Direct Method of Generating Floor Response Spectra for Structures under Earthquake Excitations at Multiple Supports

by

Rui Wang

A thesis
presented to the University of Waterloo
in fulfilment of the
thesis requirement for the degree of
Doctor of Philosophy
in
Civil Engineering

Waterloo, Ontario, Canada, 2023

Examining Committee Membership

The following served on the Examining Committee for this thesis. The decision of the Examining Committee is by majority vote.

External Examiner	NAME: Katsuichiro Goda Title: Associate Professor
Supervisor(s)	NAME: Wei-Chau Xie Title: Professor
	NAME: Mahesh Pandey Title: Professor
Internal Member	NAME: Giovanni Cascante Title: Professor
Internal Member	NAME: Shunde Yin Title: Professor
Internal-external Member	NAME: Jun Liu Title: Associate Professor

Author's Declaration

I hereby declare that I am the sole author of this thesis. This is a true copy of the thesis, including any required final revisions, as accepted by my examiners.

I understand that my thesis may be made electronically available to the public.

Abstract

Floor Response Spectra (FRS) are commonly used as seismic input in the safety assessment for secondary systems in the nuclear power industry. Efficient and accurate determination of FRS is crucial in the design of nuclear power facilities. It has been demonstrated that time history analysis can lead to large variabilities in the generation of FRS, especially at FRS peaks. Therefore, FRS from only a single or a small set of time history analyses is not reliable, while a large number of time history analyses are needed to achieve sufficiently accurate FRS. However, this procedure is time-consuming and computational expensive in practice. Although some direct methods have been developed for the accurate generation of FRS, such as the method proposed by Jiang *et al*. (2015), they do not focus on structures under earthquake excitations from multiple supports.

The purpose of this study is to develop a method of generating FRS for multiply supported structures which can overcome the deficiencies of the time history method. A direct spectra-to-spectra method is analytically developed for generating FRS of structures with earthquake excitations from multiple supports without performing any time history analyses. Only ground response spectra (GRS), "t-response spectra (tRS)", and basic modal information of primary and secondary structures, including natural frequencies, modal damping ratios, modal participation factors, and mode shapes, which can be readily obtained from modal analyses, are needed. A new combination rule for generating FRS of multi-supported structures, called FRSMS-CQC, is developed based on random vibration theory. FRSMS-CQC fully accounts for the correlations between various components affecting FRS: the correlation between the responses of oscillators excited by any two vibration modes, the correlation between the response of an oscillator excited by a vibration mode and the response of an oscillator mounted directly on a support, and the correlation between the responses of oscillators mounted on different supports.

Practical methods are developed for determining the seismic response of multiply-supported secondary structures as well as Tertiary Response Spectra (TRS) using FRS as input. The formulations in two special cases, i.e., the seismic input are fully correlated or independent, which have wide applications in practice are derived explicitly. Two assump-

tions on the correlation of FRS in the seismic evaluation of secondary systems, i.e., FRS in the same direction at different nodes of the same primary structure can be considered as fully-correlated, while they can be treated as independent if the nodes are located at different primary structures, are proposed for the practical evaluation of multi-supported secondary systems. It is demonstrated that the proposed methods can generate accurate seismic responses of secondary systems as well as TRS efficiently.

The proposed direct spectra-to-spectra method for multi-supported structures is further extended to generate FRS considering the effect of soil-structure interaction (SSI) in incorporation with the substructure method, which allows the superstructure and the surrounding soil can be analyzed individually. Based on the soil stiffness and structural modal information, FLIRS transfer matrix and modification factor are derived to convert Foundation Input Response Spectra (FIRS) into Foundation Level Input Response Spectra (FLIRS), which is then used as the seismic input to the decoupled model to generate FRS using the proposed direct spectra-to-spectra method.

The methods developed in this thesis are efficient and accurate for the generation of seismic responses, FRS, and TRS comparing to the benchmarks obtained from time history analyses using a large number of spectrum-compatible time histories.

Acknowledgement

I would like to express my great gratitude to my supervisors, Professor Wei-Chau Xie and Professor Mahesh D. Pandey, who have been tremendous mentors for me. I would like to thank them for supporting, encouraging my research and the great help in completing this thesis.

I would like to extend my gratitude to Professors Giovanni Cascante, Shunde Yin, and Jun Liu for the serving as my thesis committee members and their insightful comments on my research.

Thanks also go to my friends and colleagues, Dr. Wei Jiang, Dr. Yang Zhou, Dr. Bo Li, Dr. Lanlan Yang, Dr. Mengcheng Sun, Dr. Linbo Zhang, Muzi Li, Dr. Min Xiang, Dr. Yue Li, Peng Dai, Hongjuan Shi, and other graduate students in the Department of Civil and Environmental Engineering. I am extremely grateful to Dr. Wei Jiang, Dr. Yang Zhou, Dr. Bo Li, Dr. Lanlan Yang for generously providing their insightful suggestions and the sharing Matlab codes that have had a significant impact on the outcome of this research.

The financial support by the Natural Sciences and Engineering Research Council of Canada (NSERC) and the University Network of Excellence in Nuclear Engineering (UNENE) in the form of a Research Assistantship is greatly acknowledged.

I would like to express my deepest appreciation to Professor Wei-Chau Xie again and his wife Mrs. Cong-Rong Xie for their great impact on the development of my personalties and suggestions on career. With their great supports, I always feel surrounded by a sense of belonging and connection at Waterloo, as if I have found a second family here.

Last but not least, without the unflagging love, support, and encouragement from my parents, my fiancée, Xia Wu, and her parents throughout these years, this thesis would not have been possible.

Dedication

TO

My Family

Contents

List of Figures

List of Tables

Nomenclature

AR	Amplification Ratio
CPSD	Cross-Power Spectral Density
CQC	Complete Quadratic Combination
DAF	Dynamic Amplification Factor
FEM	Finite Element Method
FIRS	Foundation Input Response Spectrum
FLIRS	Foundation Level Input Response Spectrum
FRS	Floor Response Spectrum
FRS-CQC	Complete Quadratic Combination for Floor Response Spectrum
FRSMS-CQC	Complete Quadratic Combination for Floor Response Spectrum of Multiple Supports
FRSMS-SRSS	Square Root of Sum of Squares for Floor Response Spectrum of Multiple Supports
F-tRS	t-response spectrum of floor response spectrum
GRS	Ground Response Spectrum
HCLPF	High Confidence and Low Probability of Failure
LB	Lower Bound
MDOF	Multiple Degrees-of-Freedom
NEP	Non-Exceedance Probability
NPP	Nuclear Power Plant
PGA	Peak Ground Acceleration
PSSI	Primary-Secondary Structure Interaction

PSDF	Power Spectral Density Function
SDOF	Single Degree-of-Freedom
SMR	Small Modular Reactor
SPRA	Seismic Probability Risk Assessment
SRSS	Square Root of Sum of Squares
SSCs	Structures, Systems and Components
SSI	Soil-Structure Interaction
tRS	t-response spectrum
TRS	Tertiary Response Spectrum
ttRS	t-response spectrum for tertiary response spectrum
UB	Upper Bound

CHAPTER 1

Introduction

Secondary systems are structures, systems and components (SSCs) that are not part of the primary load-bearing structure such as building, dam, nuclear power stations. Secondary systems can be further classified into two broad categories: (1) non-structural secondary systems, such as control systems, mechanical systems, storage tanks; and (2) structural secondary systems, for example, stairways, steam generator tubes, steam turbine, piping systems and ducts. In spite the name, secondary systems are far from being secondary in importance. During the past decades, it was demonstrated that secondary systems were vulnerable in earthquake events as shown in Figure 1.1. Furthermore, the experience from earthquakes has shown that of the failure of secondary systems, such as the failure of equipment, the collapsed furniture as well as the debris caused by falling objects, may have critical influence on the performance of vital facilities, including fire stations, hospitals and nuclear power plants. For example, a number of hospitals were obliged to be evacuated during the Northridge earthquake in Los Angeles in the year of 1994. The main reason was not the failure of the primary buildings but the water damage caused by the break of water supply system and the breakdown of emergency power system (Hall *et al.*, 1994; Villaverde, 2009).

Over the past decades, considerable progress with some well developed methods has been made in the seismic assessment of primary systems, leading to notable improvement in the design of those structures. Contrary to main structures, which are designed to

Figure 1.1 Damage of secondary system in earthquake events.

bear external forces, such as the forces due to earthquake excitation, only the capacity of regular operational load and accidental load might be investigated in this procedure. Because secondary systems are usually anchored or attached to the walls or floors of primary structure, they will be subjected to earthquake induced vibration of the supported floor rather than the ground motions acting at the foundation of primary structure. Thus, the seismic analysis of secondary systems not only depends on ground motions, but also the dynamic characteristics of the primary structure.

Nuclear industry pays more attention to the design and analysis of secondary systems due to the specific requirement of safety of nuclear power plants (ASCE, 1998). Since

the information from seismic analysis of secondary structure is necessary to the seismic safety evaluation and the design of new-built plants, accurate and practical methods for the evaluation of seismic performance of secondary systems are required.

1.1 Seismic Analysis of Secondary Systems

Seismic risk analysis is a broad and complex process, involving a number of science and engineering disciplines. This complex procedure is illustrated schematically in Figure 1.2, which is divided into five areas: seismic hazard analysis, seismic demand analysis, seismic fragility analysis, system analysis, and seismic risk quantification.

The objective of seismic hazard analysis is to determine the seismic hazard curves and seismic input at the site of interest that can be used for seismic analysis and design. Seismic demand analysis aims to determine the seismic demands or inputs to important SSCs in the Nuclear Power Plant (NPP). Dynamic finite element models of the structures in the NPP are established first, and responses of the structures at desired locations are determined through structural dynamic analysis. The outcome of seismic demand analysis provides the input to the later seismic fragility analysis to determine the seismic fragility curves or the high confidence and low probability of failure (HCLPF) values of important SSCs. System analysis determines the seismic fragility curves or HCLPF values of the system. The objective of seismic risk analysis of a nuclear power facility is to determine the probability distribution or the frequency of occurrence of adverse consequences, such as core damage frequency or large early release frequency, due to the potential effects of earthquakes.

This research focuses on the determination of seismic inputs to secondary systems for their analysis, design, and assessment; thus, the seismic analysis in this thesis refers to seismic demand analysis. In general, seismic responses of secondary systems can be evaluated by two approaches: combined primary-secondary system approach and floor response spectrum approach.

1.1.1 Combined Primary-Secondary System Method

The primary and secondary structure are considered as an integral part in the combined primary-secondary system approach. In this method, both response spectrum methods

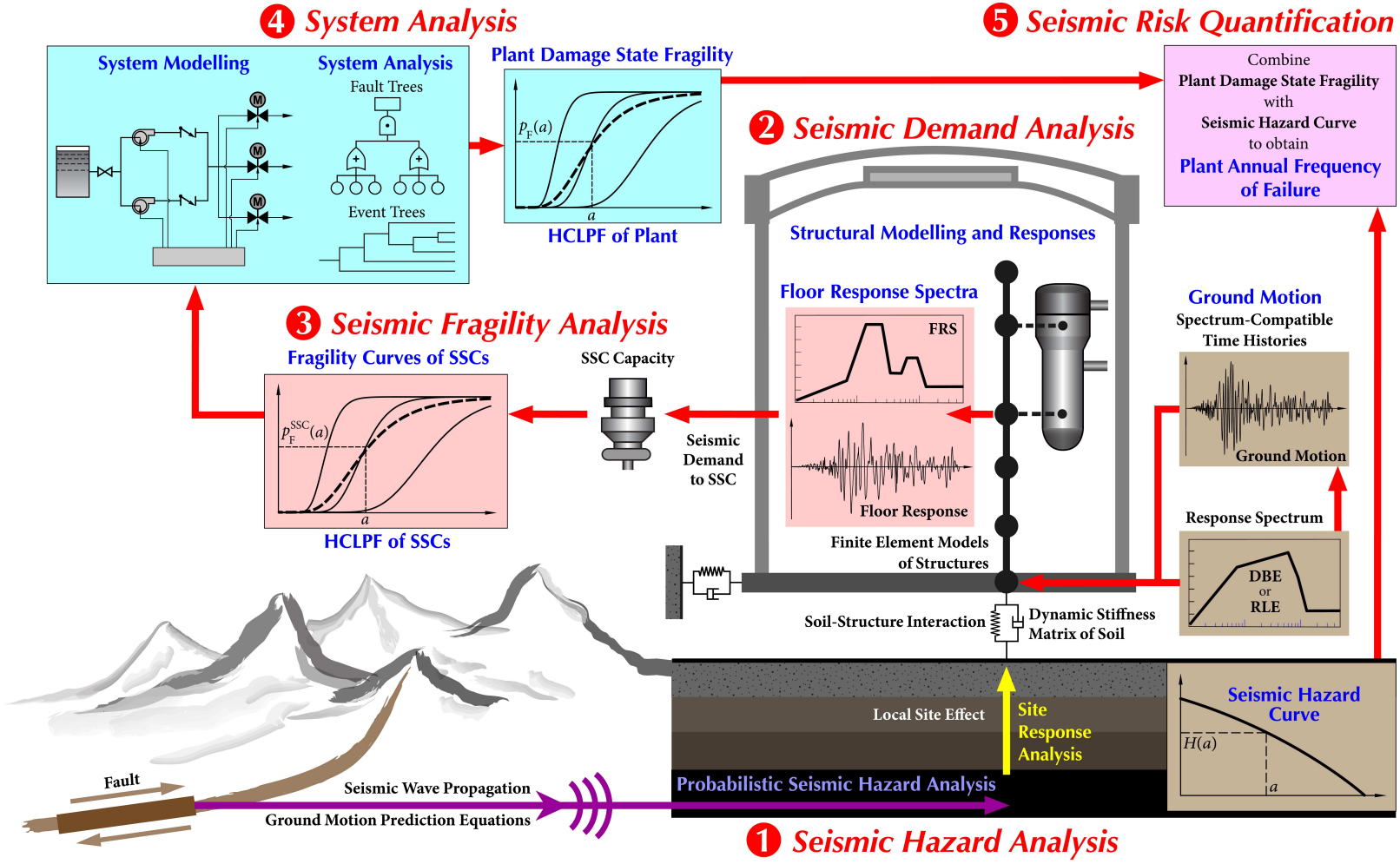

Figure 1.2 General procedure of seismic risk analysis of nuclear power plants.

based on modal analysis and time history method can be utilized to obtain the seismic response of secondary systems. In principle, the combined primary-secondary system approach can improve the accuracy of seismic evaluation as the effect of Primary-Secondary Structure Interaction (PSSI) is included. The consideration of PSSI effect causes the whole system to function as a coupled system, and exhibits specific characteristics that are conventionally not included if the primary and secondary structures are analyzed separately. In addition, since the method is based on the analysis in frequency domain, it also permits the exact solutions for the dynamic problems to be obtained (Lim and Chouw, 2015).

However, the combined primary-secondary structure method is not favored in practice because a large number of rigorous numerical integrations need to be solved. It is generally found that secondary systems are difficult to be evaluated accurately and sufficiently because a combined primary-secondary system may lead to serious numerical problems due to the large difference between two systems as well as the excessive number of degrees of freedom. For example, a secondary system may be built with materials which are different from those used by primary structure, because secondary systems are usually designed to perform specific functions rather than to bear loads. This gap between the properties of materials generally causes complex modal frequency and non-classical damping.

For example, the equation of motion for a two degrees-of-freedom coupled inelastic system may be written as (Adam and Furtmüller, 2008)

$$\begin{bmatrix} 1 & 0 \\ 0 & \bar{m} \end{bmatrix} \begin{Bmatrix} \ddot{\mathbf{x}}_\mathrm{p} \\ \ddot{\mathbf{x}}_\mathrm{s} \end{Bmatrix} + \begin{bmatrix} 2\zeta_\mathrm{p}\omega_\mathrm{p} + 2\zeta_\mathrm{s}\omega_\mathrm{s}\bar{m} & -2\zeta_\mathrm{s}\omega_\mathrm{s}\bar{m} \\ 2\zeta_\mathrm{s}\omega_\mathrm{s}\bar{m} & 2\zeta_\mathrm{s}\omega_\mathrm{s}\bar{m} \end{bmatrix} \begin{Bmatrix} \dot{\mathbf{x}}_\mathrm{p} \\ \dot{\mathbf{x}}_\mathrm{s} \end{Bmatrix} + \begin{bmatrix} \omega_\mathrm{p}^2 + \omega_\mathrm{s}^2\bar{m} & -\omega_\mathrm{s}^2\bar{m} \\ -\omega_\mathrm{s}^2\bar{m} & \omega_\mathrm{s}^2\bar{m} \end{bmatrix} \begin{Bmatrix} \mathbf{x}_\mathrm{p} \\ \mathbf{x}_\mathrm{s} \end{Bmatrix} - \begin{Bmatrix} \omega_\mathrm{p}^2 \\ 0 \end{Bmatrix} \mathbf{x}_\mathrm{p}^\mathrm{pl} = -\begin{Bmatrix} 1 \\ \bar{m} \end{Bmatrix} \ddot{\mathbf{u}}_\mathrm{g}, \tag{1.1.1}$$

in which $\bar{m}$ is the mass ratio of secondary system to primary structure, $\mathbf{x}$, ω, ζ are displacement, natural frequency and damping coefficient, respectively. The subscripts "p" and "s" stand for primary and secondary structures, respectively, and the superscript "pl" represents the plastic part of deformation. It can be seen that the combined system involves non-classically damped problem in which specific methods are required to diagonalize the equation of motion (Igusa *et al.*, 1987; Suarez and Singh, 1987; Singh and Suarez, 1987).

Furthermore, since the coupled equation includes the structural information of both primary and secondary systems, the whole coupled system needs to be reanalyzed every time

during the initial design of secondary system when one of the parameters of the secondary system is changed. Therefore, the iteration process required to complete the analysis is costly and time-consuming. Consequently, the combined primary-secondary system approach is only used in certain situations, for example, when the natural frequencies of secondary system coincidences with those of main structure or the mass of the attached components cannot be neglected comparing with primary structure.

1.1.2 Floor Response Spectrum Method

Unlike the combined primary-secondary system approach that treats the whole system as an integer part, the floor response spectrum approach is based on decoupled analysis in which the primary and secondary systems are analyzed separately. In this method, a dynamic analysis is performed for the primary structure first by neglecting the effect of the secondary system. The input for the primary structure can be a set of time histories compatible with prescribed ground motion spectra. The obtained responses of the primary structure at the support points of the secondary systems are then input to a set of single degree-of-freedom oscillators with different frequencies. Plotting the maximum responses of the oscillator versus the frequency of the oscillator yields FRS. The obtained FRS are further used to estimate response of secondary systems using certain modal combination rules.

Although problems associated with the assumption of decoupled analysis may result in some errors in special situations, it is still traditionally adopted due to many practical difficulties in the implementation of a coupled dynamic analysis (Saudy, 1992). Among the decoupled methods, the floor response spectrum method is one of the most widely accepted methods in practice due to its great simplicity in the application.

1.2 Previous Research on Floor Response Spectra

To obtain a reliable response of secondary system based on the decoupled method, an accurate FRS at the support points of secondary system is required. ASCE (1998) suggests that floor response spectra shall be generated by time history analyses or a direct spectra-to-spectra method (Figure 1.3).

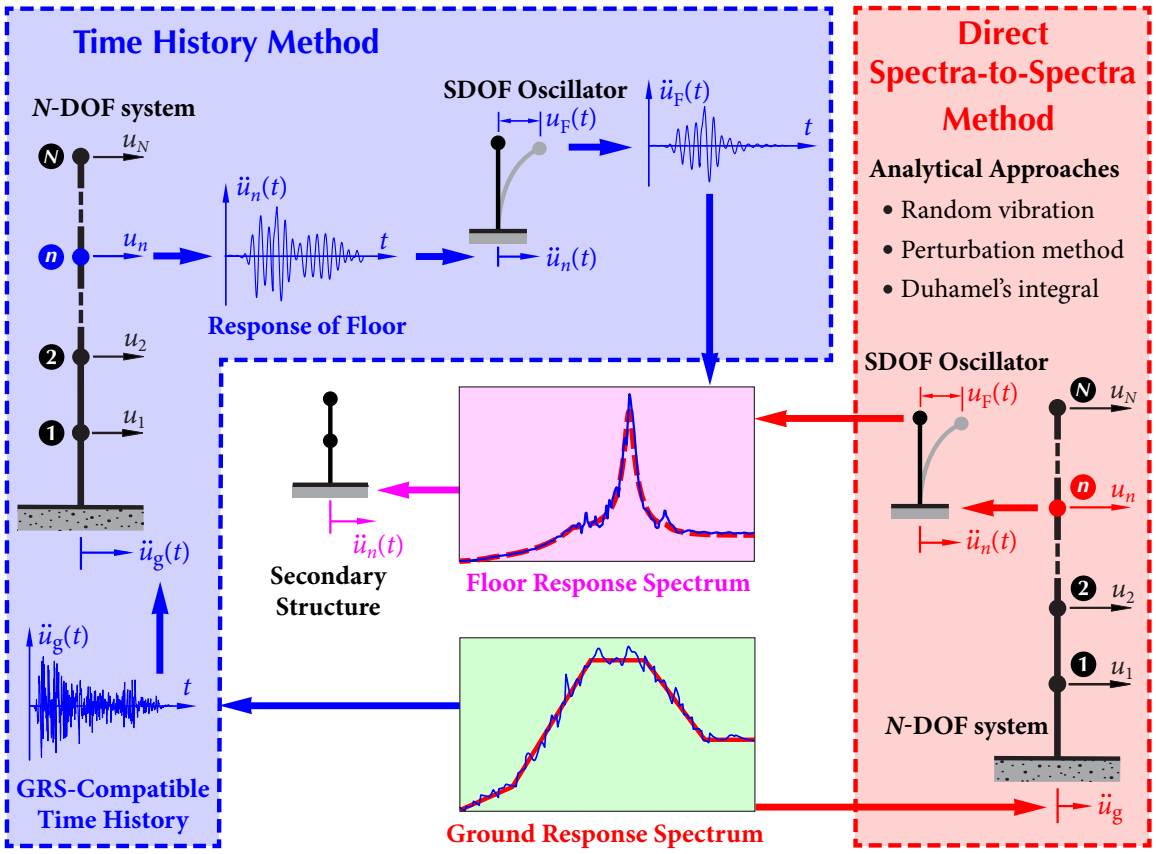

Figure 1.3 Two methods of generating floor response spectrum.

1.2.1 Time History Method

In time history method, a dynamic analysis for primary structure is performed by using modal superposition or direct time integration method. The obtained response time histories at the support point to which secondary systems are attached are then used to generate FRS.

Time history method can theoretically give exact responses for a recorded earthquake excitation. In practice, artificial time histories compatible with a target ground response spectrum are usually used in time history analysis because recorded ground motion time histories are normally not available. However, it has been demonstrated two artificial time histories can be significantly different even they are both generated from the same response

spectrum. This uncertainty in the input time histories further leads to large variabilities in FRS generated by the time history method (Singh, 1988; Villaverde, 1997; Jiang *et al.*, 2015; Xie *et al.*, 2019). Thus, if a single or a small number of time history analyses are performed, the result is not reliable, in which "not reliable" refers to the fact that the FRS obtained from two different time history analyses exhibit significant differences. As a result, a large number of earthquake time histories are required to obtain an reliable probabilistic description of FRS. However, it has been mentioned that time history method involves lengthy step-by-step numerical integrations; thus, a large number of time history analyses are very computationally costly and time consuming, which has been recognized to be impractical.

1.2.2 Direct Spectra-to-Spectra Method

To overcome the deficiencies of the time history method, some direct spectra-to-spectra methods have been developed. The "direct" means that ground response spectrum is used as input directly without generating any intermediate input such as spectrum-compatible time histories or spectrum-compatible power spectral density functions. Unlike time history method that solves the dynamic problem in time domain, floor response spectra are analytically expressed in terms of ground motion spectra and some basic modal information of the primary structure, such as modal frequencies, mode shapes, modal participation factors, and modal damping ratios, which can be readily obtained from a modal analysis.

The direct spectra-to-spectra method was first proposed by Biggs and Roesset (1970) for the direct generation of FRS without conducting any time history analysis. In this method, the maximum response of equipment is considered as the combination of GRS and the peak response of the primary structure at the location where the secondary system is attached. Two types of amplification factor for ground motion and structural response, which depends on the ratio between structure period and equipment period, were determined empirically based on four typical recorded strong ground motions. The total response of equipment is then determined using the square root of the sum of the squares (SRSS) rule.

Singh (1980) developed a method for generating FRS efficiently based on random vibration theory. Resonance case is considered to compute FRS more accurately when the natural frequency of the secondary system is close to one of the dominant frequency of the main building. This method is further extended by Singh and Sharma (1985) by employing the mode acceleration formulation in the analysis, which can eliminate the error from the neglect of missing mass effect. Unlike most of conventional direct methods that use pseudo-acceleration ground spectra as input, the seismic inputs in the approach developed by Singh and Sharma (1985) are required to be relative acceleration and relative velocity spectra, however, may usually not be prescribed in practice.

Yasui *et al.* (1993) derived a direct method for the generation of FRS, which does not need any additional modal exciting function or empirical amplification factors. This method can be applied without the distinction between non-resonant case and resonant case, which is of great simplicity comparing with the methods proposed by Singh (1980) and Singh and Sharma (1985). However, the generated FRS using this method could lead to 50% overestimation at FRS peaks. The errors were stated to be caused by the error in fitting the target spectra for the artificial seismic time histories. However, Jiang *et al.* (2015) found that the method proposed by Yasui *et al.* (1993) neglects the phase difference between responses, which is only applicable when the phase differences are π or $\pi/2$. Consequently, FRS obtained from this method could result in large errors.

Sullivan *et al.* (2013) developed a spectrum method for determining FRS of SDOF structures based on the concept of Dynamic Amplification Factor (DAF), which is the ratio of the maximum acceleration of the secondary system to the maximum acceleration of the floor where the secondary system is mounted. This method was further extended by Calvi and Sullivan (2014) to MDOF structures. Although it has been illustrated that these two methods yield acceptable FRS in the research, the expression of DAF is empirical which may lead to inaccurate FRS for some cases. More research on generating FRS based on amplification factor can also be found in Wieser *et al.* (2013), Surana *et al.* (2018A) and Surana *et al.* (2018B). However, these amplification factor functions are also obtained empirically, thus restrictions exist in the application of these methods.

Effects of Nonlinear Behavior in Primary Structure

Some direct methods of the generation of FRS involving the effect of nonlinear behavior in primary structure were developed. Lin and Mahin (1985) performed the FRS method to investigate the influence of structural nonlinearity on FRS. An amplification factor, which is the ratio of the FRS for an inelastic structure over the corresponding spectra for an elastic one, was defined to quantify the effects of inelastic deformations of primary structure on secondary structure response. It is observed that the consideration of inelastic characteristic of primary structure can decrease the spectral value of FRS, while the peak tends to be shifted toward higher frequencies.

Taghavi and Miranda (2018) and Aragaw and Calvi (2018) also conducted research on structural inelasticity and FRS using empirical modal reduction factors, which are determined by the ductility of the primary structure. The results demonstrate that the seismic demands will generally be reduced when the effect of nonlinearity in included.

Taghavi and Miranda (2012) studied the effect of nonlinearity of supporting structure on the seismic response of secondary acceleration sensitive components using time history method. The primary structure is a two-dimensional multi-story frame modelled by linear beams and nonlinear columns, which are connected through nonlinear rotational springs. They found that while floor acceleration tends to amplify ground motion in linear structure, the acceleration of secondary system might be smaller than ground acceleration, indicating that the consideration of nonlinearity of main structure could decrease the seismic demand of secondary components.

However, some research found that nonlinearity in main structure may lead to increased FRS values sometimes. For example, Chaudhuri and Villaverde (2008) performed a comprehensive parametric study on the effect of nonlinear behavior on both structural building and nonstructural components using time history analysis. It is found that spectral value of FRS may increase when the main structure varies from linear to localized nonlinear rather than to widespread nonlinear. They also concluded that the nonlinear properties in supporting structure and secondary components affects favorably the seismic performance of secondary system. As a result, secondary system can be designed following the same procedure of linear response analysis for the most of cases whereas nonlinearity should be

considered when the nonstructural component is mounted on the lower floors of a main building or when the primary and secondary systems are in resonance.

Although it has been demonstrated that structural nonlinearity of primary structures may have influence on FRS, safety-related structures in the nuclear industry are required to behave linear elastically during an earthquake. For example, Clause 6.1.2 of CSA N289.3-10 (CSA, 2010) states that "Structures that support safety-related systems shall undergo dynamic analysis to predict the responses of a system when subjected to the design basis ground motion. The responses are determined assuming that the SSCs respond within elastic stress limits". Hence, this research follows the requirement and practice of nuclear industry in conducting floor response analysis and assume that the safety-related primary structures are linear elastic with viscous damping. Structural nonlinearity is not considered in the proposed methods.

Dynamic Interaction between Primary and Secondary System

While it has been demonstrated by several studies that the interaction between the primary structure and secondary system may have some influences on the FRS, the secondary system and its supporting structure are decoupled and analyzed separately in many cases due to the limitations of the coupled analysis as mentioned before. For secondary system with mass ratio less than 1%, the dynamic interaction effect is relatively small (less than 10%) and can be ignored as a result.

However, neglecting the interaction between primary and secondary structure may provide conservative results for certain situations (Lim and Chouw, 2014; Vela *et al.*, 2008). This effect is more significant when the natural period of a secondary component is close to that of the supporting structure (Chen and Soong, 1988). A criterion of decoupling analysis was proposed by Hadjian and Ellison (1986) based on the parametric study for two types of models with 2 DOF, shown as Figure 1.4. It can be seen that the dynamic interaction effect depends on the mass ratio as well as ratio of natural frequencies between the secondary system and the primary structure. In the nuclear power industry, the mass of secondary system is generally very small comparing with primary structure, such as reactor building.

Therefore, the dynamic interaction between primary and secondary systems is supposed to relatively small and can be neglected.

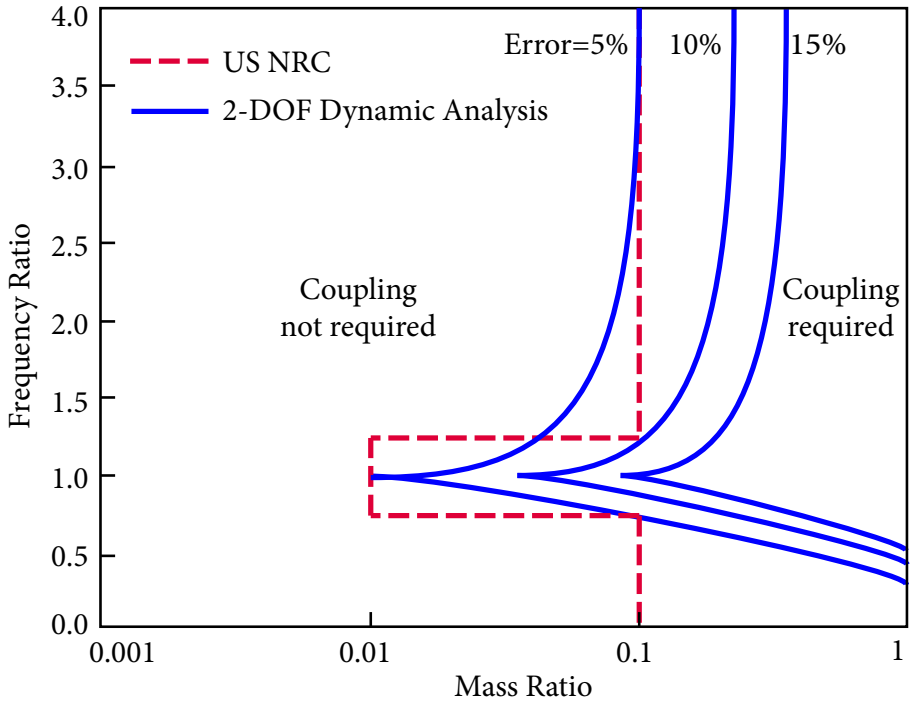

Figure 1.4 Criteria for coupling and decoupling analysis.

Although many direct spectra-to-spectra methods have been developed for the generation of FRS over the last decades, they have not been widely used in the nuclear power industry. The main reason is that those methods cannot generate accurate FRS over the entire frequency range. Some approaches provide conservative results in certain frequency ranges but unconservative results in the other frequency ranges due to various approximations or empirical amplification factors used (Yasui *et al.*, 1993; An *et al.*, 2013). Most importantly, it is unknown that when or by how much the obtained FRS is conservative or unconcervative, making it difficult to scale FRS. As a result, the process of generating FRS is separated into non-resonance and resonance cases and analyzed individually (Singh, 1980; Singh and Sharma, 1985), which is cumbersome and not user-friendly.

Recently, a new direct spectra-to-spectra method for the accurate and efficient generation of FRS was proposed by Jiang *et al.* (2015), which can give accurate FRS conveniently for

complex structures with closely-spaced modes. In this method, t-response spectrum (tRS) (Li *et al.*, 2015) was introduced to obtain FRS for the tuning or resonant case. A new modal combination method, i.e., FRS-CQC, was derived to account for various correlations between the responses of the secondary structure and the primary structure. It has been proved that this method is able to generate FRS accurately over the entire frequency range and is of much convenience and efficiency to be applied to complex structures.

It is noted that the method proposed by Jiang *et al.* (2015) focus on primary structures with single support. However, the majority of engineering structures may undergoes different seismic excitations at different supports during an earthquake event due to the following reasons:

- the wave passage effect, i.e., seismic waves may arrive at different stations at different times. This effect becomes significant for structures with large horizontal size, such as long-span bridges (Novak *et al.*, 2019).
- the loss of coherency of the ground motion due to reflections and refractions of the waves in the heterogeneous medium of the ground. Furthermore, the superposition of waves arriving from different sources at different locations may also contributes to the incoherence effect.
- the local conditions, such as local soil conditions at different stations, can also vary significantly, which can apparently affect the amplitude and phase of ground motions.

One of the typical examples of multiple excitation problem in the nuclear industry is the Small Modular Reactor (SMR). As a new trend of future nuclear power plant, SMR has its unique advantages on the relative small size and the pre-fabricated modules, which is of much convenience to be installed. Although there is no SMR has been built yet, it is generally agreed that the future SMR would be installed partially or even fully underground, as shown in Figure 1.5. As a result, in the seismic design of SMR, the earthquake excitations should not only come from the bottom foundation, but also from the side walls, leading to a multiple excitation problem.

Due the significant difference between analyzing structures with single and multiple supports, the seismic evaluation of structures with excitation from multiple supports has

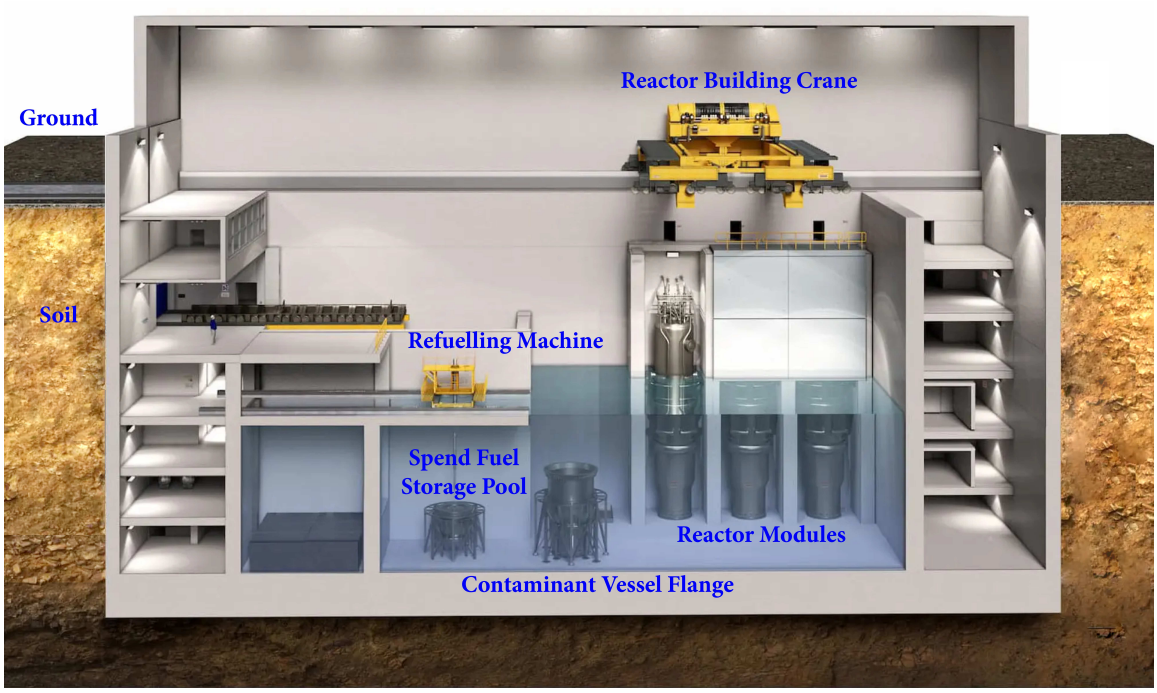

Figure 1.5 Schematic diagram of small modular reactor.

been an area of research that has received considerable attention. For example, Asfura and Der Kiureghian (1986) proposed a response spectrum method which can evaluate the total displacement spectra by introducing the concept of "cross-oscillator, cross-floor response spectrum (CCFS)". However, this method cannot be used to determine the forces in the members of the secondary system, which depends on the relative movements of the supports (Burdisso and Singh, 1987). To solve this problem, Burdisso and Singh (1987) proposed a concept of pseudo-static response that divides the response of structure into pseudo-static part and dynamic part, which were combined later based on the theory of random vibration. However, the response spectrum method proposed by Burdisso and Singh (1987) is difficult to be applied in practice, because complicated procedures to evaluate the auto-floor and cross-floor response spectra are required (Yun *et al.*, 1993). Saudy (1992) found that the method proposed by Asfura and Der Kiureghian (1986) overestimates the response of secondary systems in cases of tuned combined primary-secondary systems and an alternative modal combination rule was proposed to improve the performance.

However, the existing works on the seismic analysis of multi-supported structures mainly focus on the response of structure rather than FRS. Therefore, a direct method for generating FRS accurately and efficiently of structures under earthquake excitations from multiple supports is required. In this research, the direct method proposed by Jiang *et al.* (2015) will be extended to deal with the case of multiple seismic excitations.

1.3 Soil-Structure Interactions (SSI)

In seismic analysis, the input ground motion at the base level is commonly assumed to be the same as the free field ground motion, which is the motion of the site in the absence of the structure and of any excavation. This assumption has been justified for structures sitting on rigid rock or very stiff soil because the large stiffness of the surrounding medium can constrain the motion of foundation to be approximately the free-field motion (Zhou, 2019). However, it has been demonstrated that the soil-structure interaction (SSI) cannot be neglected when the supporting soil is relatively soft or the superstructure is massive due to (Wolf, 1985; 1987):

- Seismic responses at the foundation of the structure are different from the free-field responses at the site due to the influence of superstructure.
- The interaction between structure and its surrounding soil leads to a further change of the seismic input at the base.

It is conventionally believed that taking SSI effect into account will reduce the overall seismic responses of structure because the fundamental period of the building is elongated whereas the spectral value of ground response spectrum at lower frequencies is relatively low. Furthermore, the effective damping of a combined soil-structure system, which depends on not only structural damping but also soil material damping and soil radiation damping, is significantly higher than that of the structure itself. This larger damping causes more energy dissipation and further reduction of the responses of primary structure. For example, Kennedy *et al.* (1981) found that the soil-structure interaction tends to cause lower shear forces and moments and to higher compressive axial forces in the concrete walls, which increases the stability of the structure under strong earthquakes.

Although numerous effort has been made in studying the influence of SSI effect on the seismic performance of primary structure, only a few research investigated the effect of SSI on the floor acceleration demands. Chaudhuri and Gupta (2003) proposed a mode acceleration approach based on substructure method for generating FRS considering the effect of SSI. A numerical study of a 15-story shear building was conducted and the results indicate that soil-structure interaction should not be ignored when generating FRS unless the soil is very stiff relative to the superstructure. The extent of SSI effect is found to be highly dependent on the soil properties and the natural frequency, damping coefficient and the location of the oscillator.

The seismic response and FRS of a 4-story steel frame supported by a relative stiff soil were investigated by Raychowdhury and Ray-Chaudhuri (2015). It was found that the consideration of SSI always reduces the response of secondary components around the fundamental period of the building. It was also concluded that the maximum value of FRS tend to decrease when SSI is taken into account; however, the second or the third peak of FRS including SSI effect might be higher than that of fixed-base structure.

Zhang and Jiang (2017) studied the effect of SSI on the structural response as well as equipment response by comparing the results from experiment and finite element analysis using ANSYS. In the experiment, the equipment was modelled as a SDOF oscillator mounted on the top of the 4-story steel frame structure, which was placed on a shaking table to simulate earthquake events. The soil was modelled as a three-layer half-space medium using eight-node solid element in ANSYS. They concluded that the peak response of both main structure and secondary equipment are reduced due to the presence of soil, while the amount of reduction highly depends on the type of the ground motion and its intensity.

The typical myth about the effect of SSI on FRS is that considering SSI will benefit the seismic design of secondary components as the maximum spectral value of FRS usually decreases with the account of SSI effect. However, it is well investigated that FRS peaks occur at the frequencies of the structure dominant modes. The presence of soil results in the change of structural natural frequencies, and thus leads to shifting of FRS peaks, which could possibly approach to the resonant frequencies of equipment and its supporting building. Consequently, the seismic input to equipment could be significantly increased.

It has been pointed out by Jiang (2016) that while the maximum spectral value of FRS decreases when SSI effect is considered, the seismic input of secondary structure can be increased by 40% at certain frequencies, as shown in Figure 1.6.

Therefore, seismic input and structural analysis should not be considered independently when the structure is founded on relatively soft soil. The seismic analysis of structures considering SSI effect can be conducted through two major steps (Jiang, 2016):

1. A site response analysis is performed first to determine the foundation input response spectra (FIRS) from the GRS or response spectra prescribed at the bedrock base on the theory of wave propagation. The free-field can be generally modelled as a series of soil layers sitting on the bedrock, which is usually regarded as an elastic homogeneous half-space as shown in Figure 1.7. This step is usually conducted by earthquake professionals which is out of the scope of this study.
2. With a known FIRS, a dynamic analysis is then implemented to the structure together with the surrounding soil, considering the interaction between the structure and the surrounding soil.

The rapid progress of SSI studies after 1970s has been stimulated by the needs of the nuclear power industry. It is well understood that SSI effect should be included as one of the essential dynamic properties of NPP reactor buildings (Lou *et al.*, 2011). The methods of the investigation of SSI effect can be mainly classified into the complete method and the substructure method.

Complete Method

In the complete method or the coupled soil-structure method, the structure and a part of the surrounding soil deposit, which is denoted as near field soil, are modelled as the combined soil-structure system. Then the seismic analysis is performed to the integrated system as shown in Figure 1.8 (Wol, ; Bielak and Christiano, 1984). This model is always based on the Finite Element Method (FEM), and the system is discretized into finite elements. Since the soil deposit is actually an unbounded continuous solid and cannot be modelled by finite elements, an artificial boundary is required to model the near field soil. Furthermore, to simulate the radiation damping of semi-infinite space, the scale of the soil deposit

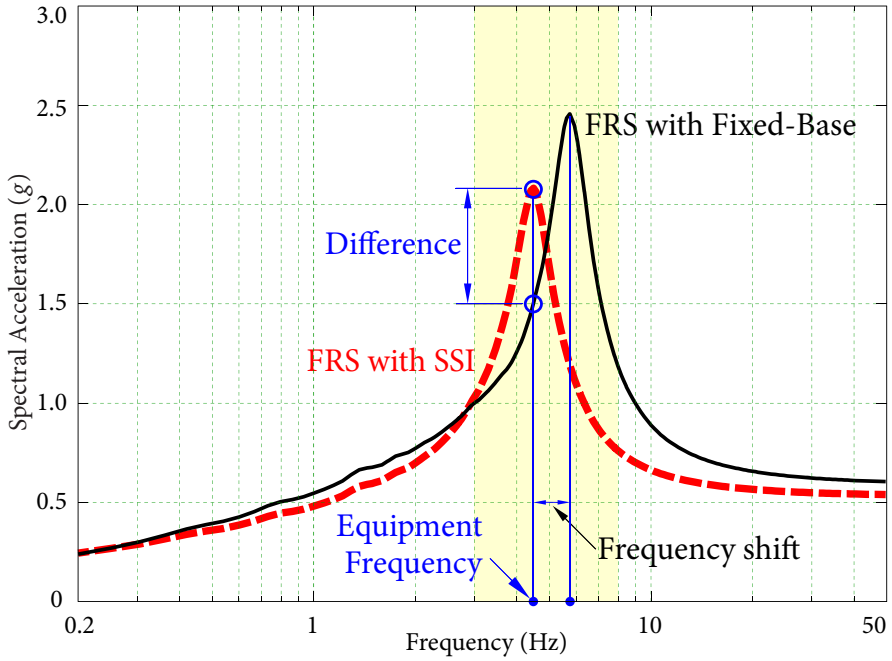

Figure 1.6 Effect of SSI on FRS.

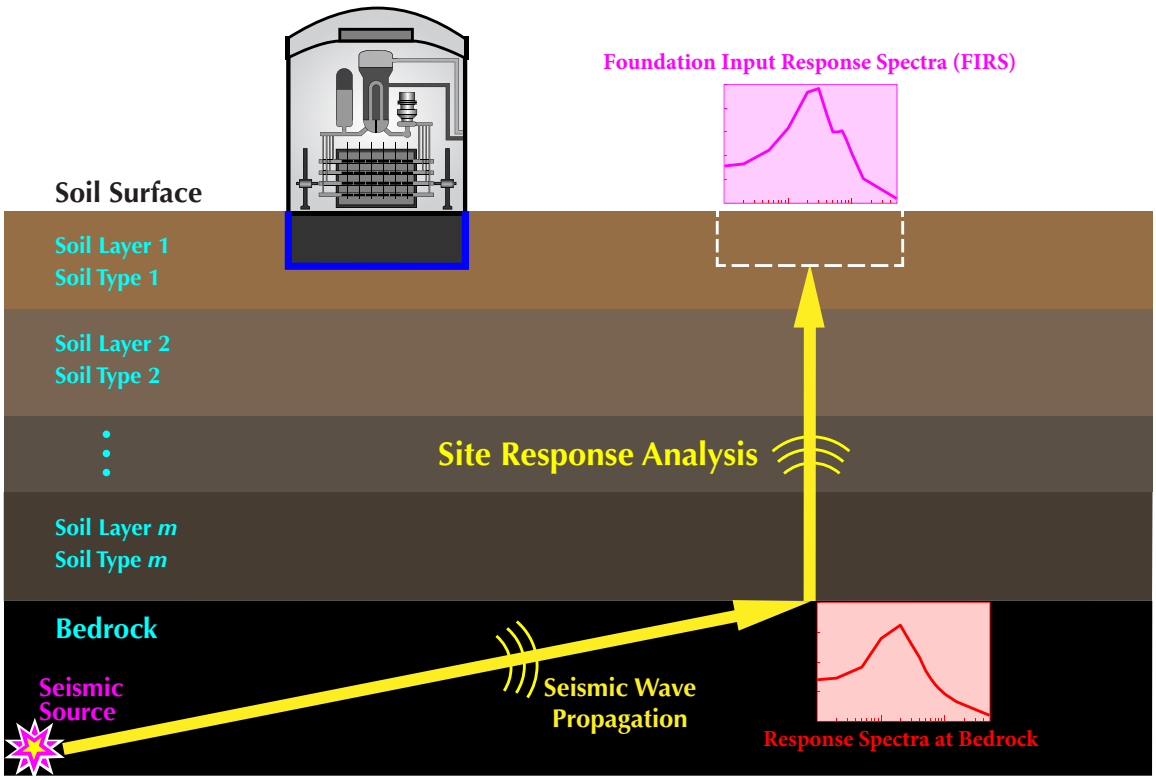

Figure 1.7 Soil-structure interaction.

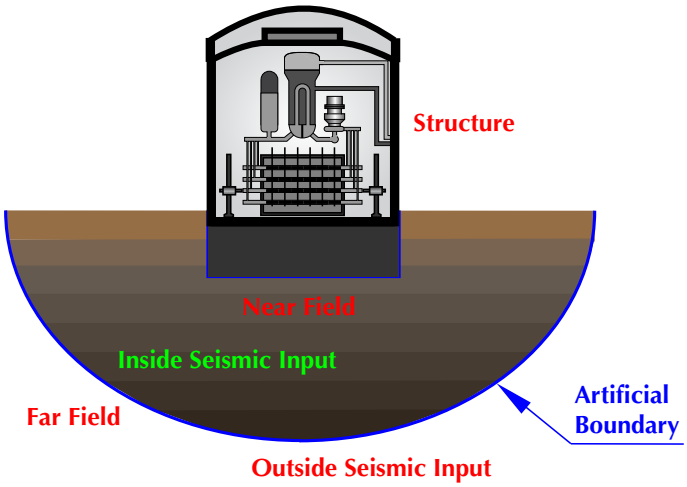

Figure 1.8 Finite element model for SSI complete method.

should be large enough (Lou *et al.*, 2011). This requirement, however, causes a tremendous consumption of time and computer resource. As a result, a number of artificial boundaries have been proposed to reduce the scale of the FEM model (Lysmer *et al.*, 1983; Higdon, 1991; Collino, 1993; Liao and Wong, 1984; Wang, 2005).

Although many transmitting boundaries were proposed to increase the efficiency of the numerical simulation, the application of the complete method still requires relatively significant time as well as computational memories because a large system of coupled equations need to solved. In addition, the use of these artificial transmitting boundaries and the necessity that the bedrock has to be located at relative shallow depth may also lead to inaccuracy by FEM. Furthermore, the entire analysis procedure has to be repeated when one of the properties of the superstructure or soil is changed, while only the responses of the structure are of interest. Therefore, the complete method is not widely used in the nuclear power industry due to the limitations above.

Substructure Method

The other method for SSI analysis is called the substructure method (Gutierrez and Chopra, 1978). This method, which is theoretically equivalent to the complete method, permits the whole system to be divided into more manageable parts and to analyze these parts separately. Some commercial finite element analysis software packages, such as **SASSI** (Lysmer *et al.*, 1983), ACS **SASSI** (Ghiocel, 2015), were developed on the basis of the substructure method,

and are currently employed in practice to analyze the seismic response of a soil-structure system. It should be noted that the entire analysis in ACS SASSI is performed in frequency domain using the complex response method and finite element techniques. The transient analysis is handled by Fast Fourier Transform techniques in which the dynamic response at each frequency can be obtained. Lastly, the vibrational behavior in time domain can be evaluated by inverse Fourier Transform. However, the dynamic analysis in frequency domain requires the seismic inputs to be spectrum-compatible time histories, which means that the deficiencies of time history analysis as discussed in Section 1.2.1, are inevitable.

Thus, it is desirable to develop an efficient and accurate method for generating FRS taking into account the SSI effect. Several studies on the generation of FRS using the direct method considering the effect of SSI have been carried out. Jiang (2016) performed a seismic analysis for structures with rigid foundation. Rigid foundation means that there is no deformation of the foundation so that the foundation can be simplified to a single point. The direct method for generating FRS proposed by the author becomes applicable in this case once the equivalent input, i.e., Foundation Level Input Response Spectra (FLIRS), is determined. This method is modified by Zhou (2019) to include the flexibilities of foundations. Although the method proposed by Zhou (2019) can deal with the situation of multiple excitations, it condenses all the deformations to a single point, which might has theoretical defect for structures undergo seismic excitation at different supports. The later part of this thesis will extend the method developed by Jiang (2016) to structures with earthquake excitations from multiple supports. In the proposed method, structural responses are not referred to a single point but are divided into dynamic and quasi-static parts.

1.4 Objectives of This Study

The objective of this study is to develop a direct spectra-to-spectra method for generating FRS for structures with earthquake excitations from multiple supports. The specific objectives of this study include:

- Extend the method proposed by Jiang (2016) to multi-supported structures.

- Develop practice-orientated methods for the seismic evaluation of secondary and tertiary system using FRS.
- Develop a direct method to generate FRS for multi-supported structures considering SSI effect.

1.5 Organization of This Thesis

In Chapter 2, a direct spectra-to-spectra method for generating FRS of structures with earthquake excitations from multiple supports is developed. Starting with the fundamentals of structural dynamics, seismic response of an MDOF primary structure is formulated by applying the concept of "quasi-static" response, which allows to divide the response into quasi-static and dynamic parts. The response of an SDOF oscillator attached to the primary structure is then obtained. A new combination rule for generating FRS of multi-supported structures, called FRSMS-CQC, is developed based on random vibration theory. FRSMS-CQC fully accounts for the correlations between various components affecting FRS: the correlation between the responses of oscillators excited by any two vibration modes, the correlation between the response of an oscillator excited by a vibration mode and the response of an oscillator mounted directly on a support, and the correlation between the responses of oscillators mounted on different supports. FRS is formulated in terms of the characteristic of input GRS and the basis modal information of primary structure, which are necessary in conventional spectrum methods and no additional information is needed. To illustrate the superiority of the proposed FRSMS-CQC combination rule, the result from conventional SRSS combination rule, called FRSMS-SRSS in this case, is also developed and the results from the two combination rules are compared.

In Chapter 3, practical methods are presented for determining the seismic responses of multiply-supported secondary structures as well as tertiary response spectra using FRS obtained by the direct method proposed in Chapter 2. Noting that the formulation of getting response of the primary structure and the secondary system is generic, it should be applicable to any structures with seismic input at multiple supports. Firstly, the implicit formulation for combining the quasi-static response and the dynamic response are

presented with the combination coefficients are given in terms of coherence function. The responses under two special cases, i.e., the seismic input are fully correlated or independent, which have wide applications in practice, are derived explicitly. Two assumptions on the correlation of FRS, i.e., the FRS in the same direction at different nodes of the same primary structure can be considered as fully-correlated, while they can be treated as independent if the nodes are located at different primary structures, are proposed for the practical generation of the seismic responses of multi-supported secondary systems. Similar to the procedure for evaluating the responses, the response spectra at the supports where the tertiary system is attached, denoted as Tertiary Response Spectra (TRS), is derived explicitly for the above two special cases.

In Chapter 4, a method is developed for generating FRS for multi-supported structures considering the effect of SSI based on the proposed direct spectra-to-spectra method and the substructure technique. Based on the soil stiffness and structural information, a transfer function is derived to convert free-field motions FIRS into FLIRS, which is then used as the seismic input to the decoupled model to generate FRS using the direct spectra-to-spectra method. The expressions of FLIRS are given implicitly in terms of the information of superstructure and soil as well as ground motions, and it can be directly and efficiently evaluated as long as such information is given. Several numerical examples are presented to verify the proposed method, and parametric studies are conducted to investigate the influence of soil conditions on FRS.

In Chapter 5, some conclusions from this study are presented, and directions for further research are proposed.

C H A P T E R 2

Generating FRS of Structures under Multiple Earthquake Excitations

For a deeply-embedded structure, such as Small Modular Reactors, the structure is subjected to earthquake excitations not only at the foundation, but also at the side walls. Hence, an SMR is subjected to seismic excitations at multiple points. Furthermore, the seismic inputs could be different at different input points because the depth of structures can not be neglected and soil properties could vary significantly with the depth. Therefore, it is necessary to extend the direct method for generating FRS developed by Jiang *et al.* (2015), which is applicable to a structure with fixed base, to structures under multiple seismic excitation inputs.

2.1 Responses of Multi-Supported Structures

Equations of Motion of the Primary Structure

Consider a general three-dimensional multiple degrees-of-freedom (MDOF) structure under multiple tridirectional seismic excitation inputs as shown in Figure 2.1. There are M seismic input nodes or supports, which are directly subjected to seismic excitations. For a typical input node m, it is subjected to tridirectional seismic excitations $\ddot{u}_g^{m,i}(t)$, $i=1,2,3$, in which $i=1$ and 2 represent the two orthogonal horizontal directions, and $i=3$ represents the vertical direction. The structure has N response nodes, or non-input nodes,

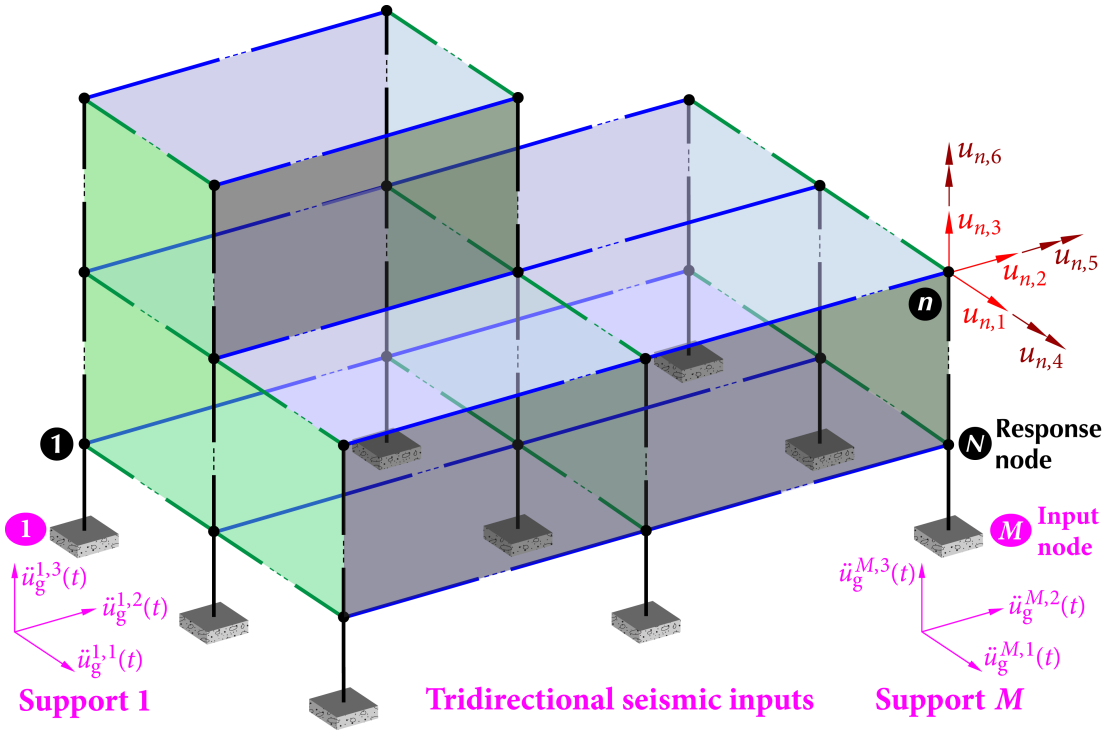

Figure 2.1 Multiple DOF primary structure under excitations at multiple supports.

which are not directly subjected to earthquake excitations. For a typical response node n, it has six DOF, including three translational DOF $u^{\mathrm{R}}_{n,1}$, $u^{\mathrm{R}}_{n,2}$, $u^{\mathrm{R}}_{n,3}$, and three rotational DOF $u^{\mathrm{R}}_{n,4}$, $u^{\mathrm{R}}_{n,5}$, $u^{\mathrm{R}}_{n,6}$. The superscript R stands for "RESPONSE". The displacement vector of the structure consists of two parts:

1. $\mathbf{u}^{\mathrm{I}} = \left\{u^{\mathrm{I}}_{1,1},\, u^{\mathrm{I}}_{1,2},\, u^{\mathrm{I}}_{1,3};\, \cdots;\, u^{\mathrm{I}}_{m,1},\, u^{\mathrm{I}}_{m,2},\, u^{\mathrm{I}}_{m,3};\, \cdots;\, u^{\mathrm{I}}_{M,1},\, u^{\mathrm{I}}_{M,2},\, u^{\mathrm{I}}_{M,3}\right\}^T$, in which there are $3M$ components of the displacements of the input or support nodes. The superscript I stands for "INPUT".
2. $\mathbf{u}^{\mathrm{R}} = \left\{u^{\mathrm{R}}_{1,1},\, u^{\mathrm{R}}_{1,2}, \ldots,\, u^{\mathrm{R}}_{1,6};\, \cdots;\, u^{\mathrm{R}}_{n,1},\, u^{\mathrm{R}}_{n,2}, \ldots,\, u^{\mathrm{R}}_{n,6};\, \cdots;\, u^{\mathrm{R}}_{N,1},\, u^{\mathrm{R}}_{N,2}, \ldots,\, u^{\mathrm{R}}_{N,6}\right\}^T$, where there are $6N$ components of the displacements of the response or non-input nodes.

The equation of dynamic equilibrium of the structure can be written in partitioned matrix form as

$$\begin{bmatrix} \mathbf{M}_{\mathrm{II}} & \mathbf{M}_{\mathrm{IR}} \\ \mathbf{M}_{\mathrm{RI}} & \mathbf{M}_{\mathrm{RR}} \end{bmatrix} \begin{Bmatrix} \ddot{\mathbf{u}}^{\mathrm{I}} \\ \ddot{\mathbf{u}}^{\mathrm{R}} \end{Bmatrix} + \begin{bmatrix} \mathbf{C}_{\mathrm{II}} & \mathbf{C}_{\mathrm{IR}} \\ \mathbf{C}_{\mathrm{RI}} & \mathbf{C}_{\mathrm{RR}} \end{bmatrix} \begin{Bmatrix} \dot{\mathbf{u}}^{\mathrm{I}} \\ \dot{\mathbf{u}}^{\mathrm{R}} \end{Bmatrix} + \begin{bmatrix} \mathbf{K}_{\mathrm{II}} & \mathbf{K}_{\mathrm{IR}} \\ \mathbf{K}_{\mathrm{RI}} & \mathbf{K}_{\mathrm{RR}} \end{bmatrix} \begin{Bmatrix} \mathbf{u}^{\mathrm{I}} \\ \mathbf{u}^{\mathrm{R}} \end{Bmatrix} = \begin{Bmatrix} \mathbf{F}^{\mathrm{I}} \\ \mathbf{F}^{\mathrm{R}} \end{Bmatrix} = \begin{Bmatrix} \mathbf{F}^{\mathrm{I}} \\ \mathbf{0} \end{Bmatrix}, \quad (2.1.1)$$

where $\mathbf{M}_{II}$, $\mathbf{C}_{II}$ and $\mathbf{K}_{II}$ are the mass, damping and stiffness matrices associated with the input nodes (supports), respectively; $\mathbf{M}_{RR}$, $\mathbf{C}_{RR}$ and $\mathbf{K}_{RR}$, respectively, are the mass, damping and stiffness matrices associated with the response nodes, while the other matrices in equation (2.1.1) describe the coupling effect between the response nodes and supports. These matrices can be determined from the properties of the structure using a finite element method, while it is desirable to determine the displacement vector $\mathbf{u}^{R}$ of the response nodes by giving the support excitations $\mathbf{F}^{I}$. Note that there are no external loading directly applied on the response nodes of the structure, i.e., $\mathbf{F}^{R}=\mathbf{0}$.

Separate the displacements in two parts as

$$\begin{Bmatrix}\mathbf{u}^{R}\\ \mathbf{u}^{I}\end{Bmatrix}=\begin{Bmatrix}\mathbf{u}^{RS}\\ \mathbf{u}^{I}\end{Bmatrix}+\begin{Bmatrix}\mathbf{x}\\ \mathbf{0}\end{Bmatrix}, \tag{2.1.2}$$

In equation (2.1.2), $\mathbf{u}^{RS}$ is the vector of displacements of the response nodes due to static load of the prescribed support displacements $\mathbf{u}^{I}$ at each time instant, which is called the *quasi-static* displacement vector. The vector $\mathbf{x}$ is called the *dynamic* displacement vector, because a dynamic analysis is needed to evaluate it. This partitioning of the response was firstly proposed by Burdisso and Singh (1987) and was also utilized by Chopra (2012).

$\mathbf{u}^{RS}$ and $\mathbf{u}^{I}$ are related through

$$\begin{bmatrix}\mathbf{K}_{II} & \mathbf{K}_{IR}\\ \mathbf{K}_{RI} & \mathbf{K}_{RR}\end{bmatrix}\begin{Bmatrix}\mathbf{u}^{I}\\ \mathbf{u}^{RS}\end{Bmatrix}=\begin{Bmatrix}\mathbf{F}^{IS}\\ \mathbf{0}\end{Bmatrix}, \tag{2.1.3}$$

where $\mathbf{F}^{IS}$ is the vector of forces at the input nodes necessary to statically impose displacement $\mathbf{u}^{I}$. If the structure is statically determinate or if the support system undergoes rigid-body motion, then $\mathbf{F}^{IS}=\mathbf{0}$.

The second block-row of equation (2.1.3) gives the relationship between quasi-static displacements and the motions of supports, i.e., $\mathbf{K}_{RI}\mathbf{u}^{I}+\mathbf{K}_{RR}\mathbf{u}^{RS}=\mathbf{0}$, which leads to

$$\mathbf{u}^{RS}=-\boldsymbol{\mathcal{I}}\mathbf{u}^{I},\qquad \boldsymbol{\mathcal{I}}=(\mathbf{K}_{RR})^{-1}\mathbf{K}_{RI}, \tag{2.1.4}$$

in which $\boldsymbol{\mathcal{I}}$ is called the *influence vector* because it describes the influence of support motions on the displacements of structures.

The second block-row of equation (2.1.1) can be written as

$$\mathbf{M}_{\mathrm{RI}}\ddot{\mathbf{u}}^{\mathrm{I}} + \mathbf{M}_{\mathrm{RR}}\ddot{\mathbf{u}}^{\mathrm{R}} + \mathbf{C}_{\mathrm{RI}}\dot{\mathbf{u}}^{\mathrm{I}} + \mathbf{C}_{\mathrm{RR}}\dot{\mathbf{u}}^{\mathrm{R}} + \mathbf{K}_{\mathrm{RI}}\mathbf{u}^{\mathrm{I}} + \mathbf{K}_{\mathrm{RR}}\mathbf{u}^{\mathrm{R}} = \mathbf{F}^{\mathrm{R}} = \mathbf{0}.$$

Substituting equation (2.1.2) into the above equation yields

$$\mathbf{M}_{\mathrm{RR}}\ddot{\mathbf{x}} + \mathbf{C}_{\mathrm{RR}}\dot{\mathbf{x}} + \mathbf{K}_{\mathrm{RR}}\mathbf{x} = \mathbf{p}_{\mathrm{e}}(t), \tag{2.1.5}$$

where $\mathbf{p}_{\mathrm{e}}(t)$ is the vector of effective earthquake forces given by

$$\mathbf{p}_{\mathrm{e}}(t) = -(\mathbf{M}_{\mathrm{RI}}\ddot{\mathbf{u}}^{\mathrm{I}} + \mathbf{M}_{\mathrm{RR}}\ddot{\mathbf{u}}^{\mathrm{RS}}) - (\mathbf{C}_{\mathrm{RI}}\dot{\mathbf{u}}^{\mathrm{I}} + \mathbf{C}_{\mathrm{RR}}\dot{\mathbf{u}}^{\mathrm{RS}}) - (\mathbf{K}_{\mathrm{RI}}\mathbf{u}^{\mathrm{I}} + \mathbf{K}_{\mathrm{RR}}\mathbf{u}^{\mathrm{RS}}). \tag{2.1.6}$$

The last term of equation (2.1.6) can be dropped due to the relationship given by equation (2.1.3). Then using the simplification proposed by Burdisso and Singh (1987), i.e., the damping terms can be neglected because their magnitudes are relatively small compared to the other terms, while $\mathbf{M}_{\mathrm{RI}}$ is a null matrix for structures with lumped masses, equation (2.1.6) can be simplified to

$$\mathbf{p}_{\mathrm{e}}(t) = -\mathbf{M}_{\mathrm{RR}}\ddot{\mathbf{u}}^{\mathrm{RS}}. \tag{2.1.7}$$

Substituting equation (2.1.4) into equation (2.1.7), the vector of effective earthquake forces becomes

$$\mathbf{p}_{\mathrm{e}}(t) = \mathbf{M}_{\mathrm{RR}}\boldsymbol{\mathcal{I}}\ddot{\mathbf{u}}^{\mathrm{I}}. \tag{2.1.8}$$

The above procedure for setting up the equation of the motion of response nodes is similar to Burdisso and Singh (1987) and Chopra (2012). Because the seismic excitations are tridirectional earthquake ground motions at the M input nodes, equation (2.1.8) can be written as

$$\mathbf{p}_{\mathrm{e}}(t) = \mathbf{M}_{\mathrm{RR}}\sum_{m=1}^{M}\sum_{i=1}^{3}\boldsymbol{\mathcal{I}}^{m,i}\ddot{u}_{\mathrm{g}}^{m,i}(t). \tag{2.1.9}$$

Hence, equation (2.1.5) becomes

$$\mathbf{M}_{\mathrm{RR}}\ddot{\mathbf{x}} + \mathbf{C}_{\mathrm{RR}}\dot{\mathbf{x}} + \mathbf{K}_{\mathrm{RR}}\mathbf{x} = \mathbf{M}_{\mathrm{RR}}\sum_{m=1}^{M}\sum_{i=1}^{3}\boldsymbol{\mathcal{I}}^{m,i}\ddot{u}_{\mathrm{g}}^{m,i}(t). \tag{2.1.10}$$

In equation (2.1.10), $\boldsymbol{\mathcal{I}}^{m,i}$ represents the $[3(m-1)+i]$-th column of the influence vector $\boldsymbol{\mathcal{I}}$, which reflects the influence of seismic input in direction i at node m on the response nodes of the structure. In equation (2.1.4), because $\mathbf{K}_{\mathrm{RR}}$ is the stiffness matrix for the

response nodes of the structure, its inverse is the flexibility matrix $\mathbf{F}_{\mathrm{RR}}$. The influence vector can be written as $\boldsymbol{\mathcal{I}} = (\mathbf{K}_{\mathrm{RR}})^{-1}\mathbf{K}_{\mathrm{RI}} = \mathbf{F}_{\mathrm{RR}}\mathbf{K}_{\mathrm{RI}}$. Therefore, $\boldsymbol{\mathcal{I}}^{m,i}$ is given by

$$\boldsymbol{\mathcal{I}}^{m,i} = \begin{Bmatrix} \sum_{\tilde{n}=1}^{N}\sum_{\tilde{j}=1}^{6} F_{1,1}^{\tilde{n},\tilde{j}} K_{\tilde{n},\tilde{j}}^{m,i} \\ \vdots \\ \sum_{\tilde{n}=1}^{N}\sum_{\tilde{j}=1}^{6} F_{1,6}^{\tilde{n},\tilde{j}} K_{\tilde{n},\tilde{j}}^{m,i} \\ \vdots \\ \vdots \\ \sum_{\tilde{n}=1}^{N}\sum_{\tilde{j}=1}^{6} F_{N,1}^{\tilde{n},\tilde{j}} K_{\tilde{n},\tilde{j}}^{m,i} \\ \vdots \\ \sum_{\tilde{n}=1}^{N}\sum_{\tilde{j}=1}^{6} F_{N,6}^{\tilde{n},\tilde{j}} K_{\tilde{n},\tilde{j}}^{m,i} \end{Bmatrix}_{6N\times 1} = \begin{Bmatrix} \vdots \\ \sum_{\tilde{n}=1}^{N}\sum_{\tilde{j}=1}^{6} F_{n,j}^{\tilde{n},\tilde{j}} K_{\tilde{n},\tilde{j}}^{m,i} \\ \vdots \end{Bmatrix}_{6N\times 1}, \tag{2.1.11}$$

in which the $[6(n-1)+j]$-th row of the vector is $\sum_{\tilde{n}=1}^{N}\sum_{\tilde{j}=1}^{6} F_{n,j}^{\tilde{n},\tilde{j}} K_{\tilde{n},\tilde{j}}^{m,i}$, which represents the influence of seismic excitation in direction i of input node m on the dynamic response in direction j of response node n of the structure. Note that in equation (2.1.11) and the remainder of this paper, for simplicity of notations, $F_{n,j}^{\tilde{n},\tilde{j}}$ refers to the element of the flexibility matrix $\mathbf{F}_{\mathrm{RR}}$ and $K_{\tilde{n},\tilde{j}}^{m,i}$ refers to the element of the stiffness matrix $\mathbf{K}_{\mathrm{RI}}$ by dropping the subscripts "RR" and "RI".

The influence vector can also be expressed in terms of the number of DOF as

$$\boldsymbol{\mathcal{I}}^{m,i} = \begin{Bmatrix} \sum_{\kappa=1}^{6N} F_1^{\kappa} K_{\kappa}^{m,i} \\ \sum_{\kappa=1}^{6N} F_2^{\kappa} K_{\kappa}^{m,i} \\ \vdots \\ \sum_{\kappa=1}^{6N} F_{6N}^{\kappa} K_{\kappa}^{m,i} \end{Bmatrix}_{6N\times 1} = \begin{Bmatrix} \vdots \\ \sum_{\kappa=1}^{6N} F_k^{\kappa} K_{\kappa}^{m,i} \\ \vdots \end{Bmatrix}_{6N\times 1}, \tag{2.1.12}$$

where the kth row in the influence vector is $\sum_{\kappa=1}^{6N} F_k^{\kappa} K_{\kappa}^{m,i}$, which reflects the influence of seismic input in direction i of node m on the kth DOF of the structure. For ease

of presentation, the two-subscript-notation n, j (node, direction) and the one-subscript-notation $k=6(n-1)+j$ are used interchangeably; the former is advantageous in describing the quantity in terms of node and direction, while the latter gives the position of the quantity in the corresponding vector.

Denoting $\mathbf{M}=\mathbf{M}_{\mathrm{RR}}$, $\mathbf{C}=\mathbf{C}_{\mathrm{RR}}$, and $\mathbf{K}=\mathbf{K}_{\mathrm{RR}}$, equation (2.1.10) can be written as

$$\mathbf{M}\ddot{\mathbf{x}}+\mathbf{C}\dot{\mathbf{x}}+\mathbf{K}\mathbf{x}=\mathbf{M}\sum_{m=1}^{M}\sum_{i=1}^{3}\boldsymbol{\iota}^{m,i}\ddot{u}_{\mathrm{g}}^{m,i}(t), \tag{2.1.13}$$

where

$$\mathbf{x}=\begin{Bmatrix}\mathbf{x}_1\\ \mathbf{x}_2\\ \vdots\\ \mathbf{x}_N\end{Bmatrix}, \qquad \mathbf{x}_n=\begin{Bmatrix}x_{n,1}\\ x_{n,2}\\ \vdots\\ x_{n,6}\end{Bmatrix}, \quad n=1,2,\ldots,N,$$

$\mathbf{M}$, $\mathbf{C}$, and $\mathbf{K}$ are, respectively, the mass, damping, and stiffness matrices of dimension $6N\times 6N$, and $\mathbf{x}_n$ is the vector of dynamic displacements of response node n.

Free Vibration

Consider undamped free vibration of the structure $\mathbf{M}\ddot{\mathbf{x}}(t)+\mathbf{K}\mathbf{x}(t)=\mathbf{0}$. Let $\omega_1, \omega_2, \ldots, \omega_{6N}$ be the $6N$ natural frequencies, $\boldsymbol{\Omega}=\mathrm{diag}\{\omega_1, \omega_2, \ldots, \omega_{6N}\}^T$, and $\boldsymbol{\Phi}=[\boldsymbol{\varphi}_1, \boldsymbol{\varphi}_2, \ldots, \boldsymbol{\varphi}_{6N}]$ be the modal matrix, where $\boldsymbol{\varphi}_k=\{\boldsymbol{\varphi}_{1,k}^T, \boldsymbol{\varphi}_{2,k}^T, \ldots, \boldsymbol{\varphi}_{N,k}^T\}^T$ is the kth mode shape, with $\boldsymbol{\varphi}_{n,k}=\{\varphi_{n,1;k}, \varphi_{n,2;k}, \ldots, \varphi_{n,6;k}\}^T$. In element $\varphi_{n,j;k}$, the first subscript n refers to the node number, the second subscript j indicates the direction of response, and the third subscript k is the mode number.

The modal matrix $\boldsymbol{\Phi}$ has the following orthogonal properties

$$\begin{aligned}\boldsymbol{\Phi}^T\mathbf{M}\boldsymbol{\Phi}&=\mathrm{diag}\{\bar{m}_1,\ \bar{m}_2,\ \ldots,\ \bar{m}_{6N}\}^T=\bar{\mathbf{m}},\\ \boldsymbol{\Phi}^T\mathbf{K}\boldsymbol{\Phi}&=\bar{\mathbf{m}}\boldsymbol{\Omega}^2=\mathrm{diag}\{\bar{m}_1\omega_1^2,\ \bar{m}_2\omega_2^2,\ \ldots,\ \bar{m}_{6N}\omega_{6N}^2\}^T,\end{aligned} \tag{2.1.14}$$

where $\bar{m}_1,\ \bar{m}_2, \ldots,\ \bar{m}_{6N}$ are the modal masses. Assume that the structure has classical damping so that the modal matrix $\boldsymbol{\Phi}$ can also diagonalize the damping matrix, i.e.,

$$\boldsymbol{\Phi}^T\mathbf{C}\boldsymbol{\Phi}=\mathrm{diag}\{\bar{c}_1, \bar{c}_2, \ldots, \bar{c}_{6N}\}^T, \qquad \bar{c}_k=\bar{m}_k\cdot 2\zeta_k\omega_k. \tag{2.1.15}$$

Forced Vibration

Let

$$\mathbf{x} = \sum_{m=1}^{M} \sum_{i=1}^{3} \mathbf{x}^{m,i}(t). \tag{2.1.16}$$

From equation (2.1.13), one has

$$\mathbf{M}\ddot{\mathbf{x}}^{m,i} + \mathbf{C}\dot{\mathbf{x}}^{m,i} + \mathbf{K}\mathbf{x}^{m,i} = \mathbf{M}\,\boldsymbol{\mathcal{I}}^{m,i}\,\ddot{u}_{\mathrm{g}}^{m,i}(t). \tag{2.1.17}$$

Apply the transformation

$$\mathbf{x}^{m,i}(t) = \boldsymbol{\Phi}\mathbf{Q}^{m,i}(t), \quad m = 1, 2, \ldots, M, \quad i = 1, 2, 3, \tag{2.1.18}$$

where

$$\mathbf{Q}^{m,i} = \begin{Bmatrix} \mathbf{Q}_1^{m,i} \\ \mathbf{Q}_2^{m,i} \\ \vdots \\ \mathbf{Q}_N^{m,i} \end{Bmatrix} = \begin{Bmatrix} \Gamma_1^{m,i} q_1^{m,i} \\ \Gamma_2^{m,i} q_2^{m,i} \\ \vdots \\ \Gamma_{6N}^{m,i} q_{6N}^{m,i} \end{Bmatrix}, \quad \mathbf{Q}_n^{m,i} = \begin{Bmatrix} \Gamma_{n,1}^{m,i} q_{n,1}^{m,i} \\ \Gamma_{n,2}^{m,i} q_{n,2}^{m,i} \\ \vdots \\ \Gamma_{n,6}^{m,i} q_{n,6}^{m,i} \end{Bmatrix}, \quad \mathbf{x}^{m,i} = \begin{Bmatrix} \mathbf{x}_1^{m,i} \\ \mathbf{x}_2^{m,i} \\ \vdots \\ \mathbf{x}_N^{m,i} \end{Bmatrix}, \mathbf{x}_n^{m,i} = \begin{Bmatrix} x_{n,1}^{m,i} \\ x_{n,2}^{m,i} \\ \vdots \\ x_{n,6}^{m,i} \end{Bmatrix},$$

$$x_{n,j}^{m,i} = \sum_{\nu=1}^{N} \sum_{\delta=1}^{6} \varphi_{n,j;6(\nu-1)+\delta}\, \Gamma_{\nu,\delta}^{m,i} q_{\nu,\delta}^{m,i} = \sum_{k=1}^{6N} \varphi_{n,j;k}\, \Gamma_k^{m,i} q_k^{m,i}, \tag{2.1.19}$$

$$\mathcal{L}_{n,j}^{m,i} = \boldsymbol{\varphi}_{6(n-1)+j}^T \mathbf{M}\boldsymbol{\mathcal{I}}^{m,i}, \quad \text{or} \quad \mathcal{L}_k^{m,i} = \boldsymbol{\varphi}_k^T \mathbf{M}\boldsymbol{\mathcal{I}}^{m,i}, \tag{2.1.20}$$

$$\Gamma_{n,j}^{m,i} = \frac{\mathcal{L}_{n,j}^{m,i}}{\bar{m}_{6(n-1)+j}}, \quad \text{or} \quad \Gamma_k^{m,i} = \frac{\mathcal{L}_k^{m,i}}{\bar{m}_k} = \frac{\boldsymbol{\varphi}_k^T \mathbf{M}\boldsymbol{\mathcal{I}}^{m,i}}{\boldsymbol{\varphi}_k^T \mathbf{M}\boldsymbol{\varphi}_k}. \tag{2.1.21}$$

$\mathcal{L}_{n,j}^{m,i}$ is the *earthquake excitation factor*, quantifying the contribution of earthquake excitation in the *i*th direction of node *m* to the modal response $q_{n,j}^{m,i}$. $\Gamma_k^{m,i}$ is the *modal participation factor*; if $\Gamma_k^{m,i}$ is small, then the contribution of mode $\boldsymbol{\varphi}_k$ to the structural response due to excitation in the *i*th direction of node *m* is small.

Substituting equation (2.1.18) into (2.1.17) and multiplying $\boldsymbol{\Phi}^T$ from the left yields

$$(\boldsymbol{\Phi}^T\mathbf{M}\boldsymbol{\Phi})\ddot{\mathbf{Q}}^{m,i}(t) + (\boldsymbol{\Phi}^T\mathbf{C}\boldsymbol{\Phi})\dot{\mathbf{Q}}^{m,i}(t) + (\boldsymbol{\Phi}^T\mathbf{K}\boldsymbol{\Phi})\mathbf{Q}^{m,i}(t) = \boldsymbol{\Phi}^T\mathbf{M}\boldsymbol{\mathcal{I}}^{m,i}\ddot{u}_{\mathrm{g}}^{m,i}(t).$$

Using relations (2.1.14), (2.1.15), (2.1.20), and (2.1.21) gives

$$\ddot{q}_k^{m,i}(t) + 2\zeta_k\omega_k\dot{q}_k^{m,i}(t) + \omega_k^2 q_k^{m,i}(t) = \ddot{u}_{\mathrm{g}}^{m,i}(t), \tag{2.1.22}$$

where $k = 1, 2, \ldots, 6N,\ m = 1, 2, \ldots, M,\ i = 1, 2, 3.$

The absolute acceleration of the nth node in direction j due to earthquake excitation in direction i at node m can be obtained using equation (2.1.2)

$$\begin{aligned}
\ddot{u}_{n,j}^{\mathrm{R},m,i}(t) &= \ddot{x}_{n,j}^{m,i}(t) + \ddot{u}_{n,j}^{\mathrm{RS},m,i}(t) = \sum_{k=1}^{6N} \varphi_{n,j;k}\, \Gamma_k^{m,i}\, \ddot{q}_k^{m,i}(t) - \mathcal{I}_{n,j}^{m,i}\, \ddot{u}_{\mathrm{g}}^{m,i}(t) \\
&= \sum_{k=1}^{6N} \varphi_{n,j;k}\, \Gamma_k^{m,i}\, \ddot{q}_k^{m,i} - \sum_{\tilde{n}=1}^{N} \sum_{\tilde{j}=1}^{6} F_{n,j}^{\tilde{n},\tilde{j}}\, K_{\tilde{n},\tilde{j}}^{m,i}\, \ddot{u}_{\mathrm{g}}^{m,i} \\
&= \sum_{k=1}^{6N} \varphi_{n,j;k}\, \Gamma_k^{m,i}\, \ddot{q}_k^{m,i} - \sum_{k=1}^{6N} F_{n,j}^{k}\, K_k^{m,i}\, \ddot{u}_{\mathrm{g}}^{m,i} \\
&= \sum_{k=1}^{6N} \varphi_{n,j;k}\, \Gamma_k^{m,i} \left(\ddot{u}_{\mathrm{g}}^{m,i} - 2\zeta_k \omega_k \dot{q}_k^{m,i} - \omega_k^2 q_k^{m,i} \right) - \sum_{k=1}^{6N} F_{n,j}^{k}\, K_k^{m,i}\, \ddot{u}_{\mathrm{g}}^{m,i} \\
&= -\sum_{k=1}^{6N} \varphi_{n,j;k}\, \Gamma_k^{m,i} \left(2\zeta_k \omega_k \dot{q}_k^{m,i} + \omega_k^2 q_k^{m,i} \right) - \left[\sum_{k=1}^{6N} \left(F_{n,j}^{k}\, K_k^{m,i} - \varphi_{n,j;k}\, \Gamma_k^{m,i} \right) \right] \ddot{u}_{\mathrm{g}}^{m,i} \\
&= -\sum_{k=1}^{6N} \varphi_{n,j;k}\, \Gamma_k^{m,i}\, \ddot{u}_k^{m,i} - \mathcal{J}_{n,j}^{m,i}\, \ddot{u}_{\mathrm{g}}^{m,i}, \qquad (2.1.23)
\end{aligned}$$

in which $\ddot{u}_k^{m,i}$ is the absolute acceleration response of the kth mode given by

$$\ddot{u}_k^{m,i} = 2\zeta_k \omega_k \dot{q}_k^{m,i} + \omega_k^2 q_k^{m,i},$$

and

$$\mathcal{J}_{n,j}^{m,i} = \sum_{k=1}^{6N} \left(F_{n,j}^{k}\, K_k^{m,i} - \varphi_{n,j;k}\, \Gamma_k^{m,i} \right)$$

represents the influence of ground input in direction i at node m to the acceleration response of the structure in direction j at node n. The similar derivation of the absolute response can also be seen in Asfura and Der Kiureghian (1986).

In earthquake engineering, negative sign has no real significance with regard to earthquake excitation and can be dropped; hence, equation (2.1.23) can be written as

$$\ddot{u}_{n,j}^{\mathrm{R},m,i}(t) = \sum_{k=1}^{6N} \varphi_{n,j;k}\, \Gamma_k^{m,i}\, \ddot{u}_k^{m,i} + \mathcal{J}_{n,j}^{m,i}\, \ddot{u}_{\mathrm{g}}^{m,i}. \qquad (2.1.24)$$

The absolute acceleration of the structure due to excitation in direction i from all supports can be obtained as

$$\ddot{u}_{n,j}^{\mathrm{R},i}(t) = \sum_{m=1}^{M} \ddot{u}_{n,j}^{\mathrm{R},m,i}(t) = \sum_{m=1}^{M} \sum_{k=1}^{6N} \varphi_{n,j;k}\, \Gamma_k^{m,i}\, \ddot{u}_k^{m,i} + \sum_{m=1}^{M} \mathcal{J}_{n,j}^{m,i}\, \ddot{u}_{\mathrm{g}}^{m,i}. \qquad (2.1.25)$$

Then the absolute acceleration of the nth node in direction j can be evaluated by

$$\ddot{u}^{\,\mathrm{R}}_{n,j}(t) = \sum_{i=1}^{3} \ddot{u}^{\,\mathrm{R},i}_{n,j}(t). \tag{2.1.26}$$

2.2 Floor Response Spectra

If the absolute response $u^{\mathrm{R},i}_{n,j}(t)$ of node n in direction j due to earthquake excitations at multiple supports in direction i is input to an SDOF oscillator (ω_0, ζ_0), the governing equations of motion are

$$\ddot{x}^{\mathrm{F},i}_{n,j}(t) + 2\zeta_0\omega_0\,\dot{x}^{\mathrm{F},i}_{n,j}(t) + \omega_0^2\,x^{\mathrm{F},i}_{n,j}(t) = -\ddot{u}^{\mathrm{R},i}_{n,j}(t), \tag{2.2.1}$$

$$\ddot{u}^{\mathrm{F},i}_{n,j}(t) = \ddot{x}^{\mathrm{F},i}_{n,j}(t) + \ddot{u}^{\mathrm{R},i}_{n,j}(t) = -2\zeta_0\omega_0\,\dot{x}^{\mathrm{F},i}_{n,j}(t) - \omega_0^2\,x^{\mathrm{F},i}_{n,j}(t), \tag{2.2.2}$$

where $x^{\mathrm{F},i}_{n,j}(t) = u^{\mathrm{F},i}_{n,j}(t) - u^{\mathrm{R},i}_{n,j}(t)$ is the displacement of the oscillator relative to node n in direction j, and $u^{\mathrm{F},i}_{n,j}(t)$ is the absolute displacement of the oscillator. The superscript "F" denotes that the oscillator is mounted on a floor. The maximum absolute acceleration of the oscillator

$$\mathcal{S}^{i}_{\mathrm{A};n,j}(\omega_0, \zeta_0) = \left|\ddot{u}^{\mathrm{F},i}_{n,j}(t)\right|_{\max} \tag{2.2.3}$$

is the floor (acceleration) response spectrum (FRS) of response node (floor) n in direction j subjected to earthquake excitations at multiple supports in direction i.

It is specified in ASCE Standard 4-98 (ASCE, 1998) that, for direct spectra-to-spectra methods, when the response spectrum of a given direction at a given location has contributions from more than one spatial component of earthquakes, these contributions shall be combined by the SRSS (Square Root of the Sum of the Squares) rule. Hence, combining contributions from tridirectional earthquake excitations, FRS of node n in direction j is given by

$$\mathcal{S}_{\mathrm{A};n,j}(\omega_0, \zeta_0) = \sqrt{\sum_{i=1}^{3}\left[\mathcal{S}^{i}_{\mathrm{A};n,j}(\omega_0, \zeta_0)\right]^2}. \tag{2.2.4}$$

2.3 Direct Method for Generating FRS for Structures under Excitations at Multiple Supports

In equation (2.1.25), the first term $\sum_{m=1}^{M}\sum_{k=1}^{6N} \ddot{u}_{n,j;k}^{m,i}$ is the response due to the interaction between the structure nodes and input nodes, which is regarded as dynamic part; whereas the second term $\sum_{m=1}^{M} \mathcal{I}_{n,j}^{m,i}\, \ddot{u}_{\mathrm{g}}^{m,i}$ is the response due to the ground motion, which can be treated as quasi-static part. Corresponding to these two terms, the absolute acceleration response of the oscillator (ω_0, ζ_0) under the excitation $\ddot{u}_{n,j}^{\mathrm{R},i}(t)$ can be written as

$$z_{n,j}^{\mathrm{R},i}(t) = \sum_{m=1}^{M}\sum_{k=1}^{6N} z_{n,j;k}^{m,i}(t) + \sum_{m=1}^{M} \mathcal{I}_{n,j}^{m,i}\, z_{\mathrm{g}}^{m,i}(t), \tag{2.3.1}$$

in which $z_{n,j;k}^{m,i}(t)$ is the absolute response of the oscillator due to $\ddot{u}_{n,j;k}^{m,i}(t)$, and $z_{\mathrm{g}}^{m,i}(t)$ is the absolute response of the oscillator due to $\ddot{u}_{\mathrm{g}}^{m,i}(t)$. It should be emphasized that it is important to separate the two terms in equation (2.3.1) so that the various correlations can be properly accounted, which is one of the novel contributions of this research.

Because the maximum values of $z_{n,j;k}^{m,i}(t)$ and $z_{\mathrm{g}}^{m,i}(t)$ do not occur at the same time, they have to be combined appropriately. In this section, a new combination rule for generating FRS of multiply supported structures is developed based on the theory of random vibration.

2.3.1 FRSMS-CQC Combination Rule

In this section, a new combination rule, called FRSMS-CQC, which can account for the correlation between FRS from any pairs of two different vibration modes, the correlation between FRS from a vibration mode and FRS due to ground input at a support, and the correlation between FRS due to ground inputs at two different supports, is developed. FRSMS-CQC stands for a Complete Quadratic Combination (CQC) rule for obtaining FRS of structures with earthquake excitations at multiple supports (MS).

Squaring both sides of equation (2.3.1) gives

$$\left\{z_{n,j}^{\mathrm{R},i}(t)\right\}^2 = \left\{\sum_{m=1}^{M}\sum_{k=1}^{6N} z_{n,j;k}^{m,i}(t) + \sum_{m=1}^{M} \mathcal{I}_{n,j}^{m,i} z_{\mathrm{g}}^{m,i}(t)\right\} \times \left\{\sum_{\hat{m}=1}^{M}\sum_{\kappa=1}^{6N} z_{n,j;\kappa}^{\hat{m},i}(t) + \sum_{\hat{m}=1}^{M} \mathcal{I}_{n,j}^{\hat{m},i} z_{\mathrm{g}}^{\hat{m},i}(t)\right\}$$

$$= \sum_{m=1}^{M}\sum_{\hat{m}=1}^{M}\sum_{k=1}^{6N}\sum_{\kappa=1}^{6N} z_{n,j;k}^{m,i}(t)\, z_{n,j;\kappa}^{\hat{m},i}(t) + 2\sum_{m=1}^{M}\sum_{\hat{m}=1}^{M}\sum_{k=1}^{6N} \mathcal{I}_{n,j}^{\hat{m},i} z_{n,j;k}^{m,i}(t)\, z_{\mathrm{g}}^{\hat{m},i}(t)$$

$$+\sum_{m=1}^{M}\sum_{\hat{m}=1}^{M}\mathcal{J}_{n,j}^{m,i}\,\mathcal{J}_{n,j}^{\hat{m},i}\,z_{\mathrm{g}}^{m,i}(t)\,z_{\mathrm{g}}^{\hat{m},i}(t).$$

Taking the expected value of both sides results in the mean-square response

$$\begin{aligned}
\mathrm{E}\Big[\big\{z_{n,j}^{\mathrm{R},i}(t)\big\}^2\Big] &= \sum_{m=1}^{M}\sum_{\hat{m}=1}^{M}\sum_{k=1}^{6N}\sum_{\kappa=1}^{6N}\mathrm{E}\Big[z_{n,j;k}^{m,i}(t)\,z_{n,j;\kappa}^{\hat{m},i}(t)\Big]+2\sum_{m=1}^{M}\sum_{\hat{m}=1}^{M}\sum_{k=1}^{6N}\mathcal{J}_{n,j}^{\hat{m},i}\,\mathrm{E}\Big[z_{n,j;k}^{m,i}(t)\,z_{\mathrm{g}}^{\hat{m},i}(t)\Big]\\
&\quad+\sum_{m=1}^{M}\sum_{\hat{m}=1}^{M}\mathcal{J}_{n,j}^{m,i}\,\mathcal{J}_{n,j}^{\hat{m},i}\,\mathrm{E}\Big[z_{\mathrm{g}}^{m,i}(t)\,z_{\mathrm{g}}^{\hat{m},i}(t)\Big]\\
&=\sum_{m=1}^{M}\sum_{\hat{m}=1}^{M}\sum_{k=1}^{6N}\sum_{\kappa=1}^{6N}\rho_{k\kappa}^{m\hat{m},i}\sqrt{\mathrm{E}\Big[\big\{z_{n,j;k}^{m,i}(t)\big\}^2\Big]}\sqrt{\mathrm{E}\Big[\big\{z_{n,j;\kappa}^{\hat{m},i}(t)\big\}^2\Big]}\\
&\quad+2\sum_{m=1}^{M}\sum_{\hat{m}=1}^{M}\sum_{k=1}^{6N}\mathcal{J}_{n,j}^{\hat{m},i}\,\rho_{k0}^{m\hat{m},i}\sqrt{\mathrm{E}\Big[\big\{z_{n,j;k}^{m,i}(t)\big\}^2\Big]}\sqrt{\mathrm{E}\Big[\big\{z_{\mathrm{g}}^{\hat{m},i}(t)\big\}^2\Big]}\\
&\quad+\sum_{m=1}^{M}\sum_{\hat{m}=1}^{M}\rho_{0}^{m\hat{m},i}\,\mathcal{J}_{n,j}^{m,i}\,\mathcal{J}_{n,j}^{\hat{m},i}\sqrt{\mathrm{E}\Big[\big\{z_{\mathrm{g}}^{m,i}(t)\big\}^2\Big]}\sqrt{\mathrm{E}\Big[\big\{z_{\mathrm{g}}^{\hat{m},i}(t)\big\}^2\Big]},
\end{aligned}\tag{2.3.2}$$

in which $\rho_{k\kappa}^{m\hat{m},i}$ is the correlation coefficient between the contribution from the kth mode due to the input at support m in direction i and the contribution from the κth mode due to the input at support $\hat{m}$ in direction i; $\rho_{k0}^{m\hat{m},i}$ is the correlation coefficient between the contribution from kth mode due to the input at support m in direction i and the contribution of an oscillator (ω_0,ζ_0) due to the input at support $\hat{m}$ in direction i; $\rho_{0}^{m\hat{m},i}$ is the correlation coefficient between the contribution of an oscillator (ω_0,ζ_0) due to the input at support m in direction i and the contribution of an oscillator (ω_0,ζ_0) due to the input at support $\hat{m}$ in direction i.

In the theory of random processes, the maximum values of $z_{n,j;k}^{m,i}$, $z_{\mathrm{g}}^{m,i}$, and $z_{n,j}^{\mathrm{R},i}$ are related to the corresponding mean-square values by peak factors. In earthquake engineering, it is reasonable to assume that the peak factors are the same, i.e.,

$$\begin{aligned}
\Big|z_{n,j;k}^{m,i}(t)\Big|_{\max} &= R_{n,j;k}^{m,i} = \mathcal{P}\sqrt{\mathrm{E}\Big[\big\{z_{n,j;k}^{m,i}(t)\big\}^2\Big]},\\
\Big|z_{\mathrm{g}}^{m,i}(t)\Big|_{\max} &= \mathcal{S}_{\mathrm{A}}^{m,i}(\omega_0,\zeta_0) = \mathcal{P}\sqrt{\mathrm{E}\Big[\big\{z_{\mathrm{g}}^{m,i}(t)\big\}^2\Big]},
\end{aligned}$$

$$\left|z_{n,j}^{\mathrm{R},i}(t)\right|_{\max} = \mathcal{S}_{\mathrm{A};n,j}^{i}(\omega_0,\zeta_0) = \mathcal{PF}\sqrt{\mathrm{E}\left[\left\{z_{n,j}^{\mathrm{R},i}(t)\right\}^2\right]}, \tag{2.3.3}$$

in which $R_{n,j;k}^{m,i}$ is the maximum absolute value of $z_{n,j;k}^{m,i}$ given by Jiang *et al.* (2015), the maximum absolute value of $z_{\mathrm{g}}^{m,i}$ is the corresponding GRS $\mathcal{S}_{\mathrm{A}}^{m,i}(\omega_0,\zeta_0)$ of an oscillator (ω_0,ζ_0), and $\mathcal{S}_{\mathrm{A};n,j}^{i}(\omega_0,\zeta_0)$ is the maximum absolute value of $z_{n,j}^{\mathrm{R},i}$.

Substituting equations (2.3.3) into equation (2.3.2) gives

$$\begin{aligned}\left\{\frac{\mathcal{S}_{\mathrm{A};n,j}^{i}(\omega_0,\zeta_0)}{\mathcal{PF}}\right\}^2 &= \sum_{m=1}^{M}\sum_{\hat{m}=1}^{M}\sum_{k=1}^{6N}\sum_{\kappa=1}^{6N}\rho_{k\kappa}^{m\hat{m},i}\left\{\frac{R_{n,j;k}^{m,i}}{\mathcal{PF}}\right\}\left\{\frac{R_{n,j;\kappa}^{\hat{m},i}}{\mathcal{PF}}\right\}\\ &\quad + 2\sum_{m=1}^{M}\sum_{\hat{m}=1}^{M}\sum_{k=1}^{6N}\mathcal{J}_{n,j}^{\hat{m},i}\,\rho_{k0}^{m\hat{m},i}\left\{\frac{R_{n,j;k}^{m,i}}{\mathcal{PF}}\right\}\left\{\frac{\mathcal{S}_{\mathrm{A}}^{\hat{m},i}(\omega_0,\zeta_0)}{\mathcal{PF}}\right\}\\ &\quad + \sum_{m=1}^{M}\sum_{\hat{m}=1}^{M}\rho_{0}^{m\hat{m},i}\,\mathcal{J}_{n,j}^{m,i}\,\mathcal{J}_{n,j}^{\hat{m},i}\left\{\frac{\mathcal{S}_{\mathrm{A}}^{m,i}(\omega_0,\zeta_0)}{\mathcal{PF}}\right\}\left\{\frac{\mathcal{S}_{\mathrm{A}}^{\hat{m},i}(\omega_0,\zeta_0)}{\mathcal{PF}}\right\}.\end{aligned} \tag{2.3.4}$$

Multiplying $\mathcal{PF}^2$ to both sides of equation (2.3.4) yields

$$\begin{aligned}\left[\mathcal{S}_{\mathrm{A};n,j}^{i}(\omega_0,\zeta_0)\right]^2 &= \sum_{m=1}^{M}\sum_{\hat{m}=1}^{M}\sum_{k=1}^{6N}\sum_{\kappa=1}^{6N}\rho_{k\kappa}^{m\hat{m},i}\,R_{n,j;k}^{m,i}\,R_{n,j;\kappa}^{\hat{m},i}\\ &\quad + 2\sum_{m=1}^{M}\sum_{\hat{m}=1}^{M}\sum_{k=1}^{6N}\mathcal{J}_{n,j}^{\hat{m},i}\,\rho_{k0}^{m\hat{m},i}\,R_{n,j;k}^{m,i}\,\mathcal{S}_{\mathrm{A}}^{\hat{m},i}(\omega_0,\zeta_0)\\ &\quad + \sum_{m=1}^{M}\sum_{\hat{m}=1}^{M}\rho_{0}^{m\hat{m},i}\,\mathcal{J}_{n,j}^{m,i}\,\mathcal{J}_{n,j}^{\hat{m},i}\,\mathcal{S}_{\mathrm{A}}^{m,i}(\omega_0,\zeta_0)\,\mathcal{S}_{\mathrm{A}}^{\hat{m},i}(\omega_0,\zeta_0).\end{aligned} \tag{2.3.5}$$

Finally, similar to equation (2.2.4), the total FRS of node n in direction j under tridirectional earthquake excitations at multiple inputs can be determined by combining $\mathcal{S}_{\mathrm{A};n,j}^{i}(\omega_0,\zeta_0)$ using the SRSS rule

$$\mathcal{S}_{\mathrm{A};n,j}(\omega_0,\zeta_0) = \sqrt{\sum_{i=1}^{3}\left[\mathcal{S}_{\mathrm{A};n,j}^{i}(\omega_0,\zeta_0)\right]^2}. \tag{2.3.6}$$

2.3.2 Determination of $\rho_{k0}^{m\hat{m},i}$, $\rho_{k\kappa}^{m\hat{m},i}$, and $\rho_{0}^{m\hat{m},i}$

The correlation coefficient between the contribution from kth mode due to the input $\ddot{u}_{n,j;k}^{m,i}(t)$ and the contribution of an oscillator (ω_0,ζ_0) due to the input $\ddot{u}_{\mathrm{g}}^{\hat{m},i}(t)$, i.e., $\rho_{k0}^{m\hat{m},i}$ in equations (2.3.2) and (2.3.5), can be obtained as follows.

The contribution from the kth mode to the response of the oscillator (ω_0, ζ_0) mounted on the MDOF structure under earthquake excitation in direction i at support m, i.e., $z_k^{m,i}$, is given by (see, e.g., Xie *et al.*, 2019)

$$z_k^{m,i}(t) = \omega_0^2\,\omega_k^2 \cdot C_k(t) * \ddot{u}_g^{m,i}(t), \quad C_k(t) = h_0(t) * h_k(t), \tag{2.3.7}$$

where "$*$" denotes the operation of convolution, while

$$h_k(t) = \mathrm{e}^{-\zeta_k\omega_k t}\,\frac{\sin\omega_{k,\mathrm{d}}t}{\omega_{k,\mathrm{d}}}, \quad \omega_{k,\mathrm{d}} = \omega_k\sqrt{1-\zeta_k^2}, \tag{2.3.8}$$

and its Fourier transform is

$$\mathcal{H}_k(\omega) = \int_{-\infty}^{\infty} h_k(\tau)\,\mathrm{e}^{-\mathrm{i}\omega\tau}\,\mathrm{d}\tau = \frac{1}{(\omega_k^2-\omega^2)+\mathrm{i}2\zeta_k\omega_k\omega}. \tag{2.3.9}$$

The contribution to the oscillator (ω_0, ζ_0) under earthquake excitation in direction i at support $\hat{m}$ is

$$z_{\mathrm{g}}^{\hat{m},i}(t) = \omega_0^2\,h_0(t) * \ddot{u}_{\mathrm{g}}^{\hat{m},i}(t). \tag{2.3.10}$$

The covariance between $z_k^{m,i}(t)$ and $z_{\mathrm{g}}^{\hat{m},i}(t)$ is given by

$$\begin{aligned}
&\mathrm{E}\Big[z_k^{m,i}(t)\; z_{\mathrm{g}}^{\hat{m},i}(t+\tau)\Big] \\
&\quad= \mathrm{E}\Big[\Big\{\omega_0^2\,\omega_k^2 \cdot C_k(t) * \ddot{u}_{\mathrm{g}}^{m,i}(t)\Big\}\cdot\Big\{\omega_0^2\,h_0(t+\tau) * \ddot{u}_{\mathrm{g}}^{\hat{m},i}(t+\tau)\Big\}\Big] \\
&\quad= \mathrm{E}\Big[\omega_0^4\,\omega_k^2\int_{-\infty}^{\infty} C_k(\tau_1)\,\ddot{u}_{\mathrm{g}}^{m,i}(t-\tau_1)\,\mathrm{d}\tau_1\int_{-\infty}^{\infty} h_0(\tau_2)\,\ddot{u}_{\mathrm{g}}^{\hat{m},i}(t+\tau-\tau_2)\,\mathrm{d}\tau_2\Big] \\
&\quad= \omega_0^4\,\omega_k^2\int_{-\infty}^{\infty}\int_{-\infty}^{\infty} C_k(\tau_1)\,h_0(\tau_2)\,\mathrm{E}\Big[\ddot{u}_{\mathrm{g}}^{m,i}(t-\tau_1)\,\ddot{u}_{\mathrm{g}}^{\hat{m},i}(t+\tau-\tau_2)\Big]\,\mathrm{d}\tau_1\,\mathrm{d}\tau_2.
\end{aligned} \tag{2.3.11}$$

Taking Fourier transform of both sides of equation (2.3.11) yields

$$\begin{aligned}
\mathcal{S}_{z_k^{m,i}z_{\mathrm{g}}^{\hat{m},i}}(\omega) &= \int_{-\infty}^{\infty}\mathrm{E}\Big[z_k^{m,i}(t)\; z_{\mathrm{g}}^{\hat{m},i}(t+\tau)\Big]\cdot\mathrm{e}^{-\mathrm{i}\omega\tau}\,\mathrm{d}\tau \\
&= \omega_0^4\,\omega_k^2\int_{-\infty}^{\infty}\int_{-\infty}^{\infty}\int_{-\infty}^{\infty} C_k(\tau_1)\,h_0(\tau_2)\,R_{\ddot{u}_{\mathrm{g}}^{m,i}\ddot{u}_{\mathrm{g}}^{\hat{m},i}}(\tau+\tau_1-\tau_2)\cdot\mathrm{e}^{-\mathrm{i}\omega\tau}\,\mathrm{d}\tau_1\,\mathrm{d}\tau_2\,\mathrm{d}\tau.
\end{aligned} \tag{2.3.12}$$

Setting $\tau_3 = \tau+\tau_1-\tau_2$, equation (2.3.12) can be written as

$$\mathcal{S}_{z_k^{m,i}z_{\mathrm{g}}^{\hat{m},i}}(\omega) = \omega_0^4\,\omega_k^2\int_{-\infty}^{\infty} C_k(\tau_1)\,\mathrm{e}^{\mathrm{i}\omega\tau_1}\,\mathrm{d}\tau_1\int_{-\infty}^{\infty} h_0(\tau_2)\,\mathrm{e}^{-\mathrm{i}\omega\tau_2}\,\mathrm{d}\tau_2\int_{-\infty}^{\infty} R_{\ddot{u}_{\mathrm{g}}^{m,i}\ddot{u}_{\mathrm{g}}^{\hat{m},i}}(\tau_3)\,\mathrm{e}^{-\mathrm{i}\omega\tau_3}\,\mathrm{d}\tau$$

$$= \omega_0^4\,\omega_k^2 \cdot \mathscr{C}_k^*(\omega) \cdot \mathcal{H}_0(\omega) \cdot \mathcal{S}_{\ddot{u}_g^{m,i}\,\ddot{u}_g^{\hat{m},i}}(\omega), \tag{2.3.13}$$

where $\mathscr{C}_k(\omega) = \mathcal{H}_0(\omega)\,\mathcal{H}_k(\omega)$ is the Fourier transform of the convolution $c_k(t)$, $\mathscr{C}_k^*(\omega)$ is the complex conjugate of $\mathscr{C}_k(\omega)$. Taking the inverse Fourier transform of equation (2.3.13) yields

$$\mathrm{E}\big[z_k^{m,i}(t)\, z_g^{\hat{m},i}(t+\tau)\big] = \frac{\omega_0^4\,\omega_k^2}{2\pi} \int_{-\infty}^{\infty} \mathscr{C}_k^*(\omega) \cdot \mathcal{H}_0(\omega) \cdot \mathcal{S}_{\ddot{u}_g^{m,i}\,\ddot{u}_g^{\hat{m},i}}(\omega)\, \mathrm{e}^{\mathrm{i}\omega\tau}\, \mathrm{d}\omega. \tag{2.3.14}$$

Setting $\tau = 0$ gives

$$\mathrm{E}\big[z_k^{m,i}(t)\, z_g^{\hat{m},i}(t)\big] = \frac{\omega_0^4\,\omega_k^2}{2\pi} \int_{-\infty}^{\infty} \mathscr{C}_k^*(\omega) \cdot \mathcal{H}_0(\omega) \cdot \mathcal{S}_{\ddot{u}_g^{m,i}\,\ddot{u}_g^{\hat{m},i}}(\omega)\, \mathrm{d}\omega. \tag{2.3.15}$$

$\mathcal{S}_{\ddot{u}_g^{m,i}\,\ddot{u}_g^{\hat{m},i}}(\omega)$ is the cross-power spectral density function of ground accelerations $\ddot{u}_g^{m,i}(t)$ and $\ddot{u}_g^{\hat{m},i}(t)$, which is usually expressed as

$$\mathcal{S}_{\ddot{u}_g^{m,i}\,\ddot{u}_g^{\hat{m},i}}(\omega) = \gamma^{\,m\hat{m},i}(\omega) \sqrt{\mathcal{S}_{\ddot{u}_g^{m,i}\,\ddot{u}_g^{m,i}}(\omega)\, \mathcal{S}_{\ddot{u}_g^{\hat{m},i}\,\ddot{u}_g^{\hat{m},i}}(\omega)}\,. \tag{2.3.16}$$

where $\mathcal{S}_{\ddot{u}_g^{m,i}\,\ddot{u}_g^{m,i}}(\omega)$ and $\mathcal{S}_{\ddot{u}_g^{\hat{m},i}\,\ddot{u}_g^{\hat{m},i}}(\omega)$ are the power density functions of ground excitations $\ddot{u}_g^{m,i}(t)$ and $\ddot{u}_g^{\hat{m},i}(t)$, respectively, $\gamma^{\,m\hat{m},i}(\omega)$ is the coherency function characterizing the spatial variation of seismic ground motions. Various theoretical and empirical models of the coherency function have been developed (Luco and Wong, 1986; Abrahamson *et al.*, 1991). Furthermore, for a site of interest, the spatial coherency function $\gamma^{\,m\hat{m},i}(\omega)$ may also be available or postulated, such as those proposed by Der Kiureghian (1996) and Zhang *et al.* (2012). For each support m, $m = 1, 2, \ldots, M$, the power spectral density function $\mathcal{S}_{\ddot{u}_g^{m,i}\,\ddot{u}_g^{m,i}}(\omega)$ may be available or postulated, such as the Kanai-Tajimi power spectral density function (Villaverde, 2009). Then equations (2.3.16) and (2.3.15) can be evaluated easily.

In the following, two important special cases, which have applications in nuclear facilities, are considered.

Case 1: Seismic Excitations $\ddot{u}_g^{m,i}(t)$ and $\ddot{u}_g^{\hat{m},i}(t)$ Identical

This case is applicable to structures of small sizes, such as SMR, which is modelled as deeply-embedded structures with flexible foundations. For these structures, earthquake

excitations in a direction do not change much at different supports, which means that the input in direction i at support m and the input in direction i at support $\hat{m}$, i.e., $\ddot{u}_{\mathrm{g}}^{m,i}(t)$ and $\ddot{u}_{\mathrm{g}}^{\hat{m},i}(t)$, are approximately the same. As a result, it can be reasonably assumed that $\ddot{u}_{\mathrm{g}}^{m,i}(t) = \ddot{u}_{\mathrm{g}}^{\hat{m},i}(t) = \ddot{u}_{\mathrm{g}}^{i}(t)$, $i = 1, 2, 3$. Equation (2.3.14) becomes

$$\mathrm{E}\big[z_k^{m,i}(t)\, z_{\mathrm{g}}^{\hat{m},i}(t)\big] = \frac{\omega_0^4\,\omega_k^2}{2\pi}\int_{-\infty}^{\infty} \mathcal{H}_0^*(\omega)\cdot\mathcal{H}_0(\omega)\cdot\mathcal{H}_k^*(\omega)\cdot\mathcal{S}_{\ddot{u}_{\mathrm{g}}^{i}\,\ddot{u}_{\mathrm{g}}^{i}}(\omega)\,\mathrm{d}\omega. \tag{2.3.17}$$

Because ground motions can be generally modelled as wide-band noises, it is reasonable to assume the seismic input $\ddot{u}_{\mathrm{g}}^{i}(t)$ as a white noise by letting the power spectral density function $\mathcal{S}_{\ddot{u}_{\mathrm{g}}^{i}\,\ddot{u}_{\mathrm{g}}^{i}}(\omega) = \mathcal{S}_{\mathrm{A}}^{i}$. Therefore, equation (2.3.17) can be written as

$$\mathrm{E}\big[z_k^{m,i}(t)\, z_{\mathrm{g}}^{\hat{m},i}(t)\big] = \frac{\omega_0^4\,\omega_k^2}{2\pi}\,\mathcal{S}_{\mathrm{A}}^{i}\int_{-\infty}^{\infty}\mathcal{H}_0^*(\omega)\,\mathcal{H}_0(\omega)\,\mathcal{H}_k^*(\omega)\,\mathrm{d}\omega = \frac{\omega_0^4\,\omega_k^2}{2\pi}\,\mathcal{S}_{\mathrm{A}}^{i}\cdot I_{0k}^*, \tag{2.3.18}$$

where

$$\begin{aligned} I_{0k}^* &= \int_{-\infty}^{\infty}\mathcal{H}_0^*(\omega)\,\mathcal{H}_0(\omega)\,\mathcal{H}_k^*(\omega)\,\mathrm{d}\omega \\ &= \int_{-\infty}^{\infty}\frac{1}{(\omega_0^2-\omega^2)^2+(2\zeta_0\omega_0\omega)^2}\cdot\frac{1}{(\omega_k^2-\omega^2)-\mathrm{i}2\zeta_k\omega_k\omega}\,\mathrm{d}\omega \\ &= \int_{-\infty}^{\infty}\frac{\omega_k^2-\omega^2}{\Delta_{0k}}\,\mathrm{d}\omega + \mathrm{i}\int_{-\infty}^{\infty}\frac{2\zeta_k\omega_k\omega}{\Delta_{0k}}\,\mathrm{d}\omega = \mathcal{R}e(I_{0k}) + \mathrm{i}\,\mathcal{I}m(I_{0k}), \\ \Delta_{0k} &= \big[(\omega_0^2-\omega^2)^2+(2\zeta_0\omega_0\omega)^2\big]\cdot\big[(\omega_k^2-\omega^2)+(2\zeta_k\omega_k\omega)^2\big], \end{aligned}$$

$\mathcal{R}e(I_{0k})$ and $\mathcal{I}m(I_{0k})$ are the real and imaginary parts of I_{0k}, respectively, and can be evaluated by the method of residue to yield (see, e.g., Xie *et al.*, 2019)

$$\mathcal{R}e(I_{0k}) = \int_{-\infty}^{\infty}\frac{\omega_k^2-\omega^2}{\Delta_{0k}}\,\mathrm{d}\omega = \frac{\pi\,\alpha_{0k}}{2\zeta_0\omega_0^5}, \qquad \mathcal{I}m(I_{0k}) = \int_{-\infty}^{\infty}\frac{2\zeta_k\omega_k\omega}{\Delta_{0k}}\,\mathrm{d}\omega = 0, \tag{2.3.19}$$

in which

$$\alpha_{0k} = \frac{(4\zeta_0^2-1)^2 + 4\zeta_0\zeta_k r_k + r_k^2}{4\zeta_0\zeta_k r_k(r_k^2+1) + 4(\zeta_0^2+\zeta_k^2)r_k^2 + (1-r_k^2)^2}, \quad r_k = \frac{\omega_k}{\omega_0}. \tag{2.3.20}$$

Substituting equations (2.3.19) and (2.3.20) into equation (2.3.18) gives

$$\mathrm{E}\big[z_k^{m,i}(t)\, z_{\mathrm{g}}^{\hat{m},i}(t)\big] = \frac{\omega_0^4\,\omega_k^2}{2\pi}\,\mathcal{S}_{\mathrm{A}}^{i}\cdot\mathcal{R}e(I_{0k}) = \frac{\omega_k^2\;\mathcal{S}_{\mathrm{A}}^{i}}{4\zeta_0\,\omega_0}\,\alpha_{0k} = \frac{\omega_0\,\mathcal{S}_{\mathrm{A}}^{i}}{4\zeta_0}\,r_k^2\,\alpha_{0k}. \tag{2.3.21}$$

The expected value of the mean-square response of $z_{\mathrm{g}}^{\hat{m},i}$, i.e., $\mathrm{E}\Big[\big\{z_{\mathrm{g}}^{\hat{m},i}(t)\big\}^2\Big]$, can be determined using the same approach. The autocorrelation function is given by

$$\mathrm{E}\big[z_{\mathrm{g}}^{\hat{m},i}(t)\, z_{\mathrm{g}}^{\hat{m},i}(t+\tau)\big] = \omega_0^4 \int_{-\infty}^{\infty}\int_{-\infty}^{\infty} h_0(\tau_1)\, h_0(\tau_2)\, \mathrm{E}\Big[\ddot{u}_{\mathrm{g}}^{\hat{m},i}(t-\tau_1)\, \ddot{u}_{\mathrm{g}}^{\hat{m},i}(t+\tau-\tau_2)\Big]\, \mathrm{d}\tau_1\, \mathrm{d}\tau_2. \tag{2.3.22}$$

Taking Fourier transform of both sides and setting $\tau_3 = \tau + \tau_1 - \tau_2$ yields

$$\mathcal{S}_{z_{\mathrm{g}}^{\hat{m},i} z_{\mathrm{g}}^{\hat{m},i}}(\omega) = \omega_0^4 \cdot \mathcal{H}_0^*(\omega) \cdot \mathcal{H}_0(\omega) \cdot \mathcal{S}_{\ddot{u}_{\mathrm{g}}^{\hat{m},i} \ddot{u}_{\mathrm{g}}^{\hat{m},i}}(\omega). \tag{2.3.23}$$

Taking the inverse Fourier transform of equation (2.3.23) yields

$$\mathrm{E}\big[z_{\mathrm{g}}^{\hat{m},i}(t)\, z_{\mathrm{g}}^{\hat{m},i}(t+\tau)\big] = \frac{\omega_0^4}{2\pi} \int_{-\infty}^{\infty} \mathcal{H}_0^*(\omega) \cdot \mathcal{H}_0(\omega) \cdot \mathcal{S}_{\ddot{u}_{\mathrm{g}}^{i} \ddot{u}_{\mathrm{g}}^{i}}(\omega)\, \mathrm{e}^{\mathrm{i}\omega\tau}\, \mathrm{d}\omega. \tag{2.3.24}$$

Setting $\tau = 0$ results in

$$\mathrm{E}\Big[\big\{z_{\mathrm{g}}^{\hat{m},i}(t)\big\}^2\Big] = \frac{\omega_0^4}{2\pi}\, \mathcal{S}_{\mathrm{A}}^{i} \int_{-\infty}^{\infty} \mathcal{H}_0^*(\omega)\, \mathcal{H}_0(\omega)\, \mathrm{d}\omega = \frac{\omega_0^4}{2\pi}\, \mathcal{S}_{\mathrm{A}}^{i} \cdot \frac{\pi}{2}\, \frac{1}{\zeta_0 \omega_0^3} = \frac{\omega_0\, \mathcal{S}_{\mathrm{A}}^{i}}{4\zeta_0}. \tag{2.3.25}$$

From equation (8.4.43) in Xie *et al.* (2019), one has

$$\mathrm{E}\Big[\big\{z_k^{m,i}(t)\big\}^2\Big] = \frac{\omega_0\, \mathcal{S}_{\mathrm{A}}^{i}}{4\zeta_0}\, \beta_k \cdot r_k^4, \tag{2.3.26}$$

in which

$$\beta_k = \frac{\zeta_0 + 4\zeta_0^2 \zeta_k r_k + 4\zeta_0 \zeta_k^2 r_k^2 + \zeta_k r_k^3}{\zeta_k r_k^3 \big(1 - 2r_k^2 + r_k^4 + 4\zeta_0 \zeta_k r_k + 4\zeta_k^2 r_k^2 + 4\zeta_0^2 r_k^2 + 4\zeta_0 \zeta_k r_k^3\big)}. \tag{2.3.27}$$

Using equations (2.3.18), (2.3.25), and (2.3.26), $\rho_{k0}^{m\hat{m},i}$ in equation (2.3.2) is given by

$$\rho_{k0}^{m\hat{m},i} = \frac{\mathrm{E}\big[z_k^{m,i}(t)\, z_{\mathrm{g}}^{\hat{m},i}(t)\big]}{\sqrt{\mathrm{E}\Big[\big\{z_k^{m,i}(t)\big\}^2\Big] \cdot \mathrm{E}\Big[\big\{z_{\mathrm{g}}^{\hat{m},i}(t)\big\}^2\Big]}} = \frac{\dfrac{\omega_0\, \mathcal{S}_{\mathrm{A}}^{i}}{4\zeta_0} \cdot r_k^2 \cdot \alpha_{0k}}{\sqrt{\dfrac{\omega_0\, \mathcal{S}_{\mathrm{A}}^{i}}{4\zeta_0}\, \beta_k \cdot r_k^4 \cdot \dfrac{\omega_0\, \mathcal{S}_{\mathrm{A}}^{i}}{4\zeta_0}}} = \frac{\alpha_{0k}}{\sqrt{\beta_k}}. \tag{2.3.28}$$

Note that $\rho_{k\kappa}^{m\hat{m},i}$ in equation (2.3.5) can be obtained from Jiang *et al.* (2015) by letting $\ddot{u}_{\mathrm{g}}^{m,i}(t) = \ddot{u}_{\mathrm{g}}^{\hat{m},i}(t) = \ddot{u}_{\mathrm{g}}^{i}(t)$, from which $\rho_{k\kappa}^{m\hat{m},i}$ can be written as

$$\rho_{k\kappa}^{m\hat{m},i} = \frac{\alpha_{k\kappa}}{\sqrt{\beta_k \beta_\kappa}}, \tag{2.3.29}$$

where $\alpha_{k\kappa}$ can be obtained using equation (2.3.30) derived by Jiang *et al.* (2015), and β_k is given by equation (2.3.27). Finally, by the assumption of Case 1, $\ddot{u}_g^{m,i}$ and $\ddot{u}_g^{\hat{m},i}$ are identical, which means $\rho_0^{m\hat{m},i}=1$.

$$\alpha_{k\kappa} = \prod_{l=1}^{3} D_{k\kappa,l}^{-1} \cdot \sum_{l=0}^{4} C_{k\kappa,l}\,\zeta_0^l, \tag{2.3.30}$$

in which $C_{k\kappa,l}$ and $D_{k\kappa,l}$ are constants in terms of ζ_0, ζ_k, ζ_κ, $r_k=\omega_k/\omega_0$, and $r_\kappa=\omega_\kappa/\omega_0$, given by

$$D_{k\kappa,1} = 1 - 2r_\kappa^2 + r_\kappa^4 + 4\zeta_0\zeta_\kappa r_\kappa + 4\zeta_0\zeta_\kappa r_\kappa^3 + 4\zeta_0^2 r_\kappa^2 + 4\zeta_\kappa^2 r_\kappa^2,$$

$$D_{k\kappa,2} = 1 - 2r_k^2 + r_k^4 + 4\zeta_0\zeta_k r_k + 4\zeta_0\zeta_k r_k^3 + 4\zeta_0^2 r_k^2 + 4\zeta_k^2 r_k^2,$$

$$D_{k\kappa,3} = (r_k^2-r_\kappa^2)^2 + 4\zeta_k\zeta_\kappa r_k r_\kappa (r_k^2+r_\kappa^2) + 4r_k^2 r_\kappa^2(\zeta_k^2+\zeta_\kappa^2),$$

$$C_{k\kappa,0} = (1 - r_k^2 - r_\kappa^2 + r_k^2 r_\kappa^2 + 4\zeta_k\zeta_\kappa r_k r_\kappa)\cdot D_{k\kappa,3},$$

$$\begin{aligned}
C_{k\kappa,1}/4 = {} & 2\zeta_k r_k + 2\zeta_\kappa r_\kappa + 8\zeta_k\zeta_\kappa r_k r_\kappa(\zeta_k r_k+\zeta_\kappa r_\kappa) - 4(\zeta_k r_k^3+\zeta_\kappa r_\kappa^3) + 8\zeta_k^3 r_k^3 + 8\zeta_\kappa^3 r_\kappa^3 \\
& - 2r_k r_\kappa(\zeta_k r_\kappa^3+\zeta_\kappa r_k^3) + 8\zeta_k\zeta_\kappa r_k r_\kappa(\zeta_k r_k^3+\zeta_\kappa r_\kappa^3) + 4r_k^2 r_\kappa^2(\zeta_k r_k+\zeta_\kappa r_\kappa) \\
& - 8r_k^2 r_\kappa^2(\zeta_k^3 r_k+\zeta_\kappa^3 r_\kappa) - 8\zeta_k\zeta_\kappa r_k^2 r_\kappa^2(\zeta_k r_\kappa+\zeta_\kappa r_k) + 32\zeta_k^2\zeta_\kappa^2 r_k^2 r_\kappa^2(\zeta_k r_k+\zeta_\kappa r_\kappa) \\
& + r_k r_\kappa(\zeta_k r_\kappa^5+\zeta_\kappa r_k^5) + r_k^2 r_\kappa^2(\zeta_k r_k^3+\zeta_\kappa r_\kappa^3) + 4\zeta_k\zeta_\kappa r_k^2 r_\kappa^2(\zeta_k r_\kappa^3+\zeta_\kappa r_k^3) \\
& - 2r_k^3 r_\kappa^3(\zeta_k r_\kappa+\zeta_\kappa r_k) + 4r_k^3 r_\kappa^3(\zeta_k^3 r_\kappa+\zeta_\kappa^3 r_k) + 8\zeta_k\zeta_\kappa r_k^3 r_\kappa^3(\zeta_k r_k+\zeta_\kappa r_\kappa),
\end{aligned}$$

$$\begin{aligned}
C_{k\kappa,2}/4 = {} & 8\zeta_k^2 r_k^2 + 8\zeta_\kappa^2 r_\kappa^2 + 16\zeta_k\zeta_\kappa r_k r_\kappa + 64\zeta_k^2\zeta_\kappa^2 r_k^2 r_\kappa^2 - 4\zeta_k\zeta_\kappa r_k r_\kappa(r_k^2+r_\kappa^2) \\
& + 32\zeta_k\zeta_\kappa r_k r_\kappa(\zeta_k^2 r_k^2+\zeta_\kappa^2 r_\kappa^2) + 6r_k^2 r_\kappa^2 - 12r_k^2 r_\kappa^2(\zeta_k^2+\zeta_\kappa^2) - 3(r_k^4+r_\kappa^4) \\
& + 8\zeta_k\zeta_\kappa r_k r_\kappa(r_k^4+r_\kappa^4) - r_k^2 r_\kappa^2(r_k^2+r_\kappa^2) + 8\zeta_k^2 r_k^4 + 8\zeta_\kappa^2 r_\kappa^4 + 4r_k^2 r_\kappa^2(\zeta_k^2+\zeta_\kappa^2)(r_k^2+r_\kappa^2) \\
& + 16\zeta_k^2\zeta_\kappa^2 r_k^2 r_\kappa^2(r_k^2+r_\kappa^2) + 16\zeta_k\zeta_\kappa r_k^3 r_\kappa^3(\zeta_k^2+\zeta_\kappa^2) + r_k^6 + r_\kappa^6,
\end{aligned}$$

$$\begin{aligned}
C_{k\kappa,3}/16 = {} & 8\zeta_k\zeta_\kappa r_k r_\kappa(\zeta_k r_k+\zeta_\kappa r_\kappa) + 2\zeta_k r_k^3 + 2\zeta_\kappa r_\kappa^3 + r_k r_\kappa(\zeta_k r_\kappa^3+\zeta_\kappa r_k^3) \\
& + 4\zeta_k\zeta_\kappa r_k r_\kappa(\zeta_k r_k^3+\zeta_\kappa r_\kappa^3) - 2r_k^2 r_\kappa^2(\zeta_k r_k+\zeta_\kappa r_\kappa) + 4r_k^2 r_\kappa^2(\zeta_k^3 r_k+\zeta_\kappa^3 r_\kappa) \\
& + 8\zeta_k\zeta_\kappa r_k^2 r_\kappa^2(\zeta_k r_\kappa+\zeta_\kappa r_k) + \zeta_k r_k^5 + \zeta_\kappa r_\kappa^5,
\end{aligned}$$

$$C_{k\kappa,4}/16 = D_{k\kappa,3}.$$

Case 2: Independent Seismic Excitations

This case also has important applications in nuclear power plants. For example, consider the main steam line that has some supports on the reactor building and some supports on the service building. The support excitations of the anchors on the reactor building and those on the service building can be considered as approximately independent. The coefficient of correlation is denoted as $\bar{\rho}$ for this case.

The expectation term in equation (2.3.11) becomes zero when $m \neq \hat{m}$, which leads to $\bar{\rho}_{k0}^{m\hat{m},i} = 0$. Therefore, the correlation coefficient $\bar{\rho}_{k0}^{m\hat{m},i}$ can be written as

$$\bar{\rho}_{k0}^{m\hat{m},i} = \delta_{m\hat{m}}\, \rho_{k0}^{m\hat{m},i}, \tag{2.3.31}$$

in which $\rho_{k0}^{m\hat{m},i}$ in the right hand side is given by equation (2.3.28), and $\delta_{m\hat{m}}$ denotes the Kronecker delta function, i.e., $\delta_{m\hat{m}} = 0$ if $m \neq \hat{m}$, and $\delta_{m\hat{m}} = 1$ if $m = \hat{m}$. Similarly, $\bar{\rho}_{k\kappa}^{m\hat{m},i}$ and $\bar{\rho}_{0}^{m\hat{m},i}$ can be written as

$$\bar{\rho}_{k\kappa}^{m\hat{m},i} = \delta_{m\hat{m}}\, \rho_{k\kappa}^{m\hat{m},i}, \qquad \bar{\rho}_{0}^{m\hat{m},i} = \delta_{m\hat{m}}. \tag{2.3.32}$$

As can be seen from equations (2.3.31) and (2.3.32), the correlation coefficients are zero when the earthquake excitations are from different supports.

2.3.3 FRSMS-SRSS Combination Rule

To verify the superiority of the proposed FRSMS-CQC combination rule, the SRSS (Square Root of Sum of Squares) combination rule is also applied to combine the FRS and the results are then compared with FRS by FRSMS-CQC combination. In FRSMS-SRSS combination rule, the correlation between FRS due to vibrational mode and ground inputs, as well as the correlation between the responses of oscillators due to ground inputs at different supports are neglected, which means that the inputs at different supports are considered as independent.

FRS in direction j at node n due to earthquake excitations in direction i can be written as

$$\left[\mathcal{S}_{\mathrm{A};n,j}^{i}(\omega_0,\zeta_0)\right]^2 = \sum_{m=1}^{M}\sum_{k=1}^{6N}\sum_{\kappa=1}^{6N} \rho_{k\kappa}^{mm,i}\, R_{n,j;k}^{m,i}\, R_{n,j;\kappa}^{m,i} + \sum_{m=1}^{M}\left[\mathcal{J}_{n,j}^{m,i}\, \mathcal{S}_{\mathrm{A}}^{m,i}(\omega_0,\zeta_0)\right]^2, \tag{2.3.33}$$

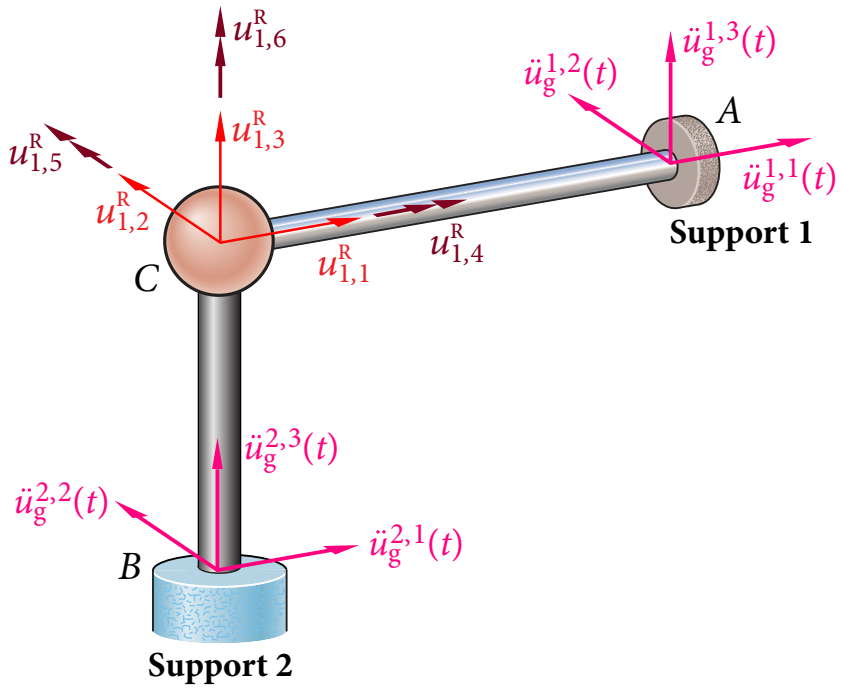

Figure 2.2 Diagram of numerical example.

and total FRS in direction j at node n can be obtained by equation (2.3.6). Equation (2.3.33) is expressed in the form of SRSS because no correlation term between FRS due to vibrational mode and ground input is considered, and is herein referred as FRSMS-SRSS. It should be mentioned that although FRSMS-SRSS neglects some correlation parts, the correlation between the responses of oscillators excited by any two vibration modes is still considered. Thus, the main advantages of the FRS-CQC method proposed by Jiang *et al.* (2015) are still applicable. As a result, FRSMS-SRSS, although cannot provide result as accurate as FRSMS-CQC, can still give much more reliable FRS than the conventional SRSS combination rule.

2.4 Numerical Examples

Two numerical examples are presented to verify the proposed method. As shown in Figure 2.2, a frame ABC with rigid right-angle at C is clamped to ground at supports A and B. It supports a lumped mass at C with three translational DOF u_1, u_2, u_3 and three rotational DOF u_4, u_5, u_6.

The length of both bars AC and BC is $L = 12$ m and the cross-section of both bars is rectangular with dimensions $0.3\,\text{m} \times 0.4\,\text{m}$. The mass at C has values 1500, 800, 2600 kg in the translational DOF 1 to 3, and 300, 400, 500 $\text{kg}\cdot\text{m}^2$ in the rotational DOF 4 to 6, respectively, while the mass of the frame is negligible. In principle, the proposed direct method is applicable to all under-damped damping values; the modal damping value of 5%, which has been widely used in earthquake engineering, is used for demonstration purpose. The Young's modulus for the frame is $3 \times 10^8\ \text{N/m}^2$, and Poisson's ratio is taken as 0.425. A model analysis is performed at first and some modal information of node C is given in Tables 2.1 and 2.2.

The frame is subjected to tridirectional earthquake excitations $\ddot{u}_g^{1,1}$, $\ddot{u}_g^{1,2}$, $\ddot{u}_g^{1,3}$ at support A and $\ddot{u}_g^{2,1}$, $\ddot{u}_g^{2,2}$, $\ddot{u}_g^{2,3}$ at support B. The input GRS follows USNRC R.G. 1.60 (USNRC, 2014) with GRS in both horizontal directions being the same and anchored at $\text{PGA} = 0.3g$ and the vertical GRS anchored at $\text{PGA} = 0.2g$ based on the relationship between horizontal and vertical GRS given in CSA N289.3-10 (CSA, 2010). Thirty sets of spectrum-compatible tridirectional acceleration time histories are generated using the Hilbert-Huang Transform method shown in Figure 2.3, from which the sets of ground inputs are selected (Ni *et al.* 2011; Ni *et al.* 2013). The sample of time histories in horizontal and vertical directions are shown in Figure 2.4.

By using different combinations of the time histories, 30 (for Case 1) and 90 (for Case 2) time history analyses are performed, respectively, and the average values are considered as the "benchmark" FRS used to evaluate the accuracy of the direct method.

2.4.1 Case 1: Identical Seismic Excitations

In this case, seismic excitations in each direction at different supports are the same, i.e., $\ddot{u}_g^{1,1} = \ddot{u}_g^{2,1}$, $\ddot{u}_g^{1,2} = \ddot{u}_g^{2,2}$, $\ddot{u}_g^{1,3} = \ddot{u}_g^{2,3}$. FRS in the three translational directions at C obtained from both time history analyses and the direct spectra-to-spectra method are shown in Figures 2.5 to 2.7. These FRS are calculated at over 200 frequencies including the natural frequencies of the structure. The mean FRS obtained from time history analyses, which are considered as the benchmark FRS, are highlighted by red dashed lines, the FRS generated by the proposed direct method with FRSMS-CQC combination rule are represented as black

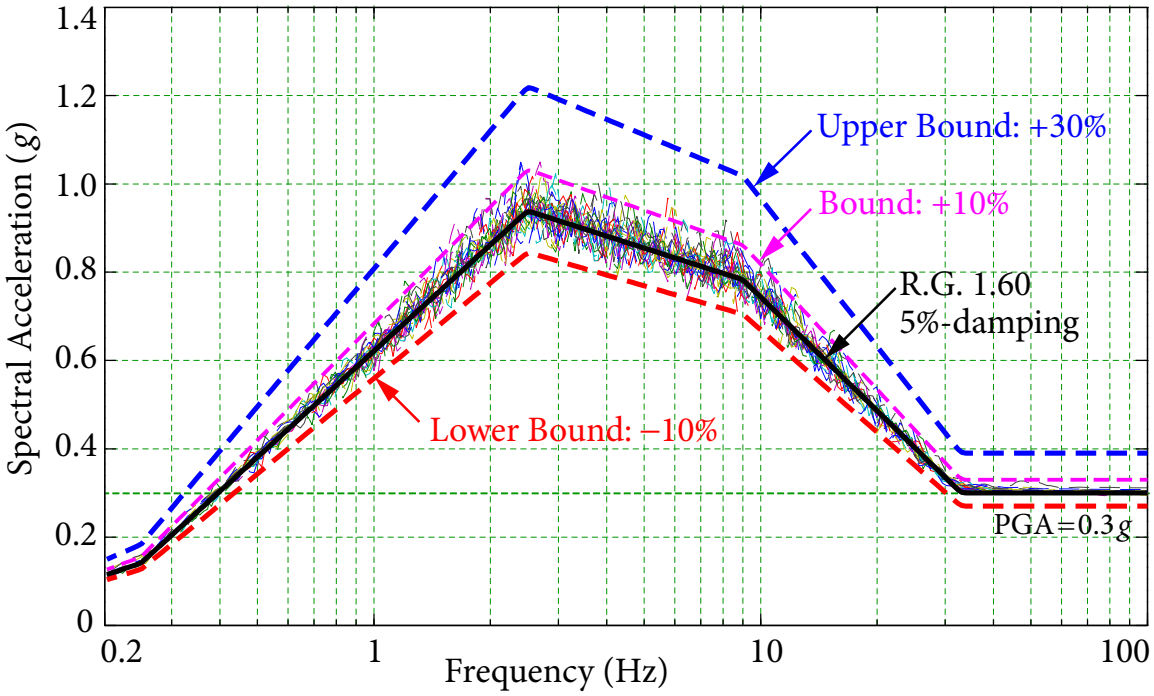

Figure 2.3 Response spectra of compatible time histories.

Table 2.1 Modal information of node C in direction 2

Mode	Frequency (Hz)	Participation factor	Modal shape
1	0.824	0.584	−0.997
5	10.492	−0.169	0.134
6	10.580	−0.139	0.086

Table 2.2 Modal information of node C in direction 3

Mode	Frequency (Hz)	Participation factor	Modal shape
2	5.411	−0.003	0.999
3	9.723	0.044	−0.105
4	10.104	−0.003	0.016

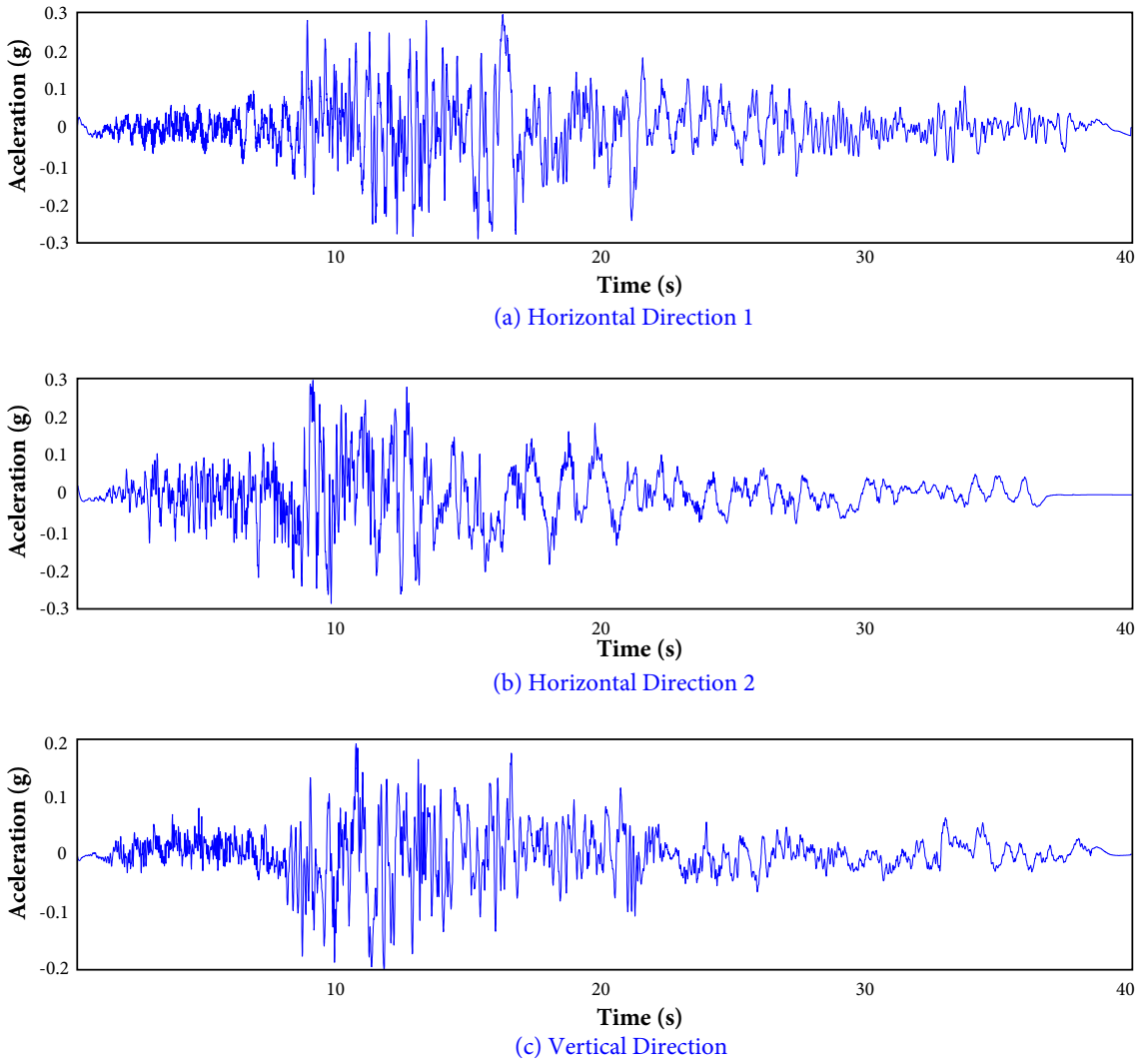

Figure 2.4 Sample of tri-directional time histories.

dashed lines, and the FRS generated by the proposed direct method using FRSMS-SRSS combination rule are represented as pink solid lines.

It is seen that FRS generated by the direct method agree remarkably well with the benchmark FRS over the entire frequency range. The relative errors are less than 4% at the peaks of FRS, whereas there are large variabilities in FRS from time history analyses, particularly at the peaks. The result of single time history analysis could be over-conservative or non-conservative, depending on which seismic input set is selected. This example demonstrates

that time history analysis can lead to approximately 31% overestimate or 27% underestimate at the FRS peaks, even though the time histories satisfy the compatibility requirements to the target GRS specified by codes and standards. Furthermore, it is observed that FRS from a single time history analysis may be over-conservative in some directions but significantly nonconservative in other directions, or over-conservative in some frequency bands but nonconservative in other frequency bands.

The results of direct method by FRSMS-CQC and FRSMS-SRSS are also compared to illustrate the effectiveness of the proposed FRSMS-CQC combination rule. As shown in Figure 2.5, although the FRS obtained by direct method with FRSMS-SRSS combination rule agree well with the benchmark result at the peak, there is a significant underestimation of FRS for frequencies between 1 Hz and 8 Hz, which is a very important frequency range in the nuclear power industry. The reason of this underestimation is that FRSMS-SRSS combination rule ignores the correlation between dynamic modal response and response of oscillator mounted directly on the ground. The maximum underestimation is 17% from Figure 2.5, indicating that FRS by the direct method with FRSMS-SRSS could be unconservative. On the contrary, FRS generated by the direct method with FRSMS-CQC combination rule agree remarkably well with the benchmark results over the entire frequency range with the relative error at the peak being only 2%.

In direction 2, as shown in Figure 2.6, FRS generated by the direct method using FRSMS-CQC match well with the benchmark results; however, FRS by FRSMS-SRSS are significantly underestimated over the entire frequency range, especially at the peak, with the relative error at the peak being -26%, leading to a very unconservative seismic input to secondary systems. This is because FRSMS-SRSS combination rule does not consider the correlation of FRS due to excitations at different supports. When tridirectional seismic inputs are identical at all supports, the peaks of responses of oscillators due to directional excitations from different supports will occur at the same time; the FRSMS-SRSS combination rule is no longer applicable because it assumes the responses are independent.

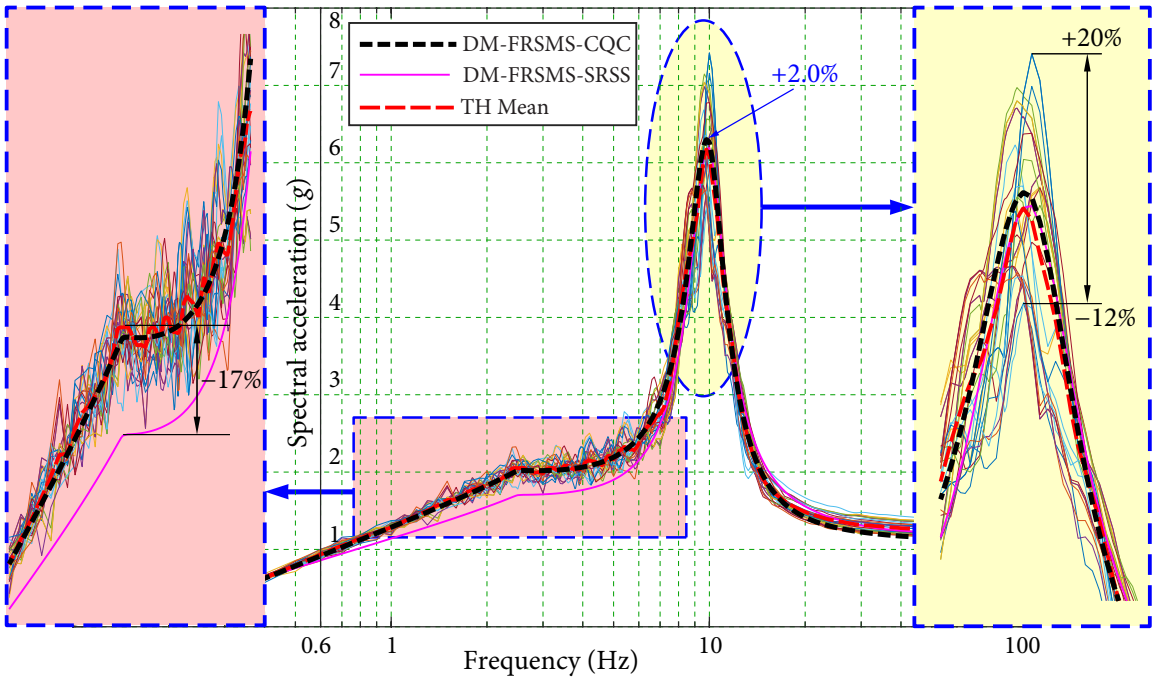

Figure 2.5 Case 1: FRS in direction 1 (Horizontal).

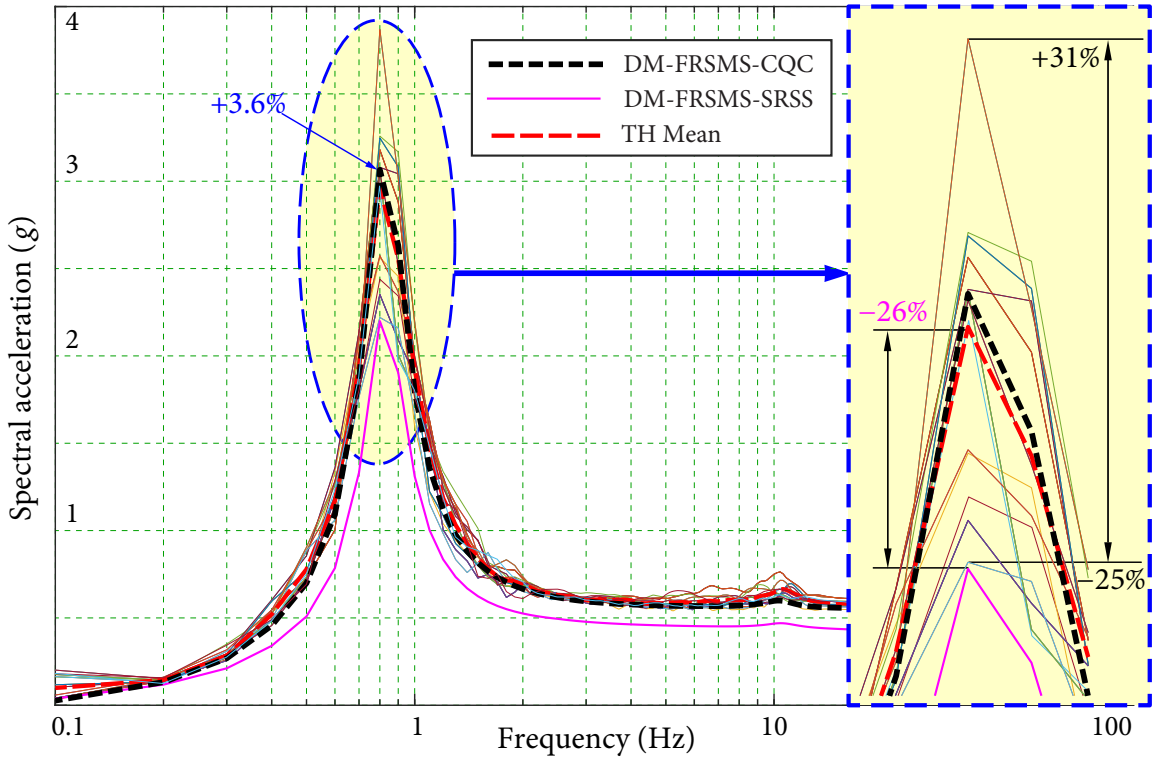

Figure 2.6 Case 1: FRS in direction 2 (Horizontal).

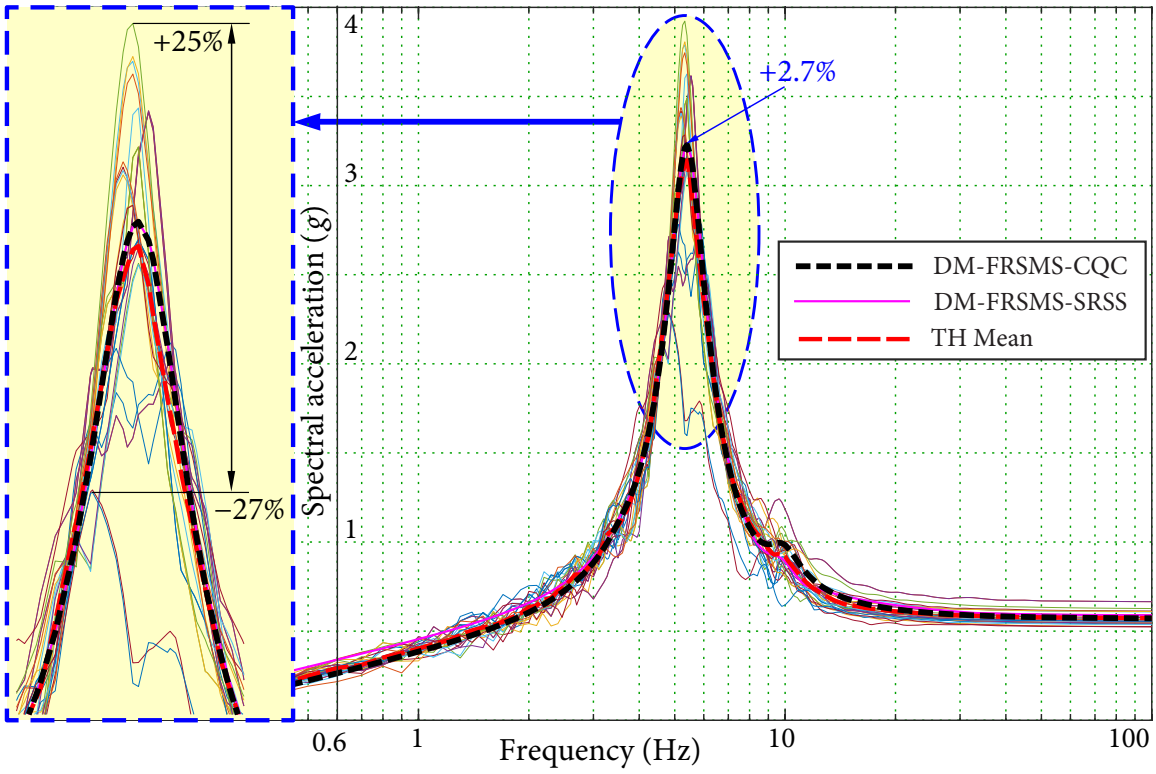

Figure 2.7 Case 1: FRS in direction 3 (Vertical).

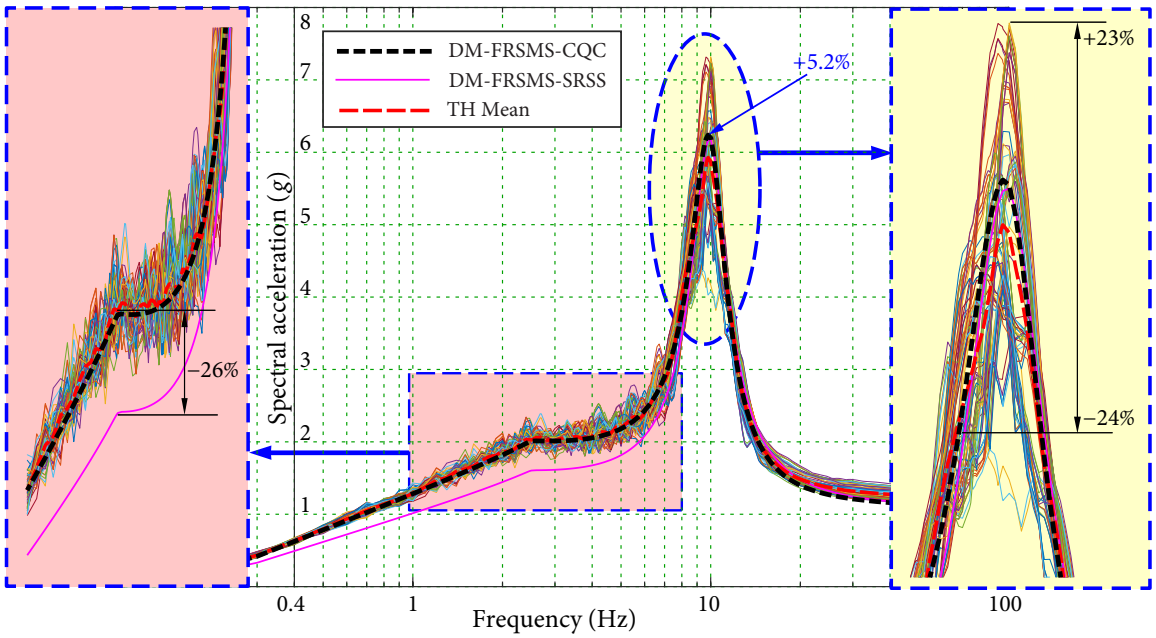

Figure 2.8 Case 2: FRS in direction 1 (Horizontal).

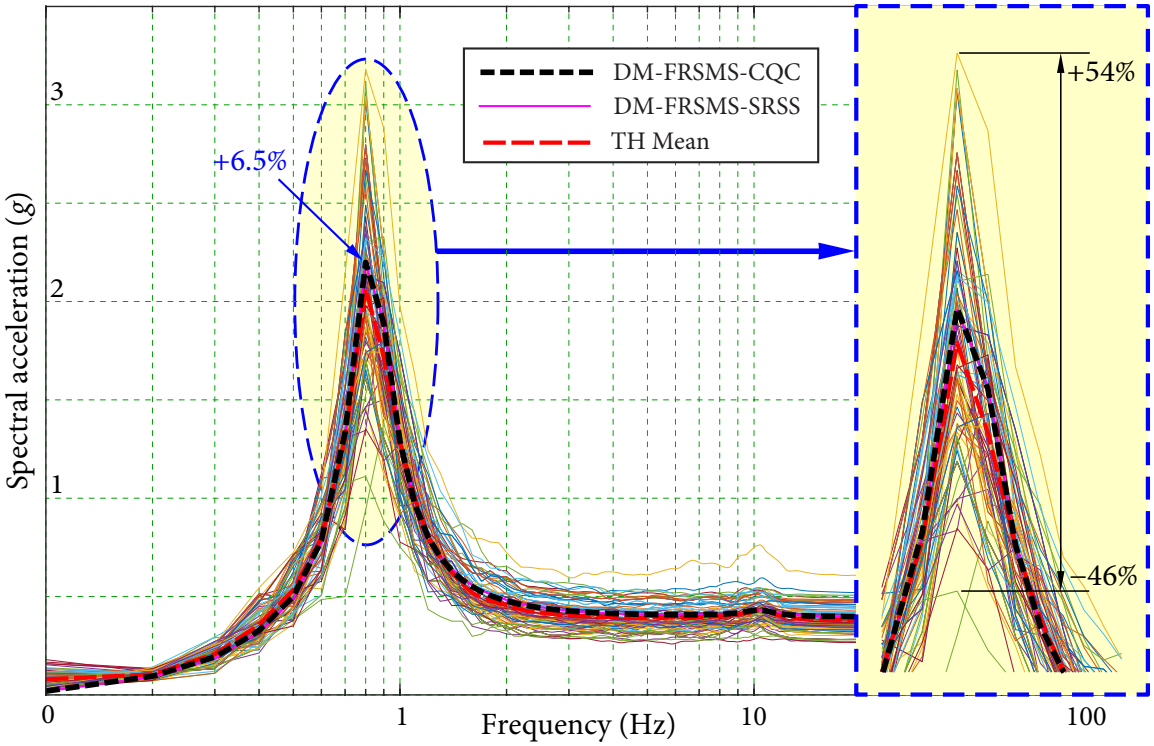

Figure 2.9 Case 2: FRS in direction 2 (Horizontal).

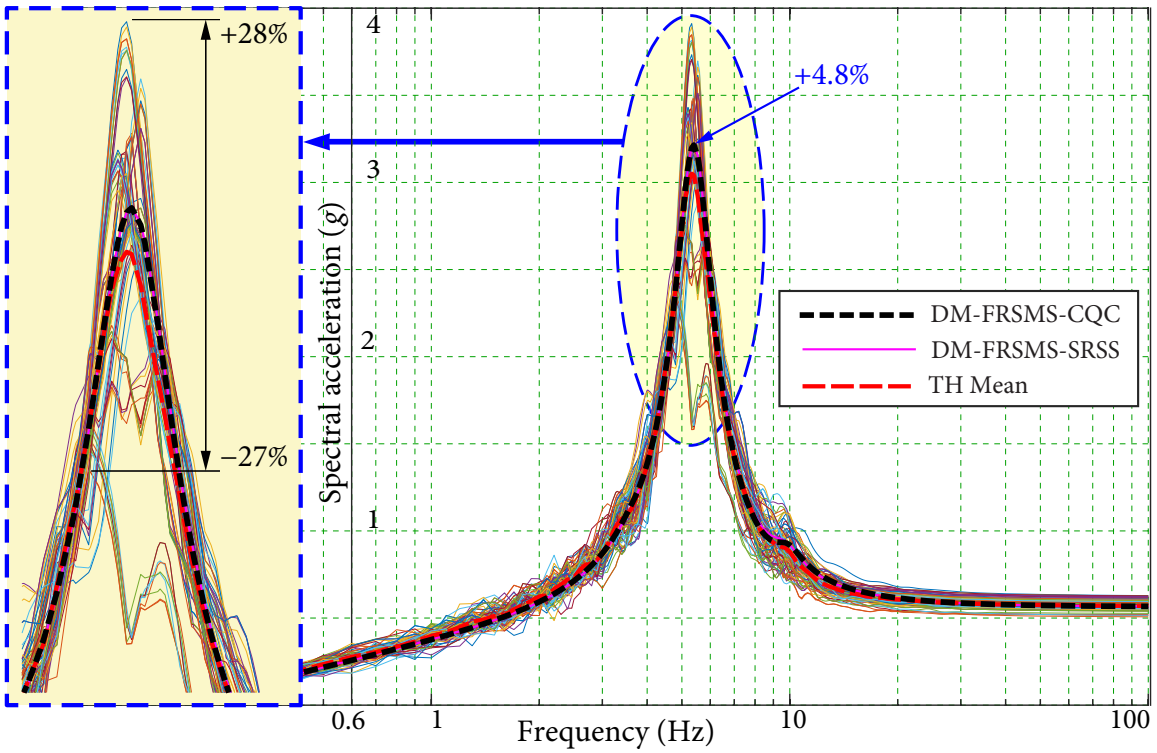

Figure 2.10 Case 2: FRS in direction 3 (Vertical).

2.4.2 Case 2: Independent Seismic Excitations

FRS in all three directions obtained from both time history analyses and the direct spectra-to-spectra method are plotted in Figures 2.8 to 2.10. FRS generated by the proposed direct method using FRSMS-CQC combination rule agree well with the benchmark results over the entire frequency range. However, it is seen that there is significant underestimation for FRS in direction 1 generated by FRSMS-SRSS for most frequencies, especially from 1 Hz to 8 Hz, as shown in Figure 2.8. In directions 2 and 3, FRS by FRSMS-CQC and FRSMS-SRSS are close. However, the discrepancy may increase for more complex structures, in which there could be many closely spaced vibrational modes.

Comparing the independent case with Case 1, it can be seen that the main change is FRS in direction 2, which is only affected by the inputs in direction 2. For the independent case, FRS obtained by the direct method using FRSMS-SRSS combination rule is very close to those by FRSMS-CQC; however, for the identical case, there is a large discrepancy between the results. It indicates that FRSMS-SRSS combination rule is not applicable when the earthquake excitations at different supports are correlated since this correlation has significant influence on FRS.

2.5 Summary

In this chapter, a direct spectra-to-spectra method for obtaining FRS of a structure under earthquake excitations at multiple supports is developed. The total response of the structure is divided into two parts and FRS of each part are evaluated separately. A new combination method FRSMS-CQC is proposed to combine the FRS of these two parts. The FRSMS-CQC combination rule fully accounts for the correlations between various components affecting FRS: the correlation between the responses of oscillators excited by any two vibration modes, the correlation between the response of an oscillator excited by a vibration mode and the response of an oscillator mounted directly on a support, and the correlation between the responses of oscillators mounted on different supports.

Numerical examples of a structure subjected to two tri-directional seismic inputs at two supports are presented. Two special cases, i.e., seismic excitations are identical or

independent, are conducted. It is shown that FRS determined by the proposed direct method in both cases agree well with the benchmark FRS, which are obtained through a large number of time history analyses. The superiority of the proposed FRSMS-CQC combination rule has been demonstrated by comparing with the conventional FRSMS-SRSS combination rule. On the other hand, FRS determined by time history analyses have large variabilities, especially at FRS peaks. Therefore, FRS determined by time history method using a single a small number of sets of time histories are not reliable. A large number of time history analyses must be performed to obtain accurate FRS, which is very time consuming.

In summary, the proposed direct method avoids the deficiencies of time history analyses and can generate FRS accurately and efficiently for structures under tri-directional seismic inputs at multiple supports.

C H A P T E R 3

Generating Responses and TRS for Secondary Structures with Multiple Supports

The generation of floor response spectrum (FRS) is essential in the seismic assessment of secondary structures as it provides the seismic input to those systems. Conventional direct methods are not widely applied in assessing the seismic performance of secondary systems because the accurate and reliable FRS over entire frequency was not available. This problem becomes more severe for multi-supported secondary structures because accurate FRS at multiple points are required. To obtain reliable FRS at these points, horizontal and vertical time histories at the supports when a secondary system is attached must be calculated based on time domain analysis of the supporting structure. This procedure, however, is very computationally expensive for structures with multiple degrees-of-freedom. Therefore, inadequate research has been carried out on the generation of the response of secondary structures. In this chapter, a practical method for the evaluation of seismic response for secondary structures with multiple supports is presented.

Besides of the responses of multiply-supported secondary structures, the Tertiary Response Spectrum (TRS) is also investigated. Tertiary systems are the systems that are attached to secondary systems, such as valves anchored on stream line. Tertiary system,

although the size is considerably smaller than secondary and primary structures, its failure could still result in a large amount of economic loss. Similar to secondary systems, tertiary systems are not intended to bear external loads. However, in case of earthquakes, they will be subjected to earthquake induced vibrations in the primary and secondary structures. However, because of their dynamic characteristics and lack of proper design in practice, those systems may pose high risk of failures even the magnitude of earthquake is relative small (Lim and Chouw, 2015). Currently few research has been done in the seismic assessment of tertiary system although it also plays an important role especially in the nuclear power industry. In this second part of this chapter, a method for generating tertiary response spectra using FRS is proposed, which can be applied to analyze tertiary systems.

3.1 A Practical Direct Method for the Generation of Responses of Multi-Supported Structures

The formulation of the total response $\ddot{u}_{n,j}^{\mathrm{R},i}(t)$ has been obtained by equation (2.1.25) in Chapter 2 in form of time history method based on modal responses, which is separated into two parts: the first part given by $\sum_{m=1}^{M}\sum_{k=1}^{6N}\varphi_{n,j;k}\,\Gamma_k^{m,i}\,\ddot{u}_{n,j;k}^{m,i}$ is the dynamic response due to vibration, whereas the second part $\sum_{m=1}^{M}\mathcal{I}_{n,j}^{m,i}\,\ddot{u}_{\mathrm{g}}^{m,i}$ is the response due to the ground motion. Note that the second part is slightly different from the quasi-static part defined in equation (2.1.3) because dynamic parameters, i.e., mode shapes and modal participation factor are included in this term. However, it can be regard as a new quasi-static term as it does not involve vibration but a product of the constant influence coefficient $\mathcal{I}_{n,j}^{m,i}$ and the ground motion $\ddot{u}_{\mathrm{g}}^{m,i}$.

In order to avoid time history analysis, a direct method based on random vibration is developed in this section.

3.1.1 Combination between Modal Response and Ground Motion

Noticing that the maximum values of the above two parts do not occur at the same time, they need to be combined using proper combination rules.

Squaring both sides of equation (2.1.24) gives

$$\begin{aligned}
&\left[\ddot{u}_{n,j}^{\mathrm{R},i}(t)\right]^2 \\
&= \left\{\sum_{m=1}^{M}\sum_{k=1}^{6N}\varphi_{n,j;k}\,\Gamma_k^{m,i}\,\ddot{u}_k^{m,i} + \sum_{m=1}^{M}\mathcal{J}_{n,j}^{m,i}\,\ddot{u}_{\mathrm{g}}^{m,i}\right\}\left\{\sum_{\hat{m}=1}^{M}\sum_{\kappa=1}^{6N}\varphi_{n,j;\kappa}\,\Gamma_\kappa^{\hat{m},i}\,\ddot{u}_\kappa^{\hat{m},i} + \sum_{\hat{m}=1}^{M}\mathcal{J}_{n,j}^{\hat{m},i}\,\ddot{u}_{\mathrm{g}}^{\hat{m},i}\right\} \\
&= \sum_{m=1}^{M}\sum_{\hat{m}=1}^{M}\sum_{k=1}^{6N}\sum_{\kappa=1}^{6N}\varphi_{n,j;k}\,\varphi_{n,j;\kappa}\,\Gamma_k^{m,i}\,\Gamma_\kappa^{\hat{m},i}\,\ddot{u}_k^{m,i}\,\ddot{u}_\kappa^{\hat{m},i} + 2\sum_{m=1}^{M}\sum_{\hat{m}=1}^{M}\sum_{k=1}^{6N}\varphi_{n,j;k}\,\Gamma_k^{m,i}\,\mathcal{J}_{n,j}^{\hat{m},i}\,\ddot{u}_k^{m,i}\,\ddot{u}_{\mathrm{g}}^{\hat{m},i} \\
&\qquad + \sum_{m=1}^{M}\sum_{\hat{m}=1}^{M}\mathcal{J}_{n,j}^{m,i}\,\mathcal{J}_{n,j}^{\hat{m},i}\,\ddot{u}_{\mathrm{g}}^{m,i}\,\ddot{u}_{\mathrm{g}}^{\hat{m},i}. \qquad (3.1.1)
\end{aligned}$$

Taking expected value of both sides results in the mean-square response

$$\begin{aligned}
\mathrm{E}\left[\left\{\ddot{u}_{n,j}^{\mathrm{R},i}(t)\right\}^2\right] &= \sum_{m=1}^{M}\sum_{\hat{m}=1}^{M}\sum_{k=1}^{6N}\sum_{\kappa=1}^{6N}\varphi_{n,j;k}\,\varphi_{n,j;\kappa}\,\Gamma_k^{m,i}\,\Gamma_\kappa^{\hat{m},i}\,\mathrm{E}\left[\left\{\ddot{u}_k^{m,i}(t)\,\ddot{u}_\kappa^{\hat{m},i}(t)\right\}\right] \\
&\quad + 2\sum_{m=1}^{M}\sum_{\hat{m}=1}^{M}\sum_{k=1}^{6N}\varphi_{n,j;k}\,\Gamma_k^{m,i}\,\mathcal{J}_{n,j}^{\hat{m},i}\,\mathrm{E}\left[\left\{\ddot{u}_k^{m,i}\,\ddot{u}_{\mathrm{g}}^{m,i}\right\}\right] \\
&\quad + \sum_{m=1}^{M}\sum_{\hat{m}=1}^{M}\mathcal{J}_{n,j}^{m,i}\,\mathcal{J}_{n,j}^{\hat{m},i}\,\mathrm{E}\left[\left\{\ddot{u}_{\mathrm{g}}^{m,i}(t)\,\ddot{u}_{\mathrm{g}}^{\hat{m},i}(t)\right\}\right] \\
&= \sum_{m=1}^{M}\sum_{\hat{m}=1}^{M}\sum_{k=1}^{6N}\sum_{\kappa=1}^{6N}\rho_{k\kappa}^{m\hat{m},i}\,\varphi_{n,j;k}\,\varphi_{n,j;\kappa}\,\Gamma_k^{m,i}\,\Gamma_\kappa^{\hat{m},i}\sqrt{\mathrm{E}\left[\left\{\ddot{u}_k^{m,i}(t)\right\}^2\right]}\sqrt{\mathrm{E}\left[\left\{\ddot{u}_\kappa^{\hat{m},i}(t)\right\}^2\right]} \\
&\quad + 2\sum_{m=1}^{M}\sum_{\hat{m}=1}^{M}\sum_{k=1}^{6N}\rho_{k0}^{m\hat{m},i}\,\varphi_{n,j;k}\,\Gamma_k^{m,i}\,\mathcal{J}_{n,j}^{\hat{m},i}\sqrt{\mathrm{E}\left[\left\{\ddot{u}_k^{m,i}(t)\right\}^2\right]}\sqrt{\mathrm{E}\left[\left\{\ddot{u}_{\mathrm{g}}^{\hat{m},i}(t)\right\}^2\right]} \\
&\quad + \sum_{m=1}^{M}\sum_{\hat{m}=1}^{M}\rho_0^{m\hat{m},i}\,\mathcal{J}_{n,j}^{m,i}\,\mathcal{J}_{n,j}^{\hat{m},i}\sqrt{\mathrm{E}\left[\left\{\ddot{u}_{\mathrm{g}}^{m,i}(t)\right\}^2\right]}\sqrt{\mathrm{E}\left[\left\{\ddot{u}_{\mathrm{g}}^{\hat{m},i}(t)\right\}^2\right]}, \qquad (3.1.2)
\end{aligned}$$

in which all earthquake excitations are in direction i, $\rho_{k\kappa}^{m\hat{m},i}$ is the correlation coefficient between the dynamic response $\ddot{u}_k^{m,i}(t)$ of the kth mode due to earthquake excitation at support m and the dynamic response $\ddot{u}_\kappa^{\hat{m},i}(t)$ of the κth mode due to earthquake excitation at support $\hat{m}$, $\rho_{k0}^{m\hat{m},i}$ is the correlation coefficient between the dynamic response $\ddot{u}_k^{m,i}(t)$ of the kth mode due to earthquake excitation at support m and ground motion $\ddot{u}_{\mathrm{g}}^{\hat{m},i}$ at support $\hat{m}$, and $\rho_0^{m\hat{m},i}$ is the correlation coefficient between ground motions $\ddot{u}_{\mathrm{g}}^{m,i}$ at support m and $\ddot{u}_{\mathrm{g}}^{\hat{m},i}$ at support $\hat{m}$.

In the theory of random processes, the maximum values of $\ddot{u}_k^{m,i}$, $\ddot{u}_{\mathrm{g}}^{m,i}$, and $\ddot{u}_{n,j}^{\mathrm{R},i}$ are related to the corresponding mean-square values by peak factors. In earthquake engineering,

it is reasonable to assume that the peak factors are the same, i.e.,

$$\left|\ddot{u}_k^{m,i}(t)\right|_{\max} = \mathcal{S}_{\mathrm{A}}^{m,i}(\omega_k,\zeta_k) = \mathcal{PF}\sqrt{\mathrm{E}\left[\left\{\ddot{u}_k^{m,i}(t)\right\}^2\right]}, \tag{3.1.3a}$$

$$\left|\ddot{u}_{\mathrm{g}}^{m,i}(t)\right|_{\max} = \mathcal{A}^{m,i} = \mathcal{S}_{\mathrm{A}}^{m,i}(\omega_{\mathrm{RIGID}}) = \mathcal{S}_{\mathrm{A,RIGID}}^{m,i} = \mathcal{PF}\sqrt{\mathrm{E}\left[\left\{\ddot{u}_{\mathrm{g}}^{m,i}(t)\right\}^2\right]}, \tag{3.1.3b}$$

$$\left|\ddot{u}_{n,j}^{\mathrm{R},i}(t)\right|_{\max} = \mathcal{A}_{n,j}^{i} = \mathcal{PF}\sqrt{\mathrm{E}\left[\left\{\ddot{u}_{n,j}^{\mathrm{R},i}(t)\right\}^2\right]}, \tag{3.1.3c}$$

in which $\mathcal{PF}$ is the peak factor, and $\mathcal{A}$ denotes the maximum (absolute value) acceleration. $\left|\ddot{u}_k^{m,i}(t)\right|_{\max}$ is the maximum absolute acceleration response of the kth vibration mode due to seismic excitation of support m in direction i, which is equivalent to the maximum absolute acceleration response of an SDOF oscillator (ω_k, ζ_k) mounted on support m in direction i. $\left|\ddot{u}_{\mathrm{g}}^{m,i}(t)\right|_{\max}$ is the maximum acceleration of support m in direction i, which is equal to the acceleration response spectrum of support m in direction i at rigid frequency ω_{RIGID} (usually taken as $\omega_{\mathrm{RIGID}} \geqslant 33\,\mathrm{Hz}$). $\left|\ddot{u}_{n,j}^{\mathrm{R},i}(t)\right|_{\max}$ is the maximum acceleration response of node n in direction j due to seismic inputs in direction i.

Substituting equation (3.1.3) into equation (3.1.2) gives

$$\begin{aligned}\left\{\frac{\mathcal{A}_{n,j}^{i}}{\mathcal{PF}}\right\}^2 = &\sum_{m=1}^{M}\sum_{\hat{m}=1}^{M}\sum_{k=1}^{6N}\sum_{\kappa=1}^{6N}\rho_{k\kappa}^{m\hat{m},i}\varphi_{n,j;k}\varphi_{n,j;\kappa}\Gamma_k^{m,i}\Gamma_\kappa^{\hat{m},i}\left\{\frac{\mathcal{S}_{\mathrm{A}}^{m,i}(\omega_k,\zeta_k)}{\mathcal{PF}}\right\}\left\{\frac{\mathcal{S}_{\mathrm{A}}^{\hat{m},i}(\omega_\kappa,\zeta_\kappa)}{\mathcal{PF}}\right\}\\ &+2\sum_{m=1}^{M}\sum_{\hat{m}=1}^{M}\sum_{k=1}^{6N}\rho_{k0}^{m\hat{m},i}\varphi_{n,j;k}\Gamma_k^{m,i}\mathcal{J}_{n,j}^{\hat{m},i}\left\{\frac{\mathcal{S}_{\mathrm{A}}^{m,i}(\omega_k,\zeta_k)}{\mathcal{PF}}\right\}\left\{\frac{\mathcal{S}_{\mathrm{A,RIGID}}^{\hat{m},i}}{\mathcal{PF}}\right\}\\ &+\sum_{m=1}^{M}\sum_{\hat{m}=1}^{M}\rho_0^{m\hat{m},i}\mathcal{J}_{n,j}^{m,i}\mathcal{J}_{n,j}^{\hat{m},i}\left\{\frac{\mathcal{S}_{\mathrm{A,RIGID}}^{m,i}}{\mathcal{PF}}\right\}\left\{\frac{\mathcal{S}_{\mathrm{A,RIGID}}^{\hat{m},i}}{\mathcal{PF}}\right\}.\end{aligned} \tag{3.1.4}$$

Multiplying $\mathcal{PF}^2$ to both sides of equation (3.1.4) yields

$$\begin{aligned}\left(\mathcal{A}_{n,j}^{i}\right)^2 = &\sum_{m=1}^{M}\sum_{\hat{m}=1}^{M}\sum_{k=1}^{6N}\sum_{\kappa=1}^{6N}\rho_{k\kappa}^{m\hat{m},i}\varphi_{n,j;k}\varphi_{n,j;\kappa}\Gamma_k^{m,i}\Gamma_\kappa^{\hat{m},i}\mathcal{S}_{\mathrm{A}}^{m,i}(\omega_k,\zeta_k)\,\mathcal{S}_{\mathrm{A}}^{\hat{m},i}(\omega_\kappa,\zeta_\kappa)\\ &+2\sum_{m=1}^{M}\sum_{\hat{m}=1}^{M}\sum_{k=1}^{6N}\rho_{k0}^{m\hat{m},i}\varphi_{n,j;k}\Gamma_k^{m,i}\mathcal{J}_{n,j}^{\hat{m},i}\mathcal{S}_{\mathrm{A}}^{m,i}(\omega_k,\zeta_k)\,\mathcal{S}_{\mathrm{A,RIGID}}^{\hat{m},i}\\ &+\sum_{m=1}^{M}\sum_{\hat{m}=1}^{M}\rho_0^{m\hat{m},i}\mathcal{J}_{n,j}^{m,i}\mathcal{J}_{n,j}^{\hat{m},i}\mathcal{S}_{\mathrm{A,RIGID}}^{m,i}\mathcal{S}_{\mathrm{A,RIGID}}^{\hat{m},i}.\end{aligned} \tag{3.1.5}$$

It is specified in ASCE 4-98 (ASCE, 1998) that, for direct methods, when the response of a given direction at a given location has contributions from more than one spatial component of earthquakes, these contributions shall be combined by the SRSS rule. Hence, combining contributions from tridirectional earthquake excitations at multiple supports, the total maximum absolute acceleration response of the nth node in direction j is given by

$$\mathcal{A}_{n,j} = \sqrt{\sum_{i=1}^{3} \left(\mathcal{A}_{n,j}^{\,i} \right)^2}\,. \tag{3.1.6}$$

3.1.2 Determination of $\rho_{k0}^{m\hat{m},i}$, $\rho_{k\kappa}^{m\hat{m},i}$, and $\rho_{0}^{m\hat{m},i}$

Determination of $\rho_{k0}^{m\hat{m},i}$: The correlation coefficient $\rho_{k0}^{m\hat{m},i}$ between $\ddot{u}_k^{m,i}(t)$ and $\ddot{u}_{\mathrm{g}}^{\hat{m},i}(t)$ is defined as

$$\rho_{k0}^{m\hat{m},i} = \frac{\mathrm{E}\left[\ddot{u}_k^{m,i}(t)\, \ddot{u}_{\mathrm{g}}^{\hat{m},i}(t) \right]}{\sqrt{\mathrm{E}\left[\left\{ \ddot{u}_k^{m,i}(t) \right\}^2 \right] \cdot \mathrm{E}\left[\left\{ \ddot{u}_{\mathrm{g}}^{\hat{m},i}(t) \right\}^2 \right]}}, \tag{3.1.7}$$

in which each term can be determined using the theory of random vibration, as shown in the following.

An approximation is made first for $\ddot{u}_k^{m,i}(t)$ to simplify the procedure,

$$\begin{aligned} \ddot{u}_k^{m,i}(t) &= 2\zeta_k \omega_k \dot{q}_k^{m,i} + \omega_k^2 q_k^{m,i} = 2\zeta_k \omega_k \cdot \dot{h}_k(t) * \ddot{u}_{\mathrm{g}}^{m,i}(t) + \omega_k^2\, h_k(t) * \ddot{u}_{\mathrm{g}}^{m,i}(t) \\ &\approx \omega_k^2\, h_k(t) * \ddot{u}_{\mathrm{g}}^{m,i}(t), \quad \text{for small } \zeta_k. \end{aligned} \tag{3.1.8}$$

The covariance between $\ddot{u}_k^{m,i}(t)$ and $\ddot{u}_{\mathrm{g}}^{\hat{m},i}(t)$ is given by

$$\begin{aligned} \mathrm{E}\left[\ddot{u}_k^{m,i}(t)\, \ddot{u}_{\mathrm{g}}^{\hat{m},i}(t+\tau) \right] &\approx \mathrm{E}\left[\left\{ \omega_k^2 \cdot h_k(t) * \ddot{u}_{\mathrm{g}}^{m,i}(t) \right\} \cdot \left\{ \ddot{u}_{\mathrm{g}}^{\hat{m},i}(t+\tau) \right\} \right] \\ &= \mathrm{E}\left[\omega_k^2 \int_{-\infty}^{\infty} h_k(\tau_1)\, \ddot{u}_{\mathrm{g}}^{m,i}(t-\tau_1)\, \mathrm{d}\tau_1 \cdot \ddot{u}_{\mathrm{g}}^{\hat{m},i}(t+\tau) \right] \\ &= \omega_k^2 \int_{-\infty}^{\infty} h_k(\tau_1)\, \mathrm{E}\left[\ddot{u}_{\mathrm{g}}^{m,i}(t-\tau_1)\, \ddot{u}_{\mathrm{g}}^{\hat{m},i}(t+\tau) \right] \mathrm{d}\tau_1. \end{aligned} \tag{3.1.9}$$

Taking Fourier transform of both sides yields

$$\mathcal{S}_{\ddot{u}_k^{m,i}\, \ddot{u}_{\mathrm{g}}^{\hat{m},i}}(\omega) = \int_{-\infty}^{\infty} \mathrm{E}\left[\ddot{u}_k^{m,i}(t)\, \ddot{u}_{\mathrm{g}}^{\hat{m},i}(t+\tau) \right] \cdot \mathrm{e}^{-\mathrm{i}\omega\tau} \mathrm{d}\tau \tag{3.1.10}$$

$$= \omega_k^2 \int_{-\infty}^{\infty}\int_{-\infty}^{\infty} h_k(\tau_1)\, R_{\ddot{u}_g^{m,i}\,\ddot{u}_g^{\hat{m},i}}(\tau+\tau_1)\cdot e^{-i\omega\tau}\, d\tau_1\, d\tau. \tag{3.1.11}$$

Setting $\tau_3 = \tau + \tau_1$, equation (3.1.11) can be written as

$$\begin{aligned} \mathcal{S}_{\ddot{u}_k^{m,i}\,\ddot{u}_g^{\hat{m},i}}(\omega) &= \omega_k^2 \int_{-\infty}^{\infty} h_k(\tau_1)\, e^{i\omega\tau_1} d\tau_1 \int_{-\infty}^{\infty} R_{\ddot{u}_g^{m,i}\,\ddot{u}_g^{\hat{m},i}}(\tau_3)\, e^{-i\omega\tau_3} d\tau_3 \\ &= \omega_k^2 \cdot \mathcal{H}_k^*(\omega) \cdot \mathcal{S}_{\ddot{u}_g^{m,i}\,\ddot{u}_g^{\hat{m},i}}(\omega), \end{aligned} \tag{3.1.12}$$

where $\mathcal{H}_k^*(\omega)$ is the complex conjugate of complex frequency response function $\mathcal{H}_k(\omega)$ given by

$$\mathcal{H}_k(\omega) = \frac{1}{(\omega_k^2 - \omega^2) + i2\zeta_k\omega_k\omega}. \tag{3.1.13}$$

$\mathcal{S}_{\ddot{u}_g^{m,i}\,\ddot{u}_g^{\hat{m},i}}(\omega)$ is the cross-power spectral density function of ground accelerations $\ddot{u}_g^{m,i}(t)$ and $\ddot{u}_g^{\hat{m},i}(t)$ given by equation (2.3.16).

Taking the inverse Fourier transform of equation (3.1.12) yields

$$E\big[\ddot{u}_k^{m,i}(t)\, \ddot{u}_g^{\hat{m},i}(t+\tau)\big] = \frac{\omega_k^2}{2\pi} \int_{-\infty}^{\infty} \mathcal{H}_k^*(\omega)\cdot \mathcal{S}_{\ddot{u}_g^{m,i}\,\ddot{u}_g^{\hat{m},i}}(\omega)\, e^{i\omega\tau}\, d\omega. \tag{3.1.14}$$

Setting $\tau = 0$ results in

$$E\big[\ddot{u}_k^{m,i}(t)\, \ddot{u}_g^{\hat{m},i}(t)\big] = \frac{\omega_k^2}{2\pi} \int_{-\infty}^{\infty} \mathcal{H}_k^*(\omega)\cdot \mathcal{S}_{\ddot{u}_g^{m,i}\,\ddot{u}_g^{\hat{m},i}}(\omega)\, d\omega. \tag{3.1.15}$$

Following the same procedure above, the mean square value of $\ddot{u}_k^{m,i}(t)$ and $\ddot{u}_g^{\hat{m},i}(t)$ can be obtained as

$$E\Big[\big\{\ddot{u}_k^{m,i}(t)\big\}^2\Big] = \frac{\omega_k^4}{2\pi} \int_{-\infty}^{\infty} \mathcal{H}_k(\omega)\, \mathcal{H}_k^*(\omega)\cdot \mathcal{S}_{\ddot{u}_g^{m,i}\,\ddot{u}_g^{m,i}}(\omega)\, d\omega, \tag{3.1.16}$$

$$E\Big[\big\{\ddot{u}_g^{\hat{m},i}(t)\big\}^2\Big] = \frac{1}{2\pi} \int_{-\infty}^{\infty} \mathcal{S}_{\ddot{u}_g^{\hat{m},i}\,\ddot{u}_g^{\hat{m},i}}(\omega)\, d\omega. \tag{3.1.17}$$

Determination of $\rho_{k\kappa}^{m\hat{m},i}$: The covariance between $\ddot{u}_k^{m,i}(t)$ and $\ddot{u}_\kappa^{\hat{m},i}(t)$ is given by

$$\begin{aligned} E\big[\ddot{u}_k^{m,i}(t)\, \ddot{u}_\kappa^{\hat{m},i}(t+\tau)\big] &\approx E\Big[\big\{\omega_k^2\cdot h_k(t) * \ddot{u}_g^{m,i}(t)\big\}\cdot\big\{\omega_\kappa^2\cdot h_\kappa(t+\tau) * \ddot{u}_g^{\hat{m},i}(t+\tau)\big\}\Big] \\ &= E\Big[\omega_k^2 \int_{-\infty}^{\infty} h_k(\tau_1)\, \ddot{u}_g^{m,i}(t-\tau_1)\, d\tau_1 \cdot \omega_\kappa^2 \int_{-\infty}^{\infty} h_\kappa(\tau_2)\, \ddot{u}_g^{m,i}(t+\tau-\tau_2)\, d\tau_2\Big] \end{aligned}$$

$$= \omega_k^2\,\omega_\kappa^2 \int_{-\infty}^{\infty}\int_{-\infty}^{\infty} h_k(\tau_1)\,h_\kappa(\tau_2)\,\mathrm{E}\Big[\,\ddot{u}_g^{m,i}(t-\tau_1)\,\ddot{u}_g^{\hat{m},i}(t+\tau-\tau_2)\Big]\,\mathrm{d}\tau_1\mathrm{d}\tau_2. \tag{3.1.18}$$

Following the same procedure of obtaining equations (3.1.11) to (3.1.16) gives

$$\mathrm{E}\Big[\,\ddot{u}_k^{m,i}(t)\,\ddot{u}_\kappa^{\hat{m},i}(t)\Big] = \frac{\omega_k^2\,\omega_\kappa^2}{2\pi}\int_{-\infty}^{\infty} \mathcal{H}_k^*(\omega)\,\mathcal{H}_\kappa(\omega)\cdot \mathcal{S}_{\ddot{u}_g^{m,i}\,\ddot{u}_g^{\hat{m},i}}(\omega)\,\mathrm{d}\omega. \tag{3.1.19}$$

Then the correlation coefficient $\rho_{k\kappa}^{m\hat{m},i}$ between $\ddot{u}_k^{m,i}(t)$ and $\ddot{u}_\kappa^{\hat{m},i}(t)$ can be evaluated by

$$\rho_{k\kappa}^{m\hat{m},i} = \frac{\mathrm{E}\Big[\,\ddot{u}_k^{m,i}(t)\,\ddot{u}_\kappa^{\hat{m},i}(t)\Big]}{\sqrt{\mathrm{E}\Big[\,\big\{\ddot{u}_k^{m,i}(t)\big\}^2\Big]\cdot \mathrm{E}\Big[\,\big\{\ddot{u}_\kappa^{\hat{m},i}(t)\big\}^2\Big]}}. \tag{3.1.20}$$

Determination of $\rho_0^{m\hat{m},i}$: The correlation coefficient $\rho_0^{m\hat{m},i}$ between $\ddot{u}_g^{m,i}(t)$ and $\ddot{u}_g^{\hat{m},i}(t)$ is defined as

$$\rho_0^{m\hat{m},i} = \frac{\mathrm{E}\Big[\,\ddot{u}_g^{m,i}(t)\,\ddot{u}_g^{\hat{m},i}(t)\Big]}{\sqrt{\mathrm{E}\Big[\,\big\{\ddot{u}_g^{m,i}(t)\big\}^2\Big]\cdot \mathrm{E}\Big[\,\big\{\ddot{u}_g^{\hat{m},i}(t)\big\}^2\Big]}}. \tag{3.1.21}$$

in which

$$\mathrm{E}\Big[\,\ddot{u}_g^{m,i}(t)\,\ddot{u}_g^{\hat{m},i}(t)\Big] = \frac{1}{2\pi}\int_{-\infty}^{\infty} \mathcal{S}_{\ddot{u}_g^{m,i}\,\ddot{u}_g^{\hat{m},i}}(\omega)\,\mathrm{d}\omega, \tag{3.1.22}$$

and the denominator can be determined using equation (3.1.17).

Equations (3.1.15) to (3.1.17), (3.1.19), and (3.1.22) can be evaluated if the spatial coherency function $\gamma^{m\hat{m},i}(\omega)$ is available or postulated, and then the correlation coefficients $\rho_{0k}^{m\hat{m},i}$, $\rho_{k\kappa}^{m\hat{m},i}$, and $\rho_0^{m\hat{m},i}$ given by equations (3.1.7), (3.1.20), and (3.1.21), respectively, can be obtained. It should be mentioned that although the correlation coefficients are derived in a theoretically rigorous way, the evaluation of the integrals could still be challenging especially for a real design. In the following, two important special cases, which have wide applications in nuclear facilities, are considered.

Case 1: Seismic Excitations $\ddot{u}_g^{m,i}(t)$ and $\ddot{u}_g^{\hat{m},i}(t)$ Fully-Correlated

In some special situations, the motions of supports may be very similiar because of their proximity to each other (Burdisso and Singh, 1987). Therefore, it is reasonable to assume the seismic excitations are approximately the same for structures of small sizes, such as

Small Modular Reactors (SMRs), which are modelled as deeply-embedded structures with flexible foundations. This approximation is also applicable to secondary structures that are mounted on primary structures with multiple supports.

For these structures, the phase of earthquake excitations in a direction do not change much at different supports, which means that the input $\ddot{u}_{\mathrm{g}}^{m,i}(t)$ in direction i at support m and the input $\ddot{u}_{\mathrm{g}}^{\hat{m},i}(t)$ in direction i at support $\hat{m}$ are approximately fully correlated, i.e., $\gamma^{m\hat{m},i}(\omega)$ in equation (2.3.16) is approximately 1. Furthermore, since ground motions can be generally modelled as wide-band noises, it is reasonable to assume the seismic input $\ddot{u}_{\mathrm{g}}^{m,i}(t)$ and $\ddot{u}_{\mathrm{g}}^{\hat{m},i}(t)$ as white noises by letting the power spectral density $\mathcal{S}_{\ddot{u}_{\mathrm{g}}^{m,i}\ddot{u}_{\mathrm{g}}^{m,i}}(\omega)=\mathcal{S}_{\mathrm{A}}^{m,i}$ and $\mathcal{S}_{\ddot{u}_{\mathrm{g}}^{\hat{m},i}\ddot{u}_{\mathrm{g}}^{\hat{m},i}}(\omega)=\mathcal{S}_{\mathrm{A}}^{\hat{m},i}$, respectively.

Therefore, in this case, the cross power spectral density of ground motions can be simplified to

$$\mathcal{S}_{\ddot{u}_{\mathrm{g}}^{m,i}\ddot{u}_{\mathrm{g}}^{\hat{m},i}}(\omega)=\sqrt{\mathcal{S}_{\mathrm{A}}^{m,i}\mathcal{S}_{\mathrm{A}}^{\hat{m},i}}. \tag{3.1.23}$$

As a result, equations (3.1.15) and (3.1.16) can be written as

$$\mathrm{E}\Big[\ddot{u}_k^{m,i}(t)\,\ddot{u}_{\mathrm{g}}^{\hat{m},i}(t)\Big]=\frac{\omega_k^2}{2\pi}\sqrt{\mathcal{S}_{\mathrm{A}}^{m,i}\mathcal{S}_{\mathrm{A}}^{\hat{m},i}}\int_{-\infty}^{\infty}\mathcal{H}_k^*(\omega)\,\mathrm{d}\omega, \tag{3.1.24}$$

$$\mathrm{E}\Big[\big\{\ddot{u}_k^{m,i}(t)\big\}^2\Big]=\frac{\omega_k^4}{2\pi}\mathcal{S}_{\mathrm{A}}^{m,i}\int_{-\infty}^{\infty}\mathcal{H}_k(\omega)\,\mathcal{H}_k^*(\omega)\,\mathrm{d}\omega. \tag{3.1.25}$$

To simplify the expression of $\rho_{k0}^{m\hat{m},i}$, denote

$$\lambda_{p,kk}=\int_{-\infty}^{\infty}\omega^p\,\mathcal{H}_k(\omega)\,\mathcal{H}_k^*(\omega)\,\mathrm{d}\omega. \tag{3.1.26}$$

Equations (3.1.24) and (3.1.25) can be then written as

$$\mathrm{E}\Big[\ddot{u}_k^{m,i}(t)\,\ddot{u}_{\mathrm{g}}^{\hat{m},i}(t)\Big]=\frac{\omega_k^2}{2\pi}\sqrt{\mathcal{S}_{\mathrm{A}}^{m,i}\mathcal{S}_{\mathrm{A}}^{\hat{m},i}}\cdot\big(\omega_k^2\,\lambda_{0,kk}-\lambda_{2,kk}\big), \tag{3.1.27}$$

$$\mathrm{E}\Big[\big\{\ddot{u}_k^{m,i}(t)\big\}^2\Big]=\frac{\omega_k^4}{2\pi}\mathcal{S}_{\mathrm{A}}^{m,i}\cdot\lambda_{0,kk}. \tag{3.1.28}$$

Substituting equations (3.1.27) and (3.1.28) into equation (3.1.7) gives

$$\rho_{k0}^{m\hat{m},i}=\frac{\mathrm{E}\Big[\ddot{u}_k^{m,i}(t)\,\ddot{u}_{\mathrm{g}}^{\hat{m},i}(t)\Big]}{\sqrt{\mathrm{E}\Big[\big\{\ddot{u}_k^{m,i}(t)\big\}^2\Big]\cdot\mathrm{E}\Big[\big\{\ddot{u}_{\mathrm{g}}^{\hat{m},i}(t)\big\}^2\Big]}}=\frac{\frac{\omega_k^2}{2\pi}\sqrt{\mathcal{S}_{\mathrm{A}}^{m,i}\mathcal{S}_{\mathrm{A}}^{\hat{m},i}}\cdot\big(\omega_k^2\,\lambda_{0,kk}-\lambda_{2,kk}\big)}{\sqrt{\frac{\omega_k^4}{2\pi}\mathcal{S}_{\mathrm{A}}^{m,i}\cdot\lambda_{0,kk}\cdot\mathrm{E}\Big[\big\{\ddot{u}_{\mathrm{g}}^{\hat{m},i}(t)\big\}^2\Big]}}$$

$$= \sqrt{\frac{\omega_k^4}{2\pi} \cdot \lambda_{0,kk} \mathcal{S}_{\mathrm{A}}^{\hat{m},i} \cdot \frac{1}{\mathrm{E}\left[\left\{\ddot{u}_{\mathrm{g}}^{\hat{m},i}(t)\right\}^2\right]}} \cdot \left(1 - \frac{\omega_{\mathrm{app},k}^2}{\omega_k^2}\right)$$

$$= \sqrt{\frac{\mathrm{E}\left[\left\{\ddot{u}_k^{\hat{m},i}(t)\right\}^2\right]}{\mathrm{E}\left[\left\{\ddot{u}_{\mathrm{g}}^{\hat{m},i}(t)\right\}^2\right]}} \cdot \left(1 - \frac{\omega_{\mathrm{app},k}^2}{\omega_k^2}\right) = \frac{\mathcal{S}_{\mathrm{A}}^{\hat{m},i}(\omega_k, \zeta_k)}{\mathcal{S}_{\mathrm{A,RIGID}}^{\hat{m},i}} \cdot \left(1 - \frac{\omega_{\mathrm{app},k}^2}{\omega_k^2}\right), \tag{3.1.29}$$

in which equations (3.1.3a) and (3.1.3b) have been used, $\omega_{\mathrm{app},k}^2 = \lambda_{2,kk}/\lambda_{0,kk}$ represents the square of the "apparent" frequency (the mean circular frequency of up-crossing the zero level) of the response in mode k due to earthquake excitation. For a lightly damped oscillator under a wide-band input, $\omega_{\mathrm{app},k}^2 \approx \omega_k^2$ (Der Kiureghian and Nakamura, 1993), resulting in $\rho_{k0}^{m\hat{m},i} \approx 0$.

Similarly, equation (3.1.19) can be written as

$$\mathrm{E}\left[\ddot{u}_k^{m,i}(t)\, \ddot{u}_\kappa^{\hat{m},i}(t)\right] = \frac{\omega_k^2 \omega_\kappa^2}{2\pi} \sqrt{\mathcal{S}_{\mathrm{A}}^{m,i} \mathcal{S}_{\mathrm{A}}^{\hat{m},i}} \cdot \lambda_{0,kk}. \tag{3.1.30}$$

Substituting equations (3.1.30) and (3.1.25) into equation (3.1.20) gives

$$\rho_{k\kappa}^{m\hat{m},i} = \frac{\mathrm{E}\left[\ddot{u}_k^{m,i}(t)\, \ddot{u}_\kappa^{\hat{m},i}(t)\right]}{\sqrt{\mathrm{E}\left[\left\{\ddot{u}_k^{m,i}(t)\right\}^2\right] \cdot \mathrm{E}\left[\left\{\ddot{u}_\kappa^{\hat{m},i}(t)\right\}^2\right]}}$$

$$= \frac{\frac{\omega_k^2 \omega_\kappa^2}{2\pi} \sqrt{\mathcal{S}_{\mathrm{A}}^{m,i} \mathcal{S}_{\mathrm{A}}^{\hat{m},i}} \cdot \lambda_{0,k\kappa}}{\sqrt{\frac{\omega_k^4}{2\pi} \mathcal{S}_{\mathrm{A}}^{m,i} \cdot \lambda_{0,kk} \cdot \frac{\omega_\kappa^4}{2\pi} \mathcal{S}_{\mathrm{A}}^{\hat{m},i} \cdot \lambda_{0,\kappa\kappa}}} = \frac{\lambda_{0,k\kappa}}{\lambda_{0,kk} \cdot \lambda_{0,\kappa\kappa}},$$

which is reduced to $\rho_{k\kappa}$ given by Wilson *et al.* (1981) (see also Xie *et al.*, 2019) as

$$\rho_{k\kappa} = \frac{8\sqrt{\zeta_k \zeta_\kappa}\,(\zeta_k + r\zeta_\kappa)\, r^{3/2}}{(1-r^2)^2 + 4\zeta_k \zeta_\kappa r(1+r^2) + 4(\zeta_k^2 + \zeta_\kappa^2) r^2}, \qquad r = \frac{\omega_\kappa}{\omega_k}. \tag{3.1.31}$$

Finally, by the assumption of Case 1, $\ddot{u}_{\mathrm{g}}^{m,i}(t)$ and $\ddot{u}_{\mathrm{g}}^{\hat{m},i}(t)$ are fully-correlated, which means $\rho_0^{m\hat{m},i} = 1$.

Case 2: Independent Seismic Excitations

This case also has important applications in nuclear power plants. For example, consider the main steam line that has some supports on the reactor building and some supports

on the service building. The support excitations of the anchors on the reactor building and those on the service building can be considered as approximately independent. The coefficient of correlation is denoted as $\bar{\rho}$ for this case.

Similar to Case 1, $\bar{\rho}_{k0}^{m\hat{m},i} = 0$. When the earthquake excitations are from different supports, the other two correlation coefficients are zero, i.e., when $m \neq \hat{m}$, $\bar{\rho}_{k\kappa}^{m\hat{m},i} = \bar{\rho}_{0}^{m\hat{m},i} = 0$. When $m = \hat{m}$,

$$\bar{\rho}_{k\kappa}^{mm,i} = \rho_{k\kappa}, \quad \bar{\rho}_{0}^{mm,i} = 1, \tag{3.1.32}$$

in which $\rho_{k\kappa}$ is given by equation (3.1.31).

3.1.3 Responses for Multi-Supported Secondary Structures

The assessment of secondary systems, such as emergency power systems and water supply piping systems in nuclear power plants, are crucial because the failure of them can causes tremendous loss (Villaverde, 2009). As illustrated in Figure 3.1, consider a secondary system supported on a total of P primary structures; there are M_p supports on the primary structure p, for $p = 1, 2, \ldots, P$, denoted as Fp-1, Fp-2, ..., Fp-M_p, in which "Fp-" indicates that the support is a "Floor" node of the pth primary structure. An example is the main steam line in a nuclear power plant that has some supports on the reactor building and some supports on the service building (see Section 3.3 for more details).

Input of Secondary Structures

The method derived in Section 3.1 or proposed by Asfura and Der Kiureghian (1986) is rigorous, thus it can be used to evaluate the seismic response of multi-supported structures in principle. For the analysis of secondary structures, the main difference is that instead of having ground motions as the input, the floor response spectra at the anchors of secondary systems are the input to secondary structures.

To obtain the FRS at these anchors, time history analysis for the primary supporting structures has been traditionally applied. However, it has been demonstrated in Chapter 2 that the result of individual time history analysis has large variabilities. Hence, a large number of time history analyses are necessary to obtain reliable FRS, which is very time

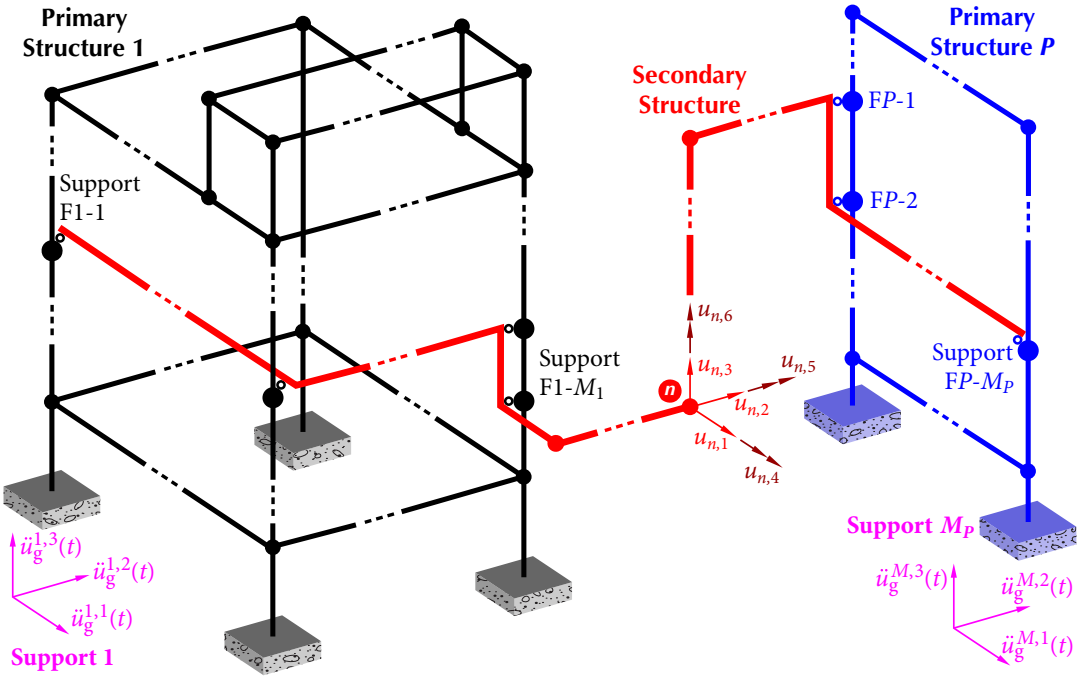

Figure 3.1 Multiple DOF secondary structure under excitations at multiple supports.

consuming. This problem can be solved by applying the direct spectra-to-spectra method developed by Jiang *et al.* (2015) or derived in Chapter 2 to generate accurate FRS.

Another problem is that similar to the coherency function of earthquake excitations, which describes the correlation between ground motions at different supports, the correlations between FRS at different anchors of secondary system are also needed. In principle, this correlation, which is characterized by cross-power spectral density (CPSD) functions, can be obtained by the theory of random vibration. For example, Singh and Burdisso (1987) conducted a comprehensive study on calculating the correlation between FRS at different supports. Asfura and Der Kiureghian (1986) also proposed a concept called "cross-oscillator, cross-floor response spectrum (CCFS)" which can approximately and implicitly consider the correlation between FRS.

However, although these methods are rigorously derived to consider the correlation between FRS at different locations, they are be not widely applied in practice because large computational effort is needed in the numerical evaluation of integrals involving CPSD

functions, especially when the structure has a large number of modes. Thus it is required to develop an approach from the practical standpoint, which can be directly applied as long as the basic model information and ground motions are given. At the same time, it should also give acceptable result with insignificant error comparing with benchmark. In this study, the assumptions below are proposed to consider the correlation between FRS of different supports. It will be verified that these assumptions, although not derived rigorously, yield good results in the seismic assessment of multi-supported secondary structures.

Simplified Relationship of Correlation between FRS

Referring to Figure 3.1, for the M_p supports of the secondary system on the pth primary structure, the seismic inputs to the secondary system are the FRS $\mathcal{S}^{\mathrm{F}p\text{-}m,i}(\omega_0,\zeta_0)$, where $i=1,2,3$ are the three orthogonal directions, and $m=1,2,\ldots,M_p$ are nodes of the supports. Because they are related to the seismic responses of the pth primary structure, it is a reasonable approximation to consider that $\mathcal{S}^{\mathrm{F}p\text{-}m,i}(\omega_0,\zeta_0)$ and $\mathcal{S}^{\mathrm{F}p\text{-}\hat{m},i}(\omega_0,\zeta_0)$ are fully correlated, i.e., FRS in the same direction at different nodes of the same primary structure can be considered as fully-correlated, as in Case 1 in Chapter 2.

It is also a reasonable approximation to consider FRS in the same direction but at nodes of different primary structures as uncorrelated because seismic responses of different primary structures are uncorrelated, i.e., the coefficient of correlation between $\mathcal{S}^{\mathrm{F}p_1\text{-}m,i}(\omega_0,\zeta_0)$ and $\mathcal{S}^{\mathrm{F}p_2\text{-}\hat{m},i}(\omega_0,\zeta_0)$ is 0 when $p_1\neq p_2$, as in Case 2 in Chapter 2. The validity of these two special cases of coefficient of correlation will be verified in Section 3.3 through numerical simulation. It should be noted that FRS in different directions at different nodes (either of the same primary structure or different primary structures) are always considered uncorrelated.

3.2 Tertiary Response Spectra (TRS)

In seismic analysis, design, and qualification of a nuclear power plant, a number of levels of response spectra are required. The first level is Ground Response Spectrum (GRS), in which the input motion to the SDOF oscillator (ω_0,ζ_0) is a ground motion. GRS are used for analysis and design of primary structures and as input for the generation of FRS. The second level is Floor Response Spectrum (FRS), in which the input motion to the SDOF

oscillator (ω_0, ζ_0) is a floor motion of the primary structure, such as reactor building. FRS are used for qualification of secondary systems, such as fueling machine and steam generator, and for the generation of TRS. The third level is the Tertiary Response Spectra (TRS), in which the input motion to the SDOF oscillator (ω_0, ζ_0) is the motion at location on a secondary system where a tertiary system is supported. TRS are used for qualifying a tertiary system, such as pumps and valves mounted on a piping.

Similar to the FRS method, the concept of TRS is also based on the decoupled analysis due to its specific advantages as mentioned in Chapter 1. Note that the method developed in Chapter 2 for the generation of FRS for multi-supported structures is generically derived, thus it can be applied to any structures with multiple supports in principle, either for primary structure or secondary structure. If the direct method is applied to secondary structure, the obtained response spectra will be TRS.

There are two things deserve to be considered in the application of the direct method in generating TRS. Firstly, instead of having ground motions as input, the seismic input to the secondary system is changed to the response spectra at the supports where secondary system is attached. These FRS may have certain correlation depending on the properties of the primary structure whereas it is difficult to consider these correlations in practice. Therefore, the same assumptions on the FRS that has been made in the generation of response of secondary structures, are applied here. Although these assumptions are not rigorously derived, it allows the explicit forms of the direct method to be exist and thus conveniently to be implemented.

The other difference in the generation of FRS and TRS is the resonance case, which is considered by using "t-Response-Spectrum (tRS)" in the direct method. Below, tRS in the generation of FRS proposed by Li *et al.* (2015) is reviewed first, followed by the two approaches of considering resonance case in evaluating TRS.

3.2.1 tRS for the Generation of Floor Response Spectra

In the direct method for generating FRS from GRS developed by Jiang *et al.* (2015), the following quantity is required when the equipment and supporting structure are in resonance

(tuning)

$$\mathcal{S}_{\mathrm{A}}^{\mathrm{t}}(\omega,\zeta) = \frac{1}{2}\left|-\omega^2 t\mathrm{e}^{-\zeta\omega t}\cos\omega t * \ddot{u}_{\mathrm{g}}(t) + \omega\mathrm{e}^{-\zeta\omega t}\sin\omega t * \ddot{u}_{\mathrm{g}}(t)\right|_{\max}. \tag{3.2.1}$$

This equation is defined as t-Response Spectrum (tRS), in which "t" indicates "tuning" or the extra "t" variable in the first convolution term as compared to GRS. However, the analytic expression of equation (3.2.1) is difficult to obtain due to the presence of "t".

The concept of "t-response-spectrum (tRS)" proposed by Li *et al.* (2015) is employed to deal with this tuning or resonant case. tRS $\mathcal{S}_{\mathrm{A}}^{\mathrm{t}}(\omega_0,\zeta_0)$ is the maximum acceleration response of an SDOF oscillator (ω_0,ζ_0) mounted on top of an SDOF structure (with the same ω_0 and ζ_0) that is mounted on ground, as shown in Figure 3.4 (a). The identical SDOF oscillator and SDOF structure are uncoupled and are in resonance or tuning (see also Xie *et al.*, 2019).

A comprehensive study on the statistical relationship between GRS and tRS is conducted by Li *et al.* (2015). A large number of real horizontal and vertical ground motions, which are selected from the Pacific Earthquake Engineering Research Center Strong Motion Database (PEER, 2010) and the European Strong Motion Database, are employed to perform numerical simulations. Statistical relationships between tRS and GRS are constructed based on three different site conditions following the the site classification criteria (ASCE, 2010; IBC, 2012):

- 49 horizontal and 49 vertical ground motions of B sites;
- 154 horizontal and 154 vertical ground motions of C sites; and
- 220 horizontal and 220 vertical ground motions of D sites.

Figures 3.2 and 3.3 show the statistical relationship between GRS and tRS for horizontal and vertical ground motions at B sites, respectively. It is found through regression analyses of the simulation results that site conditions affect the statistical relationship between tRS and GRS in vertical direction only, and the statistical relationship could be categorized by soil sites and rock sites. For a given GRS $\mathcal{S}_{\mathrm{A}}(f,\,\zeta)$, the corresponding tRS $\mathcal{S}_{\mathrm{A}}^{\mathrm{t},p}(f,\,\zeta)$ with any non-exceedance probability (NEP) can be estimated as

$$\ln\mathcal{S}_{\mathrm{A}}^{\mathrm{t},p}(f,\,\zeta) = c_1(f,\,\zeta) + c_2(f,\,\zeta)\cdot\ln\mathcal{S}_{\mathrm{A}}(f,\,\zeta) + \sigma_{\ln\mathcal{S}_{\mathrm{A}}^{\mathrm{t}}}(f,\,\zeta)\cdot\Phi^{-1}(p), \tag{3.2.2}$$

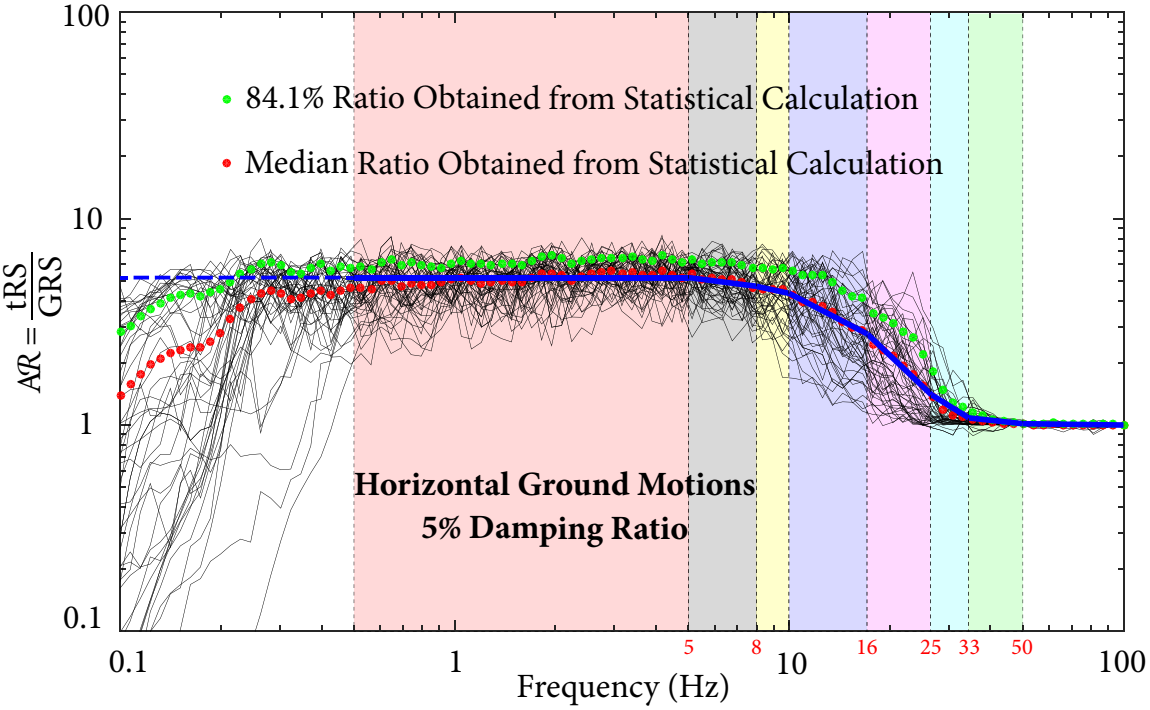

Figure 3.2 Ratio of tRS to GRS for the 49 horizontal ground motions at B sites.

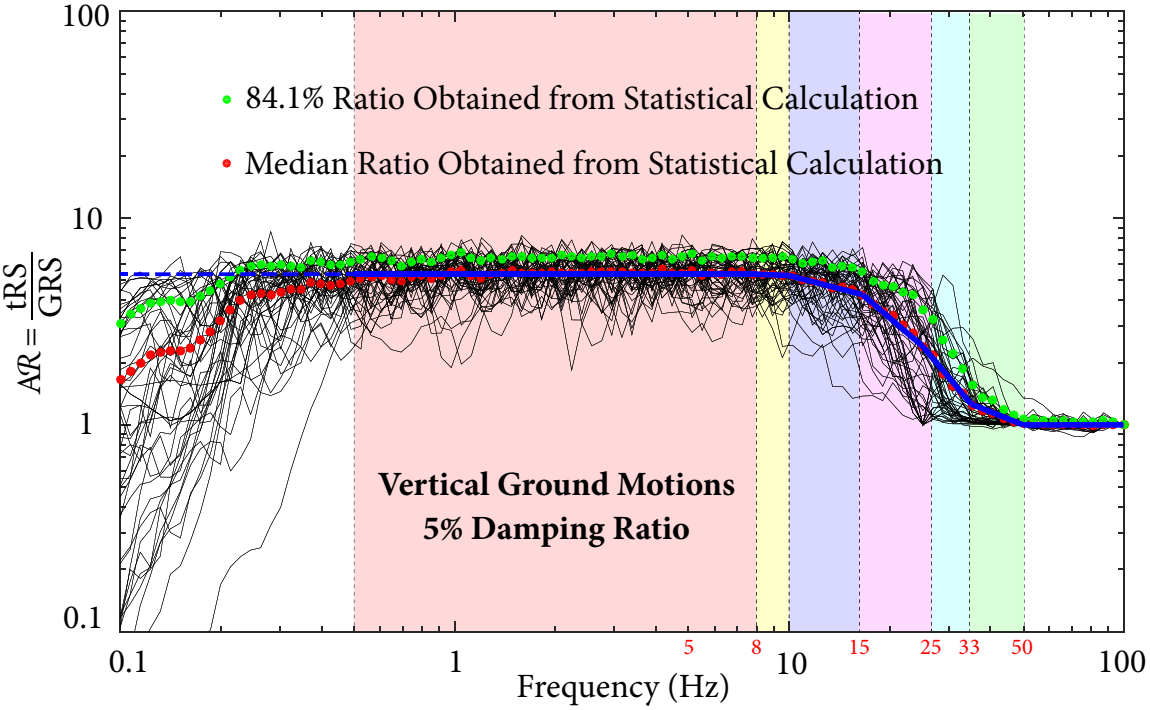

Figure 3.3 Ratio of tRS to GRS for the 49 vertical ground motions at B sites.

Table 3.1 Coefficients of simplified horizontal statistical relationship for various damping ratios

f (Hz)	Damping Ratio ζ (%)																			
	1.0			3.0			5.0			7.0			10.0			15.0			20.0		
	c_1	c_2	$\sigma_{\ln S_A^i}$	c_1	c_2	$\sigma_{\ln S_A^i}$	c_1	c_2	$\sigma_{\ln S_A^i}$	c_1	c_2	$\sigma_{\ln S_A^i}$	c_1	c_2	$\sigma_{\ln S_A^i}$	c_1	c_2	$\sigma_{\ln S_A^i}$	c_1	c_2	$\sigma_{\ln S_A^i}$
0.1∼5	3.00	1.12	0.30	2.11	1.07	0.24	1.70	1.07	0.21	1.44	1.07	0.20	1.18	1.09	0.19	0.93	1.14	0.18	0.80	1.21	0.19
8	3.00	1.33	0.27	2.14	1.45	0.25	1.76	1.51	0.24	1.54	1.55	0.23	1.34	1.61	0.21	1.20	1.69	0.16	1.09	1.69	0.14
10	2.99	1.45	0.29	2.19	1.65	0.28	1.88	1.77	0.28	1.70	1.84	0.26	1.52	1.89	0.22	1.30	1.85	0.18	1.16	1.80	0.13
16	3.31	2.21	0.43	2.72	2.57	0.40	2.39	2.58	0.33	2.15	2.52	0.27	1.86	2.38	0.21	1.48	2.14	0.15	1.30	2.01	0.11
25	6.42	5.67	0.62	5.07	5.02	0.35	3.66	3.95	0.22	2.80	3.27	0.16	2.20	2.80	0.10	1.72	2.42	0.06	1.52	2.25	0.04
33	7.35	6.68	0.49	3.77	4.02	0.21	2.32	2.88	0.11	1.67	2.36	0.07	1.30	2.06	0.04	1.20	1.98	0.03	1.18	1.97	0.02
50∼100	0.0	1.00	0.0	0.0	1.00	0.0	0.0	1.00	0.0	0.0	1.00	0.0	0.0	1.00	0.0	0.0	1.00	0.0	0.0	1.00	0.0

Table 3.2 Equations for coefficients and standard deviations of horizontal statistical relationship

f (Hz)	Coefficient c_1	Coefficient c_2	Standard deviation $\sigma_{\ln S_A^i}$
0.1∼5	$0.06(\ln\zeta)^2 - 0.92\ln\zeta + 3.03$	$0.02(\ln\zeta)^3 - 0.04(\ln\zeta)^2 - 0.02\ln\zeta + 1.12$	$-0.01(\ln\zeta)^2 - 0.05\ln\zeta + 0.30$
8	$0.10(\ln\zeta)^2 - 0.93\ln\zeta + 3.01$	$-0.01(\ln\zeta)^3 + 0.07(\ln\zeta)^2 + 0.03\ln\zeta + 1.35$	$-0.01(\ln\zeta)^3 + 0.02(\ln\zeta)^2 - 0.02\ln\zeta + 0.27$
10	$0.06(\ln\zeta)^2 - 0.80\ln\zeta + 2.99$	$-0.06(\ln\zeta)^3 + 0.21(\ln\zeta)^2 + 1.45$	$-0.01(\ln\zeta)^3 + 0.01(\ln\zeta)^2 + 0.28$
16	$-0.08(\ln\zeta)^2 - 0.45\ln\zeta + 3.32$	$-0.22(\ln\zeta)^2 + 0.58\ln\zeta + 2.24$	$0.02(\ln\zeta)^3 - 0.12(\ln\zeta)^2 + 0.07\ln\zeta + 0.43$
25	$0.39(\ln\zeta)^3 - 1.74(\ln\zeta)^2 + 0.16\ln\zeta + 6.33$	$0.35(\ln\zeta)^3 - 1.66(\ln\zeta)^2 + 0.77\ln\zeta + 5.58$	$0.02(\ln\zeta)^3 - 0.04(\ln\zeta)^2 - 0.21\ln\zeta + 0.60$
33	$0.21(\ln\zeta)^3 - 0.22(\ln\zeta)^2 - 3.16\ln\zeta + 7.23$	$0.20(\ln\zeta)^3 - 0.38(\ln\zeta)^2 - 2.15\ln\zeta + 6.58$	$0.04(\ln\zeta)^2 - 0.31\ln\zeta + 0.49$
50∼100	0	1	0

Table 3.3 Coefficients of simplified vertical statistical relationships for hard sites

f (Hz)	Damping Ratio ζ (%)																				
	1.0			3.0			5.0			7.0			10.0			15.0			20.0		
	c_1	c_2	$\sigma_{\ln \mathcal{S}_A^t}$	c_1	c_2	$\sigma_{\ln \mathcal{S}_A^t}$	c_1	c_2	$\sigma_{\ln \mathcal{S}_A^t}$	c_1	c_2	$\sigma_{\ln \mathcal{S}_A^t}$	c_1	c_2	$\sigma_{\ln \mathcal{S}_A^t}$	c_1	c_2	$\sigma_{\ln \mathcal{S}_A^t}$	c_1	c_2	$\sigma_{\ln \mathcal{S}_A^t}$
0.1∼8	3.06	1.15	0.28	2.17	1.09	0.23	1.76	1.08	0.21	1.49	1.07	0.21	1.21	1.08	0.20	0.93	1.11	0.19	0.78	1.17	0.20
10	3.07	1.23	0.20	2.19	1.28	0.19	1.80	1.35	0.19	1.58	1.42	0.20	1.37	1.48	0.19	1.14	1.51	0.16	1.00	1.52	0.14
15	3.04	1.35	0.26	2.20	1.54	0.25	1.85	1.66	0.25	1.66	1.75	0.23	1.48	1.80	0.21	1.32	1.83	0.17	1.23	1.84	0.14
25	3.28	2.28	0.6	2.64	2.53	0.43	2.33	2.55	0.33	2.14	2.53	0.27	1.94	2.48	0.20	1.62	2.28	0.13	1.45	2.16	0.09
33	3.87	3.29	0.65	3.42	3.56	0.39	2.90	3.27	0.28	2.39	2.89	0.23	1.88	2.50	0.16	1.36	2.09	0.10	1.20	1.96	0.07
50∼100	0.0	1.00	0.0	0.0	1.00	0.0	0.0	1.00	0.0	0.0	1.00	0.0	0.0	1.00	0.0	0.0	1.00	0.0	0.0	1.00	0.0

Table 3.4 Coefficients of simplified vertical statistical relationships for soft sites

f (Hz)	Damping Ratio ζ (%)																				
	1.0			3.0			5.0			7.0			10.0			15.0			20.0		
	c_1	c_2	$\sigma_{\ln \mathcal{S}_A^t}$	c_1	c_2	$\sigma_{\ln \mathcal{S}_A^t}$	c_1	c_2	$\sigma_{\ln \mathcal{S}_A^t}$	c_1	c_2	$\sigma_{\ln \mathcal{S}_A^t}$	c_1	c_2	$\sigma_{\ln \mathcal{S}_A^t}$	c_1	c_2	$\sigma_{\ln \mathcal{S}_A^t}$	c_1	c_2	$\sigma_{\ln \mathcal{S}_A^t}$
0.1∼8	3.1	1.17	0.32	2.22	1.11	0.28	1.8	1.10	0.27	1.53	1.10	0.26	1.26	1.11	0.26	0.98	1.14	0.25	0.84	1.20	0.24
10	3.06	1.24	0.22	2.18	1.32	0.18	1.78	1.35	0.18	1.53	1.38	0.18	1.28	1.39	0.18	1.06	1.42	0.16	0.88	1.37	0.14
15	3.02	1.40	0.24	2.15	1.47	0.27	1.75	1.51	0.28	1.53	1.55	0.25	1.31	1.57	0.23	1.11	1.60	0.18	1.01	1.64	0.15
25	3.20	2.62	0.73	2.70	2.84	0.48	2.51	2.88	0.34	2.34	2.82	0.27	2.12	2.68	0.22	1.81	2.45	0.17	1.59	2.28	0.12
33	3.17	2.62	0.58	3.05	3.19	0.39	2.79	3.15	0.28	2.45	2.93	0.22	2.15	2.73	0.15	1.80	2.46	0.11	1.58	2.29	0.08
50∼100	0.0	1.00	0.0	0.0	1.00	0.0	0.0	1.00	0.0	0.0	1.00	0.0	0.0	1.00	0.0	0.0	1.00	0.0	0.0	1.00	0.0

Table 3.5 Equations for coefficients and standard deviations of vertical statistical relationships for hard sites

f (Hz)	Coefficient c_1	Coefficient c_2	Standard deviation $\sigma_{\ln S_A^t}$
0.5∼8	$0.04(\ln\zeta)^2 - 0.89\ln\zeta + 3.09$	$0.01(\ln\zeta)^4 - 0.06(\ln\zeta)^3 + 0.12(\ln\zeta)^2 - 0.12\ln\zeta + 1.15$	$0.01(\ln\zeta)^2 - 0.06\ln\zeta + 0.28$
10	$0.07(\ln\zeta)^2 - 0.90\ln\zeta + 3.08$	$-0.04(\ln\zeta)^3 + 0.19(\ln\zeta)^2 - 0.13\ln\zeta + 1.24$	$-0.01(\ln\zeta)^3 + 0.05(\ln\zeta)^2 - 0.05\ln\zeta + 0.2$
15	$0.10(\ln\zeta)^2 - 0.90\ln\zeta + 3.06$	$-0.03(\ln\zeta)^3 + 0.13(\ln\zeta)^2 + 0.08\ln\zeta + 1.35$	$-0.01(\ln\zeta)^3 + 0.01(\ln\zeta)^2 + 0.25$
25	$-0.03(\ln\zeta)^2 - 0.52\ln\zeta + 3.25$	$-0.03(\ln\zeta)^3 - 0.02(\ln\zeta)^2 + 0.29\ln\zeta + 2.28$	$0.01(\ln\zeta)^3 - 0.05(\ln\zeta)^2 - 0.12\ln\zeta + 0.60$
33	$0.17(\ln\zeta)^3 - 0.98(\ln\zeta)^2 + 0.51\ln\zeta + 3.83$	$0.17(\ln\zeta)^3 - 1.10(\ln\zeta)^2 + 1.28\ln\zeta + 3.26$	$0.01(\ln\zeta)^2 - 0.26\ln\zeta + 0.65$
50∼100	0	1	0

Table 3.6 Equations for coefficients and standard deviations of vertical statistical relationships for soft sites

f (Hz)	Coefficient c_1	Coefficient c_2	Standard deviation $\sigma_{\ln S_A^t}$
0.5∼8	$0.04(\ln\zeta)^2 - 0.90\ln\zeta + 3.13$	$0.01(\ln\zeta)^3 - 0.03(\ln\zeta)^2 - 0.04\ln\zeta + 1.17$	$-0.04\ln\zeta + 0.32$
10	$0.05(\ln\zeta)^2 - 0.90\ln\zeta + 3.08$	$-0.02(\ln\zeta)^4 + 0.09(\ln\zeta)^3 - 0.14(\ln\zeta)^2 + 0.14\ln\zeta + 1.24$	$-0.01(\ln\zeta)^3 + 0.06(\ln\zeta)^2 - 0.09\ln\zeta + 0.22$
15	$0.09(\ln\zeta)^2 - 0.95\ln\zeta + 3.05$	$0.01(\ln\zeta)^4 - 0.07(\ln\zeta)^3 + 0.15(\ln\zeta)^2 - 0.03\ln\zeta + 1.40$	$-0.01(\ln\zeta)^3 - 0.01(\ln\zeta)^2 + 0.04\ln\zeta + 0.24$
25	$-0.08(\ln\zeta)^2 - 0.27\ln\zeta + 3.15$	$0.04(\ln\zeta)^4 - 0.25(\ln\zeta)^3 + 0.37(\ln\zeta)^2 + 0.06\ln\zeta + 2.63$	$0.01(\ln\zeta)^3 - 0.02(\ln\zeta)^2 - 0.24\ln\zeta + 0.74$
33	$-0.19(\ln\zeta)^2 + 3.21$	$0.07(\ln\zeta)^4 - 0.34(\ln\zeta)^3 + 0.17(\ln\zeta)^2 + 0.65\ln\zeta + 2.62$	$0.02(\ln\zeta)^3 - 0.07(\ln\zeta)^2 - 0.13\ln\zeta + 0.58$
50∼100	0	1	0

where the coefficients $c_1(f, \zeta)$ and $c_2(f, \zeta)$, and the standard deviation $\sigma_{\ln \mathcal{S}_A^t}(f, \zeta)$ are determined through the regression analyses. Table 3.2 and Tables 3.5 and 3.6 provide the values of the coefficients and the standard deviation for the horizontal and vertical tRS, respectively. Values for other frequencies can be obtained by linear interpolation in the logarithmic scale of frequency (Xie *et al.*, 2019).

3.2.2 ttRS and F-tRS for the Generation of Tertiary Response Spectra

If the secondary system cannot be decoupled from the primary structure, the problem becomes direct generation of FRS at the location of the tertiary system on the coupled system of primary structure and secondary structure from the GRS. Suppose the secondary structure not only can be, but also should be, decoupled from the primary structure (e.g., due to mass disparity). There are two approaches for generating TRS.

Approach 1. In a method for the generation of TRS directly from GRS, TRS is expressed as a triple convolution integral, making use of three levels of unit impulse response functions. The first level unit impulse response function is that of the primary structural system without the secondary structure. The second level unit impulse response function is actually a group of the secondary structure's relevant support influence functions. The third level unit impulse response function is those of a set of SDOF oscillators. Their maximum responses are the TRS. That is to say, GRS produces the FRS on the primary structure, which in turn produce the TRS on the secondary structure. The spectral responses from the same mode of the primary structure are in phase and 100% correlated. This treatment is valid even though some supports of the secondary structure may be anchored to the floors or different pieces of equipment, as long as they are included in the model of the primary structure.

The tuning situation arises when the SDOF oscillator, the secondary structure, and the primary structure are in resonance. A similar ttRS $\mathcal{S}_A^{tt}(\omega_0, \zeta_0)$, which is the maximum acceleration response of an SDOF oscillator (tertiary system) mounted on top of an SDOF oscillator (secondary system) mounted on top of another SDOF oscillator (primary structure) that is mounted on ground as shown in Figure 3.4 (b), is required to deal with

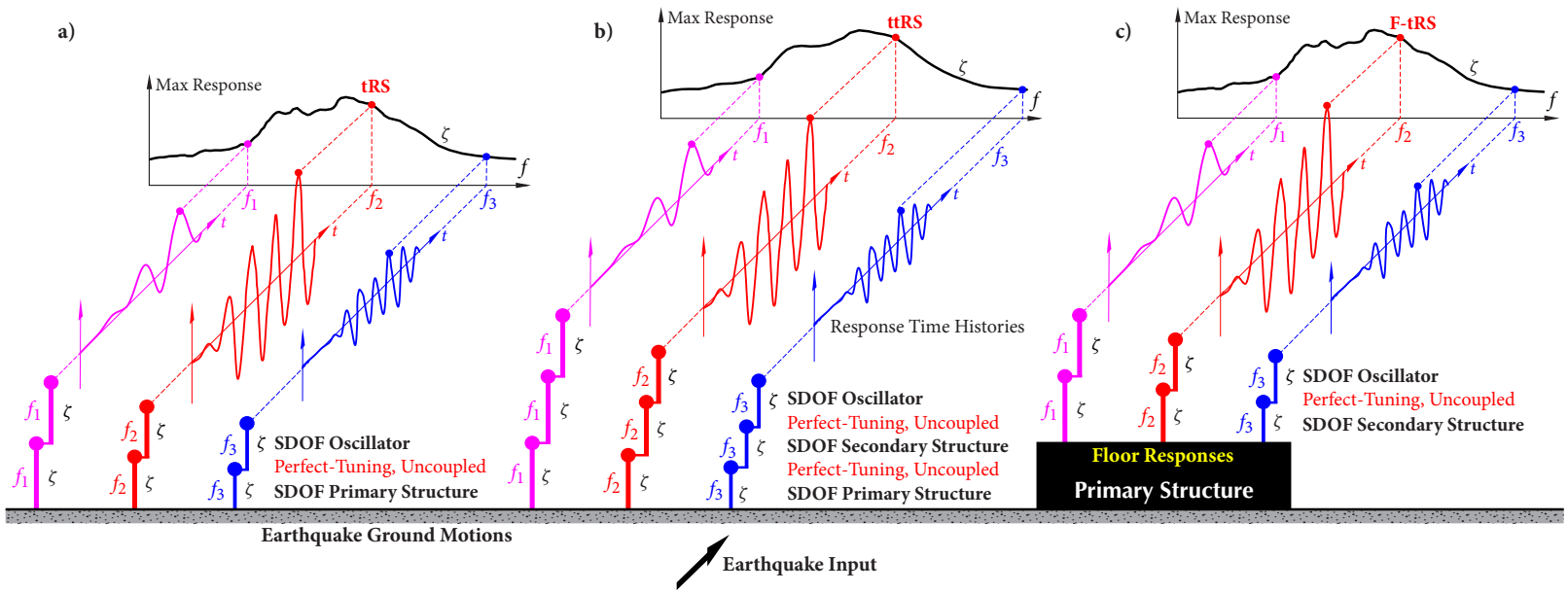

Figure 3.4 Illustration of tRS, ttRS, and F-tRS.

this tuning case. The three uncoupled SDOF oscillators (ω_0, ζ_0) are identical and are in resonance or tuning.

The inputs of this method are GRS directly, while FRS at the supports of secondary systems are not needed, which makes this approach more straightforward. However, challenge exists because in addition to theoretical derivation of the approach, a comprehensive statistical analysis has to be conducted first to obtain the relationship between ttRS and GRS. Currently, there is no such a direct method available and will be developed in a future study. An alternative approach is applied in this study to obtain TRS.

Approach 2. The second approach uses the FRS, which may be obtained from a separate analysis, as inputs. In this case, the direct method developed by Jiang *et al*. (2015) for single support or the direct method presented in Section 2.3 for multiple supports can be applied. Once these FRS are obtained, the method derived in Section 2.3, which is initially aimed to obtain FRS, can be applied to generate TRS as well. One significant advantage of Approach 2 is that it avoids the statistical analysis on the relationship between ttRS and GRS. Furthermore, the direct method for generating FRS proposed in this study can be directly applied to generate TRS, making the proposed method more widely applicable.

Instead of evaluating ttRS in Approach 1, a quantity called F-tRS as shown in Figure 3.4 (c), which is similar to tRS, is needed to deal with the tuning or resonant case when the tertiary system and the secondary structure are in resonance. F-tRS $\mathcal{S}_{\mathrm{A}}^{\mathrm{F\text{-}t}}(\omega_0, \zeta_0)$ is the maximum acceleration response of an SDOF oscillator (ω_0, ζ_0) mounted on top of an SDOF (secondary) structure under the excitations of floor responses of the primary structures.

Note that tRS developed in Li *et al*. (2015) relates FRS to GRS, which are generated from wide-band ground motion time histories, in the tuning case; whereas F-tRS relates TRS to FRS generated from floor responses, which are usually narrow-band processes, of the primary structure. Although F-tRS are conceptually somewhat different from tRS, it is expected that F-tRS and tRS are very close, and tRS can be used as an approximation of F-tRS in generating TRS from FRS. The validity of this approximation will be checked by numerical examples in Section 3.3.

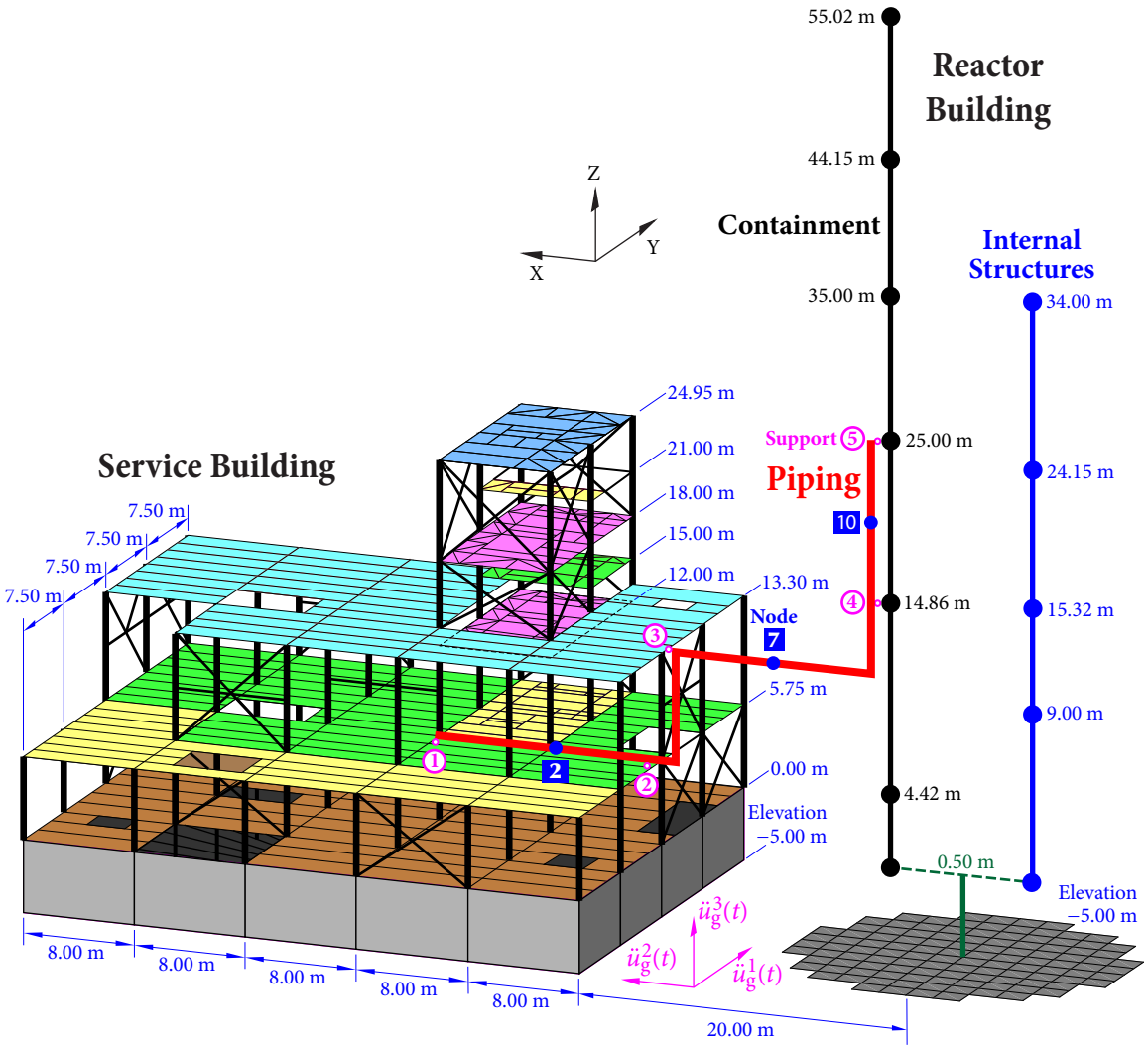

Figure 3.5 Diagram of the numerical example.

3.3 Numerical Examples

3.3.1 Description of Model and Numerical Procedure

A numerical example is presented in this section to demonstrate and verify the proposed method in generating responses as well as TRS of multi-supported secondary structures. A piping system representing the main steam line in the nuclear power industry, which is mounted on a reactor building (RB) and a service building (SB), as shown in Figure 3.5, is considered. The service building is modelled as a three-dimensional multi-storey building. The superstructure of the building consists of steel frames and concrete floor

Table 3.7 Number of elements in the finite element model

Structure	Node	Lumped Mass	Beam		Shell	
			Element	Section	Element	Section
SB	1351	120	1740	31	830	8
RB	12	12	11	7	0	0
Piping	16	16	15	1	0	0

slabs, while the foundation is constructed using concrete. Detailed information of the service building model can be found in Jiang *et al.* (2015). A stick model, which has been widely used to determine global dynamic behaviour of simple and regular structures, such as the containment, is applied to model the reactor building (Xie *et al.*, 2019). The stick model consists of beams and masses, in which masses are lumped at the floor nodes and the beams are considered as massless. Details of the reactor building model are given in Li *et al.* (2005). The foundations of SB and RB are treated as rigid. The piping system has 3 supports on the service building and 2 supports on the reactor building, which are all considered as rigid supports. Information of the numerical model is summarized in Table 3.7.

Modal analyses are performed first for the primary structures and secondary system, respectively, to obtain the modal frequencies, modal participation factors, and modal shapes of the structures. There are in total 66 DOF of the reactor building, resulting in 66 natural frequencies. Table 3.8 shows the modal information of the first 10 modes of the reactor building. The earthquake excitation factor and the ratio between the effective mass and the total mass are obtained from the results of modal analysis using ANSYS, which can be used to identify the significant modes (ANSYS, 2018). That is, the larger magnitude of the earthquake excitation factor (or the ratio) is, the more significant contribution of that mode to the total response.

As the service building has much more DOF comparing with the reactor building and the piping system in this numerical example, a mode truncation is performed. The cut-off frequency is set to be 33 Hz, resulting in 145 modes in total for the service building. This is because the mode with frequency higher than 33 Hz can be treated as rigid in the

nuclear power industry; as a result, the influence of these modes on the structural dynamic response can be neglected. The modal information of the first 10 modes of the service building is given by Table 3.9.

Besides of the information of the overall systems, the modal information at the supports of the piping system is also extracted. The results of Supports 3 and 4 are listed in Tables 3.10 and 3.11, respectively, as an example. The contribution factor is the product of the modal shape and the participation factor, representing the contribution of the corresponding mode to the total response of the node. The modes, which has absolute values of the contribution factors greater than 0.05 for the service building and 0.02 for the reactor building are listed. It can be seen that the summation of the mode contribution factors at each node is close to 1, indicating that all of the significant modes at these supports have been extracted. Moreover, there are closely-spaced modes with significant contributions to the responses at Supports 3 and 4, such as modes 65 and 67, modes 72 and 73 for Support 3; modes 37 and 38 for Support 4.

The procedure of the numerical example for generating responses of secondary system is shown in Figure 3.6. It has been mentioned in Section 3.1.3 that for secondary structures (e.g., piping systems) mounted on primary structures (e.g., buildings), the seismic inputs to the secondary structures are not the ground motions but the responses of the anchors on the supporting primary structures. Therefore, FRS at anchors of the secondary system have to be generated. In this example, the method proposed by Jiang *et al.* (2015) is applied because the foundations of the two primary buildings are considered as rigid. The generated FRS are treated as fully-correlated if the supports are located at the same building, whereas they are regarded as independent if the supports are on different buildings. After the calculation of these FRS, equation (3.1.5) is applied together with the simplified correlation coefficients to obtain the response of the piping system.

To verify the results by the proposed method, the responses of the piping system by the time history method are also generated. Firstly, 30 tri-directional acceleration time histories are input to the service building and reactor building, respectively, to obtain the response time histories at the locations when the piping system is attached. The response time histories are then treated as the inputs of the piping system to evaluate the response

Table 3.8 Modal information of the reactor building

Mode	Frequency (Hz)	Direction X		Direction Y		Direction Z	
		Excitation factor	Eff. mass / Total mass	Excitation factor	Eff. mass / Total mass	Excitation factor	Eff. mass / Total mass
1	4.44	3423.4	0.232	−2243.3	0.037	0.0	0.000
2	4.44	2243.3	0.037	3423.4	0.232	0.0	0.000
3	5.53	10.6	0.142	4057.5	0.123	0.0	0.000
4	5.53	4057.5	0.122	−10.6	0.142	0.0	0.000
5	9.43	0.0	0.000	0.0	0.000	0.0	0.000
6	12.79	−524.2	0.009	−1028.8	0.012	0.0	0.000
7	12.79	−1028.8	0.012	524.2	0.009	0.0	0.000
8	13.72	0.0	0.000	0.0	0.000	4487.1	0.324
9	14.57	1620.4	0.000	−1028.0	0.000	0.0	0.000
10	14.57	1028.0	0.020	1620.4	0.040	0.0	0.000

Table 3.9 Modal information of the service building

Mode	Frequency (Hz)	Direction X		Direction Y		Direction Z	
		Excitation factor	Eff. mass / Total mass	Excitation factor	Eff. mass / Total mass	Excitation factor	Eff. mass / Total mass
1	2.65	−219.0	0.006	1231.6	0.178	−4.3	0.000
2	2.78	1293.0	0.196	220.4	0.006	−6.8	0.000
3	4.82	−133.6	0.002	−209.9	0.005	15.4	0.000
4	5.39	−17.9	0.000	−10.5	0.0000	204.5	0.005
5	5.90	−240.3	0.007	618.0	0.050	37.5	0.000
6	6.00	62.1	0.001	−306.5	0.011	101.9	0.001
7	6.03	35.5	0.001	−196.9	0.005	191.0	0.004
8	6.13	276.4	0.009	179.4	0.004	−0.2	0.000
9	6.43	−570.0	0.040	−217.0	0.18	−17.5	0.000
10	6.99	−105.4	0.001	438.2	0.023	133.3	0.002

Table 3.10 Modal information at Support 3 in direction X

Mode	Frequency (Hz)	Participation factor	Modal shape	Contribution factor
2	2.781	1.293	0.888	1.148
3	4.820	−0.134	−0.868	0.116
11	7.647	0.466	−0.627	−0.292
65	22.794	−0.230	−0.714	0.164
67	23.304	0.226	0.535	0.121
72	24.621	0.850	−0.461	−0.392
73	24.720	−0.535	−0.316	0.169

Table 3.11 Modal information at Support 4 in direction Y

Mode	Frequency (Hz)	Participation factor	Modal shape	Contribution factor
1	4.44	3.423	0.051	0.173
2	4.44	−2.243	−0.033	0.074
9	14.57	1.620	0.180	0.291
10	14.57	−1.028	−0.114	0.117
14	24.78	0.509	0.182	0.093
18	30.72	0.936	0.327	0.306
24	43.29	0.519	0.225	0.117
25	43.29	−0.472	−0.205	0.097
31	52.36	0.292	0.096	0.028
32	52.36	0.288	0.095	0.027
37	64.46	2.130	−0.117	−0.249
38	64.46	1.745	−0.096	−0.167
45	88.65	−2.172	−0.034	0.073

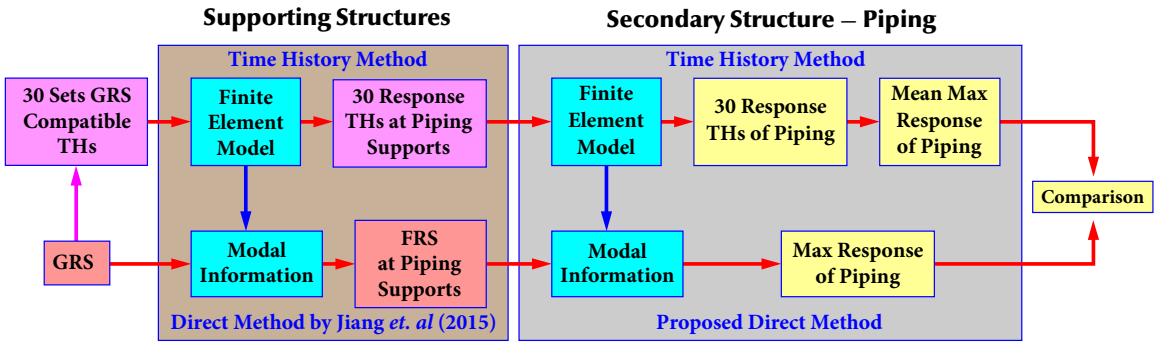

Figure 3.6 Procedure of the numerical example: generating response.

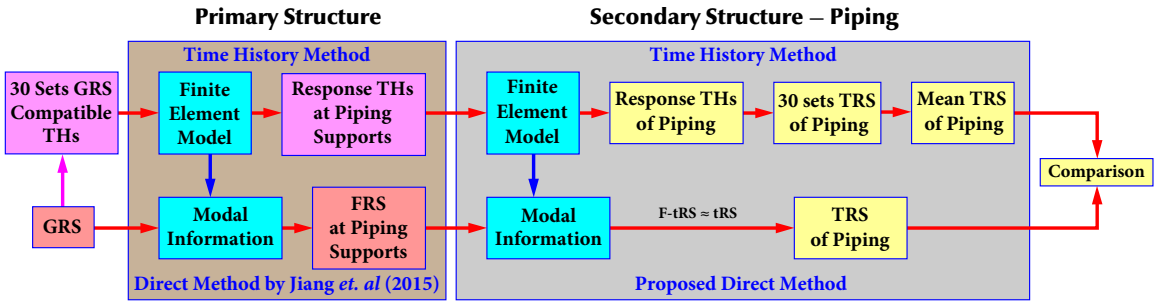

Figure 3.7 Procedure of the numerical example: generating TRS.

of the system. The average response of the piping system from 30 time history analyses is regarded as the benchmark. It should be noted that both time history analysis and direct method are based on the decoupled analysis, which the primary and secondary systems are considered individually.

The procedures for the generation of TRS is almost the same with generating response of secondary structures, shown as Figure 3.7. FRS at the supports of piping system and the modal information of the piping, which have already been obtained in the generation of responses, are utilized to generate TRS using the direct method developed in Chapter 2. In time history analysis, the response time histories at the supports of the piping system are input to a set of oscillators with different natural frequencies to obtain the corresponding response spectra, i.e., TRS. The average TRS from 30 time history analyses is regarded as the benchmark to validate the accuracy to the proposed method for generating TRS.

As can be seen from Figures 3.6 and 3.7, only GRS, tRS, and the model information of the supporting buildings and the piping system are needed in the proposed direct methods for the generation of responses and TRS, which makes the methods convenient and widely applicable in practical engineering designs.

3.3.2 Results of Response

Validation of the Input Response Spectra

Errors exists in the implementation of the most of the previous spectra methods on the response of secondary structure because an accurate FRS was not available unless a large number of time history analyses are performed. In this case, the direct method in seismic analysis loses its superiority in efficiency comparing with the time history method. This shortcoming in the previous application has been eliminated by using the direct method proposed by Jiang *et al.* (2015) for structures with single support and the direct method derived in Chapter 2 in this study for multi-supported structures.

FRS at Supports 1 and 4 of the piping, which are located on service building and reactor building, respectively, are presented in Figures 3.8 and 3.9, respectively. It can be seen that FRS obtained by the direct method agrees extremely well with the benchmark FRS which are the mean FRS from 30 time history analyses. The relative errors at FRS peaks are less than 3% except for the second peak of FRS at Support 4, which is 6.1%. However, it is still acceptable when comparing with a single time history analysis. which can result in a maximum 36.2% or a minimum -12.9% of error. It further proves that the direct method developed in Chapter 2 can generate FRS accurately and efficiently for complex three-dimensional finite element structural models with closely-spaced modes under seismic inputs.

It is found that large variabilities exist in FRS generated by time history analysis. For example, the FRS in direction Y at Support 4 obtained from an individual time history analysis can be over-estimated by up to 37.3%, while the FRS could also be underestimated by 22.1% depending on the individual set of time histories used. Therefore, a large number of time history analyses have to be conducted in order to obtain reliable FRS in the previous implementations of various direct methods, which is very time-consuming.

With the reliable FRS available, the seismic analysis of secondary systems using the direct spectra-to-spectra method can be approached. The generated FRS are treated as fully-correlated for supports on the same building, whereas they are regarded as uncorrelated if the supports are on different buildings.

Response of the Piping System by Time History Method

The acceleration response results of Nodes 2, 7, and 10 of the piping obtained by time history method are listed in Table 3.12. As can been seen from Table 3.12, the maximum mean response is $4.21g$ occurring in the X-direction of Node 7, while the minimum is $0.41g$ in the Z-direction of Node 10. To better illustrate the results, the relative errors of Node 7 in the X-direction and that of Node 10 in the Z-direction are plotted against the set of time history analysis in Figure 3.10. It can be seen from Figure 3.10 that the selection of time histories has a significant influence on the resultant response, despite that all of the time histories satisfy the code requirements and are compatible with the same response spectrum. For example, the relative error of Node 7 in the X-direction by time history set 19 is only -0.55% whereas the maximum and minimum error are 39.9% and -23.3%, respectively. Therefore, for a single or a small number of time history analyses, the result could be accurate (i.e., close to the benchmark), but it could also result in large error depending on the set of time histories used.

Comparing the results of the three nodes, time history method performs better at Node 10 with smaller variabilities in the results of individual time history analysis. However, there is still a 24% difference between the maximum and minimum relative errors. This means that the variabilities existed in time history method is not only affected by the input time histories, but is also influenced by the locations of structural nodes. Therefore, it is not possible to determine whether the response obtained by single time history analysis is either conservative or nonconservative, and/or by how much the gap is, making the result unreliable to be used in practical design. In order to obtain a reliable response, a large number of time history analyses must be performed.

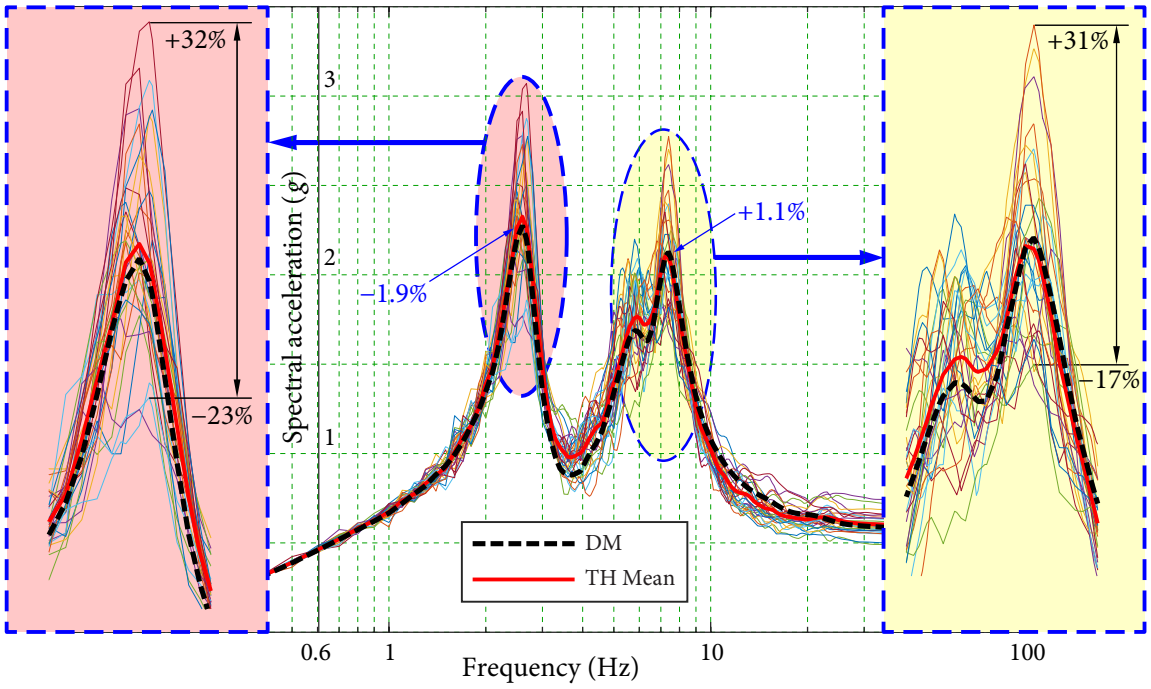

Figure 3.8 FRS at Support 1.

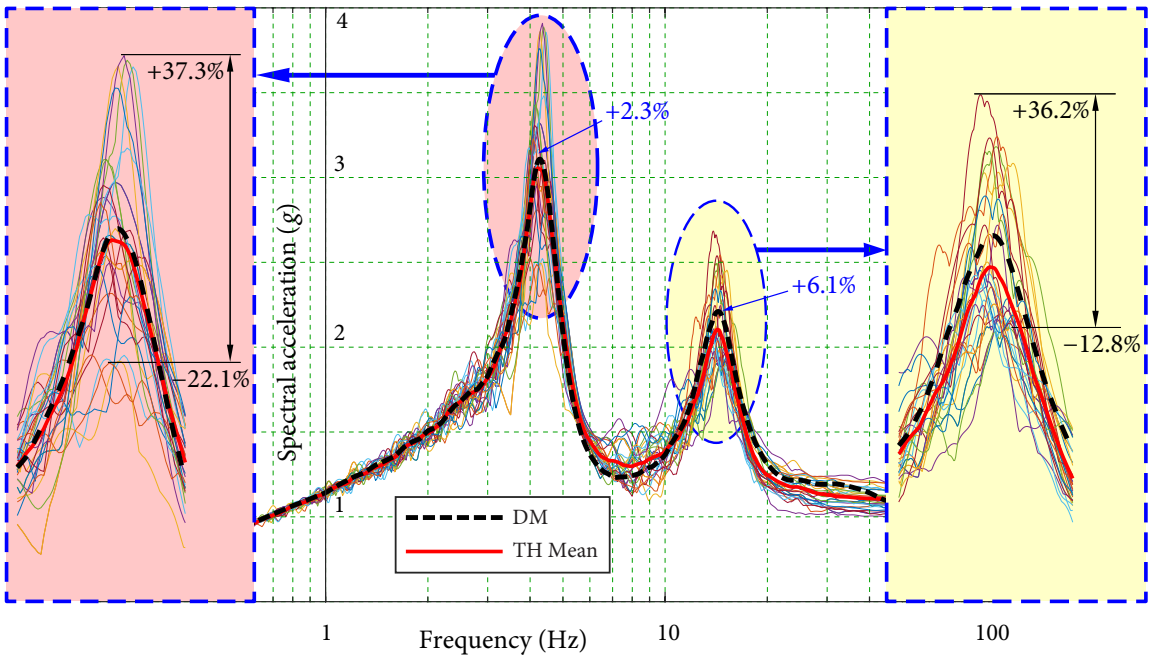

Figure 3.9 FRS at Support 4.

Table 3.12 Responses of piping using time history method

Node	Direction	Mean response (g)	Errors by different set of time history analysis (%)														
			1	2	3	4	5	6	7	8	9	10	11	12	13	14	15
2	x	2.09	4.50	11.06	20.05	−4.13	4.61	10.38	−13.49	15.61	1.74	1.85	−4.51	2.71	−13.56	−5.62	3.43
	y	0.98	4.68	−9.95	5.09	1.04	−2.65	11.57	−7.59	0.83	−12.60	−6.37	9.83	0.48	4.71	−3.75	0.46
	z	0.81	−7.39	27.59	25.02	11.73	26.85	−16.85	−7.29	3.52	3.95	1.48	9.62	1.44	−1.73	−0.81	−8.97
7	x	4.21	10.20	6.32	−2.68	4.14	−17.59	−2.25	−17.70	12.11	−18.33	34.44	−9.52	−7.86	19.29	7.99	28.54
	y	0.59	1.25	15.48	19.39	1.21	−6.10	7.40	−1.25	30.55	6.33	1.08	−9.97	25.04	18.70	4.58	29.27
	z	0.81	4.50	−6.45	−5.55	8.96	−7.72	−10.77	−7.60	8.35	−5.16	9.68	10.21	−4.57	−0.84	−0.23	6.64
10	x	0.83	−0.77	1.75	4.02	1.72	−1.63	−4.11	−0.36	−3.58	4.90	−4.05	2.77	−2.39	−0.64	5.87	8.29
	y	0.83	4.03	−0.75	−1.61	4.03	1.73	−3.56	−4.09	−0.34	−4.03	2.79	4.92	−0.63	5.89	−2.38	−0.63
	z	0.41	−0.86	14.66	0.81	−1.29	−2.46	3.50	3.50	−3.15	−4.89	4.13	−4.89	−6.88	1.19	2.37	4.48

16	17	18	19	20	21	22	23	24	25	26	27	28	29	30	Max	Min
−7.97	−3.88	−3.25	−17.50	5.74	−4.74	−7.90	15.82	−8.89	−4.76	0.40	0.00	−7.63	−0.93	10.86	20.05	−17.50
5.72	−4.74	2.11	−9.92	−3.14	2.29	−12.56	0.15	2.08	−1.64	5.17	7.74	1.84	5.56	3.55	11.57	−12.60
1.30	−2.05	−2.22	−17.25	2.41	−8.46	−2.74	−9.62	0.11	−0.61	5.97	−0.50	−11.32	−10.63	−12.58	27.59	−17.25
−8.42	5.62	5.88	−0.55	−18.65	39.94	33.42	−12.69	−22.24	−21.02	−23.26	−10.93	−5.88	−15.31	7.00	39.94	−23.26
0.42	−26.08	−13.64	−2.87	−33.04	−14.07	−21.15	2.54	−9.81	13.65	−23.63	14.69	17.95	−17.95	−30.00	30.55	−33.04
3.50	−20.67	34.14	−33.06	0.26	2.96	20.83	8.28	−20.22	−6.80	−13.68	−2.72	6.48	13.53	7.69	34.14	−33.06
−1.91	−0.87	−1.93	−5.06	−0.87	−4.11	−0.49	−2.33	0.21	4.65	−8.39	4.79	−3.01	−1.54	9.09	9.09	−8.39
1.71	1.71	−0.85	−1.91	−5.05	0.23	−4.10	−0.47	−2.32	4.81	4.66	−8.38	9.11	−2.99	−1.53	9.11	−8.38
−0.17	−2.52	3.08	3.08	−2.52	−0.63	−9.35	−7.47	−0.63	−2.01	−2.01	−1.35	−0.99	5.60	7.65	14.66	−9.35

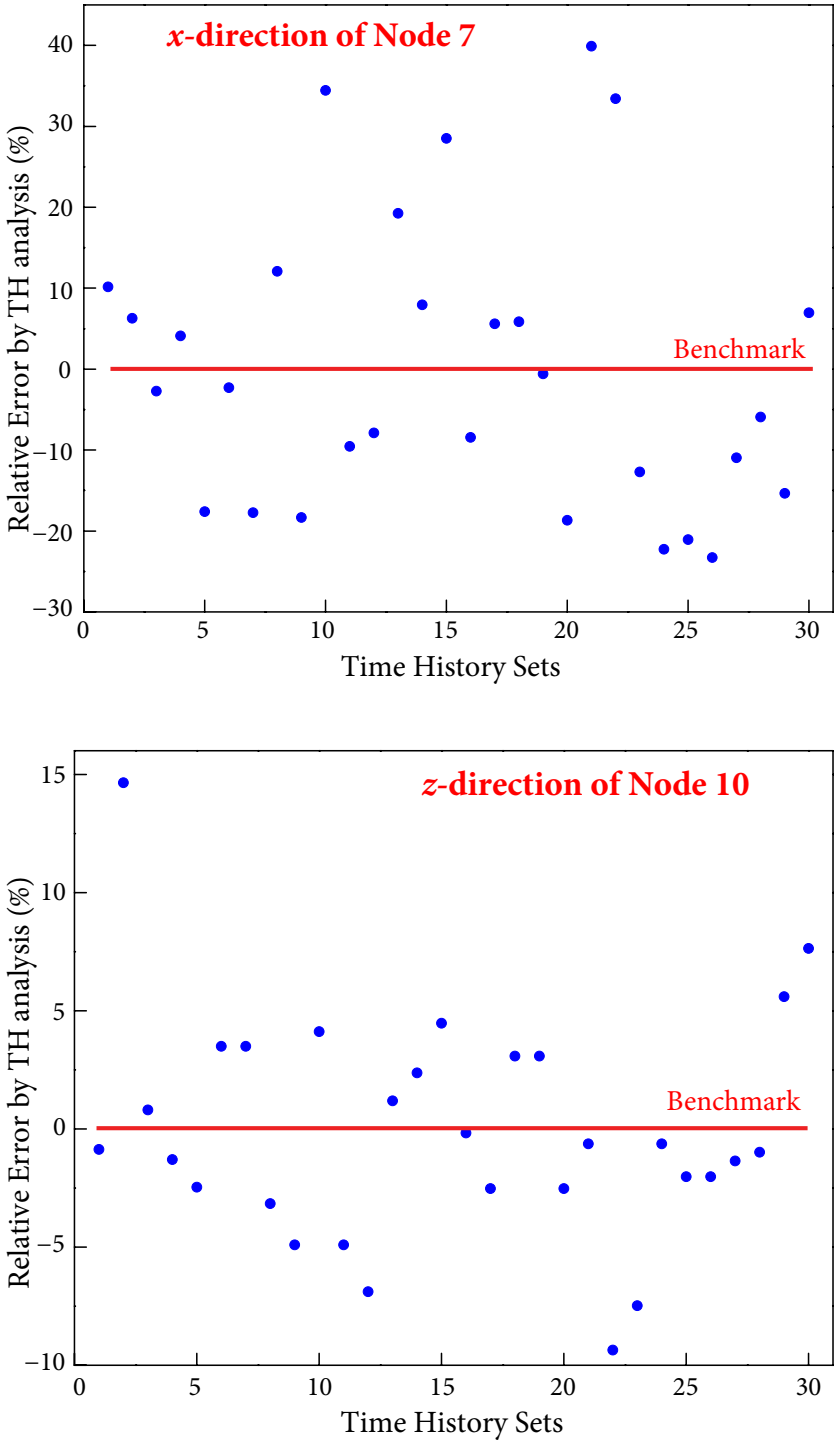

Figure 3.10 Relative errors by time history method of nodes 7 and 10.

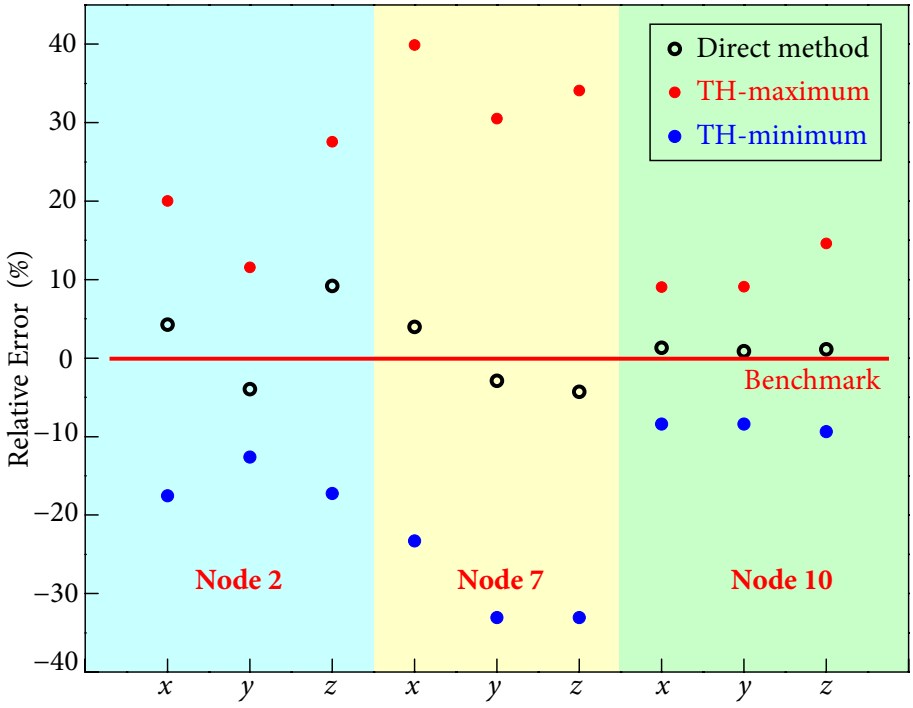

Figure 3.11 Comparison between the results by DM and TH analysis.

Response of the Piping System by the Direct Method

The responses obtained by the proposed direct method and the relative errors are listed in Table 3.13. The errors in the horizontal directions X and Y are found to be less than 4.5% for all DOF, indicating that the responses by the proposed direct method are accurate. The minimum error is 0.91% in direction Y of Node 10, while maximum error occurs at Node 2 in the Z-direction with a overestimation of 9.2%. Although this error is relatively large, it still acceptable when compare with the maximum error by a single time history analysis, which is 27.6% in this DOF. Therefore, the overall accuracy of seismic evaluation of the piping system by the proposed direct method is much better than that by single or small number of time history method. With the application of the proposed method, the deficiency and variability of time history analysis can be avoided.

To better illustrate the advantages of the proposed direct method, the relative errors by the direct method and time history method are plotted in Figure 3.11. Comparing with

Table 3.13 Responses of piping using using direct method

	Node 2			Node 7			Node 10		
Direction	x	y	z	x	y	z	x	y	z
Response-TH mean (g)	2.09	0.98	0.81	4.21	0.59	0.81	0.83	0.83	0.41
Response-DM (g)	2.18	0.94	0.88	4.38	0.57	0.78	0.85	0.84	0.41
Relative Error (%)	4.29	−3.93	9.21	4.02	−2.88	−4.29	1.32	0.91	1.12
Error-DM-Case **A** (%)	4.29	−3.93	9.21	15.35	10.22	20.77	1.32	0.91	1.12
Error-DM-Case **B** (%)	−26.25	−32.06	−22.46	4.02	−2.88	−4.29	−28.35	−28.64	−28.13

the maximum and minimum errors by time history method, the results by the proposed method agree well with the benchmark. Therefore, the proposed direct method can give maximum acceleration responses of structures under earthquake excitations from multiple supports efficiently and accurately.

Validation of the Approximation on the Correlation between FRS

To verify the feasibility of the approximation on the correlation between FRS at different locations, two additional cases are also conducted. In Case **A**, FRS at the supports of piping are all treated as fully-correlated, while they are all regarded as independent in Case **B**.

The results of Case **A** and Case **B** are presented in Table 3.13. The supports adjacent to Node 7, i.e., Supports 3 and 4, are on different buildings, and it is observed that the errors at this node increases significantly in Case **A**. For example, the relative error in direction Y increased from -2.88% to 10.22% if the FRS at the supports are treated as fully-correlated, indicating that it is not appropriate to treat FRS at nodes on different buildings as fully-correlated. By comparing with Case **B**, it is found that the independent approximation is reasonable for such nodes. On the other hand, the supports adjacent to Nodes 2 and 10 are on the same building. The errors at these nodes in Case **B** are about 28%, which is much greater than the fully-correlated case. Thus, it demonstrates that it is appropriate to treat the FRS of nodes on the same building as fully-correlated.

In principle, FRS at nodes on the same building should be correlated but not fully-correlated. On the other hand, they could have certain correlations even the supports are located on different buildings. Therefore, the proposed assumption on the correlation of FRS could cause some errors such as the response of Node 2 in direction Z (9.1%).

However, the proposed method allows the response of secondary system to be evaluated efficiently because only structural information and the input response spectra are needed. Furthermore, the generated response is of good accuracy especially when comparing with the result by single time history analysis. Therefore, the proposed method has its superiority in this aspect.

3.3.3 Results of TRS

The TRS of Nodes 2, 7, and 10 obtained from both time history analysis and the direct spectra-to-spectra method are presented in Figures 3.12, 3.13, and 3.14, respectively. These TRS are calculated at over 200 frequencies including the natural frequencies of the structures. The mean TRS obtained from 30 sets of time history analyses, which are considered as the benchmark TRS, are highlighted by red solid lines, the TRS generated by the proposed method are represented as black dashed lines.

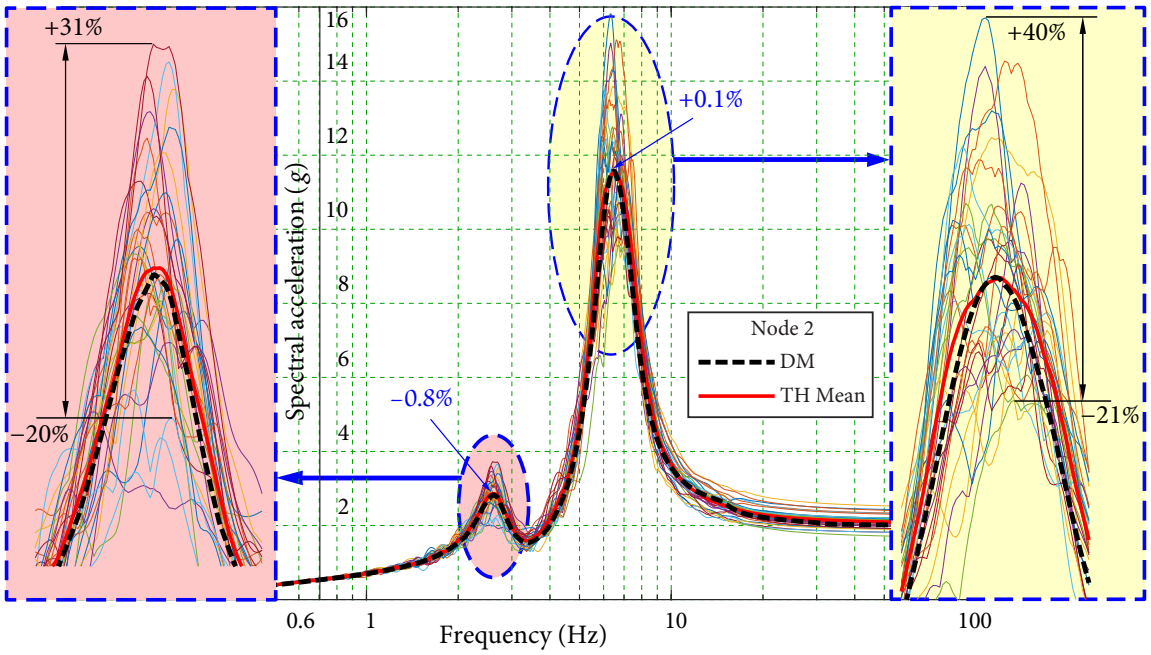

Figure 3.12 TRS at Node 2.

It is seen that TRS generated by the direct method agree extremely well with the benchmark TRS over the entire frequency range. The maximum relative error at main peaks by direct method is only -3.6% occurring at Node 7. Although the error of -8.1% at the sec-

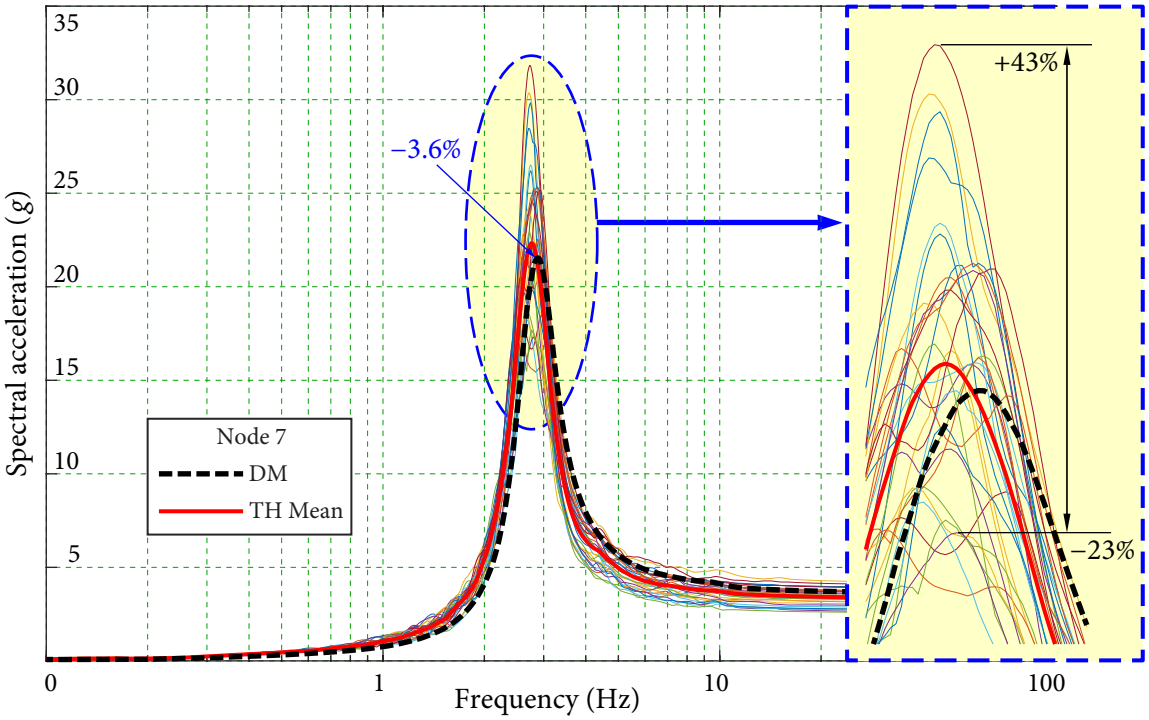

Figure 3.13 TRS at Node 7.

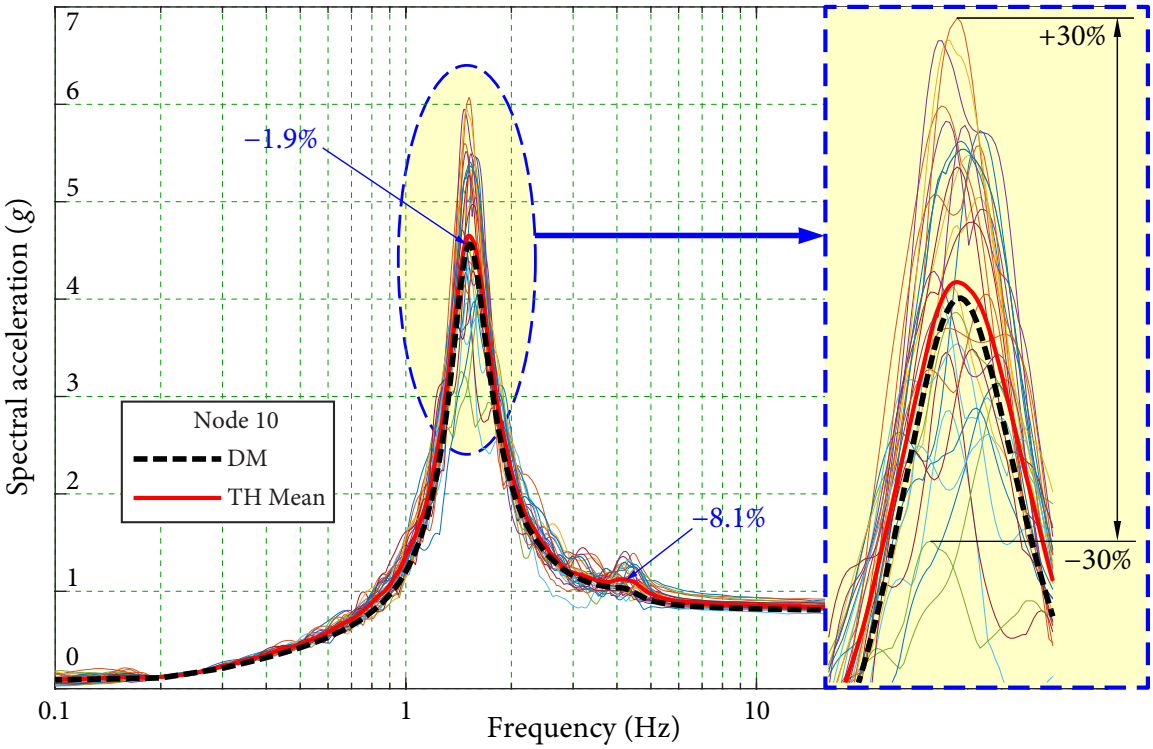

Figure 3.14 TRS at Node 10.

ond peak of Node 10 is relatively large, it does not have a significant influence on practical seismic design, because TRS at this peak is small comparing with TRS at the main peak.

However, very large variabilities are observed in the TRS generated by time history analysis, particularly at the peaks. This numerical example demonstrates that time history analysis can lead to approximately 43% overestimate or 30% underestimate at the TRS peaks, even though the time histories satisfy the compatibility requirements to the target GRS specified by codes and standards. Furthermore, it is observed that TRS from a single time history analysis may be over-conservative at some TRS peaks but nonconservative at other peaks. Therefore, the results of a single time history analysis could be over-conservative or nonconservative, depending on which set of seismic inputs is used. If a single or a small number of time history analyses are performed, the results are not reliable.

In summary, significant time and computational resources are needed to obtain reliable FRS or TRS using time history method by performing a large number of time history analyses; whereas the proposed direct method can avoid these problems and give accurate FRS or TRS.

Validating the Approximation on the Correlation between FRS: Comparing TRS

Similar to Section 3.3.2, two additional cases, i.e., Case 3 (all FRS of supports are fully-correlated) and Case 4 (all FRS of supports are uncorrelated), are also performed to further verify the approximation on the correlation between FRS at the supports. The results of TRS at Nodes 2, 7, and 10 are shown in Figure 3.15.

The supports adjacent to Node 7 are on different buildings and it is observed that the errors at this node are almost doubled in Case 3 comparing with the proposed method. It indicates that it is not appropriate to treat the FRS at nodes on different buildings as fully-correlated. By comparing with Case 4, it is found that the uncorrelated approximation is reasonable for such supports. On the other hand, the supports adjacent to Nodes 2 and 10 are on the same building. The results in Case 4 show that there are approximately 30% underestimation of TRS at the main peaks, whereas the errors are much smaller in Case 3, which are 0.1% and -3.6%, respectively. Hence, it means that it is appropriate to treat the FRS of supports on the same building as fully-correlated.

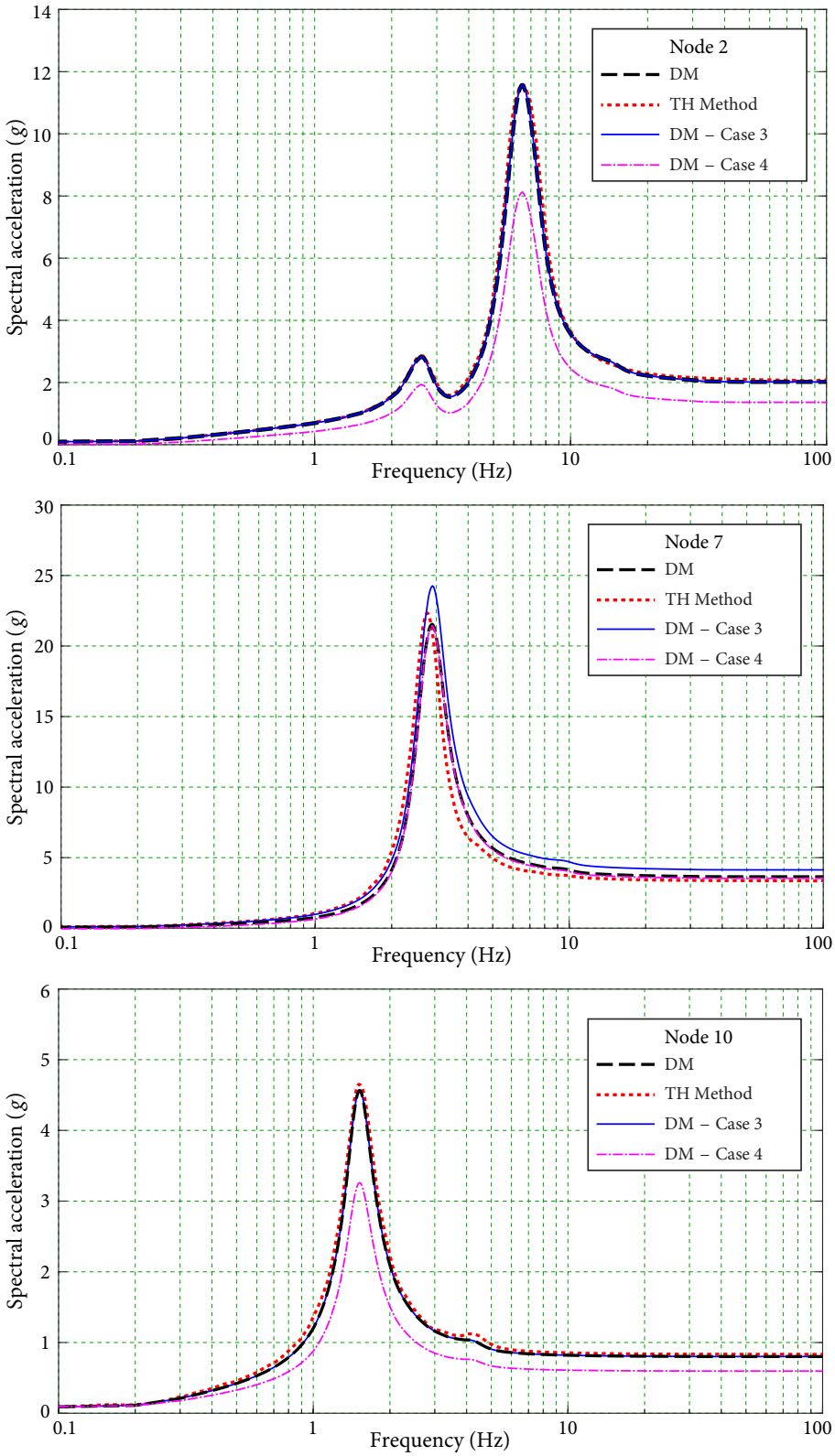

Figure 3.15 Comparison of TRS from different cases.

Comparing with the result of all the cases, TRS by the proposed method (i.e., the black dashed lines in Figure 3.15) agree extremely well with the benchmark results for all nodes over the entire frequency range. Therefore, the approximations of the correlation between FRS at supports are suitable for generating TRS for secondary structures, such as piping systems, mounted on different buildings.

Comparison between tRS and F-tRS

To validate the accuracy of using tRS as an approximation of F-tRS in generating TRS, the amplification ratio (AR) between tRS and GRS obtained by Li *et al.* (2015) is compared with that of F-tRS benchmark obtained from 30 time history analyses, as shown in Figure 3.16.

It is shown that F-tRS follows similar statistical relationship as tRS, although there are some discrepancies, especially for the frequency range from 8 Hz to 13 Hz. The discrepancies are conceptually reasonable based on the theory of random vibration. In random vibration, the response of an oscillator depends on the bandwidth of the seismic inputs. The ground motions, which are generally regarded as wide-band processes, have wider bandwidth than floor responses, which are usually narrow-band processes. This means tRS (based on ground motions) should be larger than F-tRS (based on floor responses) in the most of frequency ranges, as indicated by Figure 3.16. Therefore, the tertiary response spectra TRS generated using tRS are expected to be more conservative than those using F-tRS.

This study shows that the error caused by the use of tRS in generating TRS is acceptable as the obtained TRS is of remarkable accuracy. Therefore, it is appropriate to use tRS as an approximation of F-tRS for the generation of TRS. In some specific practical problems, however, this error could be larger when the main frequencies of floor responses are located within certain frequency ranges, for example, 8 Hz to 13 Hz. This error is expected to be reduced significantly by avoiding the use of tRS as an approximation of F-tRS when a more reliable F-tRS is available. It should be noted that the mean F-tRS obtained from 30 time history analyses in this study is not "exact". It is used as a benchmark because more statistical analyses on F-tRS are needed to obtain more accurate F-tRS in the future.

The direct method in generating TRS using ttRS is currently not available, as mentioned in Section 3.2. Therefore, statistical analyses between ttRS and tRS as well as a comprehensive theoretical derivation should be conducted in future study to develop the direct method for generating TRS using ttRS directly. Once the method has been developed, not only the use of tRS can be avoided, but also the procedure for generating TRS can be further simplified.

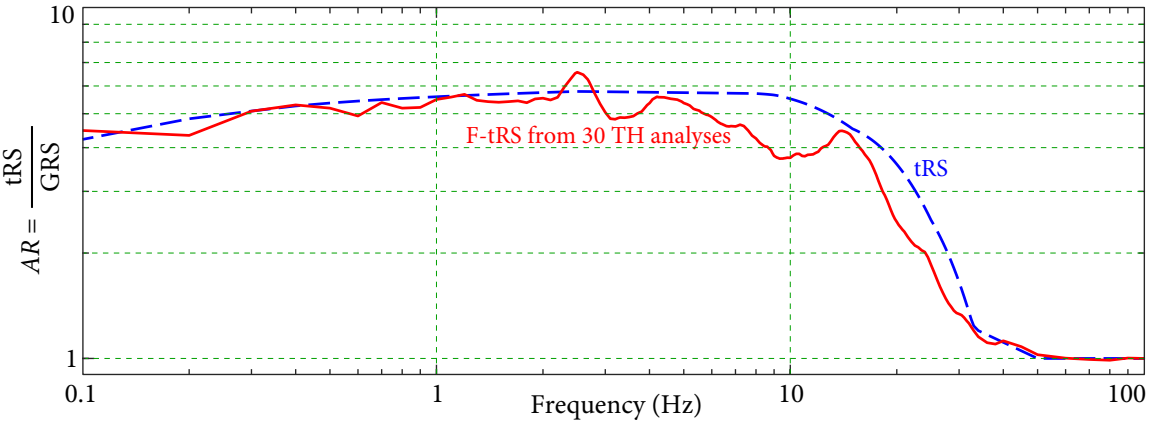

Figure 3.16 Comparison between tRS and F-tRS benchmark.

3.4 Summary

In this chapter, direct spectra-to-spectra methods for the accurate and efficient generation of the responses and TRS of multiply supported secondary structures are developed. Starting with the fundamentals in structural dynamics, the absolute response of system is derived. The expression of the absolute response consists of two parts which are related to the dynamic modal response and ground motions, respectively, which are further combined using the combination coefficients derived by theory of random vibration. On the other hand, the direct method proposed in Chapter 2 is validated to be applicable for the generation of TRS for secondary structures with multiple supports. To obtain TRS, FRS by direct method proposed by Jiang *et al.* (2015) or developed in Chapter 2 can be either applied depending on the foundation property of primary structures. The obtained FRS is then regarded as the input of secondary system and is applied together with the direct method to evaluate TRS.

In the generation of response and TRS of secondary structure with multiple supports, the correlation coefficients of FRS at different supports of a secondary structure can be approximated as follows:

- FRS can be treated as fully correlated if the supports are on the same building;
- FRS are considered as independent if the supports are on different buildings.

Moreover, the actual F-tRS in the generation of TRS is assumed to be close to tRS proposed by Li *et al*. (2015) so that time history analysis can be totally avoided. These assumptions are validated to be reasonable and can give acceptable results for the generation of both response and TRS.

A numerical example of a piping system mounted on two structure at different supports, which are subjected to tri-directional seismic inputs at foundation level, is presented. The responses and TRS determined by the proposed direct spectra-to-spectra methods agree well with the benchmarks, which are obtained through 30 time history analyses. It is demonstrated that the response as well as TRS determined by time history analyses have large variabilities. Hence, results by time history methods using a single set or a small number of sets of spectrum-compatible tri-directional time histories are not reliable. The proposed direct spectra-to-spectra methods are verified to be applicable for the seismic evaluation of secondary structures with multiple supports.

CHAPTER 4

Generating Floor Response Spectra for Structures under Excitations from Multiple Supports Considering Soil-Structure Interaction

The soil-structure interaction (SSI) must be considered when the supporting soil is relatively soft or the superstructure is massive (Wolf, 1985; 1987). Although high-level earthquake can cause nonlinear behavior in soil, the soils presented in this research are assumed to behave linearly. This is because the soil-structure interaction for earthquake excitations generally assumes the law of superposition to be applicable (Wolf, 1985). In other words, the seismic response is the sum of the free-field response and the response due to interaction where the superstructure is inserted, while conventional site response analysis of free-field soil typically assumes linear soil behavior. The main objective of this chapter is to develop a new direct method that considers SSI effects. To study the effect of soil nonlinearity, a complete understanding and verification of linear soil-structure interaction is necessary. Therefore, this study assumes soil behavior to be linear. Soil nonlinearity may be considered in future research.

4.1 General Formulation

4.1.1 Substructure Method

Dynamic Stiffness Matrix

For an MDOF linear system, the equation of motion is of the form

$$\mathbf{M}\ddot{\mathbf{x}}(t) + \mathbf{C}\dot{\mathbf{x}}(t) + \mathbf{K}\mathbf{x}(t) = \mathbf{p}(t), \tag{4.1.1}$$

where $\mathbf{M}$, $\mathbf{C}$, $\mathbf{K}$ are the mass, damping, and stiffness matrices, respectively, $\mathbf{p}(t)$ is the load vector, and $\mathbf{x}(t)$ is the response vector. Under harmonic excitation $\mathbf{p}(t) = \mathbf{P}e^{i\omega t}$, the response $\mathbf{x}(t)$ can be expressed as $\mathbf{x}(t) = \mathbf{X}e^{i\omega t}$, and equation (4.1.1) becomes

$$\mathbf{S}\mathbf{X} = \mathbf{P}, \qquad \mathbf{S} = -\omega^2\mathbf{M} + i\omega\mathbf{C} + \mathbf{K}, \tag{4.1.2}$$

where $\mathbf{S}$ is the frequency-dependent *dynamic stiffness matrix*. In terms of the dynamic stiffness matrix, equation of motion (4.1.1) can be expressed as an equation of dynamic equilibrium (4.1.2).

Substructure Model for Flexible Foundation

A coupled soil–structure model is shown in Figure 4.1. Let $\mathbf{U}_{\mathrm{R}}$ and $\mathbf{U}_{\mathrm{B}}$ be the amplitudes of the absolute displacement vectors of the structure and the foundation, respectively, where the subscript "R" stands for the "Response" DOF (nodes), which are not in contact with the soil, the subscript "B" stands for the "Boundary" DOF (nodes), which are on the boundary of soil–structure interface, and the superscript "s" stands for "Structure". The equation of dynamic equilibrium of the structure is given by

$$\begin{bmatrix} \mathbf{S}^{\mathrm{S}}_{\mathrm{RR}} & \mathbf{S}^{\mathrm{S}}_{\mathrm{RB}} \\ \mathbf{S}^{\mathrm{S}}_{\mathrm{BR}} & \mathbf{S}^{\mathrm{S}}_{\mathrm{BB}} \end{bmatrix} \begin{Bmatrix} \mathbf{U}_{\mathrm{R}} \\ \mathbf{U}_{\mathrm{B}} \end{Bmatrix} = \begin{Bmatrix} \mathbf{P}_{\mathrm{R}} \\ \mathbf{P}_{\mathrm{B}} \end{Bmatrix}, \tag{4.1.3}$$

where $\mathbf{P}_{\mathrm{R}}$ is the amplitude vector of the loads applied to the response nodes of the structure, and $\mathbf{P}_{\mathrm{B}}$ is the amplitude vector of the interaction forces between the structure and soil. For earthquake excitation, the nodes of the structure not in contact with the soil are not loaded, i.e., $\mathbf{P}_{\mathrm{R}} = \mathbf{0}$.

Let $\mathbf{S}^{\mathrm{G}}_{\mathrm{BB}}$ be the dynamic stiffness matrix of the soil with excavation, and $\mathbf{U}^{\mathrm{G}}_{\mathrm{B}}$ be the amplitudes of the absolute displacement vector of the soil with excavation under the earthquake

excitation. The superscript "G" stands for "Ground" or the soil with excavation. The interaction forces of the soil depend on the relative motion between the foundation (base) and the soil at the interface, i.e.,

$$\mathbf{P}_{\mathrm{B}} = \mathbf{S}^{\mathrm{G}}_{\mathrm{BB}} (\mathbf{U}^{\mathrm{G}}_{\mathrm{B}} - \mathbf{U}_{\mathrm{B}}). \tag{4.1.4}$$

Equation (4.1.3) becomes

$$\begin{bmatrix} \mathbf{S}^{\mathrm{S}}_{\mathrm{RR}} & \mathbf{S}^{\mathrm{S}}_{\mathrm{RB}} \\ \mathbf{S}^{\mathrm{S}}_{\mathrm{BR}} & \mathbf{S}^{\mathrm{S}}_{\mathrm{BB}} + \mathbf{S}^{\mathrm{G}}_{\mathrm{BB}} \end{bmatrix} \begin{Bmatrix} \mathbf{U}_{\mathrm{R}} \\ \mathbf{U}_{\mathrm{B}} \end{Bmatrix} = \begin{Bmatrix} \mathbf{0} \\ \mathbf{S}^{\mathrm{G}}_{\mathrm{BB}} \mathbf{U}^{\mathrm{G}}_{\mathrm{B}} \end{Bmatrix}. \tag{4.1.5}$$

The earthquake excitation is characterized by $\mathbf{U}^{\mathrm{G}}_{\mathrm{B}}$, which is the motion of the nodes on the soil–structure interface of the soil with excavation. It is desirable to replace $\mathbf{U}^{\mathrm{G}}_{\mathrm{B}}$ by the free-field motion $\mathbf{U}^{\mathrm{F}}_{\mathrm{B}}$ that does not depend on the excavation.

Free-Field Soil Model

The free-field soil can be divided into the excavated soil and the soil with excavation as shown in Figure 4.1. Regarding the excavated soil as a "structure" and referring to equation (4.1.5), one has $\tilde{\mathbf{U}}_{\mathrm{B}} = \mathbf{U}^{\mathrm{F}}_{\mathrm{B}}$, $\tilde{\mathbf{S}}^{\mathrm{S}}_{\mathrm{BR}} = \mathbf{0}$, and hence $\tilde{\mathbf{S}}^{\mathrm{S}}_{\mathrm{BB}} = \mathbf{S}^{\mathrm{E}}_{\mathrm{BB}}$, which is the dynamic stiffness matrix of the excavated soil. The superscript "E" stands for "Excavated soil". The second block-row of equation (4.1.5) gives

$$\begin{bmatrix} \tilde{\mathbf{S}}^{\mathrm{S}}_{\mathrm{BR}} & \tilde{\mathbf{S}}^{\mathrm{S}}_{\mathrm{BB}} + \mathbf{S}^{\mathrm{G}}_{\mathrm{BB}} \end{bmatrix} \begin{Bmatrix} \times \\ \mathbf{U}^{\mathrm{F}}_{\mathrm{B}} \end{Bmatrix} = \left\{ \mathbf{S}^{\mathrm{G}}_{\mathrm{BB}} \mathbf{U}^{\mathrm{G}}_{\mathrm{B}} \right\} \implies (\mathbf{S}^{\mathrm{E}}_{\mathrm{BB}} + \mathbf{S}^{\mathrm{G}}_{\mathrm{BB}}) \mathbf{U}^{\mathrm{F}}_{\mathrm{B}} = \mathbf{S}^{\mathrm{G}}_{\mathrm{BB}} \mathbf{U}^{\mathrm{G}}_{\mathrm{B}}. \tag{4.1.6}$$

Adding the excavated soil to the soil with excavation leads to the free-field system, i.e.,

$$\mathbf{S}^{\mathrm{E}}_{\mathrm{BB}} + \mathbf{S}^{\mathrm{G}}_{\mathrm{BB}} = \mathbf{S}^{\mathrm{F}}_{\mathrm{BB}}, \quad \text{or} \quad \mathbf{S}^{\mathrm{G}}_{\mathrm{BB}} = \mathbf{S}^{\mathrm{F}}_{\mathrm{BB}} - \mathbf{S}^{\mathrm{E}}_{\mathrm{BB}}. \tag{4.1.7}$$

Hence, equation (4.1.6) can be written as

$$\mathbf{S}^{\mathrm{F}}_{\mathrm{BB}} \mathbf{U}^{\mathrm{F}}_{\mathrm{B}} = \mathbf{S}^{\mathrm{G}}_{\mathrm{BB}} \mathbf{U}^{\mathrm{G}}_{\mathrm{B}}, \tag{4.1.8}$$

in which $\mathbf{S}^{\mathrm{F}}_{\mathrm{BB}}$ is the dynamic stiffness matrix of the free-field discretized at the nodes where the structure is inserted, and $\mathbf{U}^{\mathrm{F}}_{\mathrm{B}}$ is the free-field motion at the nodes of the soil–structure interface. Hence, $\mathbf{U}^{\mathrm{F}}_{\mathrm{B}}$ is the free-field response of the soil at the foundation level; the

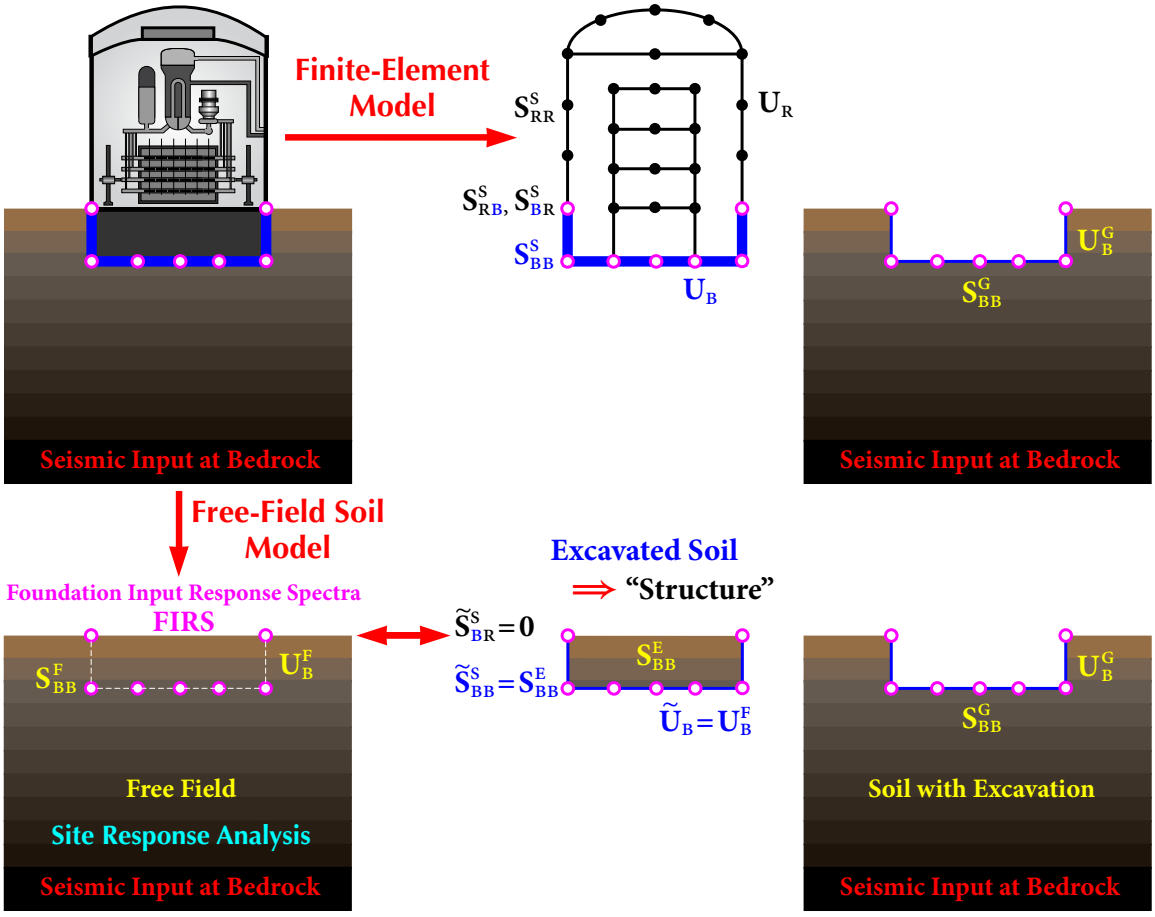

Figure 4.1 Substructural model for flexible foundation.

acceleration response spectra of $\ddot{\mathbf{u}}^F_B$ are the *Foundation Input Response Spectra* (FIRS), which can be obtained from a site response analysis of the free-field.

Using equation (4.1.8), equation (4.1.5) becomes

$$\begin{bmatrix} \mathbf{S}^S_{RR} & \mathbf{S}^S_{RB} \\ \mathbf{S}^S_{BR} & \mathbf{S}^S_{BB}+\mathbf{S}^G_{BB} \end{bmatrix} \begin{Bmatrix} \mathbf{U}_R \\ \mathbf{U}_B \end{Bmatrix} = \begin{Bmatrix} \mathbf{0} \\ \mathbf{S}^F_{BB}\,\mathbf{U}^F_B \end{Bmatrix}. \tag{4.1.9}$$

This is the equation of motion of the structure supported on a *generalized soil spring* characterized by the dynamic stiffness matrix $\mathbf{S}^G_{BB}$, and the other end of the spring is subjected to earthquake excitation $\mathbf{U}^F_B$, which is free-field response at the foundation level.

Using (4.1.7), equation (4.1.9) can also be written as

$$\begin{bmatrix} \mathbf{S}^{\mathrm{S}}_{\mathrm{RR}} & \mathbf{S}^{\mathrm{S}}_{\mathrm{RB}} \\ \mathbf{S}^{\mathrm{S}}_{\mathrm{BR}} & (\mathbf{S}^{\mathrm{S}}_{\mathrm{BB}} - \mathbf{S}^{\mathrm{E}}_{\mathrm{BB}}) + \mathbf{S}^{\mathrm{F}}_{\mathrm{BB}} \end{bmatrix} \begin{Bmatrix} \mathbf{U}_{\mathrm{R}} \\ \mathbf{U}_{\mathrm{B}} \end{Bmatrix} = \begin{Bmatrix} \mathbf{0} \\ \mathbf{S}^{\mathrm{F}}_{\mathrm{BB}} \mathbf{U}^{\mathrm{F}}_{\mathrm{B}} \end{Bmatrix}. \tag{4.1.10}$$

☞ A generalized soil spring, characterized by the dynamic stiffness matrix $\mathbf{S}^{\mathrm{G}}_{\mathrm{BB}}$, is not an elastic spring in the ordinary sense characterized by spring constant k.

Structure with Multiple Support Excitations

With $\mathbf{P}_{\mathrm{R}} = \mathbf{0}$, the first block-row of equation (4.1.3) becomes

$$\mathbf{S}^{\mathrm{S}}_{\mathrm{RR}} \mathbf{U}_{\mathrm{R}} + \mathbf{S}^{\mathrm{S}}_{\mathrm{RB}} \mathbf{U}_{\mathrm{B}} = \mathbf{0} \implies \mathbf{U}_{\mathrm{R}} = \mathbf{S}^{\mathrm{MS}} \mathbf{U}_{\mathrm{B}}, \quad \mathbf{S}^{\mathrm{MS}} = -\left(\mathbf{S}^{\mathrm{S}}_{\mathrm{RR}}\right)^{-1} \mathbf{S}^{\mathrm{S}}_{\mathrm{RB}}, \tag{4.1.11}$$

where $\mathbf{S}^{\mathrm{MS}}$ is the dynamic influence matrix for analysis of the structure with multiple support excitations, with the superscript "MS" standing for "Multiple Supports".

In seismic analysis and design, only translational ground motions are considered, while rotational ground motions are not considered. Reorganize vector $\mathbf{U}_{\mathrm{R}}$ and rewrite $\mathbf{U}_{\mathrm{B}}$ as

$$\mathbf{U}_{\mathrm{R}} = \begin{Bmatrix} \mathbf{U}_{\mathrm{R,T}} \\ \mathbf{U}_{\mathrm{R,R}} \end{Bmatrix}_{6N\times 1}, \qquad \mathbf{U}_{\mathrm{B}} = \begin{Bmatrix} \mathbf{U}^{\mathrm{MS}}_{\mathrm{I}} \\ \mathbf{0} \end{Bmatrix}_{6M\times 1}, \tag{4.1.12}$$

where the subscripts "T" and "R" stand for "Translational" and "Rotational" DOF, respectively. $\mathbf{U}^{\mathrm{MS}}_{\mathrm{I}}$ is the vector of seismic excitations in the three orthogonal translational directions at the multiple input nodes. Note that each "boundary" node "B" has six DOF; when seismic excitations at the soil–structure interface are considered, they are referred as "Input" nodes "I" with seismic excitations in the three orthogonal translational directions.

Rearranging and partitioning $\mathbf{S}^{\mathrm{MS}}$ accordingly, one has

$$\mathbf{S}^{\mathrm{MS}} = \begin{bmatrix} \mathbf{S}^{\mathrm{MS}}_{\mathrm{TT}} & \mathbf{S}^{\mathrm{MS}}_{\mathrm{TR}} \\ \mathbf{S}^{\mathrm{MS}}_{\mathrm{RT}} & \mathbf{S}^{\mathrm{MS}}_{\mathrm{RR}} \end{bmatrix}_{6N\times 6M}, \tag{4.1.13}$$

in which each submatrix is of dimension $3N\times 3M$. Equation (4.1.11) can be written as

$$\begin{Bmatrix} \mathbf{U}_{\mathrm{R,T}} \\ \mathbf{U}_{\mathrm{R,R}} \end{Bmatrix} = \begin{bmatrix} \mathbf{S}^{\mathrm{MS}}_{\mathrm{TT}} & \mathbf{S}^{\mathrm{MS}}_{\mathrm{TR}} \\ \mathbf{S}^{\mathrm{MS}}_{\mathrm{RT}} & \mathbf{S}^{\mathrm{MS}}_{\mathrm{RR}} \end{bmatrix} \begin{Bmatrix} \mathbf{U}^{\mathrm{MS}}_{\mathrm{I}} \\ \mathbf{0} \end{Bmatrix} = \begin{Bmatrix} \mathbf{S}^{\mathrm{MS}}_{\mathrm{TT}} \mathbf{U}^{\mathrm{MS}}_{\mathrm{I}} \\ \mathbf{S}^{\mathrm{MS}}_{\mathrm{RT}} \mathbf{U}^{\mathrm{MS}}_{\mathrm{I}} \end{Bmatrix}. \tag{4.1.14}$$

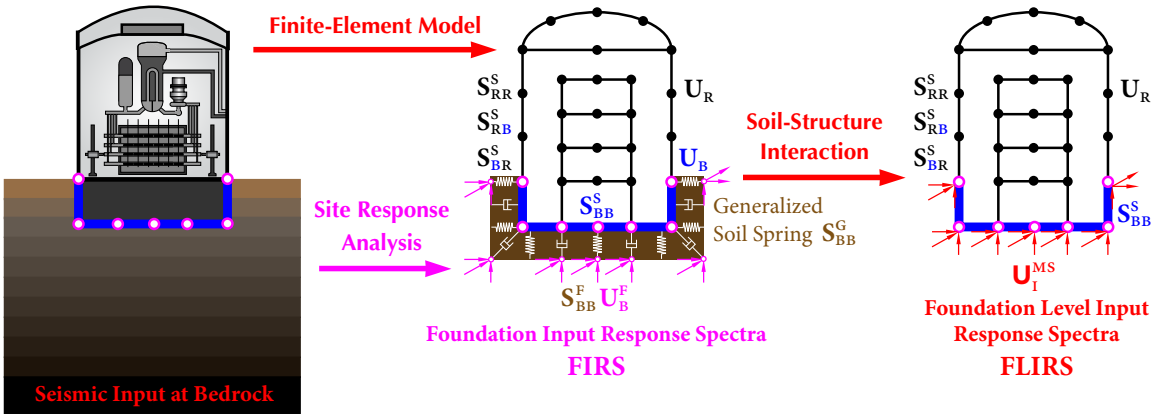

Figure 4.2 SSI using FLIRS for flexible foundation.

Multiplying the first block-row of equation (4.1.14) by $\left(\mathbf{S}_{TT}^{MS}\right)^T$ yields

$$\left(\mathbf{S}_{TT}^{MS}\right)^T \mathbf{U}_{R,T} = \left[\left(\mathbf{S}_{TT}^{MS}\right)^T \mathbf{S}_{TT}^{MS}\right] \mathbf{U}_{I}^{MS}. \tag{4.1.15}$$

The reason for performing this manipulation is to make $\left[\left(\mathbf{S}_{TT}^{MS}\right)^T \mathbf{S}_{TT}^{MS}\right]$ a square matrix of dimension $3M \times 3M$, the purpose of which will be clear in Section 4.1.2.

The tridirectional (translational) acceleration response spectra $\mathbf{U}_{I}^{MS}$ applied at multiple supports (nodes) of the flexible foundation of a structure are called *Foundation Level Input Response Spectra* (FLIRS), as shown in Figure 4.2. It is important to note that FLIRS are different from the *Foundation Input Response Spectra* (FIRS), which are the acceleration response spectra at the elevation of the foundation of the *free-field*, as illustrated in Figure 4.2.

4.1.2 Foundation Level Input Response Spectra (FLIRS)

It is desirable to determine the equivalent FLIRS for a structure with seismic excitations at multiple supports in seismic design and assessment. In SSI analysis, a seismic analysis of structures with multiple supports can be performed using the equivalent FLIRS as the seismic input, instead of a coupled soil–structure analysis using FIRS as the seismic input.

From the first block-row of equation (4.1.10), one obtains

$$\mathbf{U}_R = -\left(\mathbf{S}_{RR}^{S}\right)^{-1} \mathbf{S}_{RB}^{S} \mathbf{U}_B = \mathbf{S}^{MS} \mathbf{U}_B. \tag{4.1.16}$$

From the second block-row of equation (4.1.10), one has

$$\mathbf{S}_{\mathrm{BR}}^{\mathrm{S}}\,\mathbf{U}_{\mathrm{R}}+\left[\left(\mathbf{S}_{\mathrm{BB}}^{\mathrm{S}}-\mathbf{S}_{\mathrm{BB}}^{\mathrm{E}}\right)+\mathbf{S}_{\mathrm{BB}}^{\mathrm{F}}\right]\mathbf{U}_{\mathrm{B}}=\mathbf{S}_{\mathrm{BB}}^{\mathrm{F}}\,\mathbf{U}_{\mathrm{B}}^{\mathrm{F}}. \tag{4.1.17}$$

Substituting equation (4.1.16) into (4.1.17) yields

$$\mathbf{S}_{\mathrm{BR}}^{\mathrm{S}}\,\mathbf{S}^{\mathrm{MS}}\mathbf{U}_{\mathrm{B}}+\left[\left(\mathbf{S}_{\mathrm{BB}}^{\mathrm{S}}-\mathbf{S}_{\mathrm{BB}}^{\mathrm{E}}\right)+\mathbf{S}_{\mathrm{BB}}^{\mathrm{F}}\right]\mathbf{U}_{\mathrm{B}}=\mathbf{S}_{\mathrm{BB}}^{\mathrm{F}}\,\mathbf{U}_{\mathrm{B}}^{\mathrm{F}},$$

which gives

$$\underbrace{\mathbf{U}_{\mathrm{B}}}_{6M\times1}=\underbrace{\mathbf{S}^{-1}}_{6M\times6M}\;\underbrace{\mathbf{S}_{\mathrm{BB}}^{\mathrm{F}}}_{6M\times6M}\;\underbrace{\mathbf{U}_{\mathrm{B}}^{\mathrm{F}}}_{6M\times1},\qquad \mathbf{S}=\underbrace{\mathbf{S}_{\mathrm{BR}}^{\mathrm{S}}}_{6M\times6N}\;\underbrace{\mathbf{S}^{\mathrm{MS}}}_{6N\times6M}+\underbrace{\left(\mathbf{S}_{\mathrm{BB}}^{\mathrm{S}}-\mathbf{S}_{\mathrm{BB}}^{\mathrm{E}}\right)+\mathbf{S}_{\mathrm{BB}}^{\mathrm{F}}}_{6M\times6M}. \tag{4.1.18}$$

Note that $\mathbf{S}^{-1}\mathbf{S}_{\mathrm{BB}}^{\mathrm{F}}$ is a square matrix of dimension $6M\times6M$; partition it as follows:

$$\mathbf{S}^{-1}\mathbf{S}_{\mathrm{BB}}^{\mathrm{F}}=\mathbf{T}=\begin{bmatrix}\mathbf{T}_{\mathrm{TT}} & \mathbf{T}_{\mathrm{TR}}\\ \mathbf{T}_{\mathrm{RT}} & \mathbf{T}_{\mathrm{RR}}\end{bmatrix}_{6M\times6M}, \tag{4.1.19}$$

in which each submatrix is of dimension $3M\times3M$.

In a site response analysis, the soil medium is modelled as a series of infinite layers on a half-space, and the rotational responses of free-field should be very small under the translational excitation at bedrock. Hence, the rotational input at foundation level is negligible compared to the translational input; the rotational input is usually not given by a site response analysis and is taken as 0.

From equations (4.1.16) and (4.1.18), one has

$$\mathbf{U}_{\mathrm{R}}=\mathbf{S}^{\mathrm{MS}}\,\mathbf{T}\,\mathbf{U}_{\mathrm{B}}^{\mathrm{F}}, \tag{4.1.20}$$

i.e.,

$$\begin{aligned}\begin{Bmatrix}\mathbf{U}_{\mathrm{R,T}}\\ \mathbf{U}_{\mathrm{R,R}}\end{Bmatrix}_{6N\times1}&=\begin{bmatrix}\mathbf{S}_{\mathrm{TT}}^{\mathrm{MS}} & \mathbf{S}_{\mathrm{TR}}^{\mathrm{MS}}\\ \mathbf{S}_{\mathrm{RT}}^{\mathrm{MS}} & \mathbf{S}_{\mathrm{RR}}^{\mathrm{MS}}\end{bmatrix}_{6N\times6M}\begin{bmatrix}\mathbf{T}_{\mathrm{TT}} & \mathbf{T}_{\mathrm{TR}}\\ \mathbf{T}_{\mathrm{RT}} & \mathbf{T}_{\mathrm{RR}}\end{bmatrix}_{6M\times6M}\begin{Bmatrix}\mathbf{U}_{\mathrm{B,T}}^{\mathrm{F}}\\ \mathbf{0}\end{Bmatrix}_{6M\times1},\qquad \mathbf{U}_{\mathrm{B,T}}^{\mathrm{F}}=\mathbf{U}_{\mathrm{I}}^{\mathrm{F}},\\ &=\begin{bmatrix}\mathbf{S}_{\mathrm{TT}}^{\mathrm{MS}} & \mathbf{S}_{\mathrm{TR}}^{\mathrm{MS}}\\ \mathbf{S}_{\mathrm{RT}}^{\mathrm{MS}} & \mathbf{S}_{\mathrm{RR}}^{\mathrm{MS}}\end{bmatrix}\begin{bmatrix}\mathbf{T}_{\mathrm{TT}}\,\mathbf{U}_{\mathrm{I}}^{\mathrm{F}}\\ \mathbf{T}_{\mathrm{RT}}\,\mathbf{U}_{\mathrm{I}}^{\mathrm{F}}\end{bmatrix}=\begin{Bmatrix}\mathbf{S}_{\mathrm{TT}}^{\mathrm{MS}}\mathbf{T}_{\mathrm{TT}}\,\mathbf{U}_{\mathrm{I}}^{\mathrm{F}}+\mathbf{S}_{\mathrm{TR}}^{\mathrm{MS}}\mathbf{T}_{\mathrm{RT}}\,\mathbf{U}_{\mathrm{I}}^{\mathrm{F}}\\ \mathbf{S}_{\mathrm{RT}}^{\mathrm{MS}}\mathbf{T}_{\mathrm{TT}}\,\mathbf{U}_{\mathrm{I}}^{\mathrm{F}}+\mathbf{S}_{\mathrm{RR}}^{\mathrm{MS}}\mathbf{T}_{\mathrm{RT}}\,\mathbf{U}_{\mathrm{I}}^{\mathrm{F}}\end{Bmatrix}.\end{aligned} \tag{4.1.21}$$

Note that it is not possible to have a single set of tridirectional translational FLIRS in a dynamic analysis of a structure under seismic excitations at multiple supports to give both correct translational responses $\mathbf{U}_{\mathrm{R,T}}$ and rotational responses $\mathbf{U}_{\mathrm{R,R}}$. In the generation of FRS, only translational responses are needed; hence, from the first block-row of equation (4.1.21), one has

$$\mathbf{U}_{\mathrm{R,T}} = \mathbf{S}_{\mathrm{TT}}^{\mathrm{MS}} \mathbf{T}_{\mathrm{TT}} \mathbf{U}_{\mathrm{I}}^{\mathrm{F}} + \mathbf{S}_{\mathrm{TR}}^{\mathrm{MS}} \mathbf{T}_{\mathrm{RT}} \mathbf{U}_{\mathrm{I}}^{\mathrm{F}}. \tag{4.1.22}$$

Multiplying $\left(\mathbf{S}_{\mathrm{TT}}^{\mathrm{MS}}\right)^T$ from the left yields

$$\begin{aligned}
\left(\mathbf{S}_{\mathrm{TT}}^{\mathrm{MS}}\right)^T \mathbf{U}_{\mathrm{R,T}} &= \left\{\left(\mathbf{S}_{\mathrm{TT}}^{\mathrm{MS}}\right)^T \mathbf{S}_{\mathrm{TT}}^{\mathrm{MS}} \mathbf{T}_{\mathrm{TT}} + \left(\mathbf{S}_{\mathrm{TT}}^{\mathrm{MS}}\right)^T \mathbf{S}_{\mathrm{TR}}^{\mathrm{MS}} \mathbf{T}_{\mathrm{RT}}\right\} \mathbf{U}_{\mathrm{I}}^{\mathrm{F}} \\
&= \left[\left(\mathbf{S}_{\mathrm{TT}}^{\mathrm{MS}}\right)^T \mathbf{S}_{\mathrm{TT}}^{\mathrm{MS}}\right] \left\{\mathbf{T}_{\mathrm{TT}} + \left[\left(\mathbf{S}_{\mathrm{TT}}^{\mathrm{MS}}\right)^T \mathbf{S}_{\mathrm{TT}}^{\mathrm{MS}}\right]^{-1} \left(\mathbf{S}_{\mathrm{TT}}^{\mathrm{MS}}\right)^T \mathbf{S}_{\mathrm{TR}}^{\mathrm{MS}} \mathbf{T}_{\mathrm{RT}}\right\} \mathbf{U}_{\mathrm{I}}^{\mathrm{F}}. \\
&= \left[\left(\mathbf{S}_{\mathrm{TT}}^{\mathrm{MS}}\right)^T \mathbf{S}_{\mathrm{TT}}^{\mathrm{MS}}\right] \boldsymbol{\mathcal{T}} \mathbf{U}_{\mathrm{I}}^{\mathrm{F}},
\end{aligned} \tag{4.1.23}$$

where $\boldsymbol{\mathcal{T}}$ is called FLIRS transfer matrix in frequency domain given by

$$\underbrace{\boldsymbol{\mathcal{T}}}_{3M\times 3M} = \underbrace{\mathbf{T}_{\mathrm{TT}}}_{3M\times 3M} + \underbrace{\left[\left(\mathbf{S}_{\mathrm{TT}}^{\mathrm{MS}}\right)^T \mathbf{S}_{\mathrm{TT}}^{\mathrm{MS}}\right]^{-1}}_{(3M\times 3N)\times(3N\times 3M)} \underbrace{\left(\mathbf{S}_{\mathrm{TT}}^{\mathrm{MS}}\right)^T}_{3M\times 3N} \underbrace{\mathbf{S}_{\mathrm{TR}}^{\mathrm{MS}}}_{3N\times 3M} \underbrace{\mathbf{T}_{\mathrm{RT}}}_{3M\times 3M}. \tag{4.1.24}$$

The first and second terms of $\boldsymbol{\mathcal{T}}$ denote the contributions from the translational and rotational motions of the foundation in the soil–structure system, respectively. Because $\left[\left(\mathbf{S}_{\mathrm{TT}}^{\mathrm{MS}}\right)^T \mathbf{S}_{\mathrm{TT}}^{\mathrm{MS}}\right]$ is a square matrix of dimension $3M\times 3M$, it is relative easy to determine its inverse because M is much smaller than N. Thus, the purpose of the transformation in equation (4.1.15) becomes evident.

Comparing equations (4.1.23) and (4.1.15), one obtains the equivalent FLIRS as

$$\mathbf{U}_{\mathrm{I}}^{\mathrm{MS}} = \boldsymbol{\mathcal{T}} \mathbf{U}_{\mathrm{I}}^{\mathrm{F}}. \tag{4.1.25}$$

It is important to emphasize that, although the FLIRS $\mathbf{U}_{\mathrm{I}}^{\mathrm{MS}}$ would not give correct rotational responses $\mathbf{U}_{\mathrm{R,R}}$ of a structure, it gives exact translational responses $\mathbf{U}_{\mathrm{R,T}}$ and hence exact FRS because only translational responses are required to generate FRS. Therefore, a dynamic analysis of the structure under the seismic excitations of FLIRS $\mathbf{U}_{\mathrm{I}}^{\mathrm{MS}}$ at multiple supports gives exactly the same FRS as a fully coupled soil–structure analysis under the seismic excitations of FIRS $\mathbf{U}_{\mathrm{I}}^{\mathrm{F}}$.

Based on the theory of random vibration, the relationship between the PSD functions of $\mathbf{U}_{\mathrm{I}}^{\mathrm{MS}}$ and $\mathbf{U}_{\mathrm{I}}^{\mathrm{F}}$ can be determined by (Lin, 1967)

$$\boldsymbol{\mathcal{S}}_{\ddot{U}\ddot{U}}^{\mathrm{MS}}(\omega) = \boldsymbol{\mathcal{T}}(\omega)\,\boldsymbol{\mathcal{S}}_{\ddot{U}\ddot{U}}^{\mathrm{F}}(\omega)\,\tilde{\boldsymbol{\mathcal{T}}}(\omega), \tag{4.1.26}$$

where $\boldsymbol{\mathcal{S}}_{\ddot{U}\ddot{U}}^{\mathrm{MS}}(\omega)$ and $\boldsymbol{\mathcal{S}}_{\ddot{U}\ddot{U}}^{\mathrm{F}}(\omega)$ are $3M\times 3M$ matrices of the cross PSD functions of $\ddot{\mathbf{U}}_{\mathrm{I}}^{\mathrm{MS}}$ and $\ddot{\mathbf{U}}_{\mathrm{I}}^{\mathrm{F}}$, respectively. $\tilde{\boldsymbol{\mathcal{T}}}(\omega)$ denotes the complex conjugate and transpose of the transfer function $\boldsymbol{\mathcal{T}}(\omega)$. The terms in the main diagonals of $\boldsymbol{\mathcal{S}}_{\ddot{U}\ddot{U}}^{\mathrm{MS}}(\omega)$ and $\boldsymbol{\mathcal{S}}_{\ddot{U}\ddot{U}}^{\mathrm{F}}(\omega)$ represent the auto-PSD functions of FLIRS and FIRS, respectively, while the other terms indicate the cross-PSD functions of FLIRS and FIRS, respectively. Let $\mathcal{S}_{\ddot{U}\ddot{U};\,m,\,i}^{\mathrm{MS};\hat{m},\hat{i}}(\omega)$ denotes the element of the (m,i)-th row, $(\hat{m},\hat{i})$-th column or $[3(m-1)+i]$-th row, $[3(\hat{m}-1)+\hat{i}]$-th column of $\boldsymbol{\mathcal{S}}_{\ddot{U}\ddot{U}}^{\mathrm{MS}}(\omega)$. From equation (4.1.26), the elements in the cross-PSD functions can be written as

$$\mathcal{S}_{\ddot{U}\ddot{U};\,m,\,i}^{\mathrm{MS};\hat{m},\hat{i}}(\omega) = \boldsymbol{\mathcal{T}}_{m,i}(\omega)\,\boldsymbol{\mathcal{S}}_{\ddot{U}\ddot{U}}^{\mathrm{F}}(\omega)\,\tilde{\boldsymbol{\mathcal{T}}}^{\hat{m},\hat{i}}(\omega) = \sum_{p=1}^{3M}\sum_{q=1}^{3M}\mathcal{T}_{m,i}^{p}(\omega)\,\mathcal{S}_{\ddot{U}\ddot{U};\,p}^{\mathrm{F};\,q}(\omega)\,\tilde{\mathcal{T}}_{q}^{\hat{m},\hat{i}}(\omega), \tag{4.1.27}$$

where $\mathcal{T}_{m,i}^{p}(\omega)$ and $\tilde{\mathcal{T}}_{q}^{\hat{m},\hat{i}}(\omega)$ are the (m,i)-th row, p-th column of $\boldsymbol{\mathcal{T}}(\omega)$ and q-th row, $(\hat{m},\hat{i})$-th column of $\tilde{\boldsymbol{\mathcal{T}}}(\omega)$, respectively. When $m=\hat{m}$ and $i=\hat{i}$, the term $\mathcal{S}_{\ddot{U}\ddot{U};\,m,\,i}^{\mathrm{MS};\hat{m},\hat{i}}(\omega)$ becomes $\mathcal{S}_{\ddot{U}\ddot{U};\,m,\,i}^{\mathrm{MS};m,i}(\omega)$, i.e., the auto-PSD of FLIRS at support m in direction i, denoted as $\mathcal{S}_{\ddot{U}\ddot{U}}^{\mathrm{MS};m,i}(\omega)$ for convenience.

The mean-square response of an SDOF oscillator $(\omega_0,\,\zeta_0)$ under a base excitation $\ddot{\mathrm{U}}_{m,i}^{\mathrm{F}}$ can be obtained by

$$\mathrm{E}\Big[\Big\{\ddot{R}_0^{\mathrm{F};m,i}(t)\Big\}^2\Big] = \frac{1}{2\pi}\int_{-\infty}^{\infty}\left|\omega_0^2\,\mathcal{H}(\omega)\right|^2\mathcal{S}_{\ddot{U}\ddot{U}}^{\mathrm{F};m,i}(\omega)\,\mathrm{d}\omega, \tag{4.1.28}$$

where

$$\mathcal{H}(\omega) = \frac{1}{(\omega_0^2-\omega^2)+\mathrm{i}2\zeta_0\omega_0\omega} \tag{4.1.29}$$

is the complex frequency response function of the SDOF oscillator $(\omega_0,\,\zeta_0)$ with respect to base excitation. Similarly, the mean-square response of an SDOF oscillator $(\omega_0,\,\zeta_0)$ under a base excitation $\ddot{\mathrm{U}}_{m,i}^{\mathrm{MS}}$ can be obtained by

$$\mathrm{E}\Big[\Big\{\ddot{R}_0^{\mathrm{MS};m,i}(t)\Big\}^2\Big] = \frac{1}{2\pi}\int_{-\infty}^{\infty}\left|\omega_0^2\,\mathcal{H}(\omega)\right|^2\mathcal{S}_{\ddot{U}\ddot{U}}^{\mathrm{MS};m,i}(\omega)\,\mathrm{d}\omega$$

$$= \frac{1}{2\pi} \int_{-\infty}^{\infty} \left|\omega_0^2\, \mathcal{H}(\omega)\right|^2 \sum_{p=1}^{3M} \sum_{q=1}^{3M} \mathcal{T}_{m,i}^{p}(\omega)\, \mathcal{S}_{\ddot{U}\ddot{U};\,p}^{\mathrm{F};\,q}(\omega)\, \tilde{\mathcal{T}}_{q}^{m,i}(\omega)\ \mathrm{d}\omega. \tag{4.1.30}$$

The ratio between the mean square response of an SDOF oscillator under base excitation $\ddot{U}_{m,i}^{\mathrm{F}}$ and that under base excitation $\ddot{U}_{m,i}^{\mathrm{MS}}$ can be determined by

$$\begin{aligned}
\left[\mathcal{R}^{m,i}(\omega_0,\zeta_0)\right]^2 &= \frac{\mathrm{E}\left[\left\{\ddot{R}_0^{\mathrm{MS};m,i}(t)\right\}^2\right]}{\mathrm{E}\left[\left\{\ddot{R}_0^{\mathrm{F};m,i}(t)\right\}^2\right]} \\
&= \frac{\dfrac{1}{2\pi} \displaystyle\int_{-\infty}^{\infty} \left|\omega_0^2\, \mathcal{H}(\omega)\right|^2 \sum_{p=1}^{3M} \sum_{q=1}^{3M} \mathcal{T}_{m,i}^{p}(\omega)\, \mathcal{S}_{\ddot{U}\ddot{U};\,p}^{\mathrm{F};\,q}(\omega)\, \tilde{\mathcal{T}}_{q}^{m,i}(\omega)\ \mathrm{d}\omega}{\dfrac{1}{2\pi} \displaystyle\int_{-\infty}^{\infty} \left|\omega_0^2\, \mathcal{H}(\omega)\right|^2 \mathcal{S}_{\ddot{U}\ddot{U}}^{\mathrm{F};m,i}(\omega)\, \mathrm{d}\omega} \\
&= \frac{\displaystyle\int_{-\infty}^{\infty} \left|\mathcal{H}(\omega)\right|^2 \sum_{p=1}^{3M} \sum_{q=1}^{3M} \mathcal{T}_{m,i}^{p}(\omega)\, \mathcal{S}_{\ddot{U}\ddot{U};\,p}^{\mathrm{F};\,q}(\omega)\, \tilde{\mathcal{T}}_{q}^{m,i}(\omega)\ \mathrm{d}\omega}{\displaystyle\int_{-\infty}^{\infty} \left|\mathcal{H}(\omega)\right|^2 \mathcal{S}_{\ddot{U}\ddot{U}}^{\mathrm{F};m,i}(\omega)\, \mathrm{d}\omega}.
\end{aligned} \tag{4.1.31}$$

The maximum response of an SDOF oscillator, which is by the definition of the response spectrum, is usually related to its root-mean-square response through a peak factor as

$$\mathcal{S}_{\mathrm{A}}(\omega_0,\zeta_0) = \left|\ddot{R}_0(t)\right|_{\max} = \mathcal{P}_{\mathcal{F}} \cdot \sqrt{\mathrm{E}\left[\ddot{R}_0^2(t)\right]}. \tag{4.1.32}$$

Combining equations (4.1.31) and (4.1.32) yields the tridirectional FLIRS in direction i of input node m for a structure with multiple supports

$$\mathcal{S}_{\mathrm{A}}^{\mathrm{MS};m,i}(\omega_0,\zeta_0) = \frac{\mathcal{P}_{\mathcal{F}}^{\mathrm{MS}}}{\mathcal{P}_{\mathcal{F}}^{\mathrm{F}}}\ \mathcal{R}^{m,i}(\omega_0,\zeta_0)\ \mathcal{S}_{\mathrm{A}}^{\mathrm{F};m,i}(\omega_0,\zeta_0). \tag{4.1.33}$$

For responses in earthquake engineering, the values of peak factors $\mathcal{P}_{\mathcal{F}}^{\mathrm{MS}}$ and $\mathcal{P}_{\mathcal{F}}^{\mathrm{F}}$ do not differ significantly, i.e., $\mathcal{P}_{\mathcal{F}}^{\mathrm{MS}} \approx \mathcal{P}_{\mathcal{F}}^{\mathrm{F}}$. Hence

$$\mathcal{S}_{\mathrm{A}}^{\mathrm{MS};m,i}(\omega_0,\zeta_0) = \mathcal{R}^{m,i}(\omega_0,\zeta_0)\ \mathcal{S}_{\mathrm{A}}^{\mathrm{F};m,i}(\omega_0,\zeta_0), \tag{4.1.34}$$

in which $\mathcal{R}^{m,i}(\omega_0,\zeta_0)$ can be interpreted as the response spectrum modification factor from FIRS to FLIRS.

If the structure is only excited by tri-directional seismic input at a single support while the ground motions in different directions are generally regarded as independent, equation (4.1.26) is reduced to

$$\boldsymbol{\mathcal{S}}_{\ddot{U}\ddot{U}}^{\mathrm{SS}}(\omega) = \left[\left|\boldsymbol{\mathcal{T}}(\omega)\right|^2\right] \boldsymbol{\mathcal{S}}_{\ddot{U}\ddot{U}}^{\mathrm{F}}(\omega), \tag{4.1.35}$$

where the superscript "ss" stands for single support and $\left[\left|\boldsymbol{\mathcal{T}}(\omega)\right|^2\right]$ denotes a matrix in which each element is equal to the squared modulus of the corresponding element in $\boldsymbol{\mathcal{T}}$. For a complex number $a+\mathrm{i}b$, its modulus is defined as $\left|a+\mathrm{i}b\right| = \sqrt{a^2+b^2}$.

As a result, the FLIRS modification factor can be written as

$$\left[\mathcal{R}^i(\omega_0,\zeta_0)\right]^2 = \frac{\dfrac{1}{2\pi}\displaystyle\int_{-\infty}^{\infty} \left|\omega_0^2\,\mathcal{H}(\omega)\right|^2 \left[\left|\boldsymbol{\mathcal{T}}_i(\omega)\right|^2\right] \mathcal{S}_{\ddot{U}\ddot{U}}^{\mathrm{F};i}(\omega)\ \mathrm{d}\omega}{\dfrac{1}{2\pi}\displaystyle\int_{-\infty}^{\infty} \left|\omega_0^2\,\mathcal{H}(\omega)\right|^2 \mathcal{S}_{\ddot{U}\ddot{U}}^{\mathrm{F};i}(\omega)\,\mathrm{d}\omega}, \tag{4.1.36}$$

in which $\boldsymbol{\mathcal{T}}_i(\omega)$ is the i-th row of $\boldsymbol{\mathcal{T}}(\omega)$. For excitations with wide-band power spectral densities, $\mathcal{S}_{\ddot{U}\ddot{U}}^{\mathrm{F};m,i}(\omega)$ can be approximated by constant $\mathcal{S}_{\ddot{U}\ddot{U}}^{\mathrm{F};m,i}$. Therefore, equation (4.1.36) can be simplified to

$$\left[\mathcal{R}^i(\omega_0,\zeta_0)\right]^2 = \frac{\dfrac{1}{2\pi}\displaystyle\int_{-\infty}^{\infty} \left|\mathcal{H}(\omega)\right|^2 \left[\left|\boldsymbol{\mathcal{T}}_i(\omega)\right|^2\right]\mathbf{1}\ \mathrm{d}\omega}{\dfrac{1}{2\pi}\displaystyle\int_{-\infty}^{\infty} \left|\mathcal{H}(\omega)\right|^2\ \mathrm{d}\omega}, \tag{4.1.37}$$

where $\mathbf{1}$ is the 3×1 vector with all elements being 1. Equation (4.1.37) is the same as equation (4.3.14) in Jiang (2016).

Comparing equation (4.1.31) with equation (4.1.37), it is observed that for the situation of multiple excitations, the modification factor in direction i at support m not only depends on the ground motion at that support, but is also influenced by the ground motions at other supports.

4.1.3 Generating FRS of Multiply Supported Structures under Earthquake Excitations Considering SSI

As mentioned before, the decoupled model with FLIRS as input is equivalent to the combined soil-structure model under the excitation FIRS. Therefore, the FLIRS obtained by the

proposed method in Section 4.1.2 can be directly input to the decoupled model to generate FRS in conjunction with the direct method developed in Chapter 2.

However, it should be noted that the explicit form of the combination coefficients in FRSMS-CQC combination rule developed in Section 2.3.1 is not available when considering SSI. As can be seen in equation (2.3.16), for the generation of FRS of structures with excitations at multiple supports, the coherence function of the ground inputs (i.e., FIRS) at different supports is involved. This is changed to the coherence function of FLIRS with the presence of soil. From the view of practice, it is reasonable to simplify the coherence function of ground motions, such as by assuming fully-correlated or independent cases discussed in Chapter 2, so that the explicit form of the coefficients in FRSMS-CQC combination rule can be obtained. However, it is not proper to deal with FLIRS in a similar way, because the correlation between FLIRS is highly related to the properties of soil and the superstructure, as can be seen from equation (4.1.26). For example, the motions of supports may be correlated to some extent even if the corresponding FIRS are independent.

Therefore, the significant difference between the case of the excitations at multiple supports and at a single support is that the correlations of the generated FLIRS in the former case need to be considered. Neglecting this correlation of FLIRS at different supports will result in a significant error in the generation of FRS using FLIRS.

To consider the correlation of FLIRS at different supports, the cross-power density function of FLIRS specified by equation (4.1.26) must be considered. As a result, the integrals in equations (2.3.15) need to be evaluated numerically for multi-supported structures with SSI effect. This indicates that the direct method for the generation of FRS of multi-supported structures considering SSI effect involves more computational cost than singly supported structures. However, it is still much more efficient than a set of time history analyses. Furthermore, significant variabilities in the time history method can be eliminated with the implementation of the proposed method.

Procedure – Generating FRS Considering SSI

For a structure in an NPP plant with its flexible foundation embedded in layered soil, a procedure for generating FRS considering SSI is illustrated in Figure 4.3 and is summarized as follows:

1. Consider the layered soil as a free-field. With seismic input applied at the bedrock, a site response analysis is performed to obtain the FIRS $\mathbf{U}_{\mathrm{I}}^{\mathrm{F}}$, at the elevation of the foundation.
2. Establish a model of the layered soil. Determine the dynamic stiffness matrices of the excavated soil $\mathbf{S}_{\mathrm{BB}}^{\mathrm{E}}$ and the soil with excavation $\mathbf{S}_{\mathrm{BB}}^{\mathrm{G}}$. The dynamic stiffness matrix of the free-field is $\mathbf{S}_{\mathrm{BB}}^{\mathrm{F}} = \mathbf{S}_{\mathrm{BB}}^{\mathrm{G}} + \mathbf{S}_{\mathrm{BB}}^{\mathrm{E}}$.
3. Set up a finite element model of the structure. Determine the dynamic stiffness matrices $\mathbf{S}_{\mathrm{RR}}^{\mathrm{S}}$, $\mathbf{S}_{\mathrm{RB}}^{\mathrm{S}}$, $\mathbf{S}_{\mathrm{BR}}^{\mathrm{S}}$, $\mathbf{S}_{\mathrm{BB}}^{\mathrm{S}}$.
4. Determine the FLIRS:

   - Partition matrix $\mathbf{S}^{\mathrm{MS}} = -\left(\mathbf{S}_{\mathrm{RR}}^{\mathrm{S}}\right)^{-1}\mathbf{S}_{\mathrm{RB}}^{\mathrm{S}} = \begin{bmatrix} \mathbf{S}_{\mathrm{TT}}^{\mathrm{MS}} & \mathbf{S}_{\mathrm{TR}}^{\mathrm{MS}} \\ \mathbf{S}_{\mathrm{RT}}^{\mathrm{MS}} & \mathbf{S}_{\mathrm{RR}}^{\mathrm{MS}} \end{bmatrix}_{6N\times 6M}$
   - $\mathbf{S} = \mathbf{S}_{\mathrm{BR}}^{\mathrm{S}}\,\mathbf{S}^{\mathrm{MS}} + \left(\mathbf{S}_{\mathrm{BB}}^{\mathrm{S}} - \mathbf{S}_{\mathrm{BB}}^{\mathrm{E}}\right) + \mathbf{S}_{\mathrm{BB}}^{\mathrm{F}}$, dimension $6M\times 6M$

     Determine the inverse $\mathbf{S}^{-1}$
   - Partition matrix $\mathbf{S}^{-1}\mathbf{S}_{\mathrm{BB}}^{\mathrm{F}} = \begin{bmatrix} \mathbf{T}_{\mathrm{TT}} & \mathbf{T}_{\mathrm{TR}} \\ \mathbf{T}_{\mathrm{RT}} & \mathbf{T}_{\mathrm{RR}} \end{bmatrix}_{6M\times 6M}$
   - Transfer matrix: $\boldsymbol{\mathcal{T}} = \mathbf{T}_{\mathrm{TT}} + \left[\left(\mathbf{S}_{\mathrm{TT}}^{\mathrm{MS}}\right)^{T}\mathbf{S}_{\mathrm{TT}}^{\mathrm{MS}}\right]^{-1}\left(\mathbf{S}_{\mathrm{TT}}^{\mathrm{MS}}\right)^{T}\mathbf{S}_{\mathrm{TR}}^{\mathrm{MS}}\,\mathbf{T}_{\mathrm{RT}}$
   - FLIRS modification factor:

$$\left[\mathcal{R}^{m,i}(\omega_0,\zeta_0)\right]^2 = \frac{\displaystyle\int_{-\infty}^{\infty}\left|\mathcal{H}(\omega)\right|^2 \sum_{p=1}^{3M}\sum_{q=1}^{3M}\mathcal{T}_{m,i}^{p}(\omega)\,\mathcal{S}_{\ddot{U}\ddot{U};\,p}^{\mathrm{F};\,q}(\omega)\,\tilde{\mathcal{T}}_{q}^{m,i}(\omega)\,\mathrm{d}\omega}{\displaystyle\int_{-\infty}^{\infty}\left|\mathcal{H}(\omega)\right|^2 \mathcal{S}_{\ddot{U}\ddot{U}}^{\mathrm{F};m,i}(\omega)\,\mathrm{d}\omega}$$

   - FLIRS: $\mathcal{S}_{\mathrm{A}}^{\mathrm{MS};m,i}(\omega_0,\zeta_0) = \mathcal{R}^{m,i}(\omega_0,\zeta_0)\;\mathcal{S}_{\mathrm{A}}^{\mathrm{F};m,i}(\omega_0,\zeta_0)$
   - Cross-power density function of FLIRS: $\boldsymbol{\mathcal{S}}_{\ddot{U}\ddot{U}}^{\mathrm{MS}}(\omega) = \boldsymbol{\mathcal{T}}(\omega)\;\boldsymbol{\mathcal{S}}_{\ddot{U}\ddot{U}}^{\mathrm{F}}(\omega)\,\tilde{\boldsymbol{\mathcal{T}}}(\omega)$

5. The FLIRS $\mathcal{S}_{\mathrm{A}}^{\mathrm{MS};m,i}(\omega_0,\zeta_0)$ together with the cross-power density function $\mathcal{S}_{\ddot{U}\ddot{U}}^{\mathrm{MS}}(\omega)$ are input to the decoupled finite element model of the structure to generate the required FRS, which are exactly the same as the FRS obtained from a fully coupled soil–structure analysis under the excitation of FIRS.

Therefore, when the direct spectra-to-spectra method presented in Chapter 2 is applied to structures with flexible foundation under the excitation of FLIRS $\mathcal{S}_{\mathrm{A}}^{\mathrm{MS};m,i}(\omega_0,\zeta_0)$, FRS with complete probabilistic descriptions of FRS peaks (FRS with any desired level of NEP p) can be obtained. If the time history method is applied, such a result could only be obtained from a large number of coupled soil–structure analyses using a commercial finite element software, such as ACS **SASSI**, with a large number of generated time-histories compatible with the FIRS.

In the following sections, two numerical examples of generating FRS considering SSI effect are presented. Although the main scope of this research is focused on structures with multiple supports, it is worthwhile to start with a singly supported structure to verify the proposed method. After the method has been verified, it is then applied to a structure with earthquake excitations from two supports to generate FRS with SSI effect. Each example contains two parts: Part 1 focuses on the theoretical validation that can verify the derivation of obtaining FLIRS from FIRS, while Part 2 presents numerical results. The theoretical validation is important for these two numerical examples because it guarantees that the procedure of generating FLIRS by the proposed method is correct. In other words, it permits the theoretical expressions of the matrices in the generation of FLIRS, such as dynamic stiffness matrix, that can be obtained. It also allows the results be verified step by step.

4.2 Numerical Example 1 : Excitations at Single Support

One of the most important tasks of generating FLIRS is to obtain the dynamic stiffness matrices of the superstructure and the supporting soil, i.e., $\mathbf{S}$ in equation (4.1.2) and $\mathbf{S}_{\mathrm{BB}}^{\mathrm{E}}$ and $\mathbf{S}_{\mathrm{BB}}^{\mathrm{F}}$ in equation (4.1.10). In this section, an example is presented to illustrate this procedure and to validate the method for generating FLIRS proposed in Section 4.1.1.

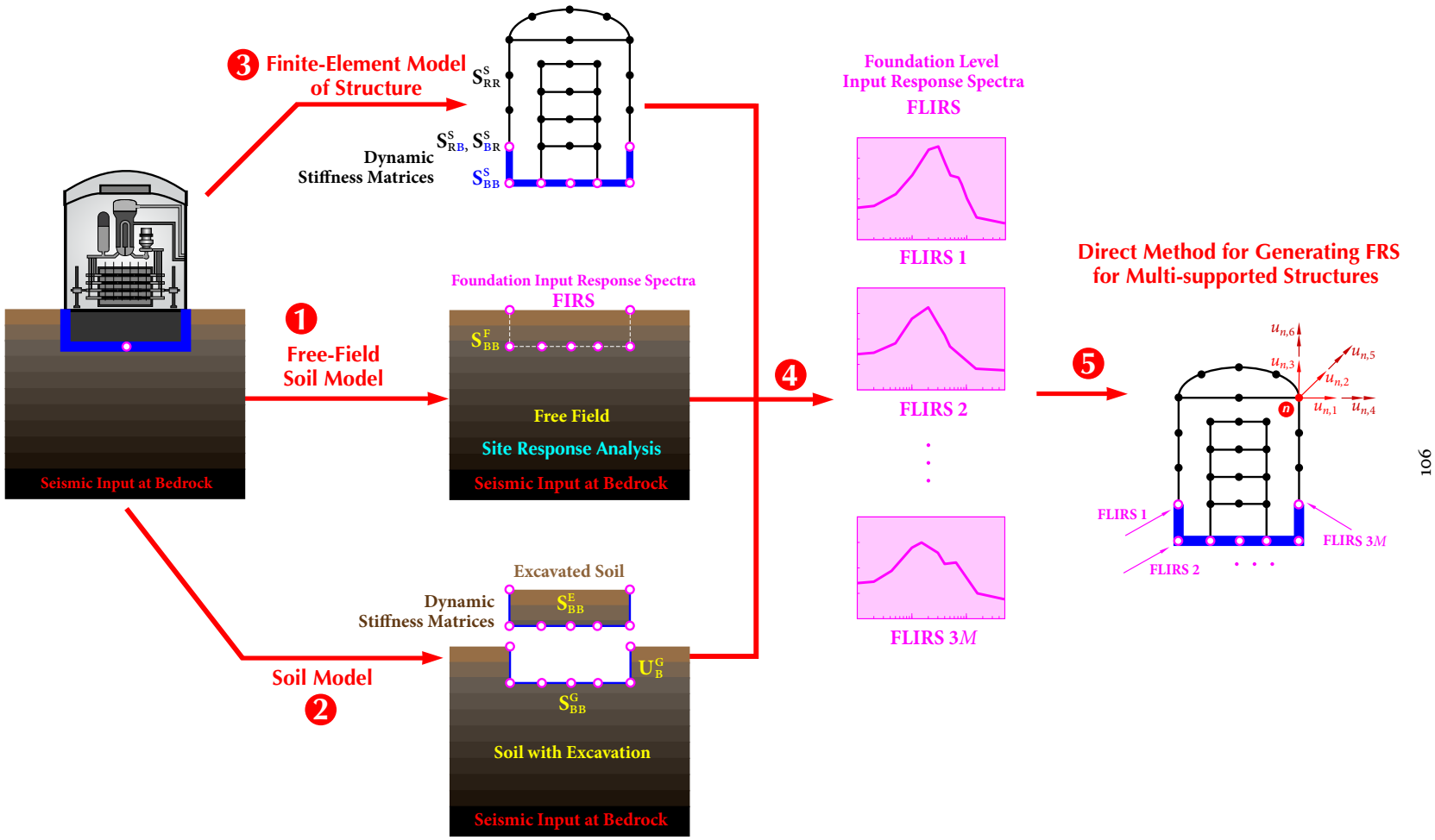

Figure 4.3 Procedure for generating FRS considering SSI.

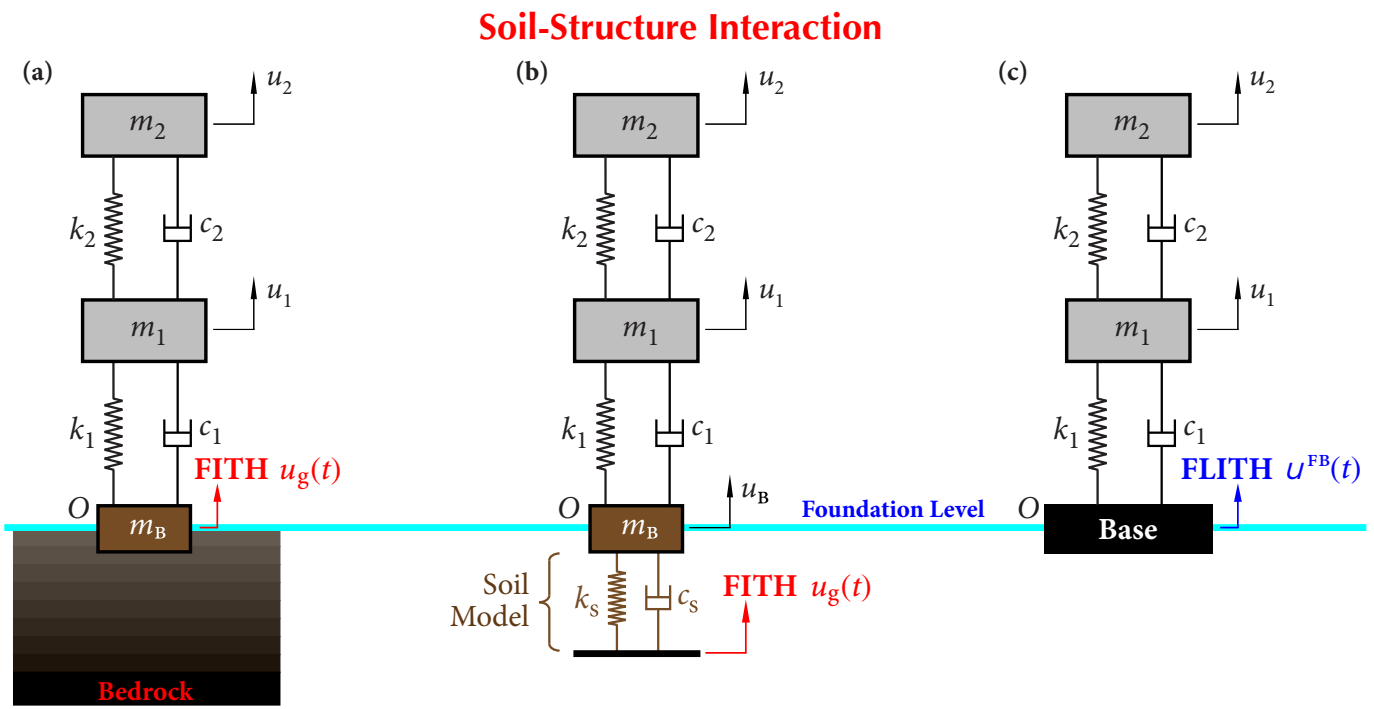

FITH: **Foundation Input Time History** (Free-field time history at foundation) $\ddot{u}_g(t)$

FIRS: **Foundation Input Response Spectrum** (Free-field response spectrum at foundation) $\mathcal{RS}\{\ddot{u}_g(t)\}$

FLITH: **Foundation Level Input Time History** (Time history at foundation level considering SSI) $\ddot{u}^{FB}(t)$

FLIRS: **Foundation Level Input Response Spectrum** (Response spectrum at foundation level considering SSI) $\mathcal{RS}\{\ddot{u}^{FB}(t)\}$

Figure 4.4 Diagram of numerical example 1.

For the purpose of clear illustration, the system has only 3 nodes including two structure nodes and one foundation node. This simple system allows the theoretical (or exact) solution to be obtained so that the results by the proposed method can be validated. As shown in Figure 4.4(a), a system with two structure nodes and one foundation node that can only move in the vertical direction is supported by soil on the top of the bedrock. The whole system undergoes earthquake excitation at the top surface of bedrock. As can be seen from Figure 4.4(b), the soil is simplified to a spring-damper element with constant stiffness and damping coefficient. The foundation input time histories FITH or foundation input response spectra FIRS obtained by site response analysis is input at the bottom of soil-damper element. As a result, the effect of soil on the response of the supported structure is included.

It should be noted that the length of the soil spring-damper element is regarded as zero when considering SSI. Therefore, FITH or FIRS is still applied at the foundation level although it is actually acting on the bottom of the soil spring. This system is called the coupled soil-structure system or the complete system and the seismic analysis of the system is called the complete method. As mentioned in Chapter 1, although the complete method theoretically allows the exact seismic response to be obtained, seismic analysis of the entire system needs to be reanalyzed when the soil property changes, which is very time-consuming for complex structures.

To overcome this disadvantage of the complete method, the coupled soil-structure system is decoupled to a 2DOF structure, as shown in Figure 4.4(c). For the decoupled structure, the inputs are the time histories at foundation level FLITH or foundation level input response spectra FLIRS applied at the bottom surface of foundation rather than soil spring-damper element.

4.2.1 Theoretical Validation of Generating FLIRS

In this section, the formulation of generating FLIRS for numerical example 1 is presented. The general formulation in Section 4.1.1 is then verified comparing with the formulation for this example.

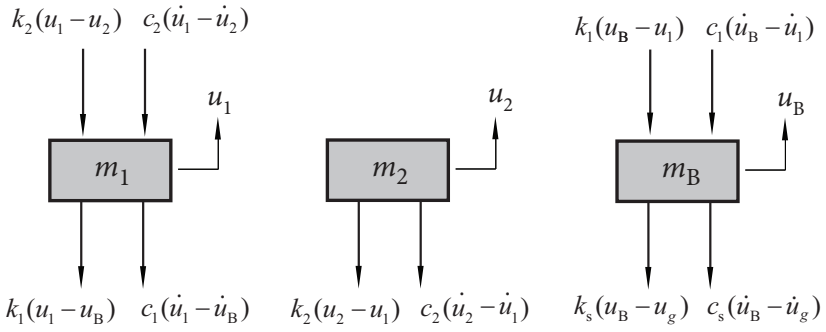

Figure 4.5 Free-body-diagram of the coupled system.

4.2.1.1 Coupled 3-DOF System

Denote $\mathbf{u}_1(t)$, $\mathbf{u}_2(t)$, and $\mathbf{u}_B(t)$ as the absolute displacement of nodes 1, 2, and the base node under earthquake excitations at the fixed end of the soil spring, respectively. The equation of motion of each node can be established by applying Newton's Second Law. For example, the free-body diagram of Node 2 is shown in Figure 4.5. Summarizing all the forces in the vertical direction gives the dynamic equilibrium equation of Node 2 as

$$m_2\,\ddot{u}_2(t) = -k_2\left(u_2(t) - u_1(t)\right) - c_2\left(\dot{u}_2(t) - \dot{u}_1(t)\right),$$

or

$$m_2\,\ddot{u}_2(t) - c_2\,\dot{u}_1(t) + c_2\,\dot{u}_2(t) - k_2\,u_1(t) + k_2\,u_2(t) = 0. \tag{4.2.1}$$

Similarly, the dynamic equilibrium equations for the other nodes can be writen as

for Node 1:

$$m_1\,\ddot{u}_1(t)+(c_1+c_2)\,\dot{u}_1(t)-c_2\,\dot{u}_2(t)+(k_1+k_2)\,u_1(t)-k_2\,u_2(t)-c_1\,\dot{u}_B(t)-k_1\,u_B(t)=0, \tag{4.2.2}$$

for base node:

$$m_B\,\ddot{u}_B(t)-c_1\,\dot{u}_1(t)+(c_1+c_s)\,\dot{u}_B(t)-k_1\,u_1+(k_1+k_s)\,u_B(t)=c_s\,\dot{u}_g+k_s\,u_g(t). \tag{4.2.3}$$

Combining equations (4.2.1), (4.2.2), and (4.2.3) yields the equation of motion of the system, given by

$$\begin{bmatrix} m_1 & 0 & 0 \\ 0 & m_2 & 0 \\ 0 & 0 & m_3 \end{bmatrix}\begin{Bmatrix} \ddot{\mathbf{u}}_1 \\ \ddot{\mathbf{u}}_2 \\ \ddot{\mathbf{u}}_B \end{Bmatrix} + \begin{bmatrix} c_1+c_2 & -c_2 & -c_1 \\ -c_2 & c_2 & 0 \\ -c_1 & 0 & c_1+c_s \end{bmatrix}\begin{Bmatrix} \dot{\mathbf{u}}_1 \\ \dot{\mathbf{u}}_2 \\ \dot{\mathbf{u}}_B \end{Bmatrix} + \begin{bmatrix} k_1+k_2 & -k_2 & -k_1 \\ -k_2 & k_2 & 0 \\ -k_1 & 0 & k_1+k_s \end{bmatrix}\begin{Bmatrix} \mathbf{u}_1 \\ \mathbf{u}_2 \\ \mathbf{u}_B \end{Bmatrix}$$

$$= \begin{Bmatrix} 0 \\ 0 \\ c_s \dot{u}_g + k_s u_g \end{Bmatrix}. \tag{4.2.4}$$

Applying the transform $\mathbf{x}(t) = \mathbf{X}e^{i\omega t}$ yields

$$\begin{Bmatrix} \mathbf{u}_1(t) \\ \mathbf{u}_2(t) \\ \mathbf{u}_B(t) \end{Bmatrix} = \begin{Bmatrix} \mathbf{U}_1 \\ \mathbf{U}_2 \\ \mathbf{U}_B \end{Bmatrix} e^{i\omega t} \Rightarrow \begin{Bmatrix} \dot{\mathbf{u}}_1(t) \\ \dot{\mathbf{u}}_2(t) \\ \dot{\mathbf{u}}_B(t) \end{Bmatrix} = \begin{Bmatrix} \mathbf{U}_1 \\ \mathbf{U}_2 \\ \mathbf{U}_B \end{Bmatrix} (i\omega) e^{i\omega t}, \quad \begin{Bmatrix} \ddot{\mathbf{u}}_1(t) \\ \ddot{\mathbf{u}}_2(t) \\ \ddot{\mathbf{u}}_B(t) \end{Bmatrix} = \begin{Bmatrix} \mathbf{U}_1 \\ \mathbf{U}_1 \\ \mathbf{U}_B \end{Bmatrix} (-\omega^2) e^{i\omega t}, \tag{4.2.5}$$

where $\mathbf{U}_1$, $\mathbf{U}_2$, and $\mathbf{U}_B$ are the amplitudes of $\mathbf{u}_1(t)$, $\mathbf{u}_2(t)$, and $\mathbf{u}_B(t)$, respectively. Similarly,

$$\mathbf{u}_g(t) = \mathbf{U_g} e^{i\omega t} \Rightarrow \dot{\mathbf{u}}_g(t) = (i\omega)\mathbf{U_g} e^{i\omega t}, \quad \ddot{\mathbf{u}}_g(t) = (-\omega^2)\mathbf{U_g} e^{i\omega t}. \tag{4.2.6}$$

Substituting equations (4.2.5) and (4.2.6) into equation (4.2.4) gives the equation of motion in frequency domain, i.e.,

$$\begin{bmatrix} m_1 & 0 & 0 \\ 0 & m_2 & 0 \\ 0 & 0 & m_3 \end{bmatrix} (-\omega^2) \begin{Bmatrix} \mathbf{U}_1 \\ \mathbf{U}_2 \\ \mathbf{U}_B \end{Bmatrix} e^{i\omega t} + \begin{bmatrix} c_1 + c_2 & -c_2 & -c_1 \\ -c_2 & c_2 & 0 \\ -c_1 & 0 & c_1 + c_s \end{bmatrix} (i\omega) \begin{Bmatrix} \mathbf{U}_1 \\ \mathbf{U}_2 \\ \mathbf{U}_B \end{Bmatrix} e^{i\omega t}$$
$$+ \begin{bmatrix} k_1 + k_2 & -k_2 & -k_1 \\ -k_2 & k_2 & 0 \\ -k_1 & 0 & k_1 + k_s \end{bmatrix} \begin{Bmatrix} \mathbf{U}_1 \\ \mathbf{U}_1 \\ \mathbf{U}_B \end{Bmatrix} = \begin{Bmatrix} 0 \\ 0 \\ i\omega c_s + k_s \end{Bmatrix} \mathbf{U_g} e^{i\omega t}. \tag{4.2.7}$$

Eliminate $e^{i\omega t}$ on the both sides so that equation (4.2.7) can be written as

$$\begin{bmatrix} -\omega^2 m_1 + i\omega(c_1+c_2) + (k_1+k_2) & -i\omega c_2 - k_2 & -i\omega c_1 - k_1 \\ -i\omega c_2 - k_2 & -\omega^2 m_2 + i\omega c_2 + k_2 & 0 \\ -i\omega c_1 - k_1 & 0 & -\omega^2 m_B + i\omega(c_1+c_s) + (k_1+k_s) \end{bmatrix} \begin{Bmatrix} \mathbf{U}_1 \\ \mathbf{U}_2 \\ \mathbf{U}_B \end{Bmatrix}$$
$$= \begin{Bmatrix} 0 \\ 0 \\ i\omega c_s + k_s \end{Bmatrix} \mathbf{U_g}. \tag{4.2.8}$$

Comparing with equation (4.1.4), one can partition equation (4.2.8) as

$$\begin{bmatrix} \mathbf{S}^{\mathrm{S}}_{\mathrm{RR}} & \mathbf{S}^{\mathrm{S}}_{\mathrm{RB}} \\ \mathbf{S}^{\mathrm{S}}_{\mathrm{BR}} & \mathbf{S}^{\mathrm{S}}_{\mathrm{BB}} + \mathbf{S}^{\mathrm{G}}_{\mathrm{BB}} \end{bmatrix} \begin{Bmatrix} \mathbf{U}_{\mathrm{R}} \\ \mathbf{U}_{\mathrm{B}} \end{Bmatrix} = \begin{Bmatrix} \mathbf{0} \\ \mathbf{S}^{\mathrm{G}}_{\mathrm{BB}}\, \mathbf{U}_{\mathbf{g}} \end{Bmatrix}, \tag{4.2.9}$$

in which

$$\begin{aligned}
\mathbf{U}_{\mathrm{R}} &= \begin{bmatrix} \mathbf{U}_1 & \mathbf{U}_2 \end{bmatrix}^{\mathrm{T}}, \\
\mathbf{S}^{\mathrm{S}}_{\mathrm{RR}} &= \begin{bmatrix} -\omega^2 m_1 + \mathrm{i}\omega(c_1+c_2) + (k_1+k_2) & -\mathrm{i}\omega c_2 - k_2 \\ -\mathrm{i}\omega c_2 - k_2 & -\omega^2 m_2 + \mathrm{i}\omega c_2 + k_2 \end{bmatrix}, \\
\mathbf{S}^{\mathrm{S}}_{\mathrm{RB}} &= \begin{bmatrix} -\mathrm{i}\omega c_1 - k_1 \\ 0 \end{bmatrix}, \quad \mathbf{S}^{\mathrm{S}}_{\mathrm{BR}} = (\mathbf{S}^{\mathrm{S}}_{\mathrm{RB}})^{\mathrm{T}} = \begin{bmatrix} -\mathrm{i}\omega c_1 - k_1 & 0 \end{bmatrix}, \\
\mathbf{S}^{\mathrm{S}}_{\mathrm{BB}} &= -\omega^2 m_{\mathrm{B}} + \mathrm{i}\omega c_1 + k_1, \quad \mathbf{S}^{\mathrm{G}}_{\mathrm{BB}} = \mathrm{i}\omega c_{\mathrm{s}} + k_{\mathrm{s}}.
\end{aligned} \tag{4.2.10}$$

From the first row of equation (4.2.9), the relationship between the dynamic responses of the structure nodes and the base nodes can be determined as

$$\mathbf{S}^{\mathrm{S}}_{\mathrm{RR}}\, \mathbf{U}_{\mathrm{R}} + \mathbf{S}^{\mathrm{S}}_{\mathrm{RB}}\, \mathbf{U}_{\mathrm{B}} = 0, \tag{4.2.11}$$

i.e.,

$$\mathbf{U}_{\mathrm{R}} = \mathbf{S}^{\mathrm{MS}}\, \mathbf{U}_{\mathrm{B}}, \tag{4.2.12}$$

where $\mathbf{S}^{\mathrm{MS}}$ is given by equation (4.1.11).

The second row of equation (4.2.9) can be written as

$$\mathbf{S}^{\mathrm{S}}_{\mathrm{BR}}\, \mathbf{U}_{\mathrm{R}} + \mathbf{S}_{\mathrm{BB}}\, \mathbf{U}_{\mathrm{B}} = \mathbf{S}^{\mathrm{G}}_{\mathrm{BB}}\, \mathbf{U}_{\mathbf{g}}, \quad \mathbf{S}_{\mathrm{BB}} = \mathbf{S}^{\mathrm{S}}_{\mathrm{BB}} + \mathbf{S}^{\mathrm{G}}_{\mathrm{BB}}. \tag{4.2.13}$$

Substituting equation (4.2.13) into equation (4.2.11) gives

$$\mathbf{S}^{\mathrm{S}}_{\mathrm{RR}}\, \mathbf{U} = \mathbf{S}^{\mathrm{S}}_{\mathrm{RB}} (\mathbf{S}_{\mathrm{BB}})^{-1} \Big[\mathbf{S}^{\mathrm{S}}_{\mathrm{BR}}\, \mathbf{U}_{\mathrm{R}} - \mathbf{S}^{\mathrm{G}}_{\mathrm{BB}}\, \mathbf{U}_{\mathbf{g}} \Big] \tag{4.2.14}$$

Note that $\mathbf{S}^{\mathrm{S}}_{\mathrm{RB}}$ may not be a square matrix when the number of DOF of the base nodes is different from the structure nodes. Therefore, without loss of generality, multiply $\mathbf{S}^{\mathrm{S}}_{\mathrm{BR}}$ to equation (4.2.14) yielding

$$\mathbf{S}^{\mathrm{S}}_{\mathrm{BR}}\, \mathbf{S}^{\mathrm{S}}_{\mathrm{RR}}\, \mathbf{U}_{\mathrm{R}} = (\mathbf{S}^{\mathrm{S}}_{\mathrm{BR}}\, \mathbf{S}^{\mathrm{S}}_{\mathrm{RB}}) (\mathbf{S}_{\mathrm{BB}})^{-1} \Big[\mathbf{S}^{\mathrm{S}}_{\mathrm{BR}}\, \mathbf{U}_{\mathrm{R}} - \mathbf{S}^{\mathrm{G}}_{\mathrm{BB}}\, \mathbf{U}_{\mathbf{g}} \Big] \tag{4.2.15}$$

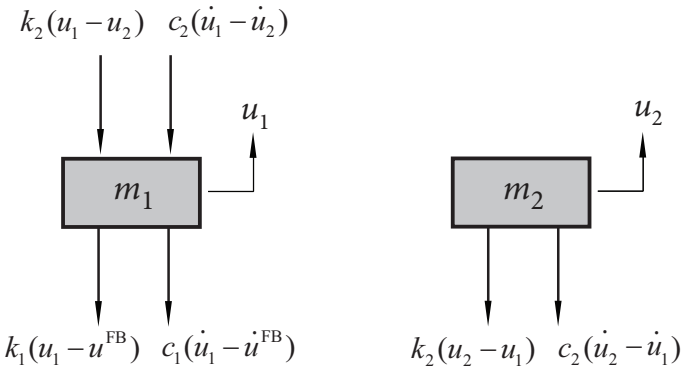

Figure 4.6 Free-body-diagram of the decoupled model.

Now the term $\mathbf{S}^{\mathrm{S}}_{\mathrm{BR}}\,\mathbf{S}^{\mathrm{S}}_{\mathrm{RB}}$ becomes a square matrix so that it can be moved to the left hand side by multiplying the inverse of it to the both sides, i.e.,

$$(\mathbf{S}^{\mathrm{S}}_{\mathrm{BR}}\,\mathbf{S}^{\mathrm{S}}_{\mathrm{RB}})^{-1}\,\mathbf{S}^{\mathrm{S}}_{\mathrm{BR}}\,\mathbf{S}^{\mathrm{S}}_{\mathrm{RR}}\,\mathbf{U}_{\mathrm{R}} = (\mathbf{S}_{\mathrm{BB}})^{-1}\Big[\mathbf{S}^{\mathrm{S}}_{\mathrm{BR}}\,\mathbf{U}_{\mathrm{R}} - \mathbf{S}^{\mathrm{G}}_{\mathrm{BB}}\,\mathbf{U}_{\mathbf{g}}\Big] \tag{4.2.16}$$

From equation (4.2.16), a relationship between the responses of the structure nodes $\mathbf{U}_{\mathrm{R}}$ and input at the bottom of supporting soil $\mathbf{U}_{\mathbf{g}}$ can be further obtained as

$$\Big[\mathbf{S}_{\mathrm{BB}}(\mathbf{S}^{\mathrm{S}}_{\mathrm{BR}}\,\mathbf{S}^{\mathrm{S}}_{\mathrm{RB}})^{-1}\,\mathbf{S}^{\mathrm{S}}_{\mathrm{BR}}\,\mathbf{S}^{\mathrm{S}}_{\mathrm{RR}} - \mathbf{S}^{\mathrm{S}}_{\mathrm{BR}}\Big]\mathbf{U}_{\mathrm{R}} = -\mathbf{S}^{\mathrm{G}}_{\mathrm{BB}}\,\mathbf{U}_{\mathbf{g}} \tag{4.2.17}$$

4.2.1.2 Decoupled 2-DOF System

Now consider if the coupled 3-DOF system can be replaced by a decoupled 2-DOF system with a modified input FLITH or FLIRS as shown in Figure 4.4(c). Based on the free-body diagram shown in Figure 4.6, the dynamic equilibrium equations can be obtained.

For Node 1:

$$m_1\,\ddot{u}_1 + (c_1 + c_2)\,\dot{u}_1 - c_2\,\dot{u}_2 + (k_1 + k_2)\,u_1 - k_2\,u_2 = c_1\,\dot{u}_{\mathrm{g}}^{\mathrm{FB}} + k_1\,u_{\mathrm{g}}^{\mathrm{FB}}, \tag{4.2.18}$$

for Node 2:

$$m_2\,\ddot{u}_2 - c_2\,\dot{u}_1 + c_2\,\dot{u}_2 - k_2\,u_1 + k_2\,u_2 = 0, \tag{4.2.19}$$

where the superscript "FB" stands for fixed base.

Combining equations (4.2.18) and (4.2.19) yields

$$\begin{bmatrix} m_1 & 0 \\ 0 & m_2 \end{bmatrix} \begin{Bmatrix} \ddot{\mathbf{u}}_1 \\ \ddot{\mathbf{u}}_2 \end{Bmatrix} + \begin{bmatrix} c_1+c_2 & -c_2 \\ -c_2 & c_2 \end{bmatrix} \begin{Bmatrix} \dot{\mathbf{u}}_1 \\ \dot{\mathbf{u}}_2 \end{Bmatrix} + \begin{bmatrix} k_1+k_2 & -k_2 \\ -k_2 & k_2 \end{bmatrix} \begin{Bmatrix} \mathbf{u}_1 \\ \mathbf{u}_2 \end{Bmatrix} = \begin{Bmatrix} c_1 \dot{\mathbf{u}}^{\mathrm{FB}} + k_1 \mathbf{u}^{\mathrm{FB}} \\ 0 \end{Bmatrix}. \tag{4.2.20}$$

Following the procedure from equation (4.2.5) to equation (4.2.8), the system of equations of motion in frequency domain can be obtained as

$$\begin{bmatrix} -\omega^2 m_1 + \mathrm{i}\omega(c_1+c_2) + (k_1+k_2) & -\mathrm{i}\omega c_2 - k_2 \\ -\mathrm{i}\omega c_2 - k_2 & -\omega^2 m_2 + \mathrm{i}\omega c_2 + k_2 \end{bmatrix} \begin{Bmatrix} \mathbf{U}_1 \\ \mathbf{U}_2 \end{Bmatrix} = \begin{Bmatrix} \mathrm{i}\omega c_1 + k_1 \\ 0 \end{Bmatrix} \mathbf{U}^{\mathrm{FB}}, \tag{4.2.21}$$

in which $\mathbf{U}^{\mathrm{FB}}$ is the amplitude of $\mathbf{u}^{\mathrm{FB}}$.

Note that the matrix on the left side of equation (4.2.21) is just $\mathbf{S}^{\mathrm{S}}_{\mathrm{RR}}$ given by equation (4.2.10) and the vector $\left\{\mathrm{i}\omega c_1 + k_1,\, 0\right\}^{\mathrm{T}}$ on the right side is $\mathbf{S}^{\mathrm{S}}_{\mathrm{RB}}$. Therefore, equation (4.2.21) can be modified to

$$\mathbf{U}_{\mathrm{R}} = -(\mathbf{S}^{\mathrm{S}}_{\mathrm{RR}})^{-1} \mathbf{S}^{\mathrm{S}}_{\mathrm{RB}} \mathbf{U}^{\mathrm{FB}} = \mathbf{S}^{\mathrm{MS}} \mathbf{U}^{\mathrm{FB}} \tag{4.2.22}$$

where $\mathbf{S}^{\mathrm{MS}}$ is given by equation (4.1.11).

Comparing equation (4.2.22) with equation (4.2.12), it can be found that

$$\mathbf{U}_{\mathrm{B}} = \mathbf{U}^{\mathrm{FB}}. \tag{4.2.23}$$

Equation (4.2.23) clearly states that the coupled 3-DOF system with earthquake excitation $\ddot{\mathbf{u}}(t)$ is equivalent to the decoupled 2-DOF system with the modified seismic input $\ddot{\mathbf{u}}^{\mathrm{FB}}(t)$. In the other words, it is theoretically correct to replace the coupled soil-structure system with input FIRS, by the decoupled system with FLIRS as input to obtain the same seismic response.

In the previous studies conducted by Jiang (2016) and Zhou (2019) involving the direct method and SSI effect, the FRS of superstructure has been verified to be accurate. However, the input of the decoupled structure, i.e., FLIRS, was not explicitly verified. This is because the verification is based on the comparison with time history analyses of the coupled soil-structure system. However, one may find that there is no such concept as FLIRS or FLITH

in the coupled system. In this study, it can be seen from equation (4.2.23) that FLIRS are the same as the response spectra at the base nodes (i.e., the FRS at the corresponding nodes) in the coupled soil-structure system. As a result, FLIRS generated by the proposed method can be verified by comparing it with FRS at the base nodes using the time history method. In this case, the input FLIRS and the resultant FRS can both be validated to better illustrate the accuracy of the proposed method.

Before moving to the next section, it is worthwhile to investigate the relationship between the amplitude of the input of the decoupled model $\mathbf{U}^{\mathrm{FB}}$ and the coupled model $\mathbf{U_g}$. Firstly, substituting equation (4.2.22) into equation (4.2.17) gives

$$\left[\mathbf{S}_{\mathrm{BB}}(\mathbf{S}^{\mathrm{s}}_{\mathrm{BR}}\,\mathbf{S}^{\mathrm{s}}_{\mathrm{RB}})^{-1}\mathbf{S}^{\mathrm{s}}_{\mathrm{BR}}\,\mathbf{S}^{\mathrm{s}}_{\mathrm{RR}}-\mathbf{S}^{\mathrm{s}}_{\mathrm{BR}}\right]\left[-(\mathbf{S}^{\mathrm{s}}_{\mathrm{RR}})^{-1}\mathbf{S}^{\mathrm{s}}_{\mathrm{RB}}\,\mathbf{U}^{\mathrm{FB}}\right]=-\mathbf{S}^{\mathrm{G}}_{\mathrm{BB}}\,\mathbf{U_g}\,, \tag{4.2.24}$$

which can be written as

$$\left[\mathbf{S}_{\mathrm{BB}}(\mathbf{S}^{\mathrm{s}}_{\mathrm{BR}}\,\mathbf{S}^{\mathrm{s}}_{\mathrm{RB}})^{-1}\mathbf{S}^{\mathrm{s}}_{\mathrm{BR}}\,\mathbf{S}^{\mathrm{s}}_{\mathrm{RR}}(\mathbf{S}^{\mathrm{s}}_{\mathrm{RR}})^{-1}\mathbf{S}^{\mathrm{s}}_{\mathrm{RB}}-\mathbf{S}^{\mathrm{s}}_{\mathrm{BR}}(\mathbf{S}^{\mathrm{s}}_{\mathrm{RR}})^{-1}\mathbf{S}^{\mathrm{s}}_{\mathrm{RB}}\right]\mathbf{U}^{\mathrm{FB}}=\mathbf{S}^{\mathrm{G}}_{\mathrm{BB}}\,\mathbf{U_g}\,. \tag{4.2.25}$$

Noting that $(\mathbf{S}^{\mathrm{s}}_{\mathrm{BR}}\,\mathbf{S}^{\mathrm{s}}_{\mathrm{RB}})^{-1}\mathbf{S}^{\mathrm{s}}_{\mathrm{BR}}\,\mathbf{S}^{\mathrm{s}}_{\mathrm{RR}}(\mathbf{S}^{\mathrm{s}}_{\mathrm{RR}})^{-1}\mathbf{S}^{\mathrm{s}}_{\mathrm{RB}}$ is an identity matrix, equation (4.2.25) can be simplified to

$$\left[\mathbf{S}_{\mathrm{BB}}-\mathbf{S}^{\mathrm{s}}_{\mathrm{BR}}(\mathbf{S}^{\mathrm{s}}_{\mathrm{RR}})^{-1}\mathbf{S}^{\mathrm{s}}_{\mathrm{RB}}\right]\mathbf{U}^{\mathrm{FB}}=\mathbf{S}^{\mathrm{G}}_{\mathrm{BB}}\,\mathbf{U_g}\,,$$

i.e.,

$$\mathbf{U}^{\mathrm{FB}}=\left[\mathbf{S}_{\mathrm{BB}}-\mathbf{S}^{\mathrm{s}}_{\mathrm{BR}}(\mathbf{S}^{\mathrm{s}}_{\mathrm{RR}})^{-1}\mathbf{S}^{\mathrm{s}}_{\mathrm{RB}}\right]^{-1}\mathbf{S}^{\mathrm{G}}_{\mathrm{BB}}\,\mathbf{U_g}\,. \tag{4.2.26}$$

It can be seen that equation (4.2.26) agrees with the relationship given by equations (4.1.18) to (4.1.25). The main difference is that equations (4.1.18) to (4.1.25) consider a more general situation, i.e., the rotational DOF and multiple supports. Although the case presented in this section is relatively simple, it provides a deeper insight of how SSI effect affects the response of structure. It also help to gain better understanding of the expression of the dynamic stiffness matrices in equations (4.1.3) and (4.1.5).

4.2.2 Numerical Verification

To further validate the derivations in Sections 4.1 and 4.2.1, numerical verification is presented. The parameters of model are given in Table 4.1 while the modal information of the coupled and uncoupled structures, which are obtained from modal analysis, are

given in Tables 4.2 and 4.3, respectively. The value of masses and stiffnesses are selected to guarantee the dominant modal frequencies are around 5 Hz and 12 Hz as this frequency range is very important in nuclear power plants. The damping coefficients are chosen to make the modal damping ratios as 5%, which is also typical in the nuclear power industry. The stiffness of soil spring is chosen to be 5×10^4 kN/m (D site) according to the soil site classification in Appendix A.

As can be seen from Tables 4.2 and 4.3, the natural frequencies of structure decrease when soil is included. For example, the dominant frequency shifts from 5.37 Hz to 5.04 Hz due to the presence of soil, indicating that the structure becomes more flexible when soil is taken into consideration. It will be shown later in a parametric study that the amount of the shift of the natural frequencies depends on the stiffness of soil.

The numerical procedure is shown in Figure 4.7. 30 sets of R.G. 1.60 spectra-compatible time histories are applied to the coupled soil-structure system. The average FLIRS (i.e.,

Table 4.1 Basic structural information in example 1

Mass (kg)			Stiffness ($\times 10^3$ kN/m)			Damping coefficient (kN · s/m)				
m_1	m_2	m_b	k_1	k_2	k_s	c_1	c_2	c_s	c_{1a}	c_{2a}
3000	1500	3000	6	5	50	4	4.5	500	8.5	3.5

Table 4.2 Modal information of the coupled soil-structure system

Mode	Frequency (Hz)	Participation factor	Modal shape
1	5.04	1.30	[0.699, 1, 0.098]
2	11.96	−0.34	[−0.696, 1, −0.144]
3	19.93	0.82	[−0.173, 0.047, 1]

Table 4.3 Modal information of the decoupled structure

Mode	Frequency (Hz)	Participation factor	Modal shape
1	5.37	1.241	[0.659, 1]
2	12.19	−0.241	[−0.759, 1]

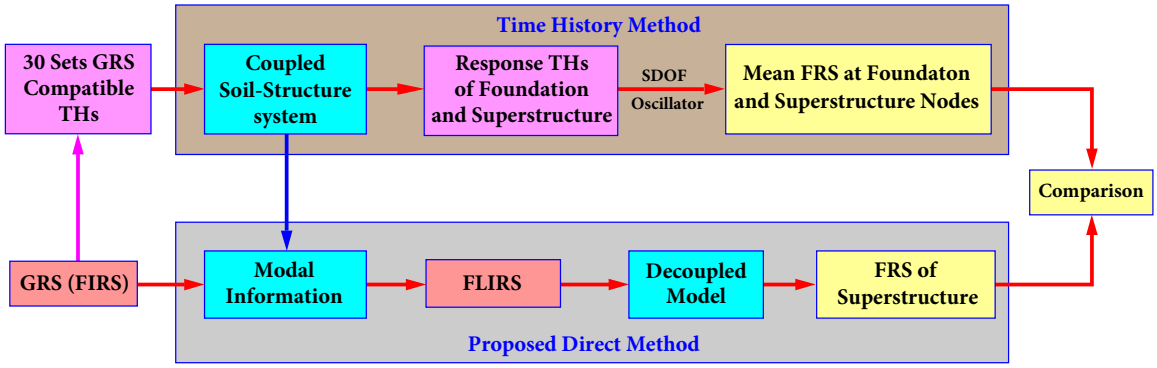

Figure 4.7 Numerical procedure for example 1.

the mean FRS at the foundation node) and FRS of the structure nodes obtained from 30 sets of time history analyses are regarded as benchmark for comparison. In the direct spectra-to-spectra method considering SSI, the formulations in Section 4.1.1 are utilized to generate FLIRS from FIRS (i.e., R.G. 1.60 response spectra) directly. The generated FLIRS is then applied together with the direct method developed in Chapter 2 to obtain FRS of the superstructure. The direct method for the generation of FRS for structures with multiple supports is reduced to single support in this numerical example. Finally, FLIRS and FRS generated by direct method are compared with the benchmarks obtained by 30 sets of time history analyses to verify the proposed method.

It should be mentioned that the coupled soil-structure system does not need to be diagonalizable for generating FLIRS. However, the superstructure (i.e., the decoupled structure) must be diagonalizable when applying a direct spectra-to-spectra method to generate FRS. This is because a direct method, either proposed in this research or previous studies, is based on modal spectral responses, which requires the structure be diagonalizable. Therefore, in order to investigate the effect of SSI on FRS, two air damping coefficients c_{1A} and c_{2A} are added, which represents the resistance from air when structure is vibrating.

Dynamic Influence Matrix

The dimensionless dynamic influence matrix $\mathbf{S}^{MS}$ of decoupled model given by equation (4.1.11) is determined for different values of ω, varying from 0.2π to 200π with an increment of 0.1. Each elements in the matrix is complex and can be regarded as a transfer function. The modulus of the elements corresponding to Node 1 and Node 2 are plotted

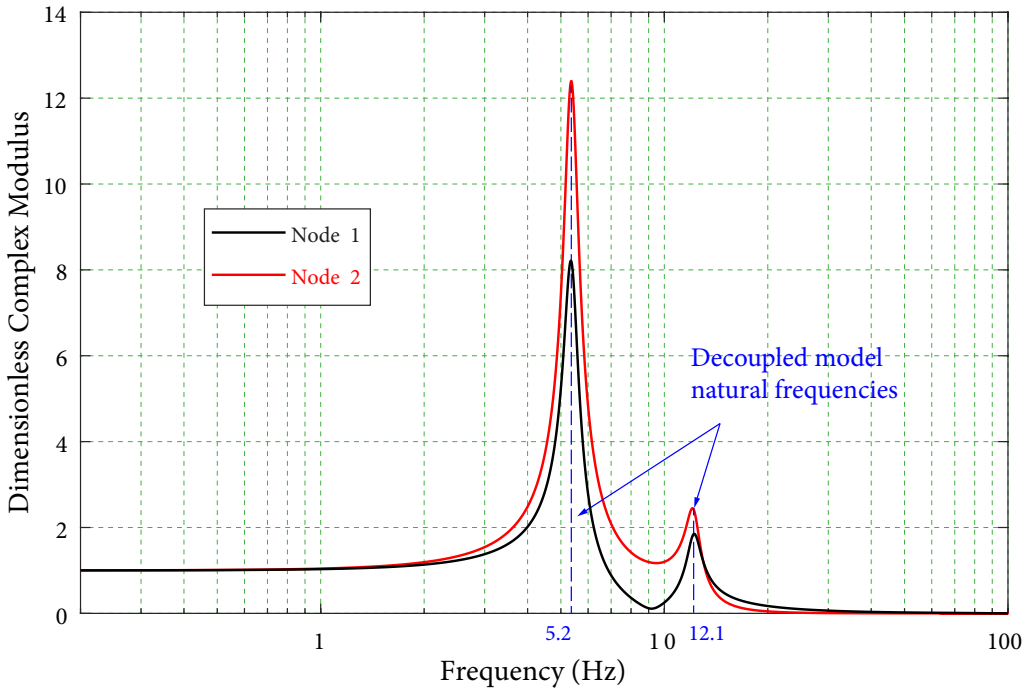

Figure 4.8 Modulus of the dynamic influence matrix for Nodes 1 and 2.

versus frequency in Figure 4.8. It can be seen that the modulus of the transfer functions peaks at the natural frequencies of the structure.

FLIRS Transfer Matrix and Modification Factor

Similar to dynamic influence matrix $\mathbf{S}^{\mathrm{MS}}$, FLIRS transfer matrix $\mathcal{T}$ and FLIRS modification factor $\mathcal{R}$ are also evaluated for the circular frequency range from 0.2π to 200π, shown in Figures 4.9 and 4.10, respectively. It is found that unlike $\mathbf{S}^{\mathrm{MS}}$, which peaks at the natural frequencies of the decoupled structure, the peaks of $\mathcal{T}$ and $\mathcal{R}$ are located near the natural frequencies of the coupled 3DOF system, whereas two valleys located at the natural frequencies of the superstructure are identified. This is because dynamic influence matrix $\mathbf{S}^{\mathrm{MS}}$ reflects the influence of base motion on superstructure; or in other words, $\mathbf{S}^{\mathrm{MS}}$ is only determined by the structural information of the decoupled structure as can be seen in equation (4.1.11). On the other hand, superstructure as well as soil properties are both considered in obtaining FLIRS transfer matrix $\mathcal{T}$ and FLIRS modification factor $\mathcal{R}$.

The valleys in $\mathcal{T}$ and $\mathcal{R}$ can be interpreted as a result of the absorption of vibration. It means that the soil in a coupled soil-structure system may play the same role as vibration absorber, in which the energy of excitation is absorbed at certain frequencies, i.e., natural frequencies of the decoupled model.

Furthermore, the result of the modification factor given in Figure 4.10 shows that the FIRS is mainly modified within the frequency range 1 Hz to 33 Hz. This is because earthquake excitations with low frequency do not have much influence on seismic vibration of this system, while a structure can be regarded as rigid when the natural frequencies exceed 33 Hz. Therefore, the modification factor in these frequency ranges is approximately 1. One more observation made from Figure 4.10 is that earthquake excitations at the dominant frequencies of either coupled or uncoupled system are changed more significantly comparing with other frequencies when SSI effect is considered. Therefore, one has to pay more attention to the dominant frequencies of both coupled and uncoupled systems in engineering practice.

Comparison of FLIRS

Having obtained the FLIRS modification factor $\mathcal{R}$, FLIRS is determined by multiplying FIRS by the modification factor. To verify if the generated FLIRS is accurate, one has to compare it with time history analysis. Although there is no concept of FLIRS in time history analysis of the coupled soil-structure system, it has been shown in Section 4.2.1 that FLIRS in the decoupled structure is equal to FRS at the corresponding base nodes in the coupled soil-structure system. Therefore, FLIRS used in the direct method can be validated by comparing it with mean FRS at Node 3 of the coupled system, shown in Figure 4.11. The black solid line is the FLIRS generated by the proposed method, while the red dash line represents the average FRS at the base node from 30 time history analyses. The blue solid line is the target response spectrum of the input time histories, i.e., FIRS.

It can be seen from Figure 4.11 that FLIRS generated by the proposed method agrees well with the corresponding mean FRS by 30 set of time history analyses. Comparing with FIRS, the modified input FLIRS has a significant valley near the dominant frequency of the superstructure (i.e., 5.3 Hz). This agrees with the conclusion that the soil in a coupled

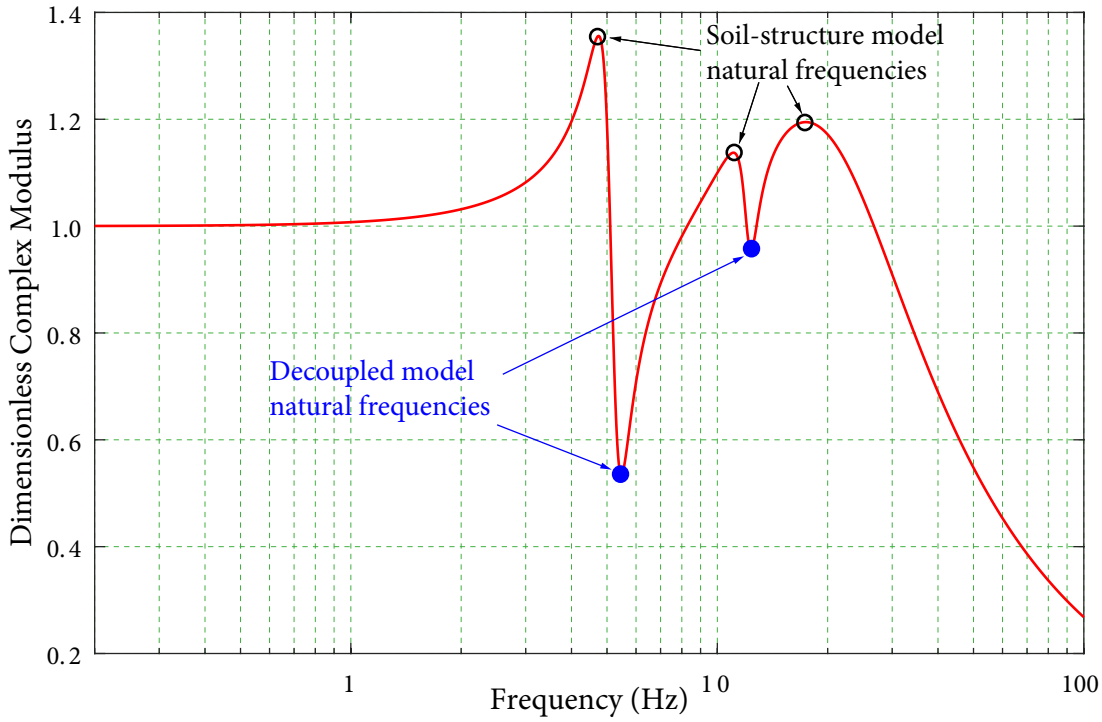

Figure 4.9 Modulus of FLIRS transfer matrix.

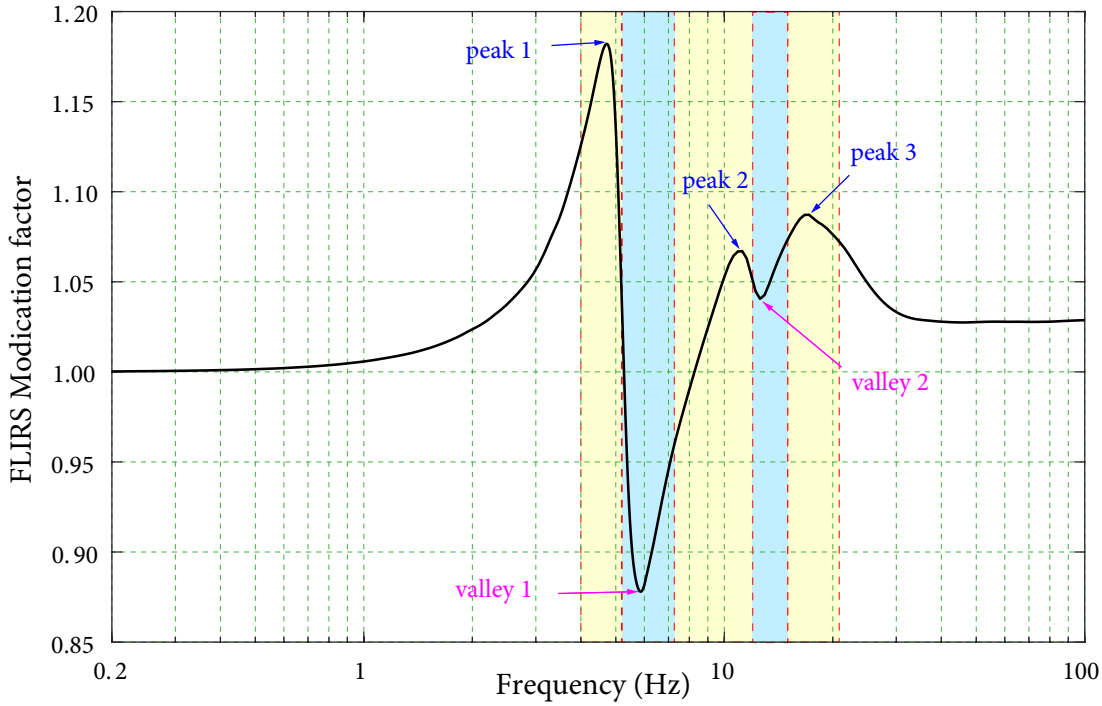

Figure 4.10 FLIRS modification factor.

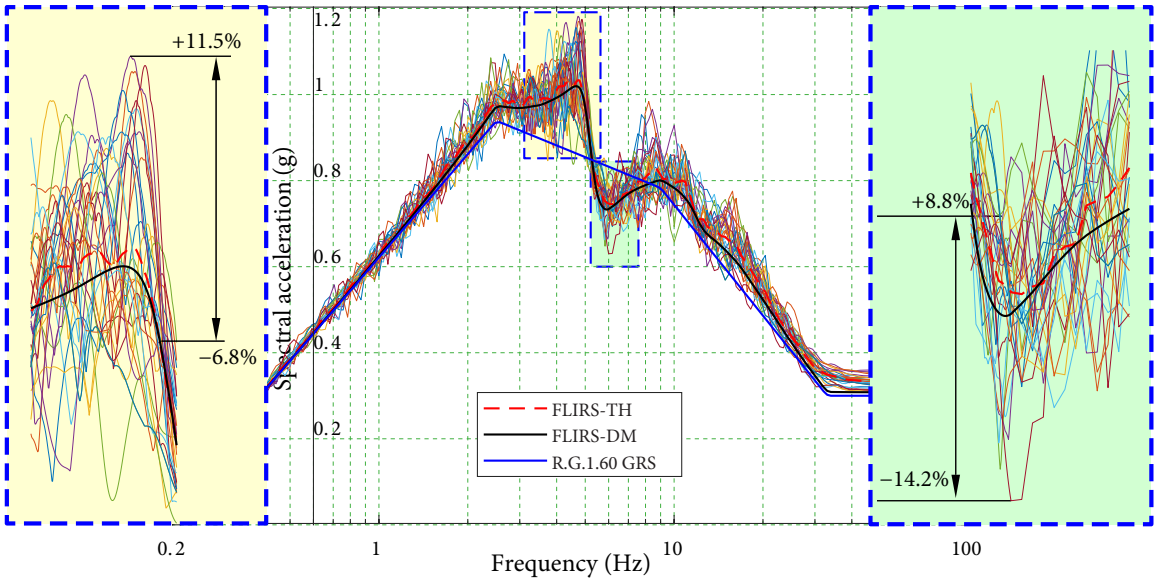

Figure 4.11 Comparison of FLIRS by direct method and time history method.

soil-structure system acts as a vibration absorber that the power of earthquake excitation near the natural frequency of the superstructure is absorbed to some extent. On the other hand, the peak located at 4.58 Hz of FLIRS indicates that the energy of seismic excitation near the natural frequency of the decoupled model is shifted to lower frequency due to the presence of soil, which could result in a larger FRS around this frequency.

While the proposed method has been proved to generate FLIRS accurately, large variabilities are found in a single time history analysis, especially at the dominant frequencies. It is observed that the peak of FLIRS can be overestimated by 11.5% whereas the valley of FLIRS may be underestimated by −14.2% in a single time history analysis. As a result, the seismic analysis considering SSI based on a single or a small number of time history analyses could be insufficient.

Comparison of FRS

The obtained FLIRS is input to the decoupled model to generate FRS, which are calculated at 200 frequencies including the natural frequencies of the structure using the direct spectra-to-spectra method. In this procedure, either the method developed in Chapter 2 or the method by Jiang (2016) can be applied because the superstructure has only one input.

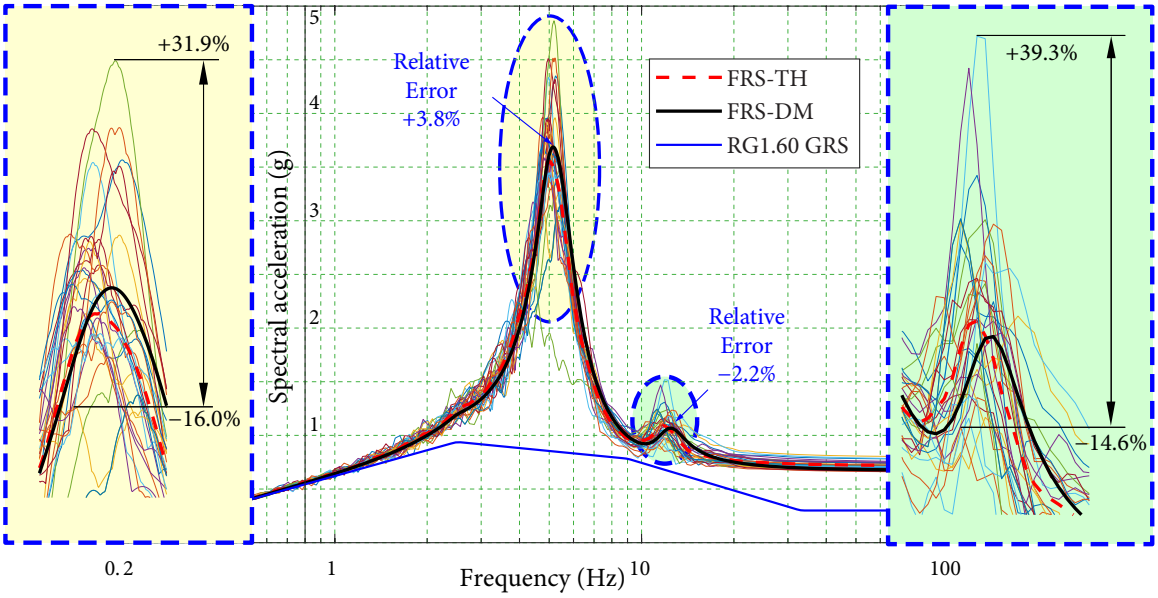

Figure 4.12 Comparison of FRS by direct method and time history method.

FRS at Node 1 obtained by the direct method is plotted along with those generated by the 30 sets of time history analyses in Figure 4.12. FRS obtained by the direct method and the mean FRS of the time history analyses, which is regarded as the "benchmark" FRS, are shown in black solid lines and red dash lines, respectively. It is seen that the FRS obtained by the direct method agrees well with the "benchmark" FRS over the entire frequency range, whereas the result from individual time history analysis exhibits large variability. Figure 4.12 shows that a single set of time history analysis can lead to a maximum 39.3% overestimation or 16.0% underestimation of FRS peak depending on the input acceleration time history used. However, the differences between the FRS peaks obtained by the direct method and "benchmark" FRS are less than 4%, which are well within the range of acceptable errors. Therefore, the proposed method is superior in accurately and efficiently generating FRS considering SSI in practice.

Effect of Soil-Structure Interaction on FRS

The effect of SSI on FRS is firstly studied by comparing the mean FRS obtained from time history analysis. 30 sets of R.G. 1.60 compatible time histories are input to the decoupled

model and soil-structure model, respectively, and the resultant mean FRS at Node 1 are plotted in Figure 4.13. The red dashed line and black solid line represent the FRS with and without the presence of soil, respectively.

It is observed that the peak value of FRS is reduced by 8.1% when the SSI effect is accounted, which indicates that the consideration of soil may decrease the seismic demand of secondary equipments. However, the peak floor acceleration, which represents the structural response and is equal to FRS at high frequencies, is decreased by only 4.5%. It means that the SSI effect is more significant on the secondary system than the main structure. Furthermore, similar to FLIRS, the main peak of FRS shifts slightly from the dominant frequency of the structure (i.e., 5.3 Hz) to lower frequency (5.0 Hz), which is between the first modal frequency of the coupled and the uncoupled systems. Although the presence of soil is conventionally considered to pose beneficial effects on seismic responses (Wolf, 1985), the shifting of FRS peaks due to SSI effect deserves more attention. For example, the shifting of FRS peak causes larger FRS values from frequency 2 Hz to 5 Hz, and neglecting this may lead to unconservative result at certain frequencies in the design of

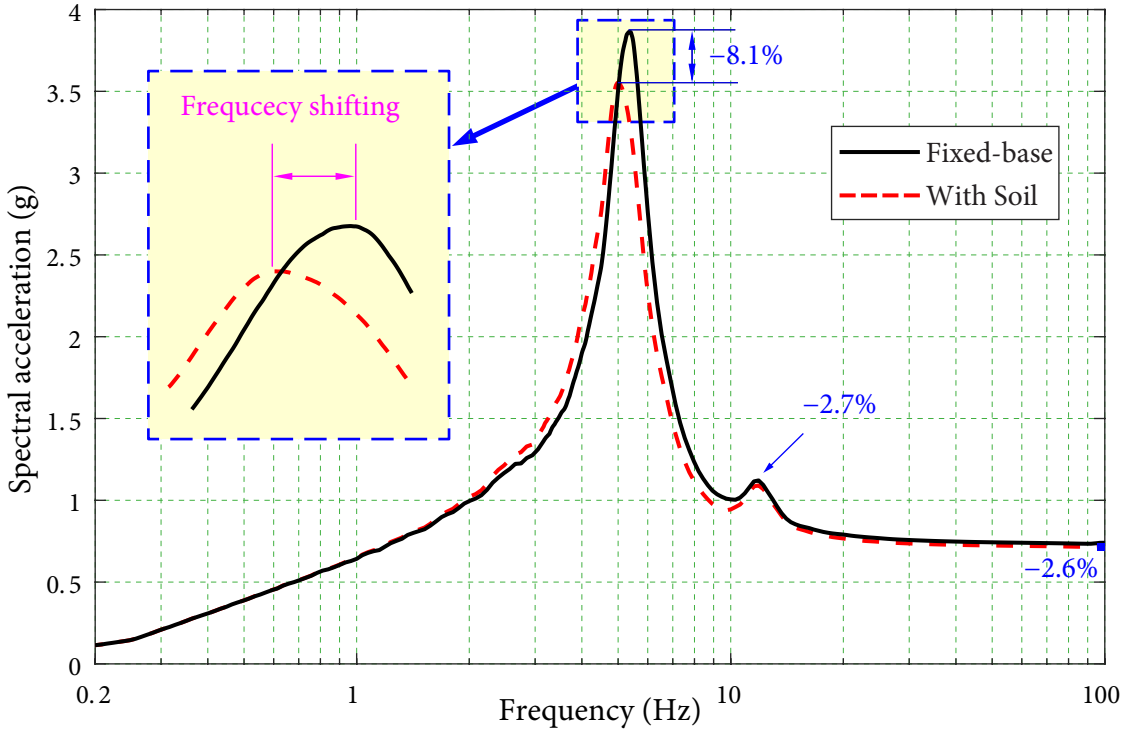

Figure 4.13 Effect of soil-structure interaction on FRS.

secondary components. Thus, SSI effect should be taken into consideration when assessing secondary system because of its significant influence on FRS.

4.2.3 Influence of Soil Conditions on FRS: A Parametric Study

In order to better investigate the effect of SSI on FRS, a parametric study in presented. There are in total 5 cases with different soil stiffness determined using Table A.3 in Appendix A. Soil ranges from soft soil to rock with the increase of soil stiffness, where Case 2 is the case presented in Section 4.2.2. The properties of the soil in different cases are given in Table 4.4, and the natural frequencies of the coupled soil-structure system are given in Table 4.5. Several parameters, such as FLIRS transfer matrix, FLIRS modification factor, and FRS, are computed for each soil case and are compared to investigate the influence of soil conditions on the seismic behavior.

It has been mentioned that the dynamic influence matrix $\mathbf{S}^{MS}$ depends on the structural information only but not soil properties. Therefore, it is same as the results given in Figure 4.8 and will not be discussed here. On the other hand, it is worthwhile to compare FLIRS transfer matrix $\mathcal{T}$ and FLIRS modification factor $\mathcal{R}$ under different soil conditions to investigate the effect of SSI as they are influenced by soil.

Table 4.4 Soil stiffness in different cases

Site class	E	D	C	B	
Case number	1	2	3	4	5
Soil type	Soft soil	Stiff soil	Very dense soil	Rock	Rock
Stiffness k_s ($\times 10^4$ kN/m)	1	5	10	50	100

Table 4.5 Natural frequencies of the coupled system under different soil cases

Soil Case		1	2	3	4	5
Natural Frequencies (Hz)	Mode 1	4.20	5.11	5.24	5.34	5.35
	Mode 2	10.58	12.02	12.11	12.17	12.18
	Mode 3	13.52	21.90	29.97	65.37	92.17

Influence of Soil Conditions on FLIRS Transfer Matrix

Figure 4.14 shows the result of the complex modulus of FLIRS transfer matrix $\mathcal{T}$ of different soil cases. It is found that all of the FLIRS in Figure 4.14 have two significant valleys located near frequencies 5.36 Hz and 12.11 Hz. Comparing with Table 4.3, it is seen that these two valleys are located at the natural frequencies of the decoupled structure despite what the value of soil stiffness is. It becomes clearer that the soil behaves like a vibration absorber that absorbs the energy in earthquake excitation near the natural frequency of the structure.

Besides of valleys, 3 peaks of the FLIRS transfer matrix are found. However, unlike the location of valleys, which are almost the same, the positions of these peaks change significantly when the soil property changes. To be more specific, the peaks are located at the natural frequencies of the combined soil-structure system, which depends on the properties of both the superstructure and the soil. With soil becoming stiffer, the peaks move toward higher frequencies along with the increase of natural frequencies of the coupled system. In addition, the first two peaks decrease along with the increase of the third peak when the soil is becoming more rigid, indicating that the power in the ground motion transfers to higher frequencies.

It is known that SSI effect becomes less significant when soil is becoming more rigid. It can also be demonstrated by Figure 4.14 that the modulus of FLIRS transfer matrix between 0.2 Hz and 33 Hz approaches to 1 when soil stiffness increases. Although the third peak of FLIRS also increases significantly, it does not affect the seismic behavior of superstructure very much, because the structure with frequency higher than 33 Hz can be regarded as rigid. As a result, FLIRS becomes very close to FIRS when soil is stiff and SSI effect does not affect structural response significantly.

Influence of Soil Conditions on FLIRS Modification Factor

The result of the FLIRS modification factor $\mathcal{R}$ is given in Figure 4.15. It is found that the modification factor also varies with the change of soil stiffness. To be more specific, FLIRS modification factor changes more significantly when soil condition is relatively soft. The modification factor in Case 4 and Case 5 are close to 1 comparing with other cases because the soil stiffness in these two cases are relative large.

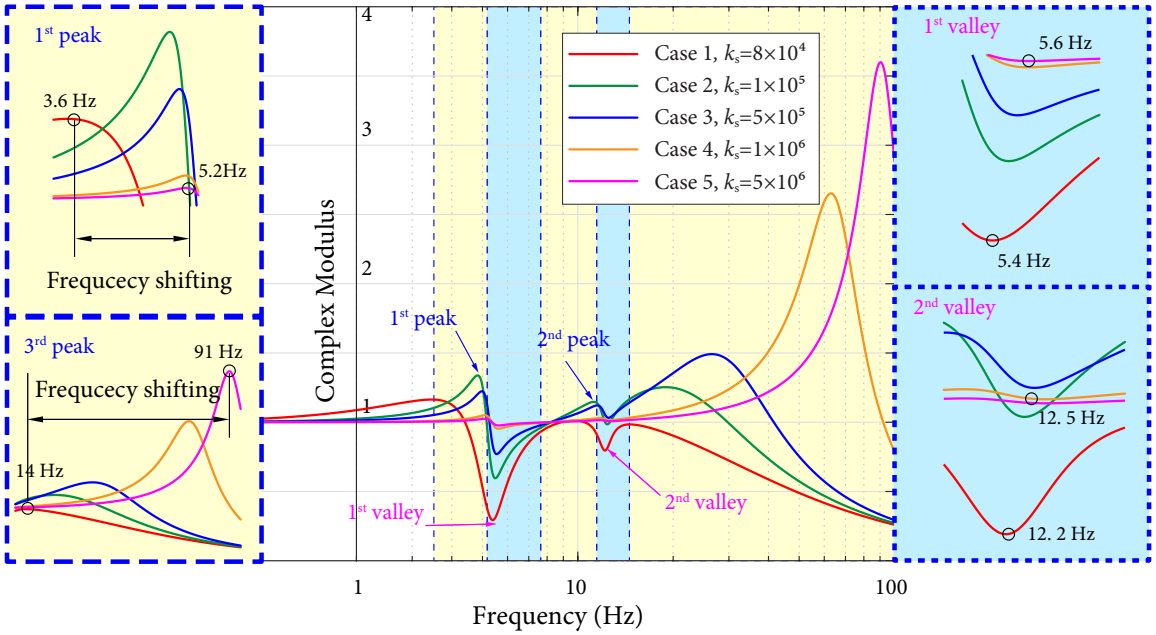

Figure 4.14 Modulus of FLIRS transfer matrix under different soil conditions.

Similar to the FLIRS transfer matrix $\mathcal{T}$, the modification factor also has two significant valleys at the natural frequencies of the superstructure under all soil conditions. In addition, the peaks at the natural frequencies of the first and second modes of the coupled soil-structure system are also presented. However, the third peak of FLIRS transfer matrix in the high frequency range, does not appear in the modification factor. This is because these peaks are located at the frequencies where the structure can be treated as rigid, and the influence of these peaks can be neglected. Therefore, the third peak of FLIRS transfer matrix does not reflect in the modification factor.

Furthermore, it is observed that the maximum value of FLIRS modification factor occurs around 5.3 Hz in Case 2, which is not the most soft case or hardest case but something in-between. This is because FLIRS will approach to FIRS when soil becomes very stiff; on the other hand, the superstructure (including the foundation nodes) will remain stable if soil is sufficiently flexible, leading to a very small modification factor. Therefore, SSI effect should be most significant when the soil stiffness is at certain value between very soft and stiff soil.

Influence of Soil Conditions on FLIRS

Figure 4.16 shows the FLIRS generated using the modification factor for each case. As FLIRS is the product of FIRS and FLIRS modification factor, it has some similar features as the modification factor, such as the locations of the peaks and valleys, which will not be discussed again. The only thing that the author wants to emphasize is the maximum value of FLIRS among these cases. While it has been shown in Figure 4.15 that FIRS is changed most significantly in Case 2, the maximum FLIRS peak appears in Case 1 at 2.6 Hz instead. This is because the spectral value of FIRS (black dashed line in Figure 4.16) at this frequency is the greatest. This highest FLIRS peak may result in higher seismic demands at low frequencies.

Influence of Soil Conditions on FRS

Figures 4.17 to 4.20 show the FLIRS and resultant FRS under different soil conditions by the direct method and the time history method, while FRS in Case 2 is given in Figure 4.12. It is observed that FRS peaks decrease when soil becomes softer, i.e., the maximum seismic response will be generally reduced when SSI effect is taken into account. For example, the maximum spectral value of FRS is reduced from $3.81g$ in Case 5 to $3.68g$ in Case 2 and further $2.34g$ in Case 1. On the other hand, the maximum value of FRS does not change apparently when soil is relative stiff as the peak FRS in Cases 3, 4 and 5 are almost the same. Moreover, the peaks of FRS, which are located at the natural frequencies of the superstructure in the relative stiff soil conditions, are slightly shifted to lower frequencies with the decrease of soil stiffness. This shifting of FRS peaks, however, can be more significant when a complex structure is analyzed, which deserves more attention in practice (Jiang, 2016).

Comparing the results by the direct method (black solid lines) and the benchmark from the time history method (red dashed lines), it can be seen that FRS by the proposed method agrees remarkably well with that by 30 sets of time history analyses for Cases 2 to 5. This indicates that the proposed direct method is accurate for generating FRS considering SSI effect for soil with classification in or higher than D sites. In nuclear industry, which has restrict requirements on safety, nuclear facilities are usually located at relative stiff soil sites,

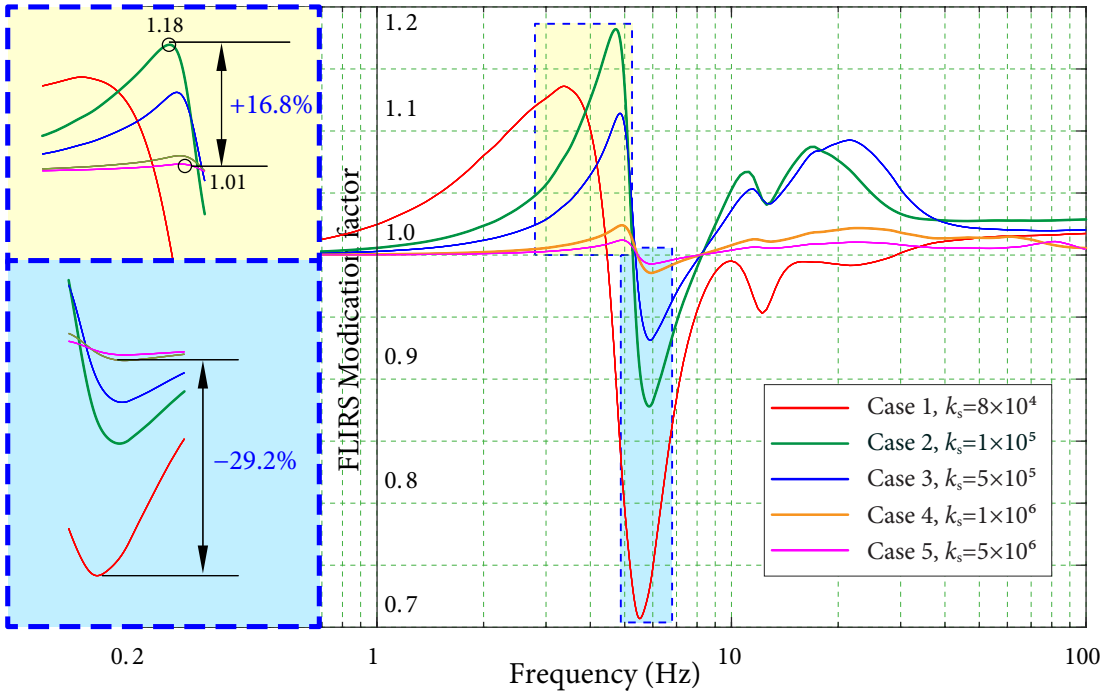

Figure 4.15 FLIRS modification factor under different soil conditions.

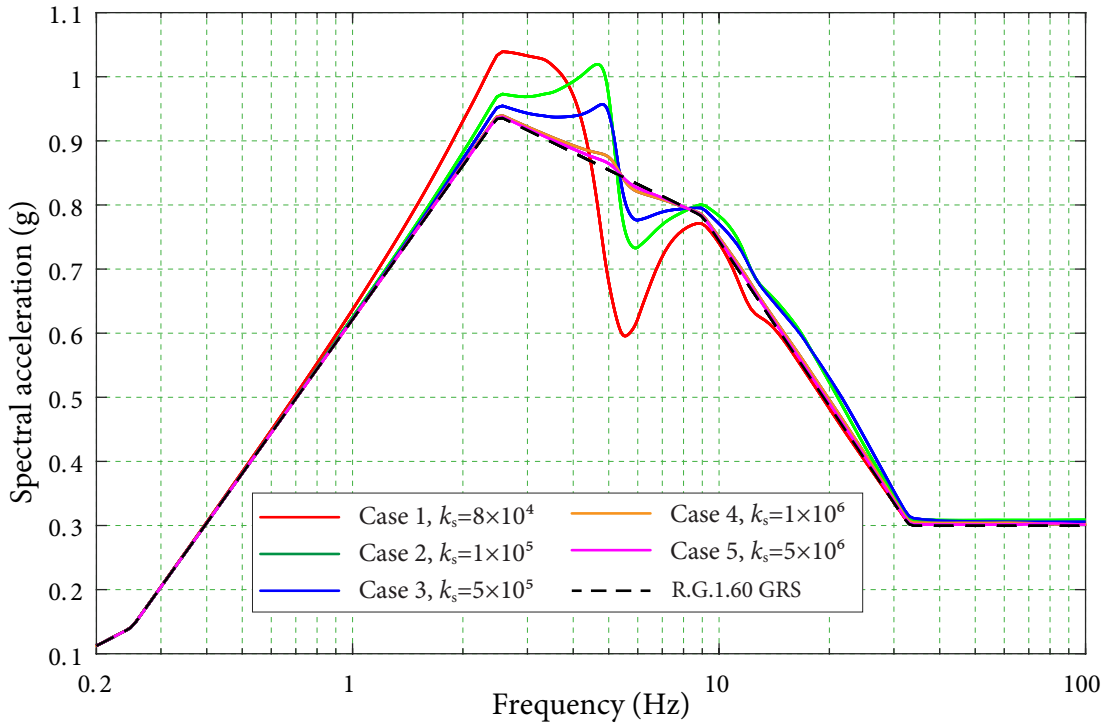

Figure 4.16 FLIRS under different soil conditions.

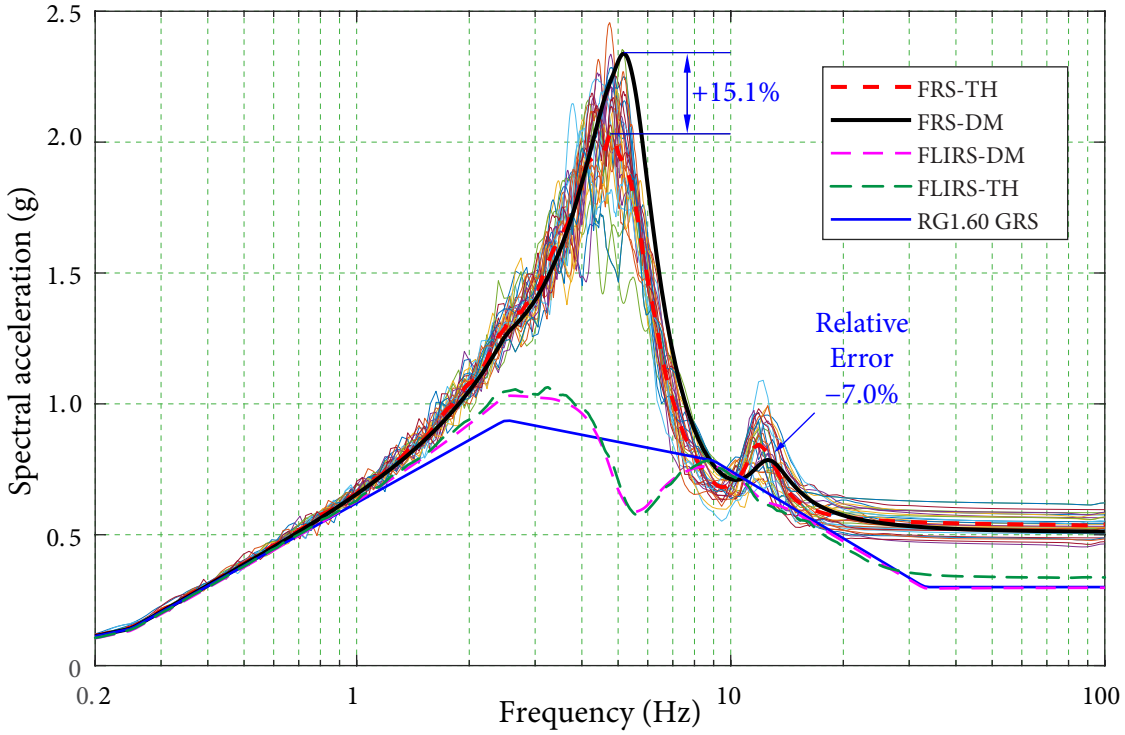

Figure 4.17 FRS at Node 1 in Case 1 (k_s=1×10^4 kN/m).

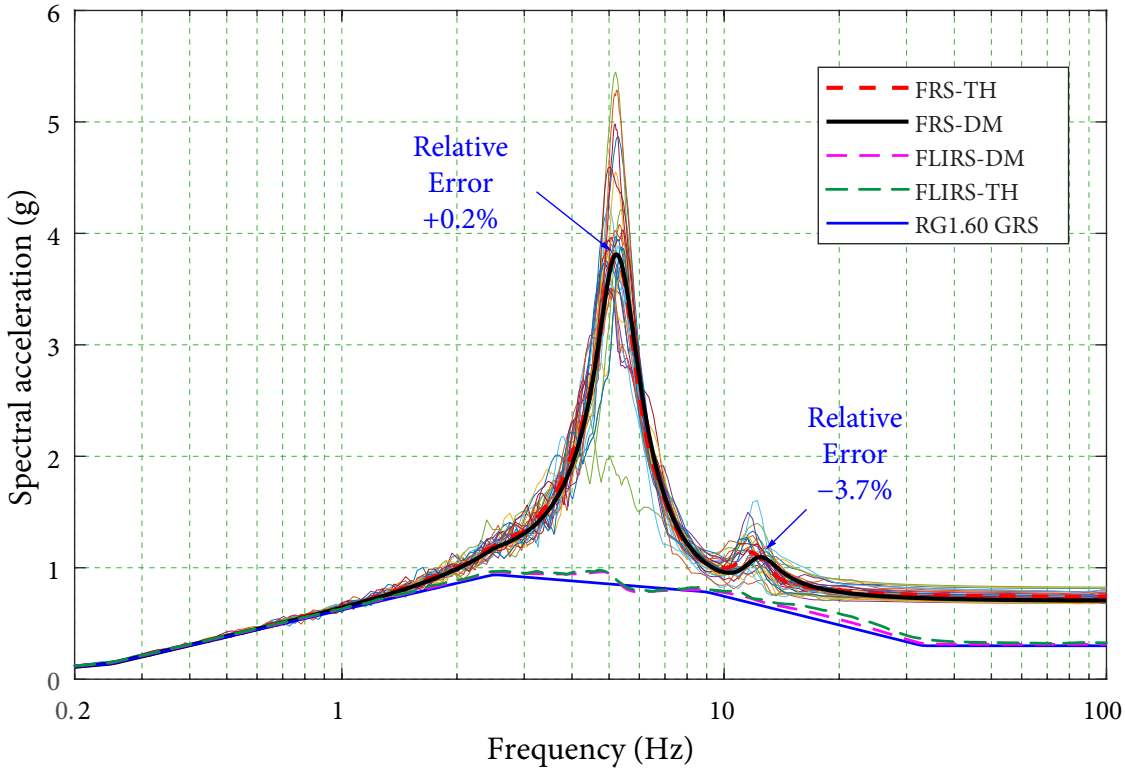

Figure 4.18 FRS at Node 1 in Case 3 (k_s=1×10^5 kN/m).

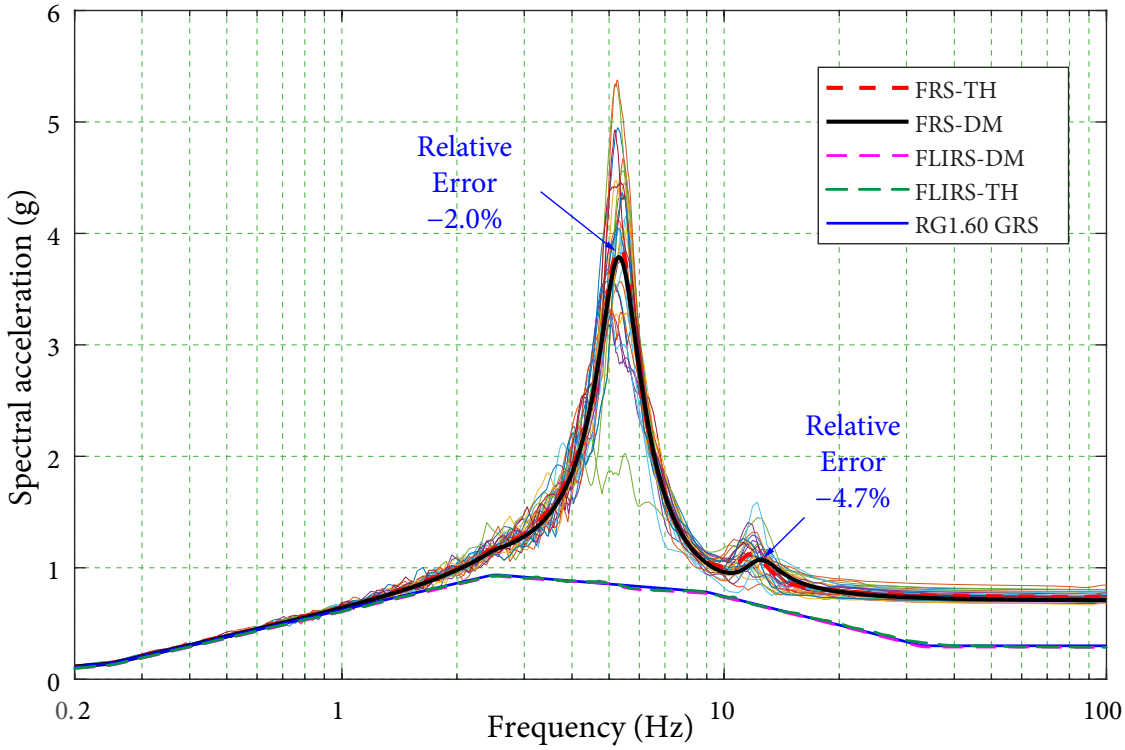

Figure 4.19 FRS at Node 1 in Case 4 (k_s=5×10^5 kN/m).

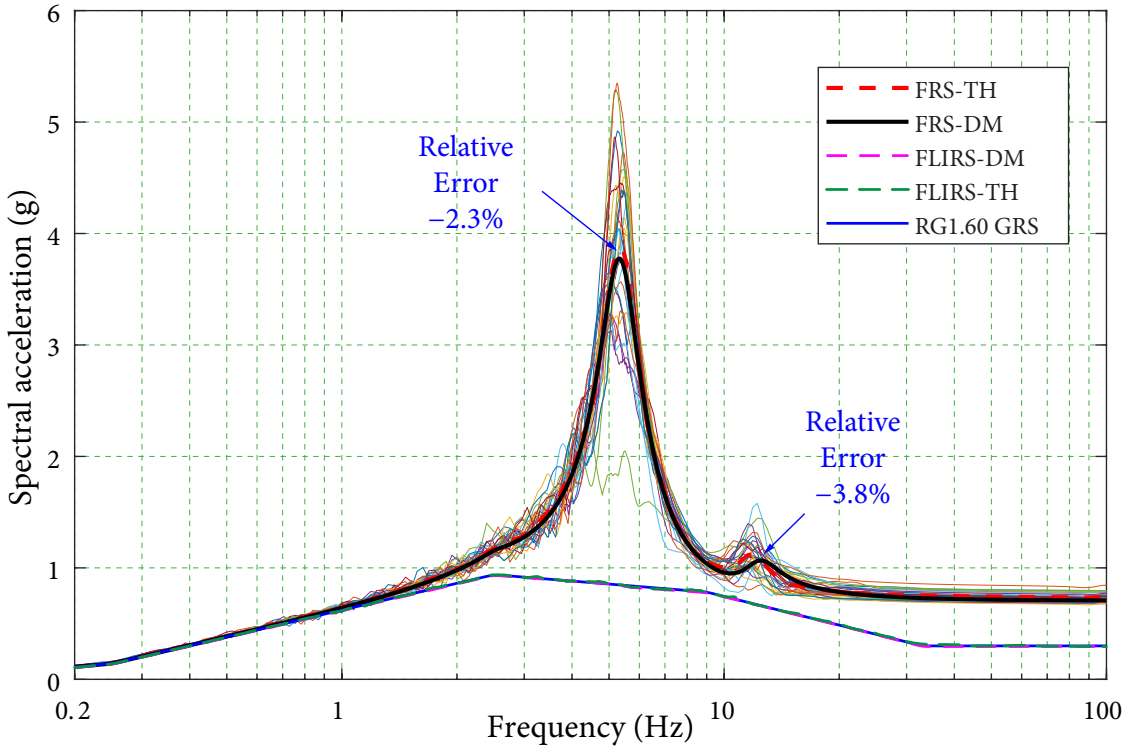

Figure 4.20 FRS at Node 1 in Case 5 (k_s=1×10^6 kN/m).

such as C sites or higher. In this cases, the proposed method can be widely applied in nuclear industry.

Although it is unlikely that nuclear buildings would be sitting on E site, the result of Case 1 is also presented in Figure 4.17. As can be seen in Figure 4.17, FRS by the proposed method can lead to a 15.1% overestimation at the main peak and -7.0% underestimation at the second peak, indicating that the proposed method has limitations in this type of soil. The reason for this restriction is studied in the following.

Limitation of the Application of tRS by Li et al. (2015) *to Very Soft Soil*

It can be found in Figure 4.17 that FLIRS obtained by the direct method agrees remarkably well with these by time history method despite of the errors in FRS. It further proved that the coupled soil-structure system can be replaced by a decoupled model with modified input FLIRS, and the proposed method for generating FLIRS is accurate for any soil conditions. Therefore, the error should not come from the seismic input but the later application of the direct method for the generation of FRS.

Noting the errors of FRS in Case 1 are mainly at the FRS peaks, it is reasonable to assume that tRS might be responsible for the errors in FRS when soil is soft because tRS is applied in the direct method to deal with the resonance case. As mentioned in Section 3.2.1, tRS is obtained by a comprehensive statistical analysis using a large number of earthquake excitations which are wide-banded (Li *et al.*, 2015). However, it can be seen that FLIRS in Case 1 is significantly different from the R.G. 1.60 response spectra. While the area under the curve of response spectrum represents the total energy of excitation, the energy in FLIRS is obviously reduced with the presence of soft soil. As a result, FLIRS in this case cannot be treated as a wide-band input, and the statistical relationship of tRS based on wide-band ground motions may be not applicable in this situation. Therefore, FRS obtained by the direct method using tRS for the soft soil case has larger error than those .

The average tRS of FLIRS under different soil cases are obtained from 30 sets of time history analyses (refer to Section 3.2.1 for details for computing tRS from time history analysis). Figure 4.21 shows the ratios between the obtained average tRS and GRS. The amplification ratios AR of Case 4 and Case 5 are found to be very close to the AR by Li

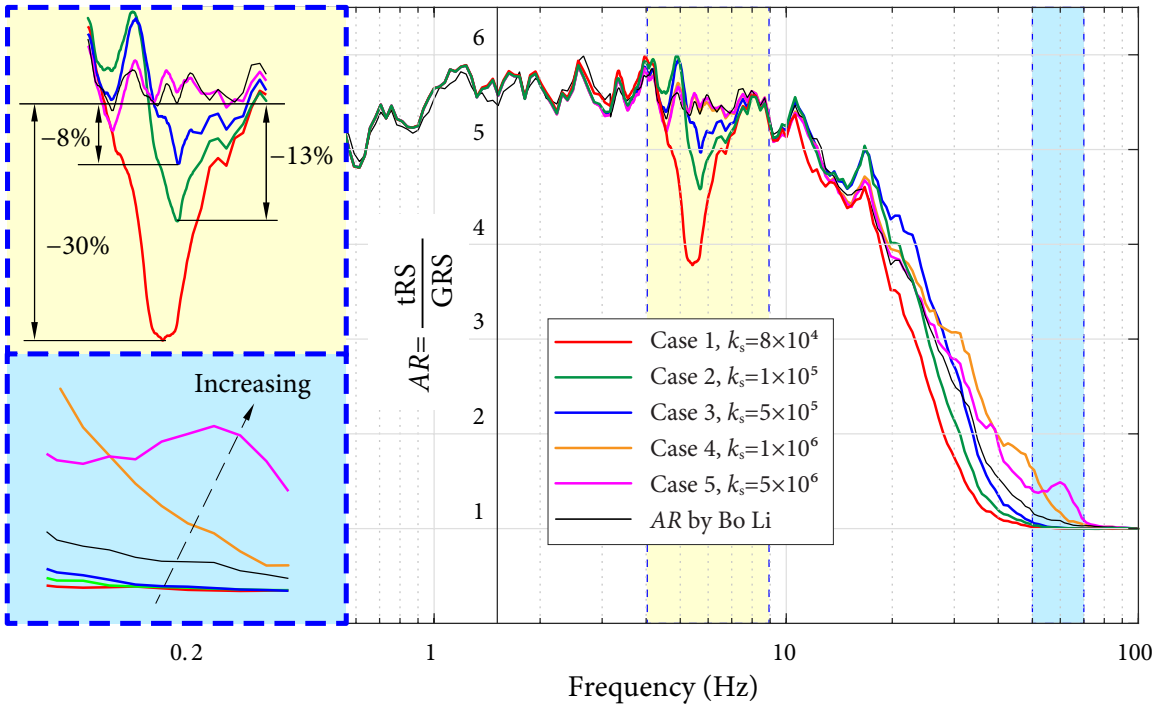

Figure 4.21 Amplification ratios in different soil cases.

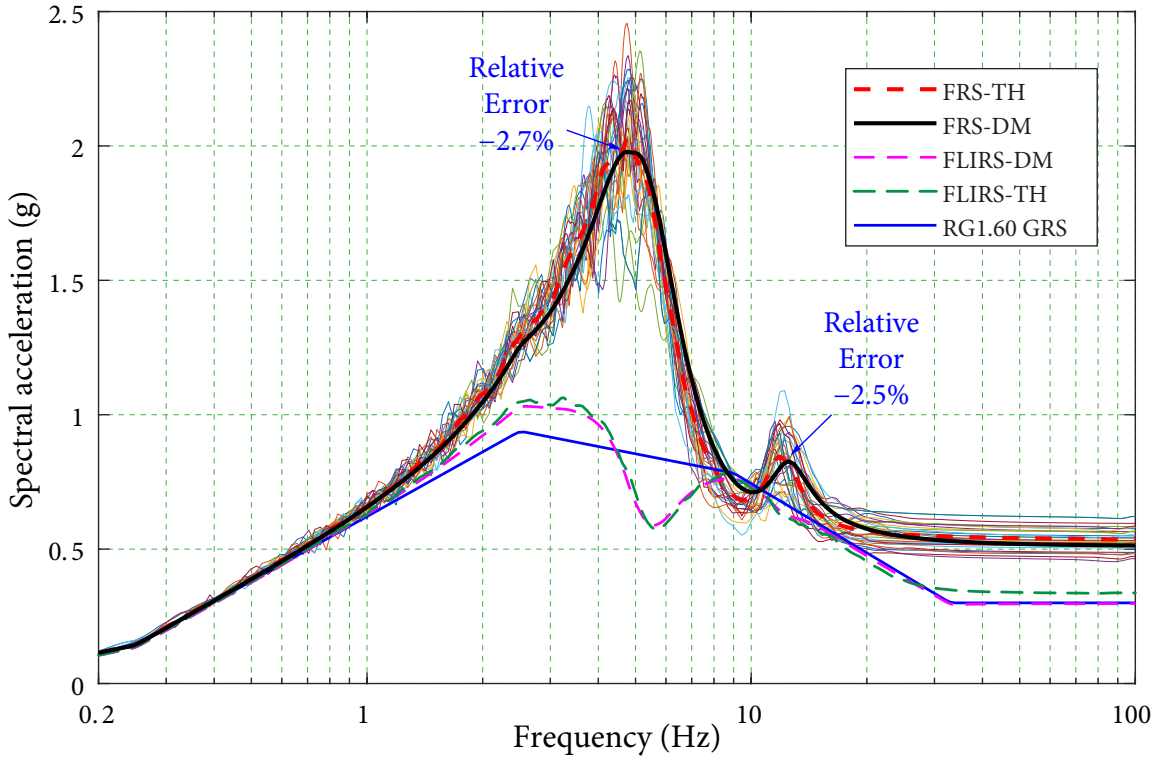

Figure 4.22 FRS using average tRS for Case 1.

et al. (2015) so that these two cases can be regarded as the rigid case as mentioned before. However, a significant valley is found around 5.4 Hz of the *AR* in Case 1 (given by red solid line in Figure 4.21), which has a 30% gap comparing with the amplification ratio by Li *et al*. (2015). This valley is corresponding to the valley in FLIRS due to the absorbed energy around the natural frequency of the superstructure. Although this gap also exists in the *AR* of Cases 2 and 3, they are not as significant as Case 1. Therefore, FRS is overestimated significantly in Case 1, while Cases 2 and 3 still give acceptable FRS. It can also be observed that the amplification ratio increases between frequency 50 Hz and 70 Hz when soil is becoming more stiff, which also indicates the energy in the earthquake excitation shifts to higher frequencies with the increase of soil stiffness.

FRS of Case 1 is regenerated using the average tRS given by Figure 4.21 instead of the tRS by Li *et al*. (2015) to better illustrate it. It is seen from Figure 4.22 that the generated FRS using the average tRS agrees very well with the mean FRS by the time history method. Comparing Figure 4.22 with Figure 4.17, the relative error at the dominant frequency drops from 15.1% to -2.6% when the mean tRS from 30 time history analyses is used. It demonstrates that the proposed method can also be applied to very flexible soil if proper tRS is available. For hard soils, tRS obtained by Li *et al*. (2015) can be directly applied, while a new relationship of tRS should be taken into consideration when soil is relative soft. Currently the tRS for the soft soil is obtained by time history analysis. A comprehensive study on the statistical relationship between tRS of soft soil and GRS needs to be conducted in the future following the approach by Li *et al*. (2015), which is out of the scope of this study.

4.3 Numerical Example 2: Earthquake Excitations at Multiple Supports

A simple structure with two supports similar to the one in Chapter 2, is presented here to illustrate the proposed method. As can be seen in Figure 4.23, a lumped mass A, which has 2 DOF in horizontal and vertical directions, is supported by two beams AB and AC (in horizontal and vertical directions respectively). The lateral stiffnesses of beams AB and AC

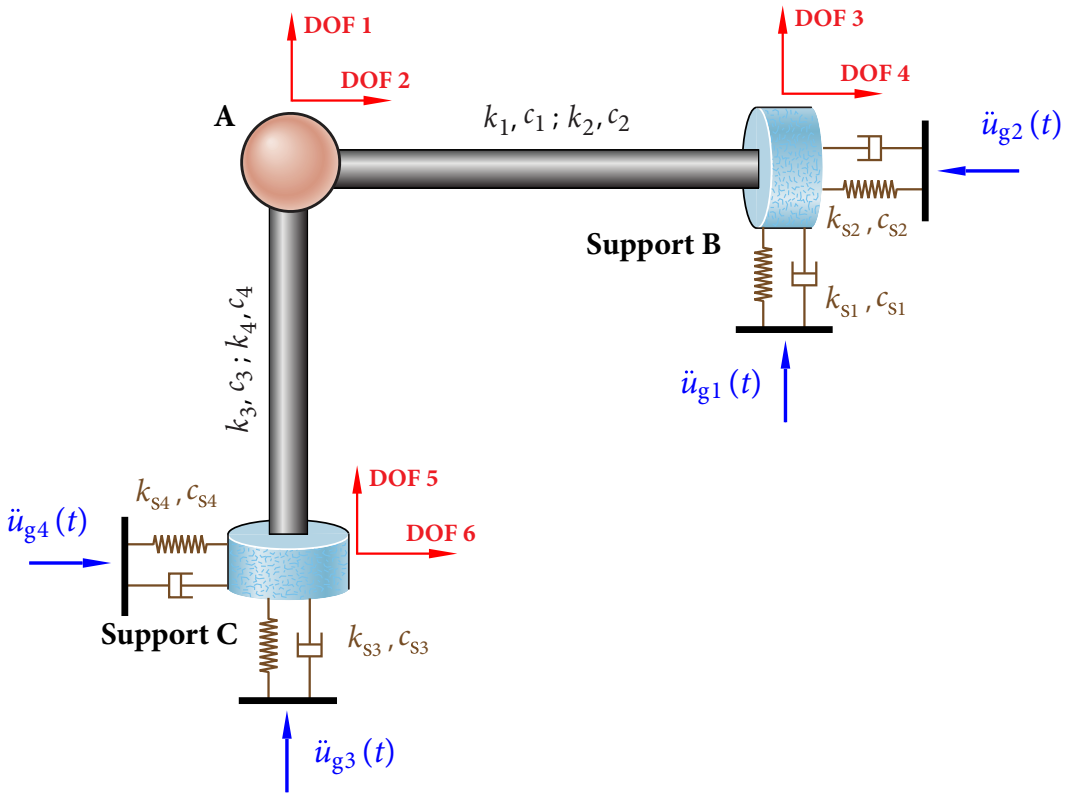

Figure 4.23 Diagram of the numerical example: FRS considering SSI.

are k_1 and k_3, respectively, and the axial stiffnesses are k_2 and k_4, respectively. Similarly, c_1, c_2, c_3, and c_4 represent the lateral and axial damping coefficients of beams AB and AC, respectively. The supports B and C are sitting on soil layers, which are characterized by a set of generalized soil springs with constant stiffnesses and damping coefficients. The combined soil-structure system has in total 6 DOF as shown by the red arrows in the diagram, and the masses are numbered from m_1 to m_6 according to the global DOF. Two set of two-directional earthquake excitations are applied to the coupled system at supports B and C, respectively. As a result, the numerical model can simulate the vibration under seismic excitations from multiple supports considering the SSI effect.

Before performing the numerical calculation, it is worthwhile to obtain the theoretical expressions of the dynamic matrices in the direct method so that those matrices can be clearer. The equations of motion can be written as

$$\begin{bmatrix} m_1 & 0 & 0 & 0 & 0 & 0 \\ 0 & m_1 & 0 & 0 & 0 & 0 \\ 0 & 0 & m_2 & 0 & 0 & 0 \\ 0 & 0 & 0 & m_2 & 0 & 0 \\ 0 & 0 & 0 & 0 & m_3 & 0 \\ 0 & 0 & 0 & 0 & 0 & m_3 \end{bmatrix} \begin{Bmatrix} \ddot{\mathbf{u}}_1 \\ \ddot{\mathbf{u}}_2 \\ \ddot{\mathbf{u}}_3 \\ \ddot{\mathbf{u}}_4 \\ \ddot{\mathbf{u}}_5 \\ \ddot{\mathbf{u}}_6 \end{Bmatrix} + \begin{bmatrix} c_1+c_4 & 0 & -c_1 & 0 & -c_4 & 0 \\ 0 & c_2+c_3 & 0 & -c_2 & 0 & -c_3 \\ -c_1 & 0 & c_1+c_{s1} & 0 & 0 & 0 \\ 0 & -c_2 & 0 & c_2+c_{s2} & 0 & 0 \\ -c_4 & 0 & 0 & 0 & c_4+c_{s3} & 0 \\ 0 & -c_3 & 0 & 0 & 0 & c_3+c_{s4} \end{bmatrix} \begin{Bmatrix} \dot{\mathbf{u}}_1 \\ \dot{\mathbf{u}}_2 \\ \dot{\mathbf{u}}_3 \\ \dot{\mathbf{u}}_4 \\ \dot{\mathbf{u}}_5 \\ \dot{\mathbf{u}}_6 \end{Bmatrix}$$

$$+ \begin{bmatrix} k_1+k_4 & 0 & -k_1 & 0 & -k_4 & 0 \\ 0 & k_2+k_3 & 0 & -k_2 & 0 & -k_3 \\ -k_1 & 0 & k_1+k_{s1} & 0 & 0 & 0 \\ 0 & -k_2 & 0 & k_2+k_{s2} & 0 & 0 \\ -k_4 & 0 & 0 & 0 & k_4+k_{s3} & 0 \\ 0 & -k_3 & 0 & 0 & 0 & k_3+k_{s4} \end{bmatrix} \begin{Bmatrix} \mathbf{u}_1 \\ \mathbf{u}_2 \\ \mathbf{u}_3 \\ \mathbf{u}_4 \\ \mathbf{u}_5 \\ \mathbf{u}_6 \end{Bmatrix} = \begin{Bmatrix} 0 \\ 0 \\ c_{s1}\,\dot{u}_{g_1}+k_{s1}\,u_{g_1} \\ c_{s2}\,\dot{u}_{g_2}+k_{s2}\,u_{g_2} \\ c_{s3}\,\dot{u}_{g_3}+k_{s3}\,u_{g_3} \\ c_{s4}\,\dot{u}_{g_4}+k_{s4}\,u_{g_4} \end{Bmatrix}. \tag{4.3.1}$$

Applying the transform $\mathbf{x}(t) = \mathbf{X}\mathrm{e}^{\mathrm{i}\omega t}$ and partitioning the matrices following the same procedure in Section 4.2.1.1, the dynamic equation of motion in frequency domain can be obtained as

$$\begin{bmatrix} \mathbf{S}^{\mathrm{S}}_{\mathrm{RR}} & \mathbf{S}^{\mathrm{S}}_{\mathrm{RB}} \\ \mathbf{S}^{\mathrm{S}}_{\mathrm{BR}} & \mathbf{S}^{\mathrm{S}}_{\mathrm{BB}} + \mathbf{S}^{\mathrm{G}}_{\mathrm{BB}} \end{bmatrix} \begin{Bmatrix} \mathbf{U}_{\mathrm{R}} \\ \mathbf{U}_{\mathrm{B}} \end{Bmatrix} = \begin{Bmatrix} \mathbf{0} \\ \mathbf{S}^{\mathrm{G}}_{\mathrm{BB}}\,\mathbf{U}_{\mathbf{g}} \end{Bmatrix}, \tag{4.3.2}$$

in which

$$\mathbf{U}_{\mathrm{R}} = \begin{bmatrix} \mathbf{U}_1 & \mathbf{U}_2 \end{bmatrix}^{\mathrm{T}}, \quad \mathbf{U}_{\mathrm{B}} = \begin{bmatrix} \mathbf{U}_3 & \mathbf{U}_4 & \mathbf{U}_5 & \mathbf{U}_6 \end{bmatrix}^{\mathrm{T}},$$

$$\mathbf{S}^{\mathrm{S}}_{\mathrm{RR}} = \begin{bmatrix} -\omega^2 m_1 + \mathrm{i}\omega(c_1+c_4) + (k_1+k_4) & 0 \\ 0 & -\omega^2 m_2 + \mathrm{i}\omega(c_2+c_3) + (k_2+k_3) \end{bmatrix},$$

$$\mathbf{S}^{\mathrm{S}}_{\mathrm{RB}} = \begin{bmatrix} -\mathrm{i}\omega c_1 - k_1 & 0 & -\mathrm{i}\omega c_4 - k_4 & 0 \\ 0 & -\mathrm{i}\omega c_2 - k_2 & 0 & -\mathrm{i}\omega c_3 - k_3 \end{bmatrix}, \quad \mathbf{S}^{\mathrm{S}}_{\mathrm{BR}} = (\mathbf{S}^{\mathrm{S}}_{\mathrm{RB}})^{\mathrm{T}},$$

$$\mathbf{S}_{\mathrm{BB}}^{\mathrm{S}} = \mathrm{diag}\begin{Bmatrix} -\omega^2 m_3 + \mathrm{i}\omega c_1 + k_1 \\ -\omega^2 m_4 + \mathrm{i}\omega c_2 + k_2 \\ -\omega^2 m_5 + \mathrm{i}\omega c_3 + k_3 \\ -\omega^2 m_6 + \mathrm{i}\omega c_4 + k_4 \end{Bmatrix}, \quad \mathbf{S}_{\mathrm{BB}}^{\mathrm{G}} = \mathrm{diag}\begin{Bmatrix} \mathrm{i}\omega c_{\mathrm{s1}} + k_{\mathrm{s1}} \\ \mathrm{i}\omega c_{\mathrm{s2}} + k_{\mathrm{s2}} \\ \mathrm{i}\omega c_{\mathrm{s3}} + k_{\mathrm{s3}} \\ \mathrm{i}\omega c_{\mathrm{s4}} + k_{\mathrm{s4}} \end{Bmatrix}. \tag{4.3.3}$$

Having obtained the dynamic stiffness matrices required in the proposed method, the direct method can be implemented to generate FLIRS. The parameters of the structure and the soil in this example are given in Table 4.6.

A modal analysis is performed for the superstructure as well as the combined soil-structure system to obtain the basic modal information. The natural frequencies of the superstructure are 4.2 Hz and 5.3 Hz, and the damping ratios are 5% for the both modes. With the presence of soil, the natural frequencies are modified to 4.1, 5.0, 11.4, 11.9, 16.0, and 16.4 Hz. It can be seen that the natural frequencies of the decoupled model decrease slightly comparing with the natural frequencies of the first two modes of the coupled model.

Table 4.6 Structural information of the numerical model

Mass (kg)	m_1	m_2	m_3	m_4	m_5	m_6		
	1000	1000	2000	2000	1000	1000		
Stiffness	k_1	k_2	k_3	k_4	k_{s1}	k_{s2}	k_{s3}	k_{s4}
($\times 10^2$ kN/m)	5	1	10	2	100	100	100	100
Damping coefficient	c_1	c_2	c_3	c_4	c_{s1}	c_{s2}	c_{s3}	c_{s4}
($\times$ kN·s/m)	2.3	1.2	1.3	1.3	50	50	50	50

The seismic input, i.e., foundation input response spectra FIRS are input at the end of the soil springs. The FIRS follows USNRC (2014) with horizontal FIRS anchored at $0.3g$ PGA, while the vertical PGA is taken as 2/3 of the horizontal direction. To validated the proposed method, 30 sets of time history analyses are performed using the acceleration time histories (i.e., FITH) compatible with the corresponding FIRS.

Although the study of coherence function is out of interest in this research, it should be noted that the proposed method of generating FRS considering the SSI effect is applicable for any ground motions as long as the coherence function is known. From the view of

practical design, two special cases, i.e., ground motions at different supports are fully-correlated or independent, are considered, respectively, to investigate the influence of the correlation between ground motions on the seismic response.

4.3.1 Case 1: Identical Seismic Excitations

In this case, the seismic excitations in the same direction are set to be identical, i.e., $\ddot{u}_{g1} = \ddot{u}_{g3}$, $\ddot{u}_{g2} = \ddot{u}_{g4}$. Note that the ground motions in different directions are usually treated as independent.

Comparison of FLIRS

FLIRS modification factor $\mathcal{R}$ and the corresponding FLIRS are determined for the circular frequency range from 0.2π to 200π, shown in Figure 4.24 and Figure 4.25, respectively. Similar to the numerical example 1, the peaks of FLIRS modification factor and FLIRS are located around the natural frequencies of the coupled structure. For example, the horizontal FLIRS at support 1, i.e., FLIRS-1, peaks at 4.9 Hz and 12.0 Hz, respectively, which are corresponding to the natural frequencies of modes 2 and 4 of the coupled soil-structure system. Additionally, it is observed from Figures 4.24 and 4.25 that FLIRS are mainly modified within the frequency range from 2 Hz to 20 Hz, which covers the natural frequencies of the coupled model. For other frequencies, however, the difference between FIRS and FLIRS is negligible, indicating that the SSI effect is not significant for the frequencies out of the natural frequency range of the coupled system. Furthermore, it is found that FIRS-1 and FIRS-2 are modified more than FIRS-3 and FIRS-4. This is because the beam AB is stiffer than beam AC, leading to greater values of the elements in the corresponding FLIRS transfer matrix, which further causes larger FLIRS modification factors.

Comparison of FRS

The generated FLIRS are then used as the input of the decoupled structure to generate FRS using the direct method. Figure 4.26 shows the FRS in the two directions. The red and blue solid lines represent the results by the proposed method in directions 1 and 2, respectively. To verify the accuracy of the proposed method, FRS are also generated using 30 sets of time

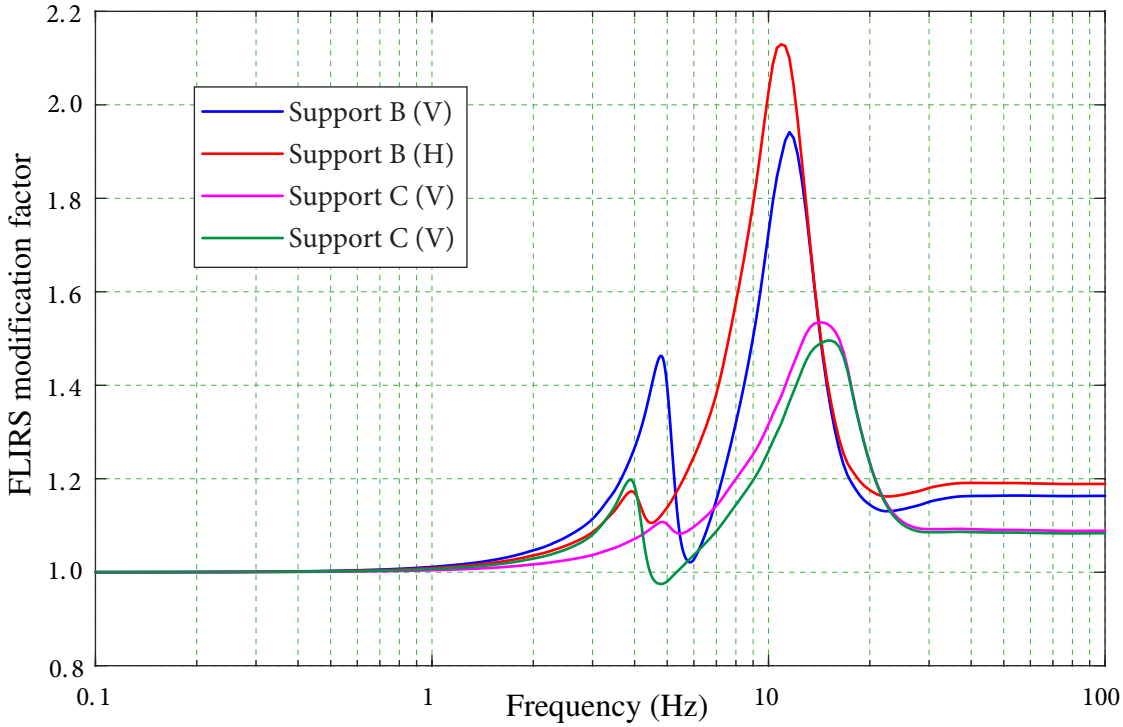

Figure 4.24 FLIRS Modification factors (correlated case).

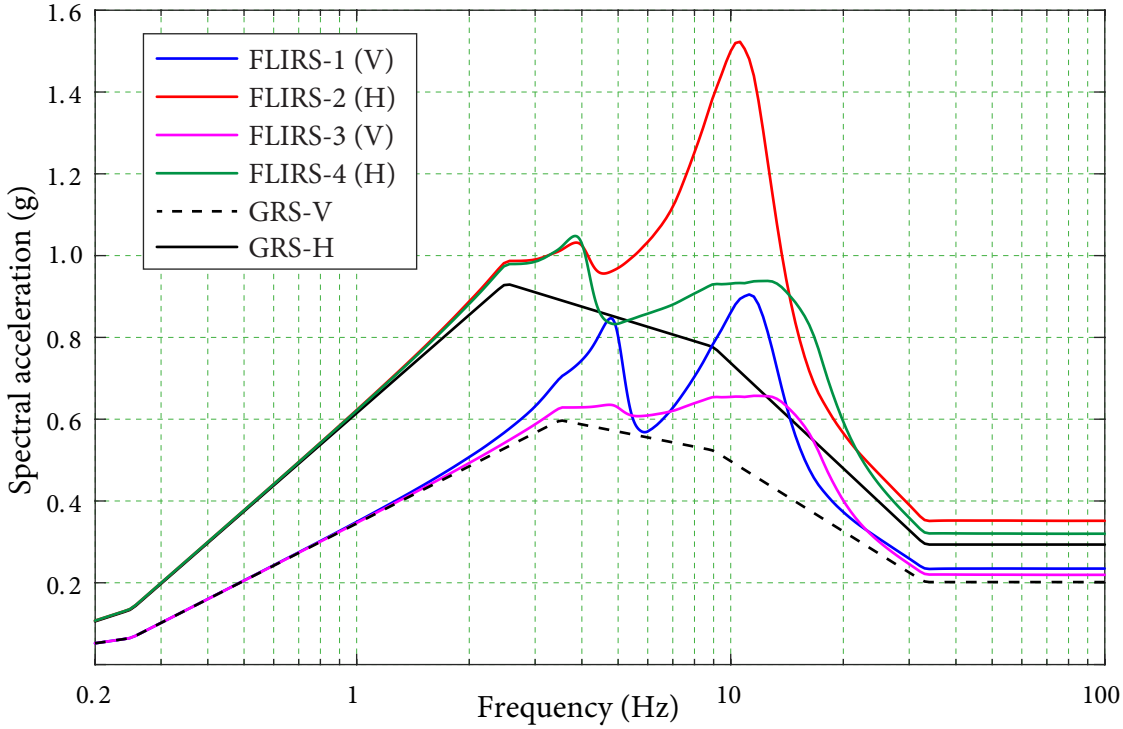

Figure 4.25 FLIRS in different directions (correlated case).

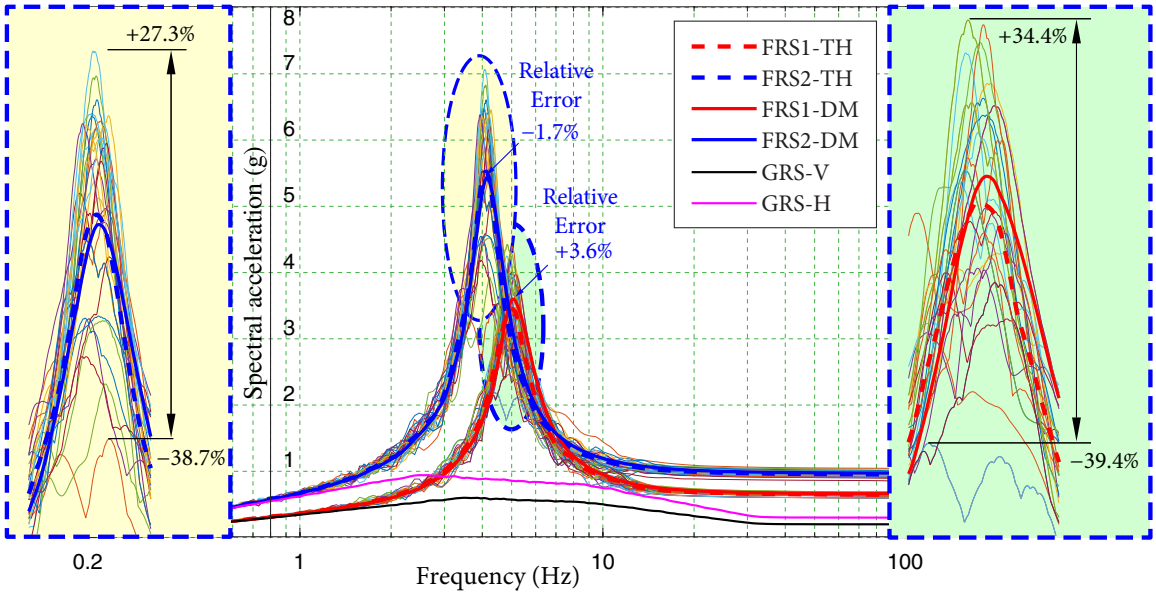

Figure 4.26 Comparison of FRS in directions 1 and 2 (correlated case).

history analyses, in which the average FRS are treated as the benchmarks given by the red and blue dashed lines for directions 1 and 2, respectively.

It is seen that FRS obtained by a single time history analysis has large variabilities. For example, the maximum relative error of FRS in direction 2 is 27.3%, while the minimum relative error is -38.7%, which yields 66% of variability. On the other hand, the error between the corresponding FRS obtained by the direct method and the benchmark is only -1.7%, from which the accuracy of the proposed method is validated. Furthermore, the large variability in time history analysis has been eliminated. Therefore, the proposed method can generate FRS accurately and efficiently considering the SSI effect.

4.3.2 Case 2: Independent Seismic Excitations

In this case, seismic excitations at different supports are chosen to be independent, while these ground motions are still compatible with R.G. 1.60 response spectra.

Result of FLIRS

FLIRS in the independent case is shown in Figure 4.27. It can be seen that FLIRS in the both two cases are very similar. For example, the FLIRS-1 in the fully-correlated and independent cases are plotted in Figure 4.28. This is because the structural information and the soil

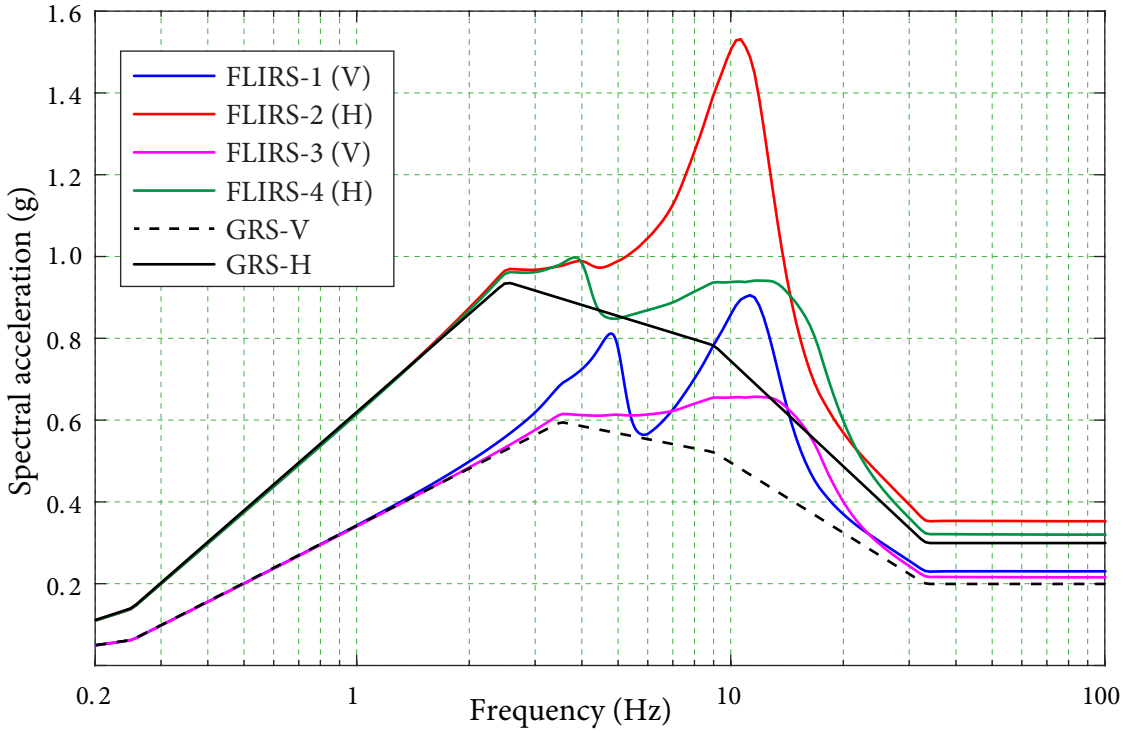

Figure 4.27 FLIRS in different directions (independent case).

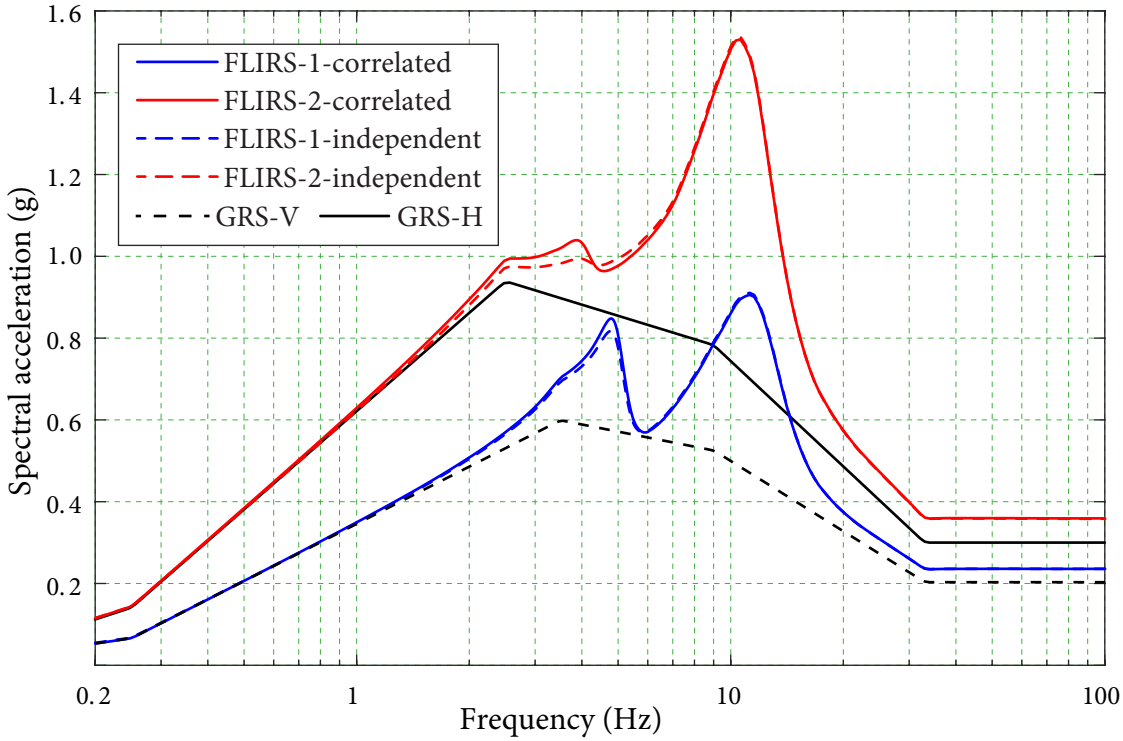

Figure 4.28 Comparison of FLIRS in different cases.

properties for the two cases are the same, while the soil is relative stiff comparing with the structure. As a result, the non-diagonal terms in FLIRS transfer matrix $\mathcal{T}$ is relatively small comparing with the terms on the main diagonal, indicating that the contributions from FIRS in other directions to FLIRS are not significant. Therefore, FLIRS in the fully-correlated case are just slightly higher than FLIRS in the independent case.

As mentioned in Section 4.1.3, FLIRS at different supports have certain correlations depending on the properties of the superstructure and the soil, even when the corresponding FIRS are independent. The cross-power density function of FLIRS at $\omega = 31$ is given in Table 4.7, in which the diagonal terms represent the auto-power density functions of FLIRS, while the non-diagonal terms are the cross-power density functions. It is found that FLIRS in the same directions at different supports are not independent although the corresponding FIRS are independent. For example, the cross power density of FLIRS-1 and FLIRS-3 is 0.03 $\times 10^{-5}$, which is 8.4% of the auto power density of FLIRS-1 and 20% of the auto power density of FLIRS-3, respectively. Therefore, neglecting this correlation between FLIRS-1 and FLIRS-3 may underestimate the FRS in the vertical direction. On the other hand, FLIRS-2 and FLIRS-4 are negatively correlated as the cross power density is less than 0. As a result, the corresponding FRS will be overestimated if the correlation is not considered. Moreover, similar to FIRS, it is observed that FLIRS in orthogonal directions are also independent.

Table 4.7 Power spectral density function of FLIRS ($\times 10^{-5}$ dBm/Hz)

	FLIRS 1	FLIRS 2	FLIRS 3	FLIRS 4
FLIRS 1	0.355	0	0.030	0
FLIRS 2	0	0.388	0	−0.023
FLIRS 3	0.030	0	0.150	0
FLIRS 4	0	−0.023	0	0.255

Comparison of FRS

Figure 4.29 shows the results of FRS generated by the direct method and time history analyses. As can be seen from Figure 4.29, FRS obtained by the proposed direct method agrees very well with the average FRS by 30 time history analyses. The relative errors of

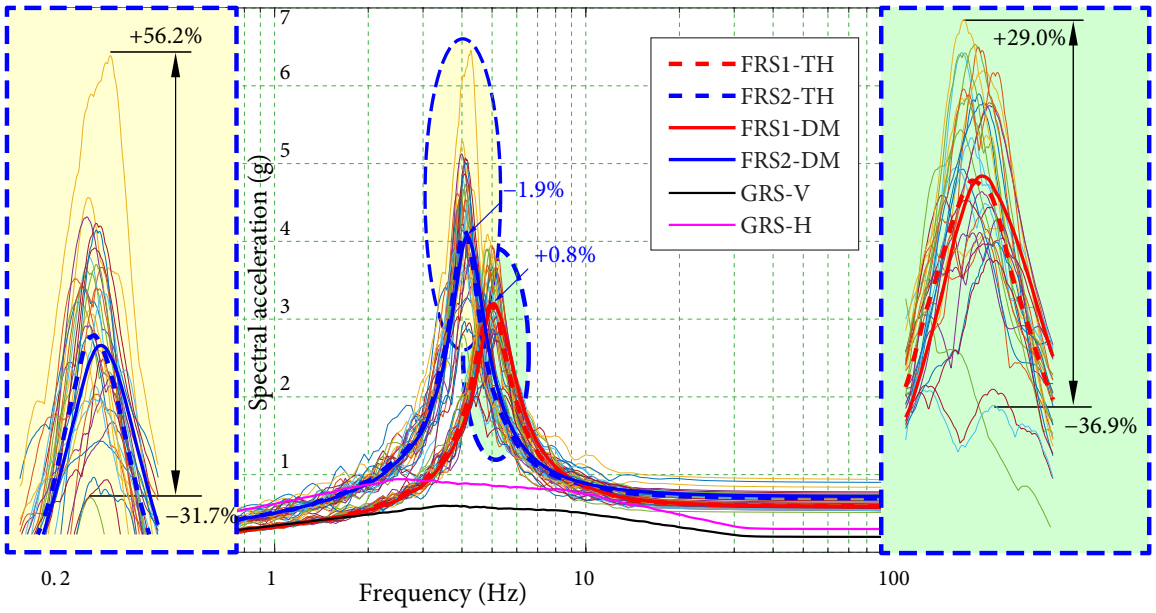

Figure 4.29 FRS in directions 1 and 2 (independent case).

the peaks of FRS are only -1.9% and 0.8% for directions 1 and 2, respectively, indicating that the proposed method has great accuracy in generating FRS considering SSI. However, a single time history analysis still results in large variabilities.

Comparing the results of the fully-correlated and the independent cases, it is found that the magnitudes of FRS are significantly different although the FLIRS in the two cases are almost the same. In Case 1, the peak value of FRS in direction 2 is $5.4g$, which is reduced to $4.1g$ in the independent case. The peak of FRS in direction 1 also decreases by 10% when the ground motions are independent. Therefore, the correlation of the ground motions has considerable influence on FRS. In general, the fully-correlated ground motions and independent ground motions provide the upper and lower bounds of FRS.

4.3.3 Influence of Soil Conditions on FRS: A Parametric Study

A parametric study is performed in this section to investigate the influence of soil stiffness on FRS for multi-supported structures. The input FIRS are chosen to be fully-correlated and the properties of the soils in each case are shown in Table 4.8. From Case 1 to Case 6, the stiffness of the soil springs at different supports in all directions are still assumed to

be the same, while they are different in Case 7 and 8. Case 2 is the fully-correlated case presented in Section 4.3.1.

Table 4.8 Soil stiffness in different cases ($\times 10^4$ kN/m)

	k_{s1}	k_{s2}	k_{s3}	k_{s4}
Case 1	0.5	0.5	0.5	0.5
Case 2	1	1	1	1
Case 3	5	5	5	5
Case 4	10	10	10	10
Case 5	100	100	100	100
Case 6	1000	1000	100	100
Case 7	1	0.5	2	1
Case 8	1	1.5	1.5	2

Soil Springs are Consistent at Different Supports

While the change of soil stiffness does not affect the structural information, such as natural frequencies of the superstructure, it has significant influence on FLIRS and the resultant FRS. Figures 4.30 and 4.31 show the results of FRS of different cases by the direct method and the average of 30 time history analyses. It is observed that the difference between FRS in Case 5 and Case 6 by either the direct method or the time history method is very small, thus they can be both regarded as the rigid case. Comparing these two figures, FRS by the direct method of the most cases are very close to those by the time history method, except for Case 1. The relative errors of FRS peaks are 3.6%, -1.9%, -1.5%, -0.6%, and -1.9% from Case 2 to Case 6, respectively. Therefore, the proposed method can be applied to most soil sites. The peak FRS in Case 1 by the direct method is $3.58g$, while it is $3.22g$ in time history analysis, leading to 11.2% of overestimation of FRS peak. This error is due to the application of the statistical relationship of tRS by Li *et al.* (2015) in this soil case.

Error in FRS caused by tRS. As mentioned before, the tRS relationship is based on the wide-banded ground motions. However, it has been shown in Section 4.2.2 that this assumption may cause errors when soil is soft, such as the soil in Case 1 in this parametric study. The average tRS of FLIRS-1 and FLIRS-4 obtained by 30 time history analyses, which

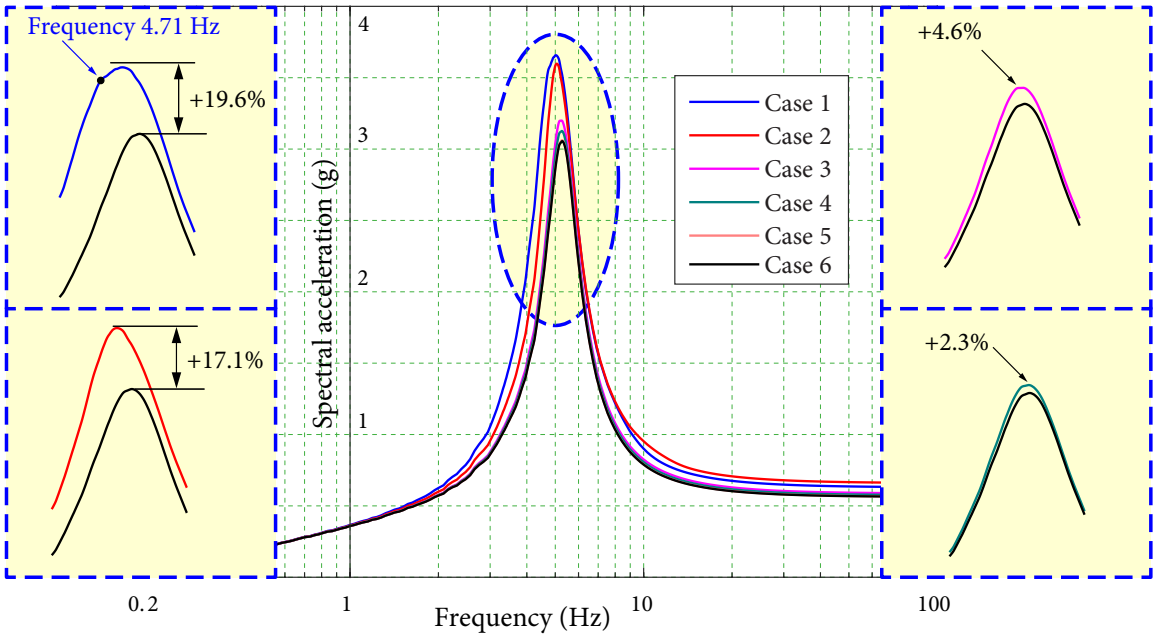

Figure 4.30 FRS in direction 2 by direct method in different cases.

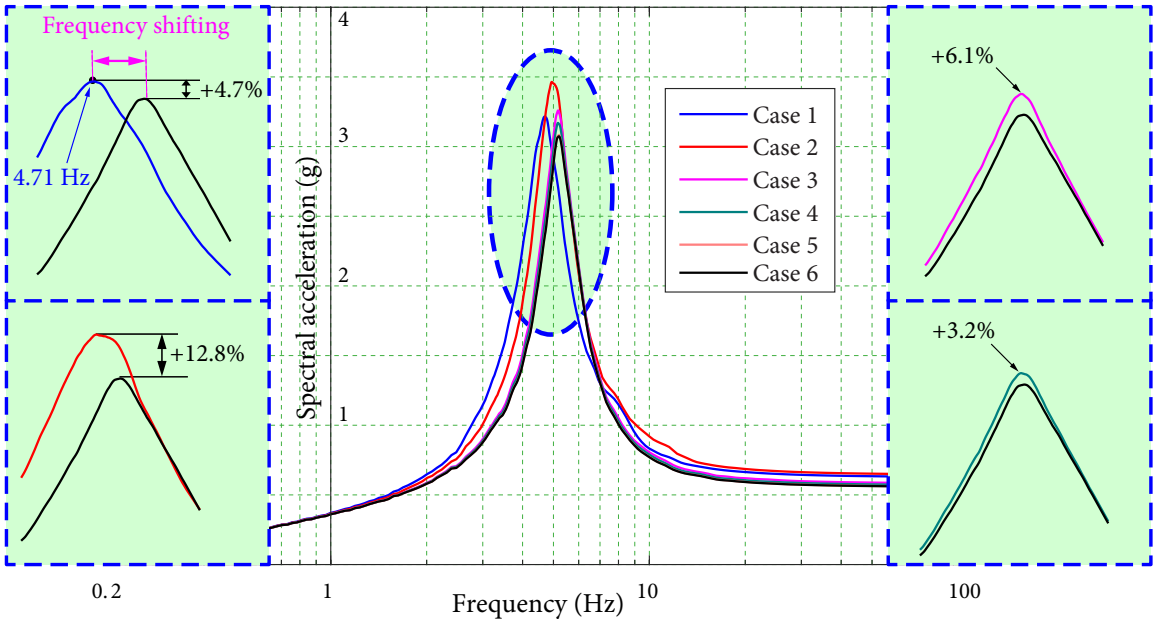

Figure 4.31 FRS in direction 2 by time history method in different cases.

can be regarded as the "benchmark" tRS of the corresponding FLIRS, are shown in Figures 4.32 and 4.33, respectively. It can be seen that the average tRS in Case 5 and Case 6 are close because the soils in these two cases are very stiff. Therefore, the difference between the FRS in these two cases is negligible.

Although the significant gaps between tRS in Case 3 (pink line), Case 4 (green line), and Case 6 are found in the frequency range from 13 Hz to 40 Hz, the resultant FRS are still close. This is because the two natural frequencies of the superstructure are located between 4 Hz and 6 Hz, while the tRS in Case 3 and Case 4 are not modified obviously within this frequency range. However, the average tRS of FLIRS-1 and FLIRS-4 are decreased by 27.7% and 15.6%, respectively, at the natural frequencies of the superstructure, which further results in the overestimation of FRS using the tRS by Li *et al.* (2015). On the other hand, the average tRS in Case 2, although has certain difference with the rigid one, the obtained FRS is still acceptable as the difference between tRS is relatively small comparing with Case 1.

Frequency shift of FRS peaks. FRS peaks are found to shift toward lower frequencies when the soil becomes more flexible. For example, the peak of FRS by the time history method in Case 6 is located at frequency 5.2 Hz and it is shifted to 4.7 Hz in Case 1. The shift of the frequency of FRS peak is relatively small when FRS are generated by the direct method in Case 1. However, as mentioned above, it is due to the problem in the application of tRS for relative soft soil case. Since tRS by Li *et al.* (2015) is more conservative than the benchmark tRS near the natural frequencies of the superstructure, the corresponding FRS keeps increasing between 4.7 Hz and 5.1 Hz when the conservative tRS is applied. As a result, the FRS peak in Case 1 by the direct method is located at the frequency 5.0 Hz, which is slightly higher than that by the time history method (i.e., 4.7 Hz). It is reasonable to assume that this peak by the direct method will be modified to 4.7 Hz with proper tRS being used.

Influence of soil stiffness to the magnitude of FRS peaks. It is observed that unlike the FRS peak increases with the increase of soil stiffness in the numerical example 1 (i.e., the 3-DOF system), greater soil stiffness can lead to either greater or smaller FRS for multi-supported structures. For example, as can be seen from Figure 4.31, the peak FRS increases

from 3.21g to 3.46g when the soil stiffness increases from Case 1 to Case 2; however, it is reduced from 3.46g to 3.05g (by 19.5%) from Case 2 to Case 6.

This phenomenon can be explained by comparing the FLIRS of Case 2 given in Figure 4.25 with the corresponding GRS. First of all, it should be noted that the peak of FRS highly depends on the modal spectral response of an oscillator and the tRS, in which the former one can be obtained by the interpolation of the input response spectra, i.e., FLIRS in this case. It is found in Figure 4.25 that although some valleys exist in the FLIRS near the natural frequencies of the decoupled model, most of them are above the corresponding GRS except for that of FLIRS-4, which is just slightly lower than the horizontal GRS. As a result, the corresponding spectral responses of oscillators are greater than those in the rigid case. On the other hand, the difference between the average tRS in Case 2 and the rigid case are not very significant. Therefore, the spectral value of FRS peak in Case 2 is larger than the rigid case, indicating that the consideration of soil may cause the increase of the seismic demand of secondary systems.

Therefore, the influence of the soil properties on FRS is more complex for structures with earthquake excitations from multiple supports because the FRS is affected by the FLIRS from different resources. The proposed method is applicable to give accurate FRS considering SSI effect for multi-supported structures.

Soil Springs are Different at Different Supports

The stiffness of soil springs at each support are set to be different for Cases 7 and 8 as shown in Table 4.8, and the resultant FRS are given in Figures 4.34 and 4.35. It can be seen that the proposed method gives accurate FRS when soil property varies at different supports. The maximum relative errors at FRS peaks are only 3.6% and 4.0% for Cases 7 and 8, respectively. For structures such as SMR, which might be deeply embedded in soil, the soil conditions may be changed somewhat, especially in the direction of depth. Therefore, a method for accurately generating FRS with varied soil parameters is required. The results in Figures 4.34 and 4.35 demonstrate that the proposed method is applicable in this situation.

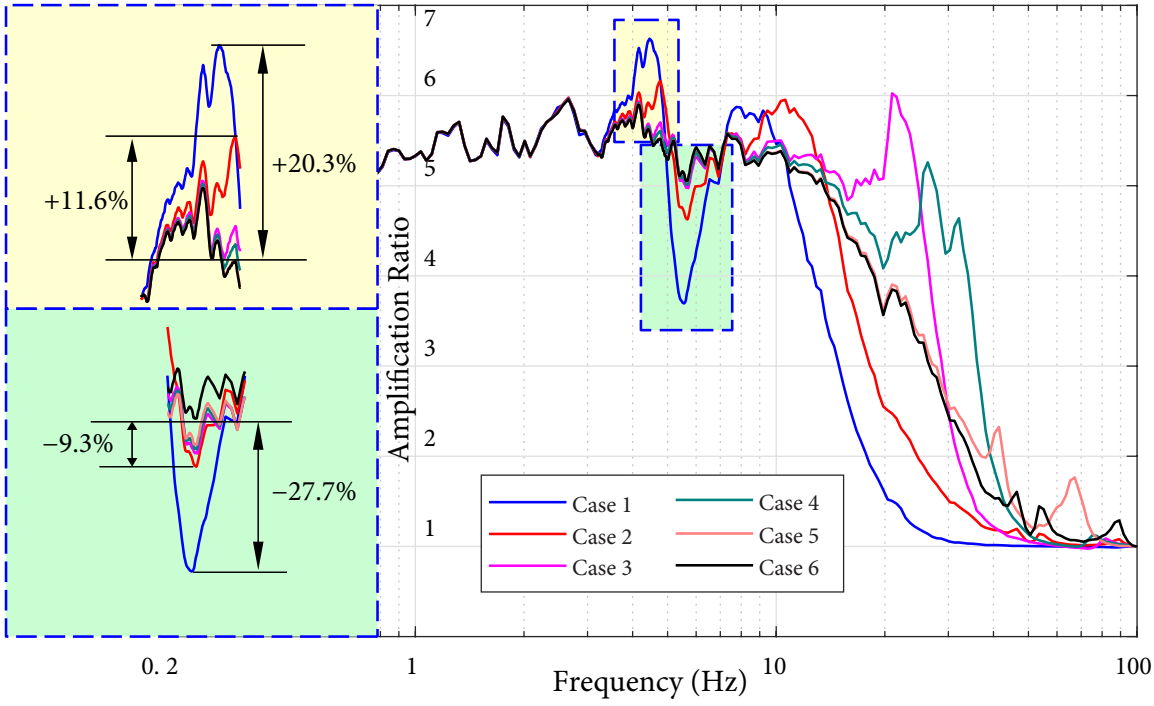

Figure 4.32 Amplification ratios of FLIRS-1 in different cases.

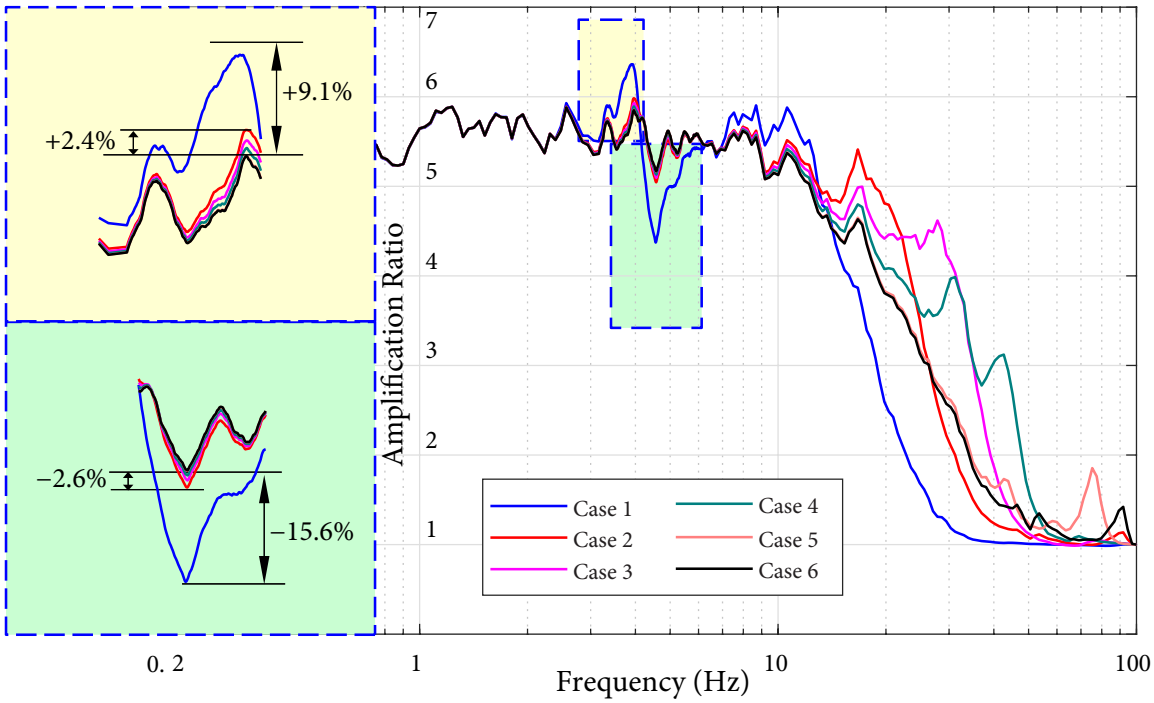

Figure 4.33 Amplification ratios of FLIRS-4 indifferent cases.

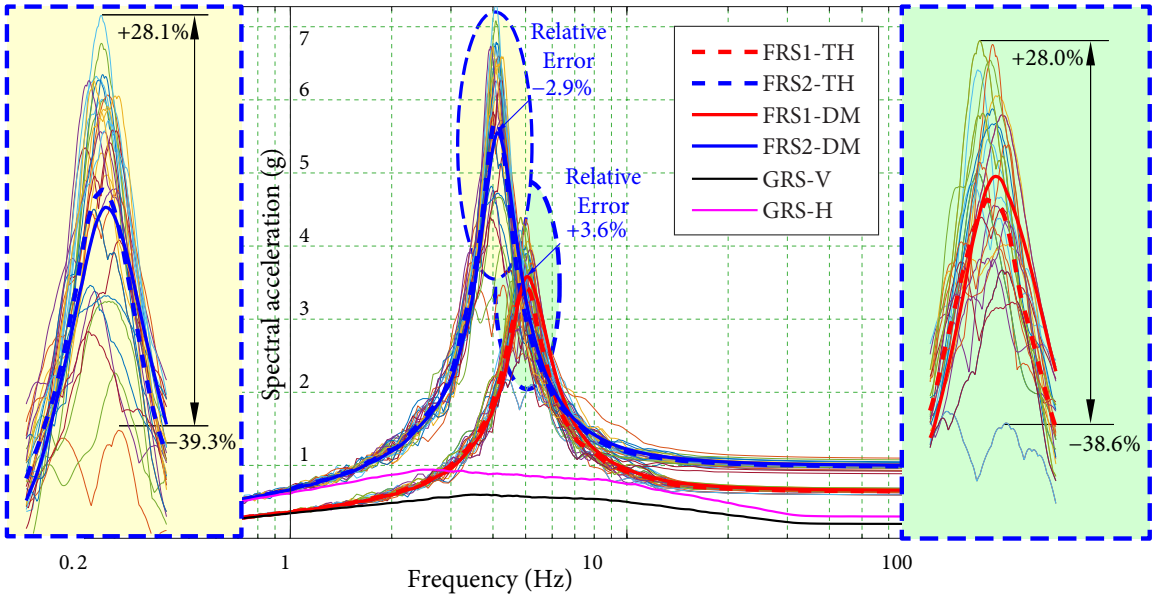

Figure 4.34 FRS of varied soil stiffness (Case 7).

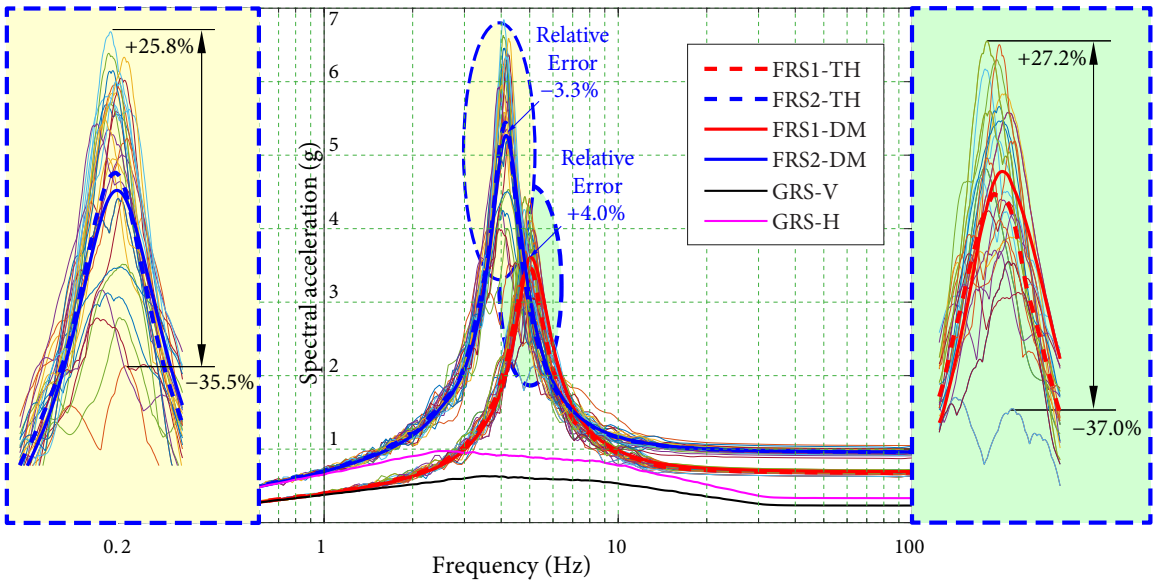

Figure 4.35 FRS of varied soil stiffness (Case 8).

4.4 Summary

In this chapter, a method for the generation of FRS for structures with earthquake excitations at multiple supports considering the effect of SSI is developed. Based on the fundamentals of structural dynamics, a transfer function, which gives the relationship between FLIRS and FIRS, is derived in frequency domain. The FLIRS modification factor, which is the ratio between FLIRS and the corresponding FIRS, is derived based on the transfer function. The modification factor is given implicitly because it depends on the structural information and the soil properties, which can be easily evaluated numerically once the information is given. Using FLIRS modification factor, FLIRS can be generated directly, which are then input to the decoupled model to generate FRS using the method proposed in Chapter 2. It has been proved that FRS of the decoupled structure using FLIRS is theoretically equivalent to that generated by the combined soil-structure system using FIRS.

Two numerical examples are presented to verify the proposed method, and to study the influence of SSI effect on FRS. Although the structures in this chapter are not complex, they allow the explicit expressions of the matrices in the formulation to be existed. A 3-DOF structure with two structure nodes and one foundation node supported by a generalized soil spring at a single support is studied. The theoretical formulation of FLIRS in this example demonstrates the seismic responses of the coupled soil-structure system under the excitations FIRS is equivalent to those of the decoupled structure under the modified inputs FLIRS. As a result, the replacement of FIRS with soil by FLIRS is theoretically rigorous. The numerical results of FRS indicate that the proposed method is of great accuracy in the generation of FRS considering the effect of SSI. A lumped mass with two supports sitting on soil is presented to illustrate the feasibility of the proposed method in the situation of multiple supports. It is shown that the proposed method can give accurate FRS of structures with multiple supports considering SSI, while the time history method still results in large variabilities.

Parametric studies are also performed to investigate the influence of soil conditions on FRS. It is found that the consideration of soil might either increase or decrease the seismic

responses of secondary structures. The effect of SSI could result in the shifting of FRS peaks. Hence, it is of great practical importance to consider SSI in the structural dynamic analysis.

In summary, the proposed method is accurate and efficient for the generation of FRS considering SSI for sites with soil classification of D or higher, which is generally the case in the nuclear power industry.

CHAPTER 5

Conclusions and Future Research

Floor Response Spectrum (FRS) is critical in seismic analysis and design of secondary systems in nuclear power facilities. In practice, most of engineering structures are supported at different points, which results in different inputs during earthquakes. This study aims at developing an accurate and efficient method for the generation of FRS for structures with seismic excitations from multiple supports. Some contributions for this purpose have been accomplished in this study, and are summarized as follows.

5.1 Direct Spectra-to-Spectra Method for Generating Floor Response Spectra

A direct spectra-to-spectra method is developed for generating FRS of multi-supported structures. "Direct" means Ground Response Spectrum (GRS) is used as seismic input directly without generating any intermediate input, such as artificial spectrum-compatible time histories. Only the information used in conventional response spectrum analysis, such as the input ground motions GRS and the basic modal information, is needed in the proposed method. Some remarkable features and advantages of the proposed direct spectra-to-spectra method are summarized as follows:

- The direct method gives accurate FRS for structures with multiple supports; FRS obtained by this method agree extremely well with the "benchmark" results obtained

from a large number of time history analyses. Particularly, the direct method can deal with the resonance cases, corresponding to FRS peaks, properly, which has not been satisfactorily solved in previous direct spectrum-to-spectrum methods. It is shown that FRS obtained by a single time history method has large variabilities. Therefore, if a single or a small number of time history analyses are performed to generate FRS, the result is not reliable, while it is very computationally expensive to perform a large number of time history analyses. The proposed method can avoid the deficiencies of the time history method.

- By using the concept of tRS, the direct method can give full probabilistic descriptions at FRS peaks, which can satisfy various seismic design and assessment requirements for SSCs with different safety margins.
- The direct method is analytically formulated and it is convenient to implement in any programming software such as MATLAB. Furthermore, the direct method is highly efficient that the computation takes only a few seconds. On the contrary, much more computational efforts are required in the application of the time history method to obtain a reliable result.

5.2 Generating Response of Secondary Structures and Tertiary Response Spectra

While the direct method mentioned above gives accurate FRS, the direct methods for generating responses and TRS of secondary structures, which are anchored on primary structures at different locations, are proposed using the obtained FRS. Some remarkable advantages of the proposed methods are summarized as follows:

- The proposed method is capable of obtaining accurate responses efficiently. Only the input GRS and the structural information of the primary and secondary systems are required.
- Two special cases, for which it is easy to obtain the explicit expressions of the proposed methods, are considered. Assumptions on the correlation between FRS at different locations are proposed and verified to be acceptable. With the two special cases

investigated and assumptions made, the proposed method can be easily implemented in practical design.

- The concept of F-tRS is proposed in the generation of TRS. F-tRS is found to follow the similar statistical relationship of tRS, and it is demonstrated that the application of tRS to the generation of TRS still yields very good result.

5.3 Generating FRS Considering Soil-Structure Interaction

The effect of soil-structure interaction (SSI) has great influence on the seismic behavior of primary structures and supported secondary systems. A methodology is developed to generate FRS for multi-supported structures considering SSI effect, using the substructure method and the proposed direct spectra-to-spectra method. Some remarkable features and advantages of the proposed method are summarized as follows:

- A method of determining FLIRS modification factors for the Foundation Input Response Spectra (FIRS), which is obtained from a free-field site response analysis, is developed to integrate the SSI effect. The modified FIRS, called Foundation Level Input Response Spectra (FLIRS), are input to the decoupled model to generate FRS using the direct spectra-to-spectra method.
- The proposed method considering SSI is demonstrated using two numerical examples. FRS obtained by the proposed method agree well with "benchmark" results obtained from a large number of time history analyses.
- Performing a large number of time history analyses can be avoided in the whole process, from which the computational cost has been considerably reduced. More importantly, the variabilities in the time history method are eliminated by applying the proposed method. A reanalysis of the entire soil-structure system can be avoided when the properties of the superstructure or soil are changed; thus the efficiency of the proposed method is further improved. Furthermore, instead of evaluating the inverse of a $6N \times 6N$ matrix, only the inverse of a $6M \times 6M$ matrix is required, in which N and M are the number of the nodes of the structure and the foundation,

respectively. Because the number of supports is generally much less than the number of structural nodes, the numerical difficulties of a large-scale system can be avoided.

- It is found that the consideration of SSI may either increase or reduce the seismic responses depending on soil conditions. Besides of the modification of the magnitude of FRS due to the presence of soil, the shifting of FRS peaks also deserves much attention in engineering practice. Neglecting this effect could lead to unconservative results around the frequencies of the combined soil-structure system.

5.4 Future Research

In future research, statistical expressions of ttRS, which represents the maximum response of an oscillator mounted on an identical oscillator supported by another identical one, will be investigated. Once ttRS has been obtained, a new direct method for generating TRS will be developed for the direct generation of TRS from GRS. This will simplify the current procedures for generating TRS using F-tRS or tRS as the intermediate outputs, such as FRS, are not required. Furthermore, the minor error in TRS obtained using the approximation on F-tRS can be further avoided.

The direct methods for generating FRS have been developed by Jiang (2016) for structures with fixed-base, and by this research for structures subjected to seismic excitations at multiple supports. More investigations on developing the criterion on determine whether the foundation of a structure can be regarded as rigid or must be modelled as flexible should be conducted, which can provide guidance in practical analysis and design.

Further studies on generating FRS considering SSI for realistic structures with multiple supports, such as SMR, will be conducted. The analysis should be performed using the proposed method and also in commercial finite element softwares to verify the results. Furthermore, parametric studies on determining the locations of the seismic inputs to SMR will be performed.

Bibliography

Abrahamson, N.A., Schneider, J.F., and Stepp, J.C., 1991. Empirical spatial coherency functions for application to soil-structre interaction analysis. *Earthquake Spectra*, **7**: 1–28.

Adam, C. and Furtmüller, T., October 12-17 2008. Response of nonstructural components in ductile load-bearing structures subjected to ordinary ground motions. In *Proceedings of the 14th world conference on earthquake engineering, paper*, (05-01). Beijing, China.

ANSYS, Inc., 2018. *Ansys Academic Research Mechanical, Structural Analysis Guide, Release 19.2*.

An, Y., Jiang, Y., and Ly, B., 2013. Direct generation of RRS from FRS. In *Proceedings of the 22nd International Conference on Structural Mechanics in Reactor Technology*.

Aragaw, L.F. and Calvi, P.M., 2018. Earthquake-induced floor accelerations in base-rocking wall buildings. *Journal of Earthquake Engineering*, p. 1–29.

ASCE, 1998. *Seismic Analysis of Safety-Related Nuclear Structures and Commentary*, **asce 4-98**. American Society of Civil Engineers (ASCE).

ASCE, 2010. *Minimum Design Loads for Buildings and Other Structures*, **asce/sei 7-10**. American Society of Civil Engineers, Reston, Virginia.

Asfura, A. and Der Kiureghian, A., 1986. Floor response spectrum method for seismic analysis of multiply supported secondary systems. *Earthquake Engineering and Structural Dynamics*, **14**(2): 245–265.

Bielak, J. and Christiano, P., 1984. On the effective seismic input for non-linear soil-structure interaction systems. *Earthquake Engineering and Structural Dynamics*, **12**: 107–119.

Biggs, J.M. and Roesset, J.M., 1970. Seismic analysis of equipment mounted on a massive structure. *Seismic Design for Nuclear Power Plants*, 319–343.

Burdisso, R.A. and Singh, M.P., 1987. Multiply supported secondary systems part i: Response spectrum analysis. *Earthquake Engineering and Structural Dynamics*, **15**(1): 53–72.

Calvi, P.M. and Sullivan, T.J., 2014. Estimating floor spectra in multiple degree of freedom systems. *Earthquakes and Structures*, **7**(1): 17–38.

Chaudhuri, S.R. and Villaverde, R., 2008. Effect of building nonlinearity on seismic response of nonstructural components: a parametric study. *Journal of Structural Engineering*, **134**(4): 661–670.

Chaudhuri, S. R. and Gupta, V.K., 2003. Mode acceleration approach for generation of floor spectra including soil-structure interaction. *ISET Journal of Earthquake Technology*, **40**(434): 99–115.

Chen, Y. and Soong, T.T., 1988. Seismic response of secondary systems. *Engineering Structures*, **10**(4): 218–228.

Chopra, A.K., 2012. *Dynamics of Structures – Theory and Applications to Earthquake Engineering*. Prentice Hall, fourth edition.

Collino, F., 1993. High order absorbing boundary conditions for wave propagation models. straight line boundaries and corner cases. *Proceedings of the Second International Conferenceon Mathematical and Numerical Aspects of Wave Propagation*, p. 161–171.

CSA, 2010. *Design Procedures for Seismic Qualification of Nuclear Power Plants*, **CSA N289.3-10**. Canadian Standard Association (CSA).

Der Kiureghian, A. and Nakamura, Yutaka, 1993. Cqc modal combination rule for high–frequency modes. *Earthquake engineering and structural dynamics*, **22**: 943–956.

Der Kiureghian, A., 1996. A coherency model for spatially varying ground motions. *Earthquake Enginnering and Structural Dynamics*, **25**(1): 99–111.

Ghiocel, D.M., 2015. **ACS SASSI, 3.0**. GP Technologies, Inc.

Gutierrez, J.A. and Chopra, A.K., 1978. A substructure method for earthquake analysis of structures including structure-soil interaction. *Earthquake Engineering and Structural Dynamics*, **6**(1): 51–69.

Hadjian, A. H. and Ellison, B., 1986. Decoupling of secondary systems for seismic analysis. *Journal of Pressure Vessel Technology*, **108**(1): 78–85.

Hall, J.F., Holmes, W.T., and Somers, P., 1994. Northridge earthquake, january 17, 1994. *Preliminary reconnaissance report*, **1**: 87–93.

Higdon, R. L., 1991. Absorbing boundary conditions for elastic waves. *Geophysics*, **56**(2): 231–241.

IBC, 2012. *2012 International Building Code*. International Code Council, Washington D.C.

Igusa, T., Der Kiureghian, A., and J.L.Sackman, 1987. Seismic response analysis of structure-equipment systems with non-classical damping effects. *Earthquake Engineering and Structural Dynamics*, **15**(7): 871–888.

Jiang, W., Li, B., Xie, W-C., and Pandey, M.D., 2015. Generate floor response spectra: Part 1. direct spectra-to-spectra method. *Nuclear Engineering and Design*, **293**: 525–546.

Jiang, W., 2016. *Direct Method of Generating Floor Response Spectra*. PhD thesis, University of Waterloo.

Kennedy, R. P., Short, S. A., and Newmark, N. M., 1981. The response of a nuclear power plant to near-field moderate magnitude earthquakes. In *Transactions of the 6th International Conference on Structural Mechanics in Reactor Technology, Palais des Congres*. Co. for the Commission of the European Communities: Paris, France.

Liao, Z. P. and Wong, H. L., 1984. A transmitting boundary for the numerical simulation of elastic wave propagation. *Soil Dynamics And Earthquake Engineering*, **3**(3): 174–183.

Lim, E. and Chouw, N., 2014. Consequence of main-secondary structures interaction for seismic response of secondary structures. In *Annual New Zealand Society of Earthquake Engineering Conference*.

Lim, E. and Chouw, N., 2015. Review of approaches for analysing secondary structures in earthquakes and evaluation of floor response spectrum approach. *International Journal of Protective Structures*, **6**(2): 237–261.

Lin, J. and Mahin, S. A., 1985. Seismic response of light subsystems on inelastic structures. *Journal of Structural Engineering*, **111**(2): 400–417.

Lin, Y.K., 1967. *Probabilistic theory of structural dynamics*. McGraw-Hill, N.

Li, B., Jiang, W., Xie, W-C., and Pandey, M.D., 2015. Generate floor response spectra: Part 2. response spectra for equipment-structure resonance. *Nuclear Engineering and Design*, **293**: 547–560.

Li, Z.-X., LI, Z.-C., and Shen, W.-X., 2005. Sensitivity analysis for floor response spectra of nuclear reactor buildings. *Nuclear Power Engineering*, **26**(1): 44–50.

Lou, M., Wang, H., Chen, X., and Zhai, Y., 2011. Structure¨csoil¨cstructure interaction: Literature review. *Soil dynamics and earthquake engineering*, **31**(12): 1724–1731.

Luco, J.E. and Wong, H.L., 1986. Response of a rigid foundation to a spatially random ground motion. *Earthquake Engineering and Structural Dynamics*, **14**: 891–908.

Lysmer, J., , Tabatabaie-Raissi, M., Tajirian, F., Vahdani, S., and Ostadan, F., 1983. **SASSI**. *System for Analysis of Soil Structure Interaction*. UC Berkeley, Department of Civil Engineering, Berkeley, CA.

Ni, S-H., Xie, W-C., and Pandey, M. D., 2011. Tri-directional spectrum-compatible earthquake time-histories for nuclear energy facilities. *Nuclear Engineering and Design*, **241**(8): 2732–2743.

Ni, S-H., Xie, W-C., and Pandey, M. D., 2013. Generation of spectrum-compatible earthquake ground motions considering intrinsic spectral variability using Hilbert-Huang transform. *Structural Safety*, **42**: 45–53.

Novak, M. S., Lazarevic, D., Atalic, J., and Uros, M., 2019. Influence of multiple-support excitation on seismic response of reinforced concrete arch bridges. *Applied Sciences*, **10**(1): 17.

PEER, 2010. *Report for the PEER Ground Motion Database Web Application*. Pacific Earthquake Engineering Research Center, Berkeley, California.

Raychowdhury, P. and Ray-Chaudhuri, S., 2015. Seismic response of nonstructural components supported by a 4-story smrf: Effect of nonlinear soil¨cstructure interaction. *Structures*, **3**: 200–210.

Saudy, A., 1992. *Seismic analysis of multiply-supported MDOF secondary systems*. PhD thesis, McMaster University.

Singh, M.P. and Burdisso, R.A., 1987. Multiply supported secondary systems part ii: Seismic inputs. *Earthquake Engineering and Structural Dynamics*, **15**(1): 73–90.

Singh, M.P. and Sharma, A.M., 1985. Seismic floor spectra by mode acceleration approach. *Journal of Engineering Mechanics*, **111**(11): 1402–1419.

Singh, M.P. and Suarez, L.E., 1987. Seismic response analysis of structure-equipment systems with non-classical damping effects. *Earthquake Engineering and Structural Dynamics*, **15**(7): 871–888.

Singh, M.P., 1980. Seismic design input for secondary systems. *Journal of the Structural Division*, **106**(2): 505–517.

Singh, M.P., 1988. Seismic design of secondary systems. *Probabilistic Engineering Mechanics*, **3**(3): 151–158.

Suarez, L.E. and Singh, M.P., 1987. Eigenproperties of non-classically damped primary structure and equipment systems by a perturbation approach. *Earthquake Engineering and Structural Dynamics*, **15**(5): 565–583.

Sullivan, T.J., Calvi, P.M., and Nascimbene, R., 2013. Towards improved floor spectra estimates for seismic design. *Earthquakes and Structures*, **4**(1): 109–132.

Surana, M., Singh, Y., and Lang, D.H., 2018a. Effect of irregular structural configuration on floor acceleration demand in hill-side buildings. *Earthquake Engineering and Structural Dynamics*, **47**(10): 2032–2054.

Surana, M., Singh, Y., and Lang, D.H., 2018b. Floor spectra of inelastic rc frame buildings considering ground motion characteristics. *Journal of Earthquake Engineering*, **22**(3): 488–519.

Taghavi, S. and Miranda, E., September 24-28 2012. Probabilistic study of peak floor acceleration demands in nonlinear structures. In *Proceedings of the 15th World conference on earthquake engineering*. Lisbon, Portugal.

Taghavi, S. and Miranda, E., 2018. Floor response spectra in hybrid base-rocking wall buildings. In *11th US National Conference on Earthquake Engineering*. Earthquake Engineering Research Institute, Los Angeles, USA.

USNRC, 2014. *Design Response Spectra for Seismic Design of Nuclear Power Plants*, **usnrc r.g. 1.60 (rev. 2)**. U.S. Nuclear Regulatory Commission.

Vela, R. R. M., Brunesi, E., and R.Nascimbene, 2008. Derivation of floor acceleration spectra for an industrial liquid tank supporting structure with braced frame systems. *Engineering Structures*, **171**: 105–122.

Villaverde, R., 1997. Seismic design of secondary structures: state of the art. *Journal of Structural Engineering*, **123**(8): 1011–1019.

Villaverde, R., 2009. *Fundamental Concept of Earthquake Engineering*. CRC Press, New York.

Wang, J., August 7-12 2005. Influence of different boundary conditions on analysis of ssi. In *18th International Conference on Structural Mechanics in Reactor Technology*. Beijing, China.

Wieser, J., Pekcan, G., Zaghi, A.E., Itani, A., and Maragakis, M., 2013. Floor accelerations in yielding special moment resisting frame structures. *Earthquake Spectra*, **29**(3): 987–1002.

Wilson, E. L., Der Kiureghian, A., and Bayo, E. P., 1981. A replacement for the srss method in seismic analysis. *Earthquake Enginnering and Structural Dynamics*, **9**(2): 187–192.

Wolf, J.P., 1985. *Dynamic Soil Structure Interaction*. Prentice Hall.

Wolf, J.P., 1987. *Soil-Structure-Interaction Analysis in Time Domain*. Structural Mechanics in Reactor Technology.

Xie, Wei-Chau, Ni, Shun-Hao, Liu, Wei, and Jiang, Wei, 2019. *Seismic Risk Analysis of Nuclear Power Plants*. Cambridge University Press.

Yasui, Y., Yoshihara, J., Takeda, T., and Miyamoto, A., 1993. Direct generation method for floor response spectra. *Proceedings of the 12th International Conference on Structural Mechanics in Reactor Technology*, **13**(4).

Yun, C.B., Hyun, C.H., Kong, C.S., J.S., and Youn, 1993. Floor response spectra analysis including correlations of multiple support motions. In *Proceedings of the Computational Structural Engineering Institute Conference*, p. 173–180. Computational Structural Engineering Institute of Korea.

Zhang, C. and Jiang, N., 2017. Effects of equipment-structure-soil interaction on seismic response of equipment and structure via real-time dynamic substructuring shaking table testing. *Shock and Vibration*, **2017**: 1–13.

Zhang, D.-Y., Xie, W.-C., and Pandey, M. D., 2012. Synthesis of spatially correlated ground motions at varying sites based on vector-valued seismic hazard deaggregation. *Soil Dynamics and Earthquake Engineering*, **41**: 1–13.

Zhou, Y., 2019. *Direct Method for Floor Response Spectra Considering Soil-Structure Interaction*. PhD thesis, University of Waterloo.

APPENDIX A

Evaluation of Soil Stiffness for Distinct Site Classes

The stiffness of foundation is the amount of force required to produce a unit deformation at the foundation level. It is a measure of the resistance of the foundation to the unit deflection. ASCE 4-98 (1998) suggests that soil-structure interaction (SSI) should be considered if the supporting soil is not rock or rock-like soil. The provision put forward that the underlying soil can be represented by general soil spring, which stiffness can be evaluated from the way exhibited in Table A.1 if the shape of the base is circular.

Table A.1 Formula for evaluating stiffness at surface for circular base

	Horizontal	Vertical
Equivalent Spring Constant	$k_{sx} = \frac{32(1-\mu)GR}{7-8\mu}$	$k_{sz} = \frac{4GR}{1-\mu}$

where G is the shear modulus of the soil, μ is the Poisson's ratio of the soil, and R is the radius of circular basemat.

To evaluate the stiffness range of underlying soil, a representative type of soil was selected for each site class. These include different properties of clay in Classes E, D, and C to represent soft soil, medium soil and dense or stiff soil; soft sandstone, medium basalt and granite were used to represent soft rock, medium rock and hard rock, respectively. Two

shear wave velocities were selected as the lower and upper bounds. To ensure a reasonable estimate of the lower bound of stiffness, a minimum radius of 3 m is set. Furthermore, a radius of 30 m, which is the typical size of the foundations of nuclear facilities, is used to evaluate the upper bound of k_s. This allows for an approximation of the idealized soil stiffness for this study. The parameters and results are listed in Table A.2 and the ranges of stiffness for different site classes of the underlying soil are estimated as shown in Table A.3.

It should be noted that the estimation of the stiffness of soil spring presented in this section is approximate. They are used as the illustration purpose in the implement of the proposed direct method. More rigorous determination of soil stiffness needs to be implemented when the structural information, the type and size of foundation as well as the site condition are given.

Table A.2 Evaluation of soil stiffness for different site classes

Site Class	Soil	Type	Bound	V_s (m/s)	μ	E (kN/m^2)	G (kN/m^2)	R=3 m		R=30 m	
								k_H (kN/m)	k_V (kN/m)	k_H (kN/m)	k_V (kN/m)
E	Soft Clay	soft soil	LB	30	0.49	4.00×10^2	134.23	2.13×10^3	3.16×10^3	2.13×10^4	3.16×10^4
			UB	120	0.42	5.00×10^3	1760.56	2.67×10^4	3.64×10^4	2.67×10^5	3.64×10^5
D	Medium Clay	stiff soil	LB	150	0.46	6.00×10^3	2054.79	3.20×10^4	4.57×10^4	3.20×10^5	4.57×10^5
			UB	300	0.38	1.80×10^4	6521.74	9.66×10^4	1.26×10^5	9.66×10^5	1.26×10^6
C	Dense Clay	very dense soil	LB	350	0.39	2.00×10^4	7194.24	1.07×10^5	1.42×10^5	1.07×10^6	1.42×10^6
	Soft sandstone	and soft rock	UB	700	0.33	9.00×10^4	33834.59	4.86×10^5	6.06×10^5	4.86×10^6	6.06×10^6
B	Medium Basalt	rock	LB	800	0.34	1.00×10^5	37313.43	5.39×10^5	6.78×10^5	5.39×10^6	6.78×10^6
			UB	1500	0.29	2.00×10^5	77519.38	1.09×10^6	1.31×10^6	1.09×10^7	1.31×10^7
A	Granite	hard rock	LB	1600	0.3	1.00×10^6	384615.38	5.43×10^6	6.59×10^6	5.43×10^7	6.59×10^7
			UB	3000	0.25	2.00×10^8	80000000	1.10×10^9	1.28×10^9	1.10×10^{10}	1.28×10^{10}

Table A.3 Approximate range of soil stiffness for different sites

Site class	E		D		C		B		A	
Bound	LB	UB	LB	UB	LB	UB	LB	UB	LB	UB
k_s (kN/m)	2×10^3	4×10^5	3×10^4	2×10^6	1×10^5	6×10^6	5×10^5	2×10^7	5×10^6	2×10^{10}